To the Graduate Council:

We are submitting herewith a dissertation written by Abdollah Haddad Tabrizi entitled "An Experimental and Theoretical Investigation of an Air Injection Type Anti-Icing System for Aircraft." We have examined the final copy of this dissertation for form and content and recommend that it be accepted in partial fulfillment of the requirements for the degree of Doctor of Philosophy, with a major in Mechanical Engineering.

W. Stanley Johnson, Major Professor

James W. White, Major Professor

We have read this dissertation
and recommend its acceptance:

Accepted for the Council:

Vice Provost
and Dean of The Graduate School

AN EXPERIMENTAL AND THEORETICAL INVESTIGATION OF AN AIR INJECTION TYPE ANTI-ICING SYSTEM FOR AIRCRAFT

A Dissertation

Presented for the

Doctor of Philosophy

Degree

The University of Tennessee, Knoxville

Abdollah Haddad Tabrizi

August 1986

DEDICATION

To

my family

ACKNOWLEDGEMENTS

The author would like to express his appreciation to all those people who have added motivation to the work presented in this thesis.

In particular, thanks are especially due to his co-chairmen, Professors W. Stanley Johnson and James W. White, and to Professor Edward G. Keshock for their encouragement and assistance. Thanks are also due to his other committee members, Professors Allen J. Baker and J. Roger Parsons.

The author is grateful to the Department of Mechanical and Aerospace Engineering at the University of Tennessee for financial support on this project. Special thanks are due to Professor Donald R. Pitts, Head of the Department of Mechanical and Aerospace Engineering, for providing the necessary funds and a teaching opportunity to the author.

Thanks are extended to Mr. Dennis W. Higdon, Senior Electronics Technician, for his invaluable help during the course of the experimental investigation and his patience, understanding, and moral support.

A great debt of thanks is owed to the author's parents, Mr. and Mrs. Sadeg H. Tabrizi, whose financial support and endless love made his education possible. Thanks are also extended to the author's brother, Mr. Mohammad H. Tabrizi for his endless support in many ways throughout his education.

Finally, the author would like to thank Ms. Theresa J. Muenks for the preparation of the final copy of the dissertation.

ABSTRACT

An anti-icing system was investigated in connection with the ice accretion on an aircraft engine inlet and wing leading edge. Air injection at the leading edge was used to prevent supercooled water droplets in the atmosphere from striking the surface. Through the consideration of the droplet dynamics in a two-phase flow, i.e. air-water droplets, the effectiveness and feasibility of the air injection as a means of anti-icing technique was studied. An experimental investigation was also undertaken to complement the analytical study. An experimental model of a circular cylinder with injection slots was tested in a two-phase flow environment in a wind tunnel. A circular cylinder was used as an approximation of the leading edge of an engine inlet and a wing. It was shown that air injection at the leading edge reduces the ice collection rate and that the ice reduction rate is dependent on the air injection rate and location of the injection as well as the number of slots. The ice reduction due to the surface injection was determined by weighing the ice collected on the model. The predicted reduction in the ice collection due to the injection at a rate of 100 ft^3/hr from each slot (slots were located at 0 and ± 50 degrees from the front stagnation point) was 42 percent. The difference between predicted and measured ice weights ranged from 1.9 to 35.4 percent. A specially designed profilometer was used to obtain ice profiles for a qualitative assessment of the system performance.

TABLE OF CONTENTS

CHAPTER		PAGE
I.	INTRODUCTION	1
II.	PURPOSE OF THE RESEARCH	9
III.	DROPLET DYNAMICS	11
IV.	THEORETICAL MODEL OF A FLOW OVER A CIRCULAR CYLINDER WITH SURFACE INJECTION	21
V.	BOUNDARY LAYER OVER A CIRCULAR CYLINDER WITH SURFACE INJECTION AND ITS EFFECT ON DROPLET TRAJECTORY	47
VI.	MAPPED POTENTIAL FLOW SOLUTION OF FLOW OVER A CIRCULAR CYLINDER WITH SURFACE INJECTION	67
	General	67
	Grid Mapping Procedure	68
	Potential Flow Solution	77
VII.	EXPERIMENTAL INVESTIGATION	83
	General	83
	Wind Tunnel	84
	Experimental Model	86
	Spray System	89
	Droplet Size Distribution	94
	Droplet Velocity in the Test Section	95
	Experimental Procedure	96
	Measured Ice Profiles	102

CHAPTER PAGE

VIII. DISCUSSION OF RESULTS 113

IX. CONCLUSIONS AND RECOMMENDATIONS 127

Conclusions 127

Recommendations 129

BIBLIOGRAPHY 131

APPENDICES 137

APPENDIX A. TWO-PHASE FLOW EFFECTS 138

APPENDIX B. EFFECT OF DROPLET EVAPORATION 141

APPENDIX C. DROPLET DRAG COEFFICIENT 144

APPENDIX D. DERIVATION OF THE TRAJECTORY EQUATION 146

APPENDIX E. SOURCE AND SINK MODEL OF A FLOW OVER A CIRCULAR CYLINDER WITH SURFACE INJECTION 149

APPENDIX F. 1-EQUATION MODEL OF LOCAL NONSIMILARITY AND SOLUTION PROCEDURE 152

Solution Procedure 153

APPENDIX G. 2-EQUATION MODEL OF LOCAL NONSIMILARITY AND SOLUTION PROCEDURE 157

Solution Procedure 158

APPENDIX H. 3-EQUATION MODEL OF LOCAL NONSIMILARITY AND SOLUTION PROCEDURE 161

Solution Procedure 162

APPENDIX I. GRID MAPPING EQUATIONS AND PROCEDURE 166

CHAPTER PAGE

APPENDIX J. MAPPED POTENTIAL FLOW EQUATIONS..... 174

APPENDIX K. THE TUNNEL FLOW AND SPRAY CHARACTERISTICS. 177

Velocity Profiles..... 177

Spray System..... 177

APPENDIX L. MISCELLANEOUS INSTRUMENTS AND EQUIPMENT... 187

APPENDIX M. INCOMPRESSIBLE VISCOUS FLOW OVER A CYLINDER WITH SURFACE INJECTION..... 191

APPENDIX N. COMPUTER PROGRAM FOR DROPLET TRAJECTORY CALCULATION..... 203

APPENDIX O. COMPUTER PROGRAM FOR STREAMLINES CALCULATION..... 210

APPENDIX P. COMPUTER PROGRAM FOR 1-EQUATION MODEL..... 214

APPENDIX Q. COMPUTER PROGRAM FOR 2-EQUATION MODEL..... 217

APPENDIX R. COMPUTER PROGRAM FOR 3-EQUATION MODEL..... 221

APPENDIX S. COMPUTER PROGRAM FOR BOUNDARY LAYER AND DISPLACEMENT THICKNESS AND VELOCITY CALCULATION..... 227

APPENDIX T. COMPUTER PROGRAM FOR INITIAL GRID GENERATION..... 230

APPENDIX U. COMPUTER PROGRAM FOR GRID MAPPING..... 235

APPENDIX V. COMPUTER PROGRAM FOR MAPPED POTENTIAL FLOW..... 240

CHAPTER PAGE

APPENDIX W. COMPUTER PROGRAM FOR VELOCITY CALCULATION FROM STREAM FUNCTION DATA IN MAPPED PLANE..... 249

APPENDIX X. COMPUTER PROGRAM FOR GENERATING SPRAY DROPLET DISTRIBUTION DATA..... 251

APPENDIX Y. COMPUTER PROGRAM FOR VISCOUS FLOW SOLUTION..... 254

APPENDIX Z. COMPUTER PROGRAM FOR STREAM FUNCTION CALCULATION FROM VELOCITY DATA OF VISCOUS FLOW SOLUTION..... 275

VITA..... 277

LIST OF FIGURES

FIGURE		PAGE
I-1.	Ice Shapes Obtained in Flight.....	2
III-1.	Droplet Coordinate System.....	19
IV-1.	Potential Flow Representation of Flow Over Cylinder With Surface Injection.....	22
IV-2.	Coordinate System of Theoretical Model.....	24
IV-3.	Collection Efficiency of Cylinder.....	28
IV-4.	Collection Efficiency of Cylinder with Surface Injection, Sources Located at ±5°, ±50°.....	30
IV-5.	Collection Efficiency of Cylinder with Surface Injection, Sources Located at ±5°, ±25°.....	32
IV-6.	Effect of Source Location on Collection Efficiency, For Two Sources Located at ±θ°, K = 5.....	33
IV-7.	Effect of Source Location on Collection Efficiency, For Two Sources Located at ±θ°, K = 50.....	34
IV-8.	Effect of Source Strength on Collection Efficiency, Three Sources Model.....	36
IV-9.	Effect of Source Numbers on Collection Efficiency, for Equally Spaced Sources Within ±90°.....	37
IV-10.	Droplet Trajectories and Streamlines, K = 10, ϕ = 1000, and Q = 0.....	39

FIGURE PAGE

IV-11. Droplet Trajectories, K = 10, ϕ = 1000, Q = 0.5, Source Angles 0°, ±30°, ±60° 40

IV-12. Droplet Trajectories and Streamlines, K = 10, ϕ = 1000, and Q = 2, Source Angles 0°, ±30°, ±60° 41

IV-13. Droplet Trajectories For Various Source Strength .. 42

IV-14. Streamlines of Flow Over Circular Cylinder 43

IV-15. Streamlines of Flow Over Circular Cylinder With Surface Injection Q = 0.5, Angles 0°, ±30°, ±60° 44

IV-16. Streamlines of Flow Over Circular Cylinder With Surface Injection Q = 2, Source Angles 0°, ±30°, ±60° 45

V-1. Wall Shear of Flow Over Circular Cylinder 57

V-2. Boundary Layer Velocity Profile at x/R = 1.3 58

V-3. Boundary Layer Velocity Profile at x/R = 1.5 59

V-4. Displacement and Boundary Layer Thickness of Flow Over Cylinder, Re_o = 2463, Free Stream Velocity = 10 ft/sec 61

V-5. Effect of Surface Mass Transfer on Boundary Layer Velocity Profile for Flow Over Circular Cylinder, Re_o = 1000 63

FIGURE PAGE

V-6. Effect of Surface Mass Transfer on Boundary Layer Velocity Profile for Flow Over Circular Cylinder, Re_o = 10,000..... 64

V-7. Effect of Surface Mass Transfer on Wall Shear For Flow Over Circular Cylinder, Boundary Layer Flow..... 65

VI-1. Grid Mapping Coordinates, (a) Transformed Plane, (b) Physical Plane..... 70

VI-2. Initial Coordinate of Grid Mapping..... 73

VI-3. Initial Coordinate After Mapping..... 74

VI-4. Initial Coordinate with Modified Top Boundary..... 75

VI-5. Initial Modified Grid After Mapping..... 76

VI-6. Mapped Coordinate of Initial Modified Grid With Suction Applied at the Bottom Plane..... 78

VI-7. Contour Plot of Streamlines Obtained From Mapped Solution With Surface Injection at ±50°, and 0° (Front Stagnation Point), Wall Velocity = $17.3*U_\infty$..... 80

VI-8. Contour Plot of Streamlines Obtained From Theoretical Solution With Surface Injection at ±50° and 0° From Stagnation, Wall Velocity = $17.3*U_\infty$..... 81

FIGURE PAGE

VI-9. Contour Plot of Streamlines Obtained From Theoretical Solution With No Surface Injection..... 82

VII-1. Wind Tunnel..... 85

VII-2. Wind Tunnel Test Section And The Model..... 87

VII-3. Hot Wire/Film Anemometer Used For Velocity Measurement..... 88

VII-4. Dimensional Details of the Experimental Model..... 90

VII-5. Descriptive Details of the Experimental Model..... 91

VII-6. Schematics of the Spray System Used in Experiments..... 92

VII-7. Schematic of a Pneumatic Atomizing Nozzle..... 93

VII-8. Spray Droplet Deceleration Distance..... 97

VII-9. Schematic of the Cooling and the Nitrogen Supply System..... 99

VII-10. Profilometer Used for Ice Profile Measurements, Experimental Model is Also Shown..... 100

VII-11. Typical Ice Shapes on Cylinder With And Without Surface Injection..... 103

FIGURE PAGE

VII-12. Axial Ice Profiles Along the Cylinder at θ = +5° From the Front Stagnation Point. Injection Rates Are: Curve #1 = 0, 0, 0; Curve #2 = 0, 200, 0; Curve #3 = 100, 200, 100 (ft^3/hr)..... 105

VII-13. Angular Ice Profiles Around the Cylinder at L = 5 inches. The Front Stagnation Point is at θ = 0°. Injection Rates Are: Curve #1 = 0, 0, 0; Curve #2 = 0, 200, 0; Curve #3 = 100, 200, 100 (ft^3/hr)..... 106

VII-14. Angular Ice Profiles Around the Cylinder at L = 6.25 inches. The Front Stagnation Point is at θ = 0°. Injection Rates Are: Curve #1 = 0, 0, 0; Curve #2 = 0, 200, 0; Curve #3 = 100, 200, 100 (ft^3/hr)..... 107

VII-15. Angular Ice Profiles Around the Cylinder at L = 7.5 inches. The Front Stagnation Point is at θ = 0°. Injection Rates Are: Curve #1 = 0, 0, 0; Curve #2 = 0, 200, 0; Curve #3 = 100, 200, 100 (ft^3/hr)..... 108

VII-16. Axial Ice Profile Along the Cylinder at θ = +5° From The Front Stagnation Point. Injection Rates Are: Curve #1 = 0; Curve #2 = 200 (ft^3/sec)..... 110

FIGURE PAGE

VII-17. Angular Ice Profile Around the Cylinder at L = 6.25 inches..... 111

VIII-1. Comparison of Theoretical and Experimental Ice Weights, No Surface Injection..... 124

B-1. The Drag Coefficient Divided By That in the Absence of Blowing as a Function of Blowing Number For Various Reynolds Number [39]..... 143

E-1. Potential Flow Model of a Source Near a Cylinder.. 150

K-1. Hot Wire Probe Calibration Curve and Velocity Equation..... 178

K-2. Hot Film Probe Calibration Curve and Velocity Equation..... 179

K-3. Test Section Velocity Profile, Average Velocity = 4.1 ft/sec..... 180

K-4. Test Section Velocity Profile, Average Velocity = 6.3 ft/sec..... 180

K-5. Test Section Velocity Profile, Average Velocity = 13.3 ft/sec..... 181

K-6. Test Section Velocity Profile, Average Velocity = 39 ft/sec..... 181

K-7. Pneumatic Nozzle Water Mass Flow Calibration Curve 182

FIGURE PAGE

K-8. Frequency of Occurence of a Droplet Size in the Spray..... 186

L-1. Schematic of Smoke Generator..... 190

LIST OF TABLES

TABLE		PAGE
VIII-1.	Experimental Ice Weights Collected on the Model, Set No. 1	114
VIII-2.	Experimental Ice Weights Collected on the Model, Set No. 2	115
VIII-3.	Predicted Ice Weights Collected on the Model For 7 Minutes of Exposure, Set No. 1	118
VIII-4.	Predicted Ice Weights Collected on the Model For 7 Minutes of Exposure, Set No. 2	119
VIII-5.	Percent Difference of Predicted and Experimental Ice Weights	120
C-1.	Experimental Drag Coefficient of Solid Sphere [42]	145
F-1.	First Order Equations For 1-Equation Model	156
G-1.	First Order Equations For 2-Equation Model	160
H-1.	First Order Equations For 3-Equation Model	164
K-1.	Nozzle Water Flow Rate Calibration Data Tunnel LWC	184
K-2.	Spray Droplet Characterization	185

NOMENCLATURE

C_d	Droplet drag coefficient
c_p	Specific heat of air
D	Cylinder diameter
d	Droplet diameter
E	Collection efficiency
Eö	Eötvos number
F_a	Apparent mass force
F_B	Basset force
F_d	Drag force
F_g	Gravity force
F_M	Magnus force
Fr	Froud number
f'	Nondimensional velocity in the boundary layer
f"	Nondimensional shear stress in the boundary layer
g	Gravitational constant
h	Convective heat transfer coefficient
h_{fg}	Latent heat of vaporization
J	Coordinate transformation Jacobian
K	Inertia parameter
k	Thermal conductivity
L	Reference length
LWC	Liquid water content of clouds

$\dot{m}$	Mass flow rate
m_d	Droplet mass
N_o	Number of droplets per unit volume
Nu	Nusselt number
P	Coordinate control parameter
P_a	Air pressure
Q	Nondimensional slot (source) flow rate, also coordinate control parameter
$\dot{Q}$	Volumetric flow rate
q	Slot flow rate or source/sink strength
R	Cylinder radius
Re_d	Droplet relative Reynolds number, $d(\|U_a - U_d\|)/\nu$
Re_{o_d}	Droplet Reynolds number, dU_∞/ν
Re_o	Flow Reynolds number, RU_∞/ν
r	Radial coordinate vector
r_d	Droplet radial position coordinate
S	Droplet position vector
$\dot{\vec{S}}$	Droplet velocity vector
$\ddot{\vec{S}}$	Droplet acceleration vector
T_a	Air temperature
T_{wb}	Wet bulb temperature
t	Time
U	Velocity at the edge of the boundary layer
U_a	Air velocity vector
U_d	Droplet velocity vector

U_o Reference velocity

U_∞ Free stream velocity

u_a Air velocity in the streamwise (x) direction

u_d Droplet velocity in the streamwise (x) direction

v_a Air velocity in the y direction

v_d Droplet velocity in the y direction

v_w Wall air velocity perpendicular to the cylinder surface

We Weber number

w Slot width

X Cartesian coordinate used in mapping

x Cartesian coordinate, also used as an initial guess for f" at the cylinder surface

x_i Position of a slot (source) on the cylinder in the x direction

Y Cartesian coordinate used in mapping

y Cartesian coordinate also used as an initial guess for g" at the cylinder surface

y_i Position of a slot (source) on the cylinder in the y direction

Z Droplet loading in the tunnel

z Initial guess for h" at the cylinder surface

Greek Symbols

α Grid transformation parameter defined by Equation (VI-4)

β	Grid transformation parameter defined by Equation (VI-4), also parameter defined by Equation (V-12)
Γ, Γ^*	Boundary segment identifiers
γ	Grid transformation parameter defined by Equation (VI-4), also parameter defined by Equation (V-12)
δ	Boundary layer thickness
$\delta_{\eta\eta}, \delta_{\xi\xi}$	Second order finite difference operators
δ^*	Displacement thickness
η	Transformed coordinate of the boundary layer and mapped plane
θ	Angle
λ	Blowing number
μ	Air viscosity
ν	Air kinematic viscosity
ξ	Transformed coordinate of the mapped plane
ρ_a	Air density
ρ_d	Droplet density
σ_d	Droplet surface tension
τ	Shear stress
ϕ	Parameter defined by Re_0^2/K
Ψ	Stream function
ω	Droplet angular velocity

CHAPTER I

INTRODUCTION

Problems associated with aircraft icing have been recognized since the early days of aircraft technology and have been subject to a number of investigations. The undesirable effects of icing on aircraft performance and potential hazards associated with these effects have been well documented [1,2].

Brun [3], outlines that aircraft icing occurs when an aircraft enters an atmosphere containing supercooled water droplets. Under such conditions, when a supercooled water droplet strikes the aircraft, the ice which forms immediately adheres to the surface. If the aircraft is exposed to this kind of condition for a period of time (on the order of minutes [2]) an ice layer will form and grow with time on the aircraft surface. Resulting ice shapes differ for different atmospheric conditions. In general two types of accreted ice formation appear on an airfoil, rime and glaze ice [3,4,5], as illustrated in Figure I-1. Icing intensity depends upon the temperature and liquid water content of the clouds. It is known that the liquid water content of clouds decreases, and the temperature increases as the altitude increases.

Ice accreted on the wing surface increases the aerodynamic drag coefficient and decreases the lift [1]. On the other hand icing of a helicopter rotor blade increases the blade drag and results in a

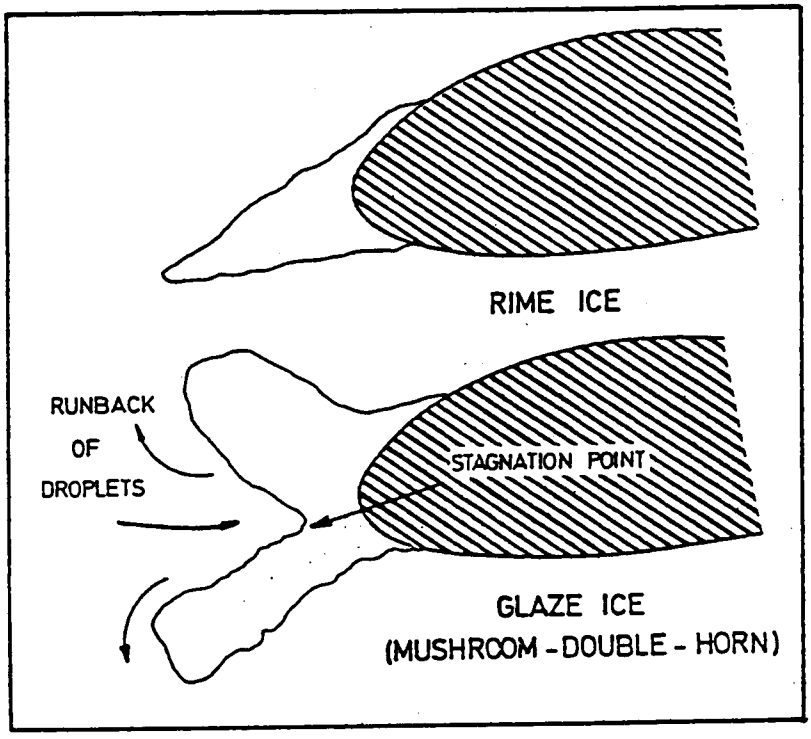


Figure I-1. Ice Shapes Obtained in Flight .

torque rise on the rotor shaft, but causes little change in the blade lift [1].

In practice, wind tunnel facilities are used to create conditions under which icing occurs, but testing of a full-scale model is obviously not always possible or convenient. Both economic and physical constraints make this type of experimentation undesirable when considering tests on aircraft wings, engines, and helicopter rotors. Therefore, it is desirable to perform the experiments on a small-scale model. This necessitates obtaining certain similitude conditons by which the behavior of the full-scale model may be simulated [6,7,8].

The majority of the investigations performed by the aircraft industries have focused on preventive measures through experimental evaluations and little has been done on the theoretical aspects of the icing phenomena.

Brun categorizes the protection techniques as anti-icing, prevention of ice formation, and deicing, i.e. the periodic removal of ice already formed. Examples of anti-icing techniques are the chemical and coating processes, which are used to prevent the ice from adhering. Continuous heating of the surface was considered by Nichols [9]. He investigated the anti-icing heat flux requirements to provide an ice free leading edge of the engine inlet for cruise missiles with a strip heater configuration. He reports that, for the ambient temperature of $-9.4°C$ and heating element surface temperature of $14°C$, total anti-ice capability of the inlet leading edge was

found possible with a power input of 1.94 Watts/sq-cm. Continuous heating is considered to be the only universal means of protection against icing. A glycol-exuding porous leading edge ice protection system has been experimentally investigated by NASA Lewis and performance of this system is found to be very effective [10]. This particular technique is more popular with the British aircraft industries and is utilized in certain types of British aircraft [11]. Another deicing system includes pneumatic deicers ("rubber shoes" which covers the leading edge and are periodically inflated and deflated). Also, intermittent heating of airfoils utilizing hot air is considered by Hauger [12]. He has studied the feasibility of the technique and has developed the critical heating time for the deicing of an ice covered surface. However, there are problems associated with each one of the above techniques, among which are the high power demand for heating systems and short life for pneumatic deicers.

Investigation of an airfoil icing and ice collection rate requires a knowledge of the liquid water content and droplet size distribution of the atmospheric clouds and the collection efficiency of the icing surface. The liquid water content of the clouds was determined by Brun et al. [13] using the rotating multicylinder method. They also determined the droplet size distribution and reported that in a typical cloud the mean droplet size is about 20 microns. The liquid water content in a typical icing cloud was determined to be as high as 2.5 gm/m^3. The droplet size distribution was determined by exposing several cylinders of different diameters from an airplane in

flight to the supercooled droplets in the icing cloud. The number of supercooled droplets that strike and freeze on the cylinders is a function of the cylinder size and of the flight and atmospheric conditions, as well as the inertial properties of the droplets. The liquid water content and droplet size distribution in the cloud are determined by a comparison of the amount of the measured weight of ice collected on each of the cylinders with the amount of droplet impingement obtained from the calculated water droplet trajectories for cylinders of the same size and for the same flight and atmospheric conditions. In a laboratory environment, however, the droplet size distribution in a given droplet laden flow can be determined by a variety of methods depending on the flow system under consideration and, most importantly, on the availability of the equipment required. The Laser Doppler Anemometer measurement is among the most sophisticated techniques and microscopic measurement of the sampling slides is among the simplest and most reliable techniques. Azzopardi [14] presents a fairly complete review of the droplet size measuring techniques.

In practice, the majority of experimental investigation of the icing phenomenon is carried out in a two-phase flow wind tunnel such as the one in NASA Lewis in Cleveland, Ohio. The droplets in a two-phase tunnel were produced by an array of spray nozzles. Pneumatic atomizers are the most widely used spray nozzles in two-phase flow applications in which spray is produced by the disruptive action of a high velocity gas upon a liquid jet. Because two fluid streams are

involved, it is sometimes called two-fluid atomization. Pneumatic nozzles are particularly well suited to produce fine sprays, that is, less than 50 microns in mass median diameter. Kim and Marshall [15] have studied pneumatic nozzles and have developed empirical droplet size distribution correlations for a number of design conditions. Other methods of atomization, such as pressure nozzles and spinning disks, are not generally capable of producing sprays of this drop size range except under extreme operating conditions. However, the fine size production from pneumatic atomizers is accomplished only with relatively modest capacities, several gallons per hour at most. Nevertheless, this type of atomization has an advantage in that liquid and air streams can be controlled independently. Pressure nozzles have been studied by Schnider [16] in connection with the stability of electrified liquid surfaces and by Dabora [17] in connection with production of monodisperse sprays. Their analyses are based on the Rayleigh's analysis of the instability of capillary jets.

Ice shapes formed on a surface can be predicted analytically by considering the energy transfer processes taking place at the interface of ice and adjacent air layer above the surface. Such an investigation has been conducted by Stallabrass [18] and fair agreements have been obtained with the experimental results. The presence of droplets in a flow over a surface enhances the heat transfer rate up to 9 times that of the case with no droplets in the flow. Goldstein [19] analyzed the boundary layer of two-phase gas

liquid flow over a cylinder and Hodgson [20] studied heat transfer from an isothermal cylinder exposed to air-water flow. The above investigations, however, have been conducted based on very approximate boundary layer analyses.

The droplet collection efficiency of a given surface, in general, is a function of air speed, surface shape and size, and droplet diameter. The collection efficiency of a surface can be calculated by considering the droplet trajectories about that particular surface. A droplet is collected on the surface if its trajectory intersects the collecting surface. Capture by interception assumes that the center of a small nondiffusing spherical particle follows exactly along an undisturbed fluid streamline near a larger collector until the particle and the collector touch, whereupon the particle is retained by contact adhesion. On the other hand, owing to inertia, sufficiently massive particles are unable to follow curvilinear fluid motion and tend to continue along a straight path as the carrier fluid curves around the collector. Particles can also be deposited on a surface by the action of Brownian diffusion. However, only submicron particles are affected by this type of diffusion. Review of particle impaction mechanisms is given by Spielman [21]. From the above discussion on droplet collection it is obvious that determination of the droplet trajectories require detailed knowledge of the flow field, i.e. flow velocities at every point in the flow. Thus for a given flow situation the velocity distribution should be calculated along with the droplet trajectory. Unless one is dealing

with a very simple geometry, the governing differential equations for the flow, in general, should be integrated numerically using techniques such as finite difference or finite elements. The selection of a particular technique usually depends on the problem under consideration and required accuracy. A review of numerical techniques is given by Peyret [22].

The boundary layer flow effects on the droplet trajectory are customarily neglected by the aircraft icing investigators. Consequently, droplet trajectories have never been obtained inside a boundary layer. Even though the boundary layer may be thin enough so that it does not perturb the flow field, it is of interest to know the behavior of the droplet inside the boundary layer. In fact this is of particular interest when one is dealing with scaling of pipes in the geothermal power plants [23] and erosion of the gas turbine blades [24].

Solutions of the boundary layer flow with surface mass transfer have been obtained by many investigators. The solution techniques range from analytical similarity methods to numerical procedures. Lindow and Greber [25] obtained a similarity solution for the jet flowing along a curved surface. Tennant et al [26] presented a solution technique for calculating boundary layers along rotating cylinders. On the other hand, boundary layer flows with surface injection have been investigated by Cole and Aroesty [27] for the case of large blowing rates. Strong blowing into supersonic laminar flows have been studied by Inger and Gaitatzes [28].

CHAPTER II

PURPOSE OF THE RESEARCH

An anti-icing technique was investigated in connection with aircraft wing icing. The technique is based on air injection at the leading edge of the icing surface, through a slot (or slots), which alters the flow field about the surface, thus affecting the droplet trajectories as they approach the leading edge. Preventing the droplet trajectories from intercepting the leading edge is the main objective with this technique. In the analysis that follows, the leading edge has been approximated by a circular cylinder and the flow is considered to be two dimensional. Both analytical and experimental investigations of the anti-icing system were conducted. The objectives of the research program are:

1. Analytical modeling of a droplet laden inviscid potential flow over a circular cylinder with surface mass transfer. The entire flow was represented by a series of sources and sinks. Thus the flow field velocities were calculated from a set of exact relationships.

2. Analytical modeling of the boundary layer flow over a circular cylinder with surface mass transfer. The boundary layer was modeled based on the "local nonsimilarity" method and its effect on the droplet trajectories as well as the blow-off limits of the boundary layer as a function of surface injection rate was investigated.

3. Comparison of the stream functions obtained from an exact theoretical solution of part (1) and those obtained numerically by integrating the Laplace equation for the stream function with appropriate boundary conditions. A factored implicit finite differencing technique was used for the solution. The physical plane was first mapped onto a rectangular cartesian plane and the flow equation was then transformed and solved in the mapped plane.

4. Experimental investigation of the air injection anti-icing technique. An experimental model, circular cylinder, with three injection slots located at 0 and ±50 degrees from the front stagnation point was tested in the wind tunnel.

5. Modeling of a flow over a circular cylinder including viscous effects. Momentum (Navier-Stokes) equations describing velocities, along with an artificial compressibility equation, were solved in a vectorial form to obtain solutions to the flow field. This section is discussed entirely in Appendix M and the corresponding computer programs are given in Appendices Y and Z.

CHAPTER III

DROPLET DYNAMICS

The motion of droplets in a gas stream is influenced by a variety of forces and factors: thus, analysis of the dynamics of droplets is a formidable task. Fortunately, however, in any given two-phase flow situation it is possible to reduce the problem, without loss of generality, to a more manageable size by neglecting parameters with second order effects. Therefore the problem becomes one of identifying the parameters that govern a particular flow. Simplification of the problem is then possible by an order of magnitude analysis.

A droplet dynamics analysis was performed to obtain the trajectories of the droplets in the icing environment. It was assumed that the mean droplet diameter could effectively represent the average effect of all of the droplet sizes present in the stream. The air stream is assumed to be uniform, steady and laminar and that the water droplets are distributed uniformly in the air. Thus, under these conditions the droplet trajectories, in general, would be affected by the following factors and forces:

1. Two-phase flow effects
2. Pressure gradient force
3. Magnus lift force
4. Saffman lift force
5. Temperature gradient effects

6. Basset memory force
7. Asphericity and brake up effects
8. Brownian motion
9. Electrostatic precipitation
10. Electrostatic repulsive force between droplets
11. Mass transfer, i.e. droplet evaporation, effects
12. Apparent or virtual mass force
13. Gravity force
14. Drag force

However, it will be shown that not all of the above listed items are important in the icing problem under consideration.

In many two-phase flow systems each phase is generally considered to be a continuum with two way coupling between the phases. The two-phase flow encountered in the icing situation, i.e. the air-water droplet mixture, does not possess the above characteristics since the droplet loading, i.e. ratio of the droplet mass to the air mass in a given volume, of the air stream is small (< 0.1) and thus the droplet phase is dilute and cannot be considered as a continuum. Furthermore, it can be shown that in dilute suspensions the particle motion is controlled by the gas flow as opposed to particle collisions. Since in a continuum the flow information is transferred by molecular interaction (collisions), a dilute droplet cloud cannot be considered a continuum [29]. In dilute droplet clouds information is transmitted only along trajectories. In Appendix A it is shown that based on the above conditions the two-phase flow effects in the

icing flow situation can be assumed negligible. This assumption makes it possible to calculate the individual droplet trajectories once the air stream velocities are known.

Droplets are influenced by the pressure gradient in the air stream. However, only the droplets near the icing surface will be affected by the pressure gradient and even then this effect compared to drag force is on the order of $\rho_{air} / \rho_{water} \simeq 10^{-3}$. Thus pressure gradient force was assumed to be negligible [30].

The droplets when introduced into the air stream may have initial rotation. Rotation causes fluid entrainment adding to the velocity on the one side of the droplet and lowering the velocity on the other side. Lower pressure on the higher velocity region generates lift on the droplet which is known as the Magnus lift force. The Magnus force can be calculated from [31]

$$F_M = \frac{\pi}{8} d^3 \rho_a \bar{\omega} \times \bar{U}_d \qquad \text{(III-1)}$$

where d, $\bar{\omega}$, and $\bar{U}_d$ are droplet diameter, angular speed of rotation, and droplet velocity vector respectively. The Magnus force compared to the drag force is on the order of $\rho_{air} / \rho_{water} \simeq 10^{-3}$. Thus the effect of the Magnus lift force was assumed to be negligible.

Rotation of a droplet may also arise due to the presence of a velocity gradient in the fluid such as the shear layer near a wall. Thus the presence of a velocity gradient in the flow gives rise to a

lift force which is called the Saffman lift force. This force can be calculated from [32]

$$F_S = \frac{18.1}{4} \frac{\mu_a d^2}{\nu^{\frac{1}{2}}} \left| \bar{U}_a - \bar{U}_d \right| \left(\frac{du_a}{dy} \right)^{\frac{1}{2}} \qquad \text{(III-2)}$$

However, this force may be important in the boundary layer region where a steep velocity gradient exists. The effect of boundary layer is neglected in the present study.

The temperature gradient in the air stream could cause a viscosity gradient and therefore a velocity gradient could result which in turn produces the Saffman lift. However, the air stream was considered to be uniform in temperature except near the surface where a temperature gradient may result due to frictional effects. The effect of temperature gradient, if any, is confined to the boundary layer region which was assumed to be unimportant for the icing problem.

The Basset force is due to unsteady development of a boundary layer on the droplet. In another words, this term accounts for the error in using the steady state drag coefficient for the accelerating droplets. The magnitude of this term depends on the history of the droplets acceleration and can be calculated from [33]

$$F_B = \frac{3}{2} d^2 (\pi \rho_a \mu_a)^{\frac{1}{2}} \int_{t_o}^{t} \frac{(\bar{U}_a - \bar{U}_d)_{t'}}{(t - t')} dt' \qquad \text{(III-3)}$$

The Basset force term is important in situations where particle density is small and the acceleration rates are high. For the case under consideration Hines [33] has shown that this force is several orders of magnitude smaller than drag force. Thus the effect of this force was neglected.

Droplet instability may result in the deformation of the droplet which increases the drag, and could lead to the break up of the droplet. The droplet break up can occur for Weber number greater than 10 [29] where the Weber number is defined as

$$We = \frac{d\,\rho_a(\bar{U}_a - \bar{U}_d)^2}{\sigma_d} \qquad \text{(III-4)}$$

However, the droplet deformation and break up criterion is quantified by [34]

$$\frac{We}{Re_d^{\frac{1}{2}}} \leq 1.0 \qquad \text{(III-5)}$$

For a droplet of 100 microns in diameter and a velocity of 10 m/sec this ratio is equal to 0.02. Therefore the droplet deformation and break up for the present problem is very unlikely.

Submicron droplets can undergo Brownian motion, which promotes their deposition during flow past a collector. In the present study all the analyses were conducted using the mean droplet diameter of the icing clouds, which in a typical icing cloud is about 20 microns.

Since the effect of the Brownian diffusion is only appreciable on the submicron droplets, it was assumed that droplet deposition by this type of diffusion is negligible.

During the flight, an electrostatic charge will be produced on the icing surface due to the striking of atmospheric ions with the surface so that the droplets near the surface may be affected by it. This force is important when dealing with submicron droplets [35], thus it was assumed to be unimportant for the present case.

Due to the striking of unipolar ions in the atmosphere with the droplets, an electrostatic charge will be produced in the droplets. If all the droplets have the same polarity, there will be a repelling force between the droplets. This action could have an effect on the droplet trajectories. Furthermore, if a droplet carries two charges, repulsive force would give an ellipsoid as a stable shape rather than the sphere, due to surface tension. The stability of a charged droplet was studied by Ailam and Gallily [36]. The electrostatic effect was not considered in the present study.

Evaporation of a droplet affects the drag force on the droplet in two different ways. Firstly, mass transfer reduces the diameter of the droplet, thus changing the drag coefficient and the drag force [37,38]. Secondly, surface mass transfer reduces the drag force on a droplet suspended in a fluid. The drag reduction by surface blowing can be as high as 60 percent at a blowing number (i.e. blowing velocity/free stream velocity) of 3 [39]. As shown in Appendix B, evaporation effects are not important for the icing problem.

The apparent mass force is the force required to accelerate the droplet added mass, that is the air entrained in the droplet boundary layer. This force can be calculated from [40]

$$F_a = \frac{1}{2}\frac{\pi}{6}\rho_a d^3 \frac{d}{dt}(\bar{U}_a - \bar{U}_d) \qquad \text{(III-6)}$$

The trajectory of the droplet can be influenced by the gravity force acting on the droplet. The gravitational effect in comparison to drag force acting on the droplet is small in the droplet size range encountered in an icing situation.

Generally, the drag coefficient of a droplet is less than that of a solid sphere. Zuber and Ishii [41] indicate that drag coefficient on a pure water droplet could be 33 percent smaller than that of a solid sphere (due to internal circulation). However, small amounts of impurities are sufficient to eliminate this drag reduction. Based on the analysis and justification provided in Appendix C it was assumed that the drag coefficient of a solid sphere could accurately represent the drag coefficient on the droplets considered in the present study. The experimental drag coefficients for solid spheres [42] are also given in Table C-1 in Appendix C. These coefficients were used in the analytical computation.

With the above assumptions the trajectory equation for the droplet was obtained by application of Newton's second law, i.e. conservation of momentum, thus

$$m_d \frac{d^2 \bar{S}}{dt^2} = \bar{F}_g + \bar{F}_a + \bar{F}_d \qquad \text{(III-7)}$$

where m_d is droplet mass, $\bar{S}$ is the droplet displacement vector, $\bar{F}_g$ is the gravity force, $\bar{F}_a$ is the apparent mass force, and $\bar{F}_d$ is the drag force. After inclusion of appropriate expressions and assuming that $\rho_d >> \rho_a$, the nondimensional droplet trajectory equation was obtained (details of the derivation are given in Appendix D and the coordinate system is shown in Figure III-1) as follows

$$\ddot{\bar{S}}^* = \frac{1}{Fr^2} \frac{\bar{g}}{g} - \frac{c_d Re_d}{24K} (\dot{\bar{S}}^* - \bar{U}_a) \qquad \text{(III-8)}$$

where

$$K = \frac{\rho_d d^2 U_\infty}{9 D \mu_a} \quad , \quad Fr = \frac{U_\infty}{(Rg)^{\frac{1}{2}}}$$

subject to the following initial conditions:

$$\begin{aligned} t = 0 \qquad & u_d(x = 10) = u_a \\ & v_d(x = 10) = v_a \end{aligned} \qquad \text{(III-9)}$$

The validity of the above initial condition was examined in connection with the experimental investigation and results are given in Chapter VIII.

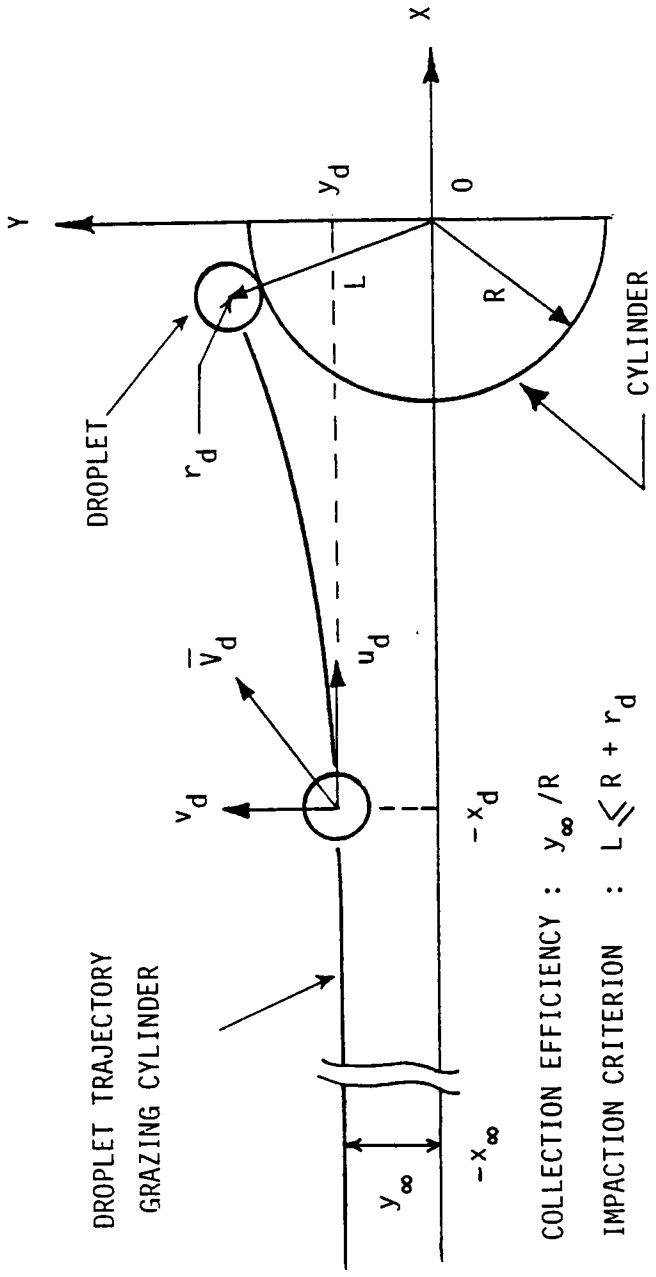


Figure III-1. Droplet Coordinate System.

Equation (III-8) was integrated to obtain the droplet trajectories about the cylinder. Equation (III-8) contains air velocities which must be supplied before the integration can be performed. The following chapters present methods for calculating flow velocities.

CHAPTER IV

THEORETICAL MODEL OF A FLOW OVER A CIRCULAR CYLINDER WITH SURFACE INJECTION

A theoretical model was developed to calculate the velocities in the flow over a circular cylinder with surface injection. It was assumed that the boundary layer on the cylinder is thin and that the entire flow can be represented by an inviscid flow. This approximation greatly simplifies the analysis because of the fact that the solution of the flow field around a circular cylinder is mathematically simple for a potential flow.

The free stream is assumed to be uniform and undisturbed by the presence of droplets. The entire flow is considered to be two dimensional with the cylinder represented by the superposition of a doublet within the uniform stream. Injection slots are considered as line sources on the cylinder, which in turn requires the inclusion of sinks at the center of the cylinder as shown in Figure IV-1. Specifically, for every source with strength of (q) located on the cylinder it is required to add a sink with the strength of (0.5q) at the center of the cylinder (circle). The requirement for the addition of sinks will be evident if one considers the image of a source outside a curved surface and application of the optical relationships [40,43]. A detailed modeling analysis of the above is presented in Appendix E. Both the stream and potential functions for the entire flow can now be obtained directly by summing up the stream

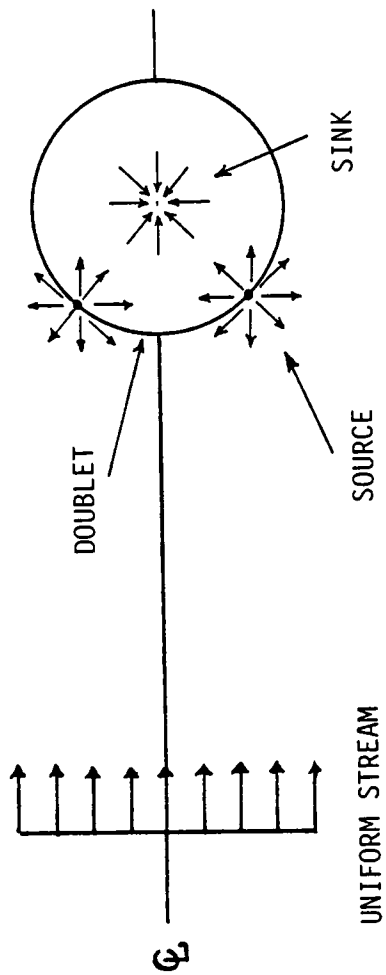


Figure IV-1. Potential Flow Representation of Flow Over Cylinder With Surface Injection.

functions for the uniform stream, doublet, sources, and sinks (using the principle of superposition). Thus

$$\Psi = \Psi_{\substack{\text{uniform}\\\text{stream}}} + \Psi_{\text{doublet}} + \sum_{i=1}^{n} \Psi_{i\ \text{source}} + \sum_{i=1}^{n} \Psi_{i\ \text{sink}} \qquad \text{(IV-1)}$$

$$\Phi = \Phi_{\substack{\text{uniform}\\\text{stream}}} + \Phi_{\text{doublet}} + \sum_{i=1}^{n} \Phi_{i\ \text{source}} + \sum_{i=1}^{n} \Phi_{i\ \text{sink}} \qquad \text{(IV-2)}$$

Substituting appropriate stream and potential functions, Equations (IV-1) and (IV-2) become (see Figure IV-2 for coordiante details)

$$\Psi = U_\infty y - \frac{R^2 U_\infty y}{(x^2 + y^2)} + \sum_{i=1}^{n} \frac{(q_i)(\theta_{\text{source}})_i}{2\pi} - \sum_{i=1}^{n} \frac{(q_i)(\theta_{\text{sink}})_i}{4\pi} \qquad \text{(IV-3)}$$

where

$$(\theta_{\text{source}})_i = \tan^{-1}\left(\frac{y - y_i}{x - x_i}\right)$$

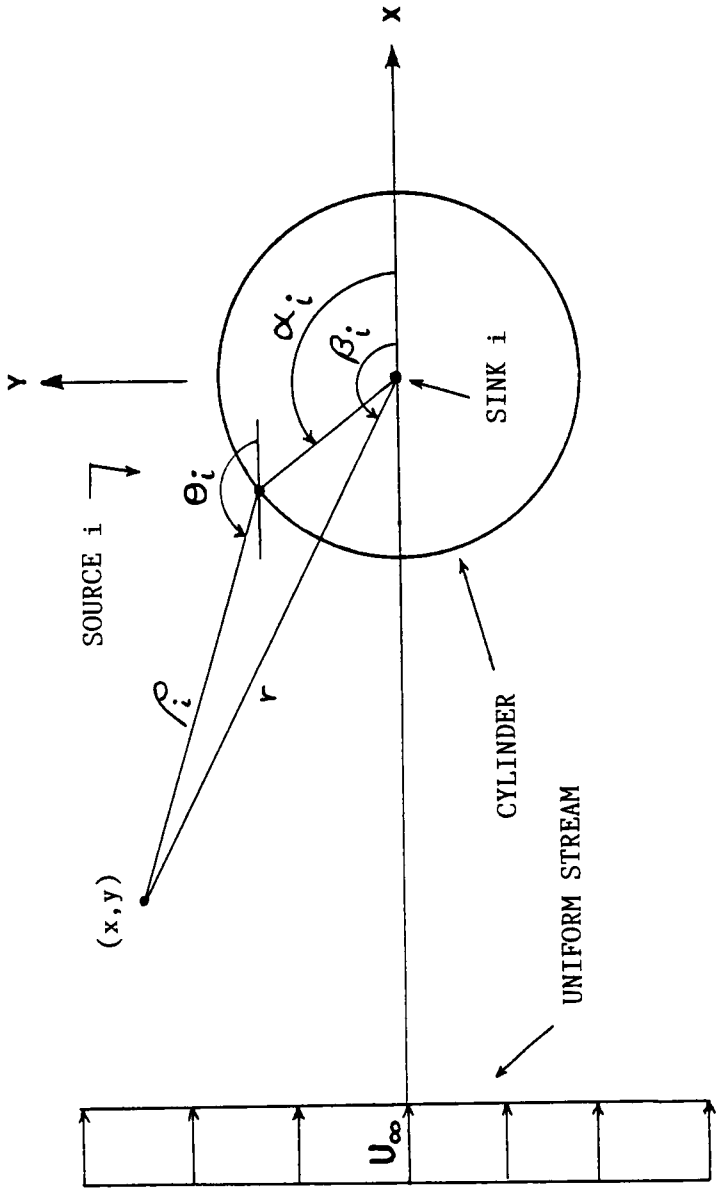


Figure IV-2. Coordinate System of Theoretical Model

$$(\theta_{sink})_i = \tan^{-1}\left(\frac{y}{x}\right)$$

$$x_i = R\cos(\alpha_i)$$

$$y_i = R\sin(\alpha_i)$$

$$x = r\cos\beta_i$$

$$y = r\sin\beta_i$$

$$\Phi = U_\infty x + \frac{R^2 U_\infty x}{(x^2 + y^2)} + \sum_{i=1}^{n} \frac{q_i}{2\pi} \ln \rho_i - \sum_{i=1}^{n} \frac{q_i}{4\pi} \ln r \qquad \text{(IV-4)}$$

where

$$\rho_i = \left[(x - x_i)^2 + (y - y_i)^2\right]^{\frac{1}{2}}$$

$$r = [x^2 + y^2]^{\frac{1}{2}}$$

The velocities were obtained from

$$u_a = + \frac{\partial \Phi}{\partial x}$$

$$u_a = U_\infty \left[1 - \frac{R^2(x^2 + y^2)}{(x^2 + y^2)^2}\right]_{\text{uniform stream}}$$

$$+ \sum_{i=1}^{n} \frac{q_i}{2\pi} \frac{(x - x_i)}{(x - x_i)^2 + (y - y_i)^2} - n \sum_{i=1}^{n} \frac{q_i}{4\pi} \frac{x}{(x^2 + y^2)} \qquad \text{(IV-5)}$$

Similarly

$$v_a = + \frac{\partial \Phi}{\partial y}$$

$$v_a = - \frac{2R^2 U_\infty x y}{(x^2 + y^2)^2} + \sum_{i=1}^{n} \frac{q_i}{2\pi} \frac{y - y_i}{(x - x_i)^2 + (y - y_i)^2} - n \sum_{i=1}^{n} \frac{q_i}{4\pi} \frac{y}{(x^2 + y^2)} \qquad \text{(IV-6)}$$

The trajectory equations can now be integrated with the aid of the above air velocities. The trajectory of a droplet is obtained as follows. The numerical integration of the droplet dynamics equation starts by releasing a droplet from a distance far from the cylinder ($x = -10R$) at which point the velocity of the droplet is assumed to be equal to the local velocity of the main stream. Then integration was performed over a preselected time interval and the new droplet position was calculated. Air velocities corresponding to the new droplet position are computed from the exact potential flow Equations (IV-5,6). This procedure was then repeated to obtain the complete droplet trajectory. The integration process was terminated when the trajectory intercepted the cylinder or passed the cylinder (see Figure III-1, page 19 for coordinate details). It was assumed that the droplet was collected on the cylinder when the (impaction) criterion, i.e. $L \leq R + d/2$, was satisfied as shown in Figure III-1.

It should be noted that the criterion used to evaluate the system performance is the parameter called "collection efficiency" which is represented by the symbol (E). Figure III-1 also graphically presents the definition of the collection efficiency. The effectiveness of the system is then judged by the reduction in collection efficiency. The collection efficiency of a circular cylinder was first determined and plotted against the inertia parameter (K) (defined by Equation (III-8)) as shown in Figure IV-3. A dimensionless parameter ϕ, defined as

$$\phi = \frac{Re_{o_d}^2}{K}$$

$$Re_{o_d} = \frac{U_\infty d}{\nu} \qquad \text{(IV-7)}$$

was adopted for the presentation of the data. The parameter ϕ is valuable in that ϕ is not a function of droplet size. Furthermore, the magnitude of ϕ is a measure of the deviation from Stokes' law for the forces acting on the water droplets. It can be seen that the droplet collection rate increases with an increase in the droplet diameter. The collection efficiency decreases with an increase in the cylinder diameter. Finally, the efficiency increases with an increase in the free stream velocity. At this point, a note of justification for neglecting the boundary layer on the cylinder is in order. The boundary layer displaces the stream lines of the flow by the amount equal to the displacement thickness. Accordingly, the

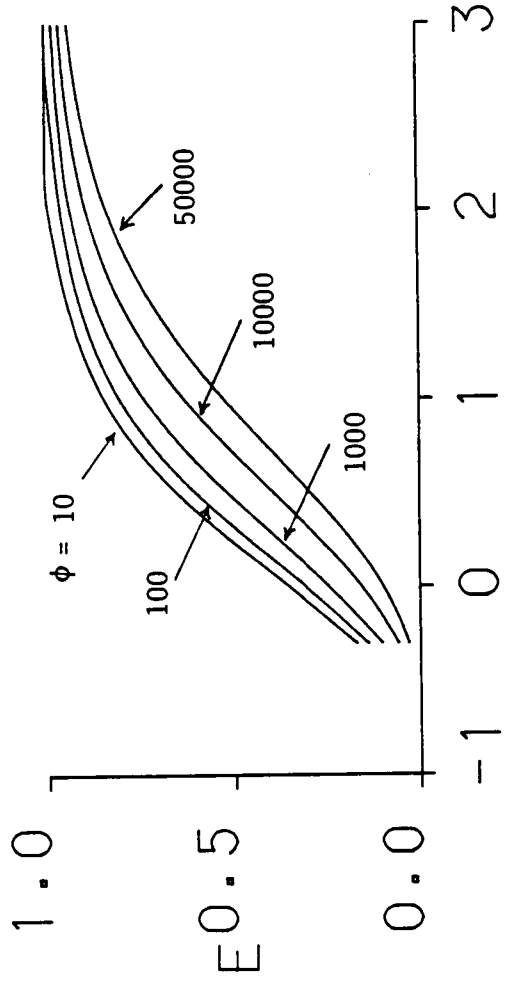


Figure IV-3. Collection Efficiency of Cylinder.

droplet trajectories are also displaced which results in a decrease in the collection rate. Thus, neglecting the boundary layer results in a conservative estimate of the ice collection.

The collection efficiency of the circular cylinder with surface injection depends on the injection rates and the location of the injection. In the present study air was injected through the slots located on the cylinder. These slots were approximated by the line sources in the theoretical model. Thus, to evaluate the performance of the injection system, the effects of the following factors should be investigated:

1 – Source (slot) location
2 – Source (slot) flow rate
3 – Number of sources (slots)

The collection efficiency of a circular cylinder, in which the two sources are located at $\pm$ θ degrees from the front stagnation point (line), have been calculated and plotted for a value of the (ϕ) parameter of 10 in Figure IV-4. For the two sources located at $\pm$ 50 degrees from the front stagnation point, with the source strength of $Q = 5$, (Q is the nondimensional source strength, i.e. $Q = q/RU_{\infty}$), it is apparent that the collection efficiencies (E) have been reduced considerably compared to the case where there is no injection, i.e. where $Q = 0$. It will be shown later that as the source strength is increased the collection efficiencies are further reduced. Figure IV-4 also presents another case where the sources are located at ± 5

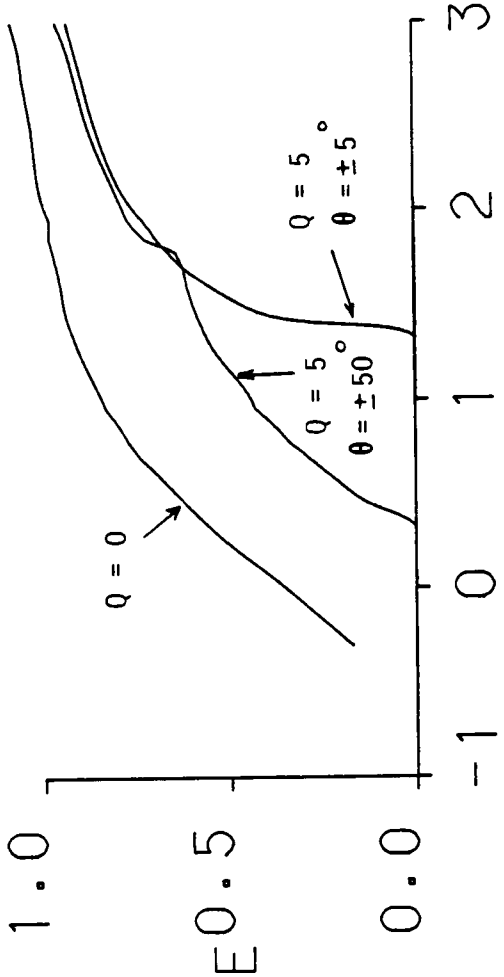


Figure IV-4. Collection Efficiency of Cylinder with Surface Injection, Sources Located at ±5°, ±50°.

degrees with the Q = 5. In this case the reduction in the collection efficiency values are even higher than those reported above. Consider another case where the slots are located at ±25 degrees and ±5 as shown in Figure IV-5. Once again the reduction in the collection efficiency is evident. Examining the region where the two curves cross over in both Figure IV-4 and IV-5 one can anticipate that there should be an optimum location where the sources have their maximum effect on the collection efficiency. Then the next step of the analysis would be to find this particular location. Collection efficiencies have been plotted versus the source location (actually two sources, located at ±θ degrees for purpose of symmetry) and shown in Figure IV-6. A general reduction in the collection efficiency compared to the case of no injection is realized. However, it can be seen that there is an optimum source location at about θ = ±34 degrees where the injection effect is a maximum, i.e. there is a maximum reduction in the collection efficiency, which is indicated by a dip on the curve. Figure IV-6 also indicates that the effect of injection diminishes as the sources move toward θ = ±90 degrees. Figure IV-6 also contains a case with a higher source strength (Q) which shows that the optimum source location has been moved even further toward the front stagnation point with further reduction in the collection efficiencies. The same analysis has been done with a larger value of (K) and the results are presented in Figure IV-7. It is easily seen that in this case the location of the sources do not seem to have too much of an effect on the collection efficiency.

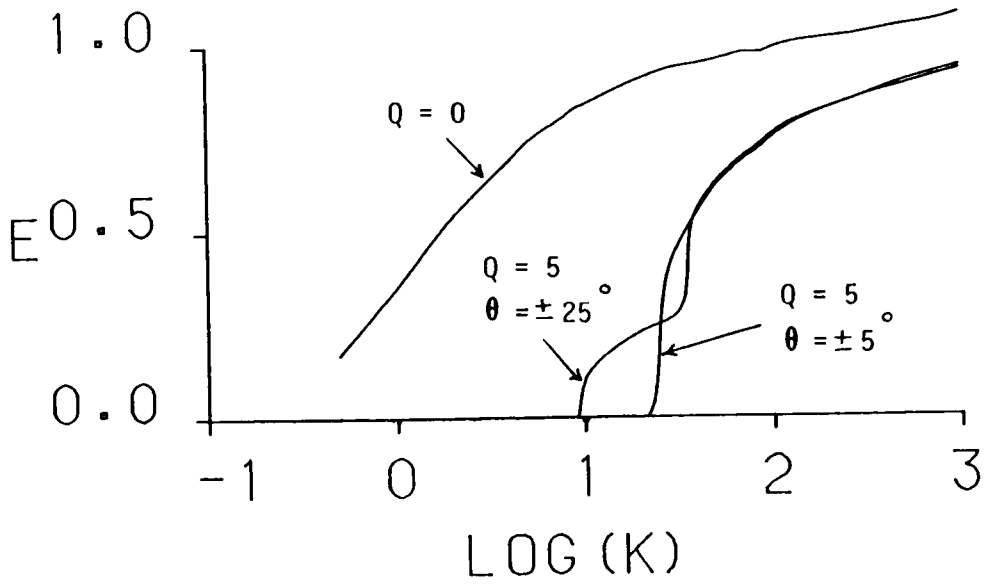


Figure IV-5. Collection Efficiency of Cylinder with Surface Injection, Sources Located at ±5°, ±25°.

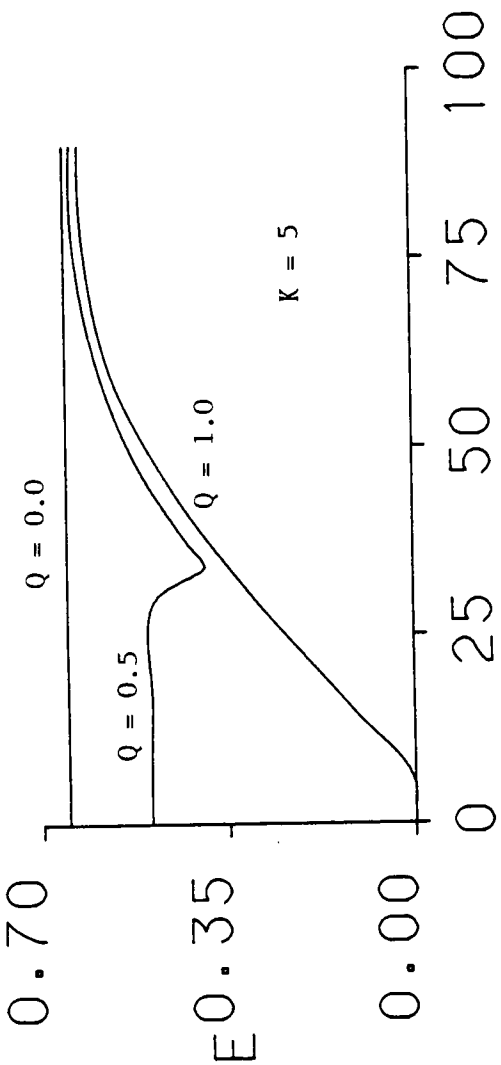


Figure IV-6. Effect of Source Location on Collection Efficiency, For Two Sources Located at $\pm\theta^\circ$, K = 5.

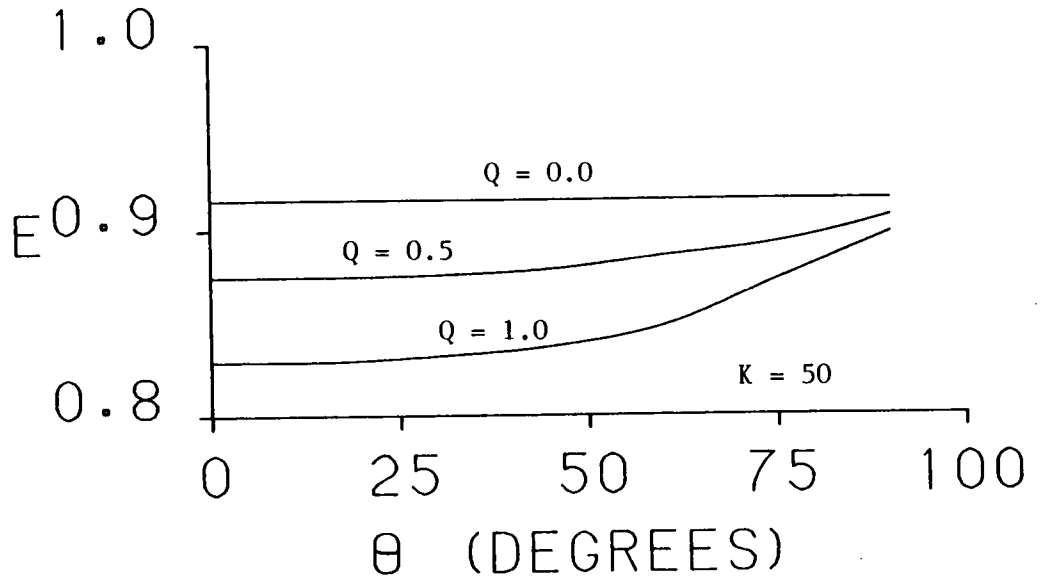


Figure IV-7. Effect of Source Location on Collection Efficiency, For Two Sources Located at ±θ°, K = 50.

This observation leads one to believe that for the two slot models there is only one optimum source location for a particular case with certain droplet diameter, cylinder diameter, and free stream velocity.

Dependence of the collection efficiency on the injection flow rate is shown in Figure IV-8. This figure presents the case in which there are three injection slots (sources) on the cylinder which are located at −50, 0, and +50 degrees (where 0 degree corresponds to the front stagnation line). It can be seen that as the injection flow rates are increased the collection efficiency of the cylinder is decreased. Furthermore, the required injection for the 100 percent reduction in efficiency is greater for a larger inertia parameter (K). This is obvious from physical grounds since a larger value of K implies either a larger free stream velocity or a larger droplet size.

The effect of the number of injection slots on the collection efficiency was studied and results are shown in Figure IV-9. The slots were considered to be equally spaced on the front half of the cylinder (i.e. from +90 to −90 degrees where angles are measured from the front stagnation line). For example, in the case of the three slot model, the slots are located at the front stagnation point and at ±90 degrees. As shown in Figure IV-9 the collection efficiency decreases with the increase in source numbers. However, it should be noted that the same reduction in efficiency can also be achieved by holding the source numbers constant and increasing the injection rate

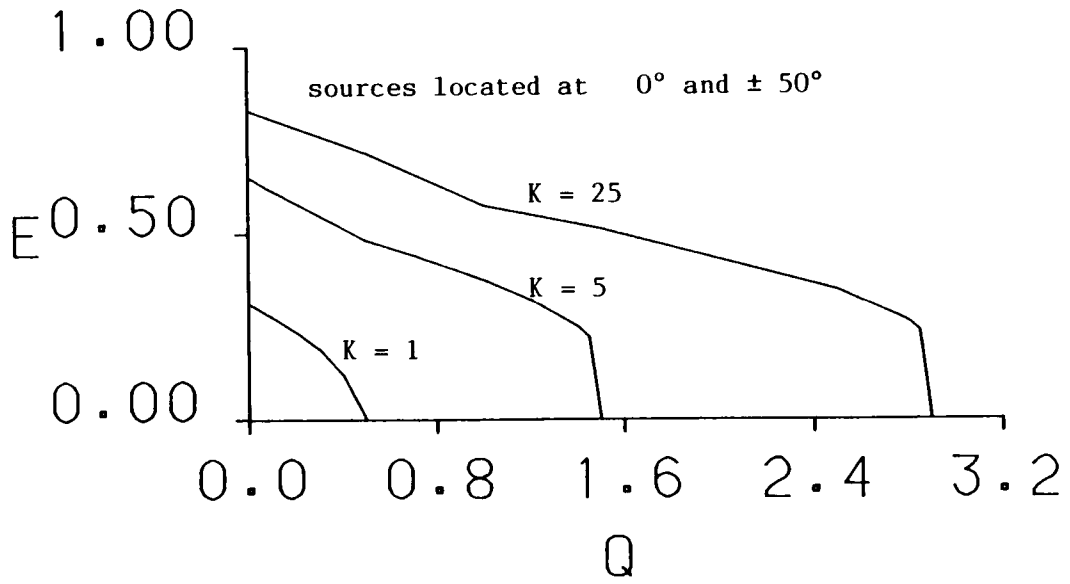


Figure IV-8. Effect of Source Strength on Collection Efficiency, Three Sources Model.

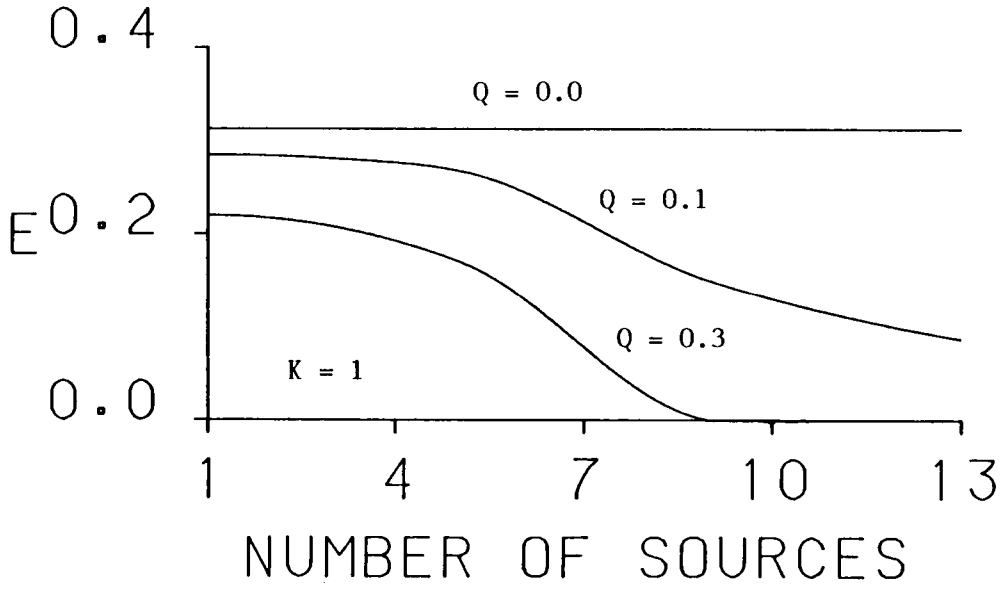


Figure IV-9. Effect of Source Numbers on Collection Efficiency, for Equally Spaced Sources Within ± 90°.

as shown in this figure. It should also be noted that there is an optimum number of sources for which the collection efficiency is E = 0. It is shown in Figure IV-9 that the minimum number of sources required to reduce efficiency to E = 0 for the case of K = 1.0 and injection rate of Q = 0.3 is 9.

The trajectories of the droplets for the case of flow over a circular cylinder with no surface injection are shown in Figure IV-10. This figure also contains the corresponding streamlines at x = −10R where trajectories coincide with the streamlines. The separation of trajectories from streamlines as droplets approaching the cylinder is noted. The effects of surface injection on droplet trajectories are shown in Figure IV-11. A total of five sources, located at 0, ±30, and ±60 degrees from the front stagnation point, with source flow of Q = 0.5 were considered. Finally, Figure IV-12 presents a case of strong blowing for the same case presented above. In this case droplets are being repelled or blown away from the surface. The closest trajectory to the surface is most affected. The effect of various injection rates on a particular trajectory is shown in Figure IV-13. This figure presents three curves for three different values of source strength, i.e. Q = 0, 1.0, and 2.0, for droplets initially released from y = 0.3 and x = 10R. The source numbers and their locations on the cylinder are the same as those discussed above. Figures IV-14, IV-15, and IV-16 show the effect of surface blowing on the flow streamlines. Elevation of streamlines ahead and behind the cylinder is indicated. Once again a total of

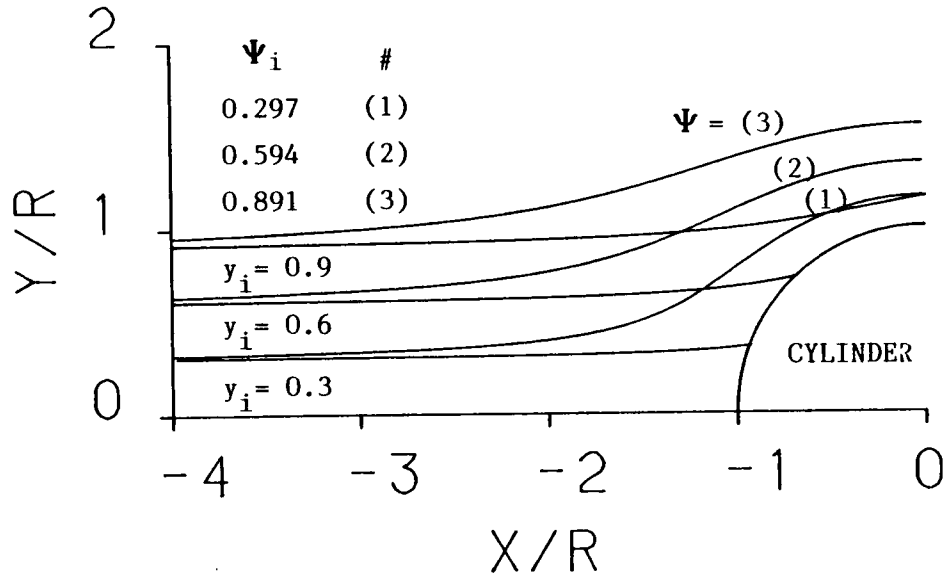


Figure IV-10. Droplet Trajectories and Streamlines, K = 10, Φ = 1000, and Q = 0.

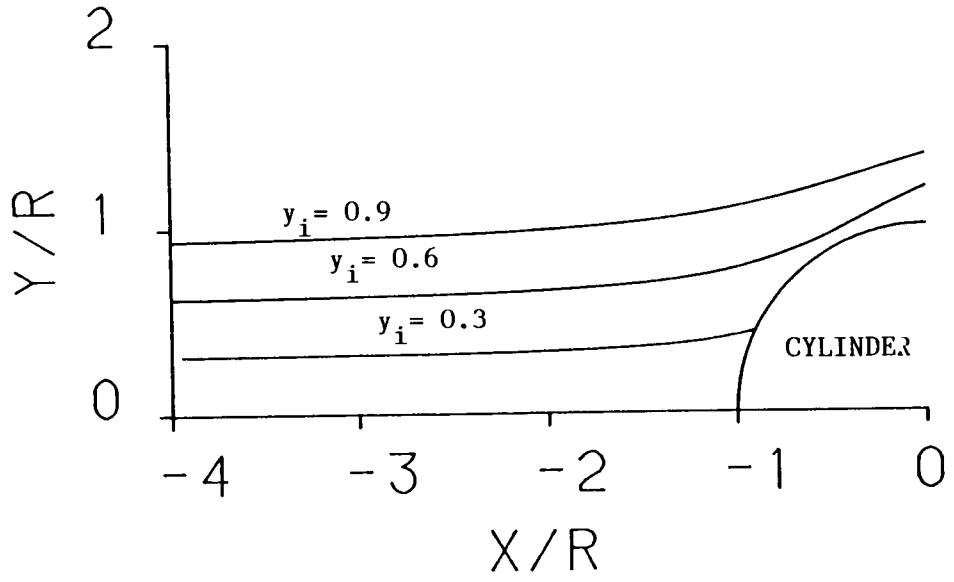


Figure IV-11. Droplet Trajectories, K = 10, Φ = 1000, Q = 0.5, Source Angles 0°, ±30°, ±60°.

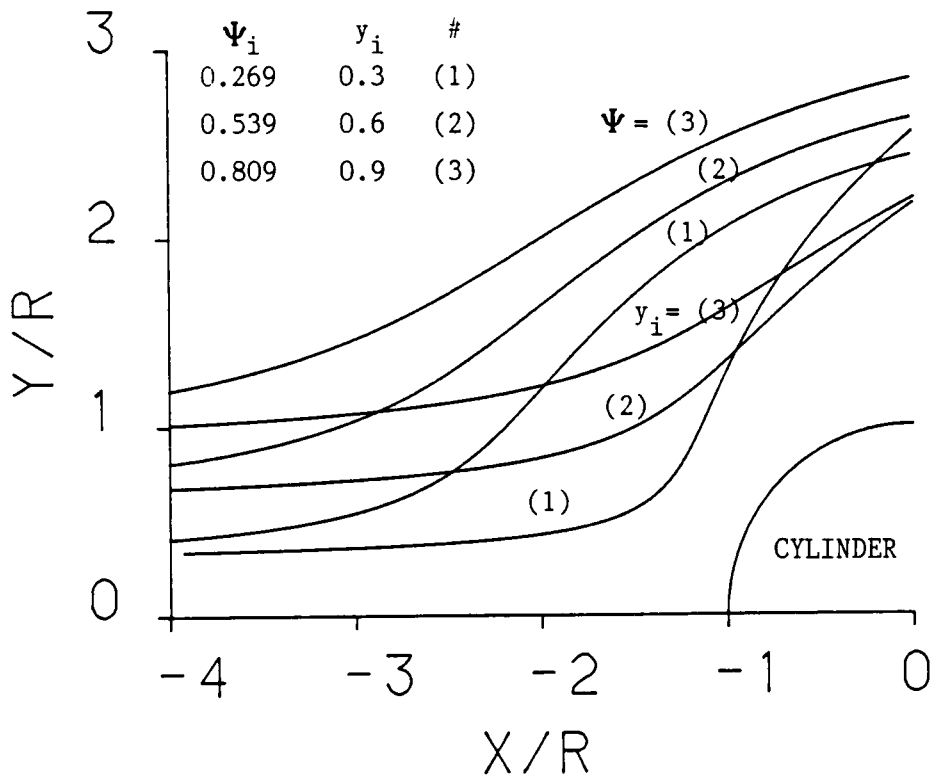


Figure IV-12. Droplet Trajectories and Streamlines, K = 10, Φ = 1000, and Q = 2, Source Angles 0°, ±30°, ±60°.

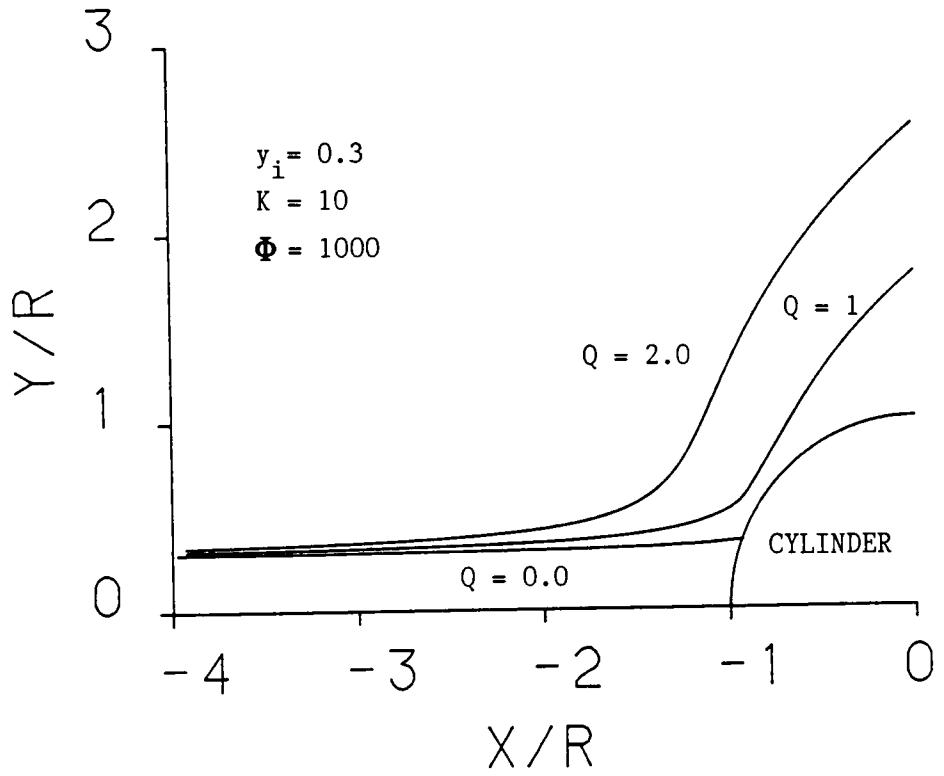


Figure IV-13. Droplet Trajectories For Various Source Strength.

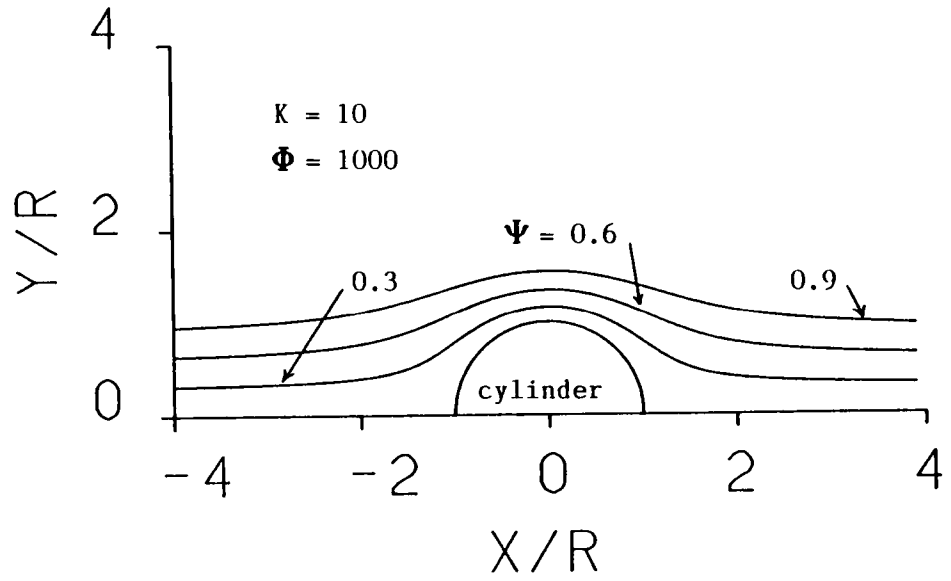


Figure IV-14. Streamlines of Flow Over Circular Cylinder.

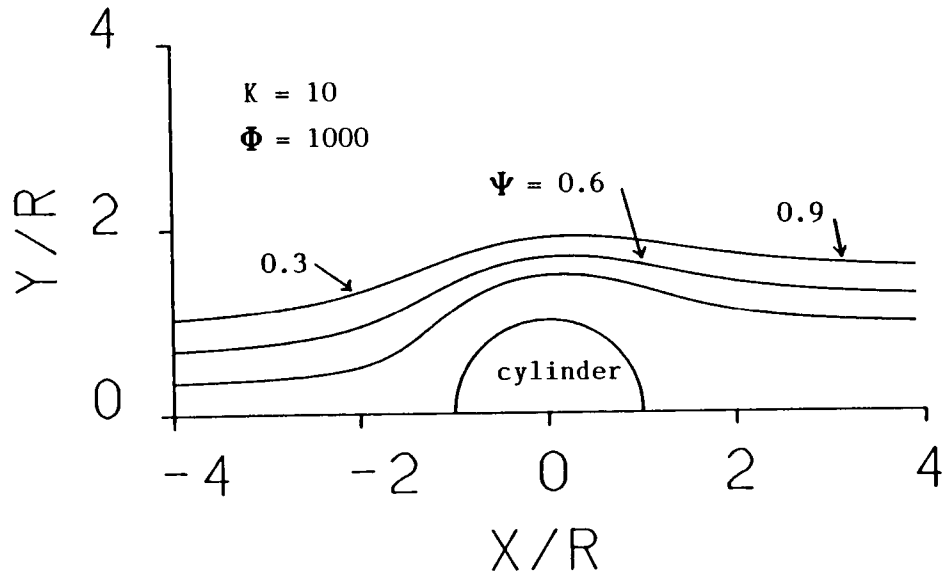


Figure IV-15. Streamlines of Flow Over Circular Cylinder With Surface Injection Q = 0.5, angles 0°, ±30°, ±60°.

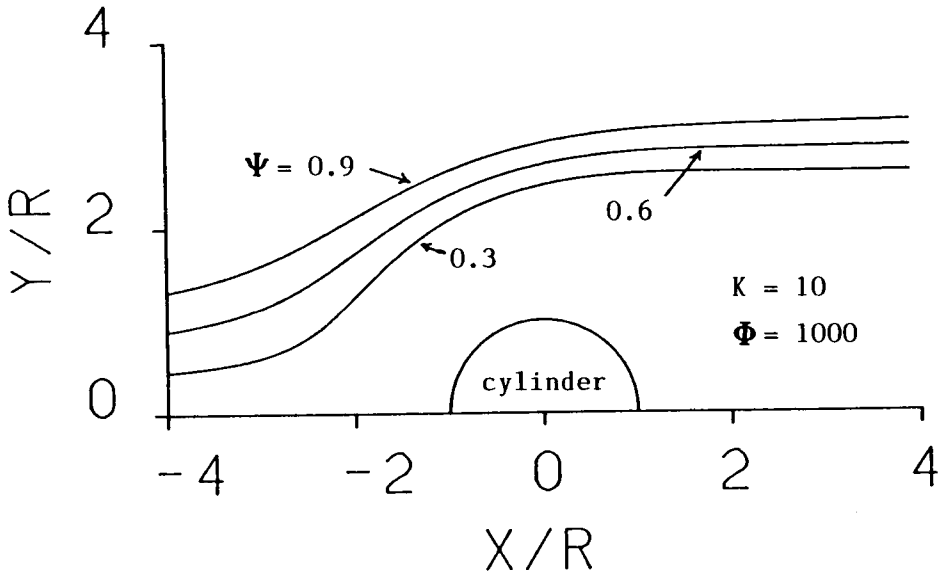


Figure IV-16. Streamlines of Flow Over Circular Cylinder With Surface Injection Q = 2, Source Angles 0°, ±30°, ±60°.

five sources located at 0, ±30, and ±60 degrees from the stagnation point were considered.

The amount of ice collection on the model can now be calculated from

$$m_{ICE} = (LWC)(E)(U_\infty)(D)(t) \qquad (IV\text{-}7)$$

where LWC is the liquid water content of the flow, D is the diameter of the model, and t is the icing duration. Calculated ice weights corresponding to the experimental conditions will be presented in Chapter VIII.

Computer programs for calculating droplet trajectories and correpsonding streamlines are given in Appendices N and O respectively.

CHAPTER V

BOUNDARY LAYER OVER A CIRCULAR CYLINDER WITH SURFACE INJECTION AND ITS EFFECT ON DROPLET TRAJECTORY

In the previous section it was assumed that the boundary layer on the cylinder was thin and that its effect on the droplet trajectory could be neglected. In this section, the boundary layer solution with and without surface injection is presented to further substantiate the above assumption. The boundary layer thickness and the displacement thickness were calculated for many surface injection velocities. The boundary layer blow off limits were established for a number of injection rates.

The solution of the boundary layer over the circular cylinder was modeled based on the "local nonsimilarity" method of Sparrow [44,45]. Nonsimilarity in the present problem is caused by the spatial variation of the free stream velocity and surface mass transfer. Consideration is given here to the laminar ($Re_0 < 1.8 \times 10^4$) two-dimensional steady constant property flow. The boundary layer studied in this section is then described by

$$uu_x + vu_y = UU_x + \nu u_{yy} \tag{V-1}$$

Boundary conditions are

$$\begin{aligned} y = 0 \qquad & u = 0 \\ & v = v_{wall} \\ y \to \infty \qquad & u \to U(x) \end{aligned} \tag{V-2}$$

where x and y denote the streamwise and transverse coordinates, respectively measured along and normal to the surface of the cylinder. U(x) is the free stream velocity, which is a known function of x.

The above boundary layer equation was first transformed from the x, y coordinate system to the ξ, η system, where η is related to x and would be a similarity variable if the boundary layer were similar. Employing the Gortler and Meksyn transformation one defines

$$\xi = \int_0^x \frac{U(x)}{U_o} \frac{dx}{L} \tag{V-3}$$

$$\eta = \frac{y\, U(x)}{(2\nu L U_o \xi)^{\frac{1}{2}}} \tag{V-4}$$

in which L is a reference length and U_o is a reference velocity that is taken as the velocity of the oncoming flow. The stream function is defined in terms of the new coordinate system as

$$\Psi = (2\nu\, L\, U_o\, \xi)^{\frac{1}{2}} f(\xi,\eta) - \int_0^{x/R} \left(\frac{v_w}{U_\infty} \right) d\,(x/R) \tag{V-5}$$

where $f(\xi,\eta)$ is the nondimensional stream function in the new coordinate system and the last term accounts for the mass transfer at the surface. For a circular cylinder subjected to irrotational crossflow the spatial variation of the free stream velocity is represented by

$$U(x) = 2U_{\infty} \sin\left(\frac{x}{R}\right) \tag{V-6}$$

in which U_{∞} is the free stream velocity far away from the cylinder, R is the cylinder radius, and x is the circumferential distance measured from the forward stagnation point. In the above equation the U_{∞} and R are taken to be the reference quantities U_0 and L respectively. The ξ and η functions can now be expressed in terms of x and y as

$$\xi(x) = 2\left[1 - \cos\left(\frac{x}{R}\right)\right] \tag{V-7}$$

$$\eta(x,y) = \frac{\left(\frac{y}{R}\right) Re_0^{\frac{1}{2}} \sin\left(\frac{x}{R}\right)}{\left[1 - \cos\left(\frac{x}{R}\right)\right]^{\frac{1}{2}}} \tag{V-8}$$

where:

$$Re_0 = \frac{U_{\infty} R}{\nu} \tag{V-9}$$

The boundary layer equation was transformed using the following relationships and definitions

$$u = \frac{d\Psi}{dy} \quad , \quad v = -\frac{d\Psi}{dx}$$

$$u = U(x) f' \quad , \quad f' = \frac{df}{d\eta} \tag{V-10}$$

Finally the boundary layer equation in the new coordinate system takes the form of

$$(f''' + ff'') + \beta(1 - f'^2) + \gamma f'' = 2\xi(f'_\xi f' - f_\xi f'') \tag{V-11}$$

where

$$\beta = \frac{2\cos\left(\frac{x}{R}\right)}{1 + \cos\left(\frac{x}{R}\right)}$$

$$\gamma = \frac{-\mathrm{Re}_o^{\frac{1}{2}}\left[1 - \cos\left(\frac{x}{R}\right)\right]^{\frac{1}{2}}}{\sin\left(\frac{x}{R}\right)}\left(\frac{v_{wall}}{U_\infty}\right)$$

$$v_{wall} > 0 \quad \text{INJECTION}$$

$$v_{wall} < 0 \quad \text{SUCTION} \tag{V-12}$$

Boundary conditions are:

$$f'(\xi,0) = 0$$

$$f(\xi,0) = 0$$

$$f(\xi,0) + 2\xi f_{\xi}(\xi,0) = 0$$

$$f'(\xi,\infty) = 1.0 \qquad \text{(V-13)}$$

The local similarity equation can now be obtained, if desired, by deleting terms of the form $\xi(\partial/\partial\xi)$ from the Equation (V-11) and the boundary conditions (Equation (V-13)). These terms may be deleted under the assumption that either ξ or $(\partial/\partial\xi)$ is small, which is a fair assumption in the region close to the stagnation point. The solution procedure for obtaining the local similarity model (or the 1-equation model of the local nonsimilarity) is given in Appendix F. It will be shown later that the accuracy of the solution obtained from the local similarity model diminishes in the streamwise direction (increasing x along the cylinder surface) which indicates that the above assumption becomes questionable, if not invalid depending on the accuracy sought, for large x. To improve the results, a 2-equation model of local nonsimilarity was obtained by differentiating the Equation (V-11) with respect to ξ and defining

$$g = f_{\xi} \quad , \quad g' = f'_{\xi}$$

$$g'' = f''_{\xi} \quad , \quad g''' = f'''_{\xi} \qquad \text{(V-14)}$$

Once again neglecting terms of the form $\xi(....)_\xi$ based on similar argument presented above or by assuming

$$\xi(\cdot\ \cdot\ \cdot\ \cdot\ \cdot\ \cdot\ \cdot)_\xi \sim 0 \tag{V-15}$$

The 2-equation model then becomes

$$g''' + fg'' + f''g - 2\beta f'g' + \gamma g'' + (1 - f'^2)\beta_\xi$$

$$+ \gamma_\xi f'' = 2(g'f' - g f'') + 2\xi(g'^2 + g'g'') \tag{V-16}$$

Boundary conditions are:

$$\begin{aligned} f'(\xi,0) &= 0.0 \\ f(\xi,0) &= 0.0 \\ f'(\xi,\infty) &= 1.0 \\ g'(\xi,0) &= 0.0 \\ g\ (\xi,0) &= 0.0 \\ g'(\xi,\infty) &= 0.0 \end{aligned} \tag{V-17}$$

The details of the solution of the 2-equation model are given in Appendix G.

Finally, the 3-equation model of the local nonsimilarity solution was obtained by taking the second derivative of Equation (V-11) with respect to ξ and defining

$$h = g_\xi \quad , \quad h' = g'_\xi$$

$$h'' = g''_\xi \quad , \quad h''' = g'''_\xi \tag{V-18}$$

neglecting terms of $(....)_\xi$ from the resulting equations based on a similar argument presented above, the 3-equation model becomes

$$h''' + (6g + 2\gamma_\xi)g'' + (-2\beta g' - 4g' - 4\beta_\xi f')g' + (f + \gamma)h''$$

$$+ 5f''h - (4 + 2\beta)f'h' + (1 - f'^2)\beta_{\xi\xi} + \gamma_{\xi\xi}f'' = 0 \tag{V-19}$$

Boundary conditions are:

$$f'(\xi,0) = 0.0$$

$$f(\xi,0) = 0.0$$

$$f'(\xi,\infty) = 1.0$$

$$g'(\xi,0) = 0.0$$

$$g(\xi,0) = 0.0$$

$$g'(\xi,\infty) = 0.0$$

$$h'(\xi,0) = 0.0$$

$$h(\xi,0) = 0.0$$

$$h'(\xi,\infty) = 0.0 \qquad \text{(V-20)}$$

The 3-equation model, and the first and the second derivatives of the boundary layer equation (Equation (V-11)) were solved simultaneously along with appropriate boundary conditions. See Appendix H for the complete listing of the equations and solution procedure. The method of Nachtsheim and Swigert [46,47] in conjunction with the 4th order Runge-Kutta integration scheme with variable step size [48] was adopted for the solution procedure. This method requires an initial guess for each of the unknown functions, i.e., f, g, and h, and also requires asymptotic conditions for these functions as they approach the edge of the boundary layer as

Initial guesses:

$$f''(\xi,0) = x$$

$$g''(\xi,0) = y$$

$$h''(\xi,0) = z \qquad \text{(V-21)}$$

Asymptotic conditions:

$$f''(\xi,\infty) = 0.0$$

$$g''(\xi,\infty) = 0.0$$

$$h''(\xi,\infty) = 0.0 \qquad \text{(V-22)}$$

The above equations were converted into 36 ordinary differential equations of the first order and, integrated along η from $\eta = 0$ to η_{max} (η_{max} was initially guessed), then the $f(\xi,\eta_{max})$, $f''(\xi,\eta_{max})$, $g(\xi,\eta_{max})$, $g''(\xi,\eta_{max})$, $h(\xi,\eta_{max})$, and $h''(\xi,\eta_{max})$ were calculated. With these values known the corrections for the initial guesses were then made, i.e. Δx, Δy, and Δz. The integration was repeated until the percent correction was less than the preselected small value ε ($=10^{-4}$). Finally, to obtain η the following conditions were imposed on the solution:

$$E_f(\xi,\eta_{max}) = (1-f')^2 + f''^2 + f'''^2$$

$$E_g(\xi,\eta_{max}) = g'^2 + g''^2 + g'''^2$$

$$E_h(\xi,\eta_{max}) = h'^2 + h''^2 + h'''^2 \qquad \text{(V-23)}$$

if E's $> \varepsilon$ then $\eta_{max} = \eta_{max} + \Delta\eta$ and once again the integration was repeated until E's $< \varepsilon$ and Δx, Δy, $\Delta z < \varepsilon$. This completes the solution of the boundary layer equation at a particular point. The

solution of the entire boundary layer was obtained from x = 0 (front stagnation) up to around 90 degrees (see Appendix H for details).

To gain confidence in the equations and the solution procedure, the boundary layer solution with no surface mass transfer was obtained based on the 1-equation model (local similarity solution), 2-equation model, and the 3-equation model and were compared to the finite difference solution [49]. Figure V-1 presents the nondimensional wall shear in the streamwise direction obtained from the above models. The result of the finite difference solution is also shown for comparison. Inspection of the figure reveals that increasingly more accurate results are obtained as one passes from the local similarity model to the 2-equation model and thence to the 3-equation model. Furthermore, it appears that the successive curves from these models bracket the finite difference solution. For further comparison, the nondimensional velocity profiles are shown in Figures V-2 and V-3. Once again in these figures the finite difference solution was taken as a standard against which the nonsimilarity solutions were compared.

The results from the 3-equation model are seen to deviate from the exact solution beyond approximately 80 degrees from the front stagnation point. This is due to the effect of downstream flow separation. To improve the result even more one can develop the 4-equation model for the problem. However, in the present analysis since the region of interest was the front half of the cylinder it

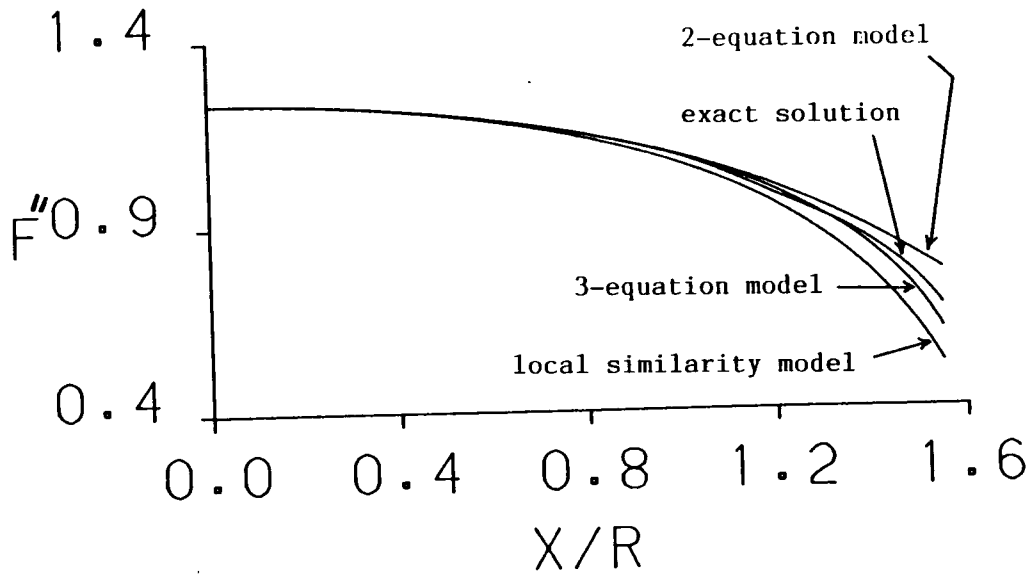


Figure V-1. Wall Shear of Flow Over Circular Cylinder.

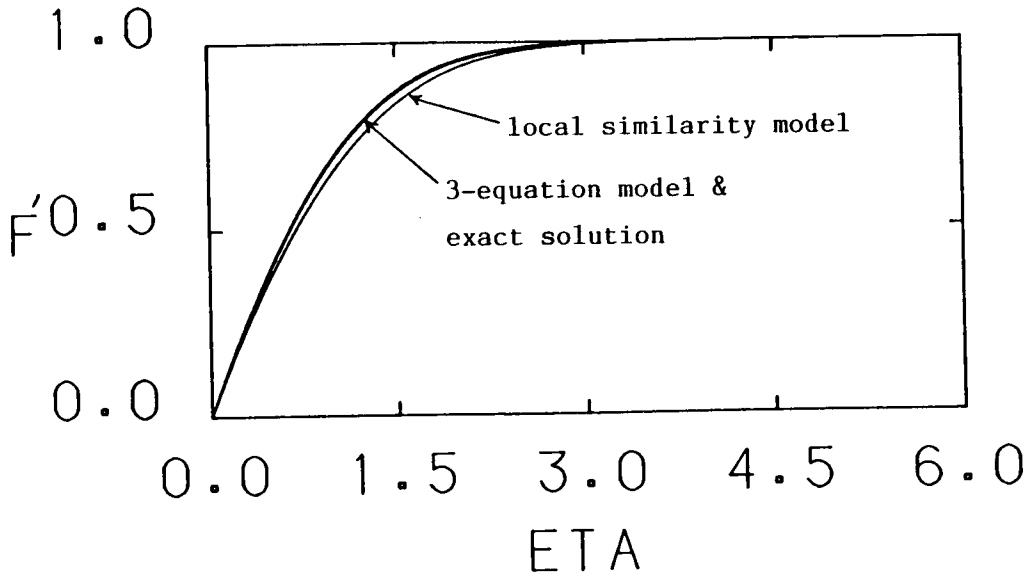


Figure V-2. Boundary Layer Velocity Profile at x/R = 1.3.

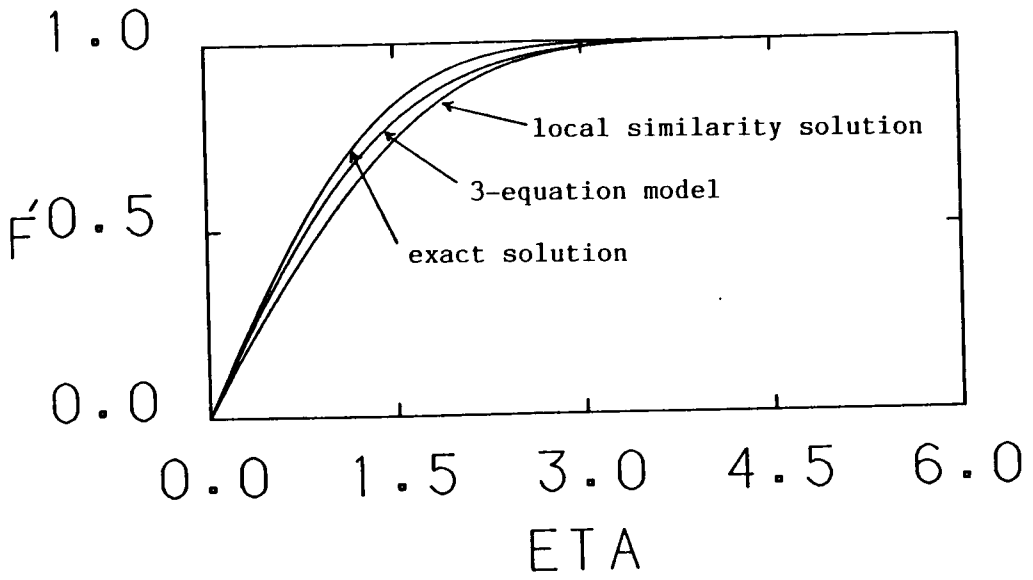


Figure V-3. Boundary Layer Velocity Profile at x/R = 1.5.

was reasoned that the 3-equation model provides an adequate solution for the problem.

Boundary layer and displacement thickness were calculated from

$$\delta(x) = A\,\eta_{edge}$$

$$\delta^*(x) = A\,(\eta_{edge} - f'_{edge}) \qquad \text{(V-24)}$$

where

$$A = \frac{R\left[1 - \cos\left(\frac{x}{R}\right)\right]^{\frac{1}{2}}}{Re_o^{\frac{1}{2}} \sin\left(\frac{x}{R}\right)}$$

$$f'_{edge} = 0.995$$

$$\eta_{edge} = \text{Interpolated} \qquad \text{(V-25)}$$

Figure V-4 presents the boundary layer thickness (δ) and the displacement thickness (δ^*) for flow over a circular cylinder with no surface injection. These values were obtained for a flow Reynolds number of 2463.

The complete boundary layer solution, i.e. velocities, for the case of no surface mass transfer was calculated around the cylinder from the front stagnation point up to 90 degrees. In the streamwise direction, ξ, a total of 15 equally spaced points were considered while in the direction perpendicular to the surface, η, the boundary

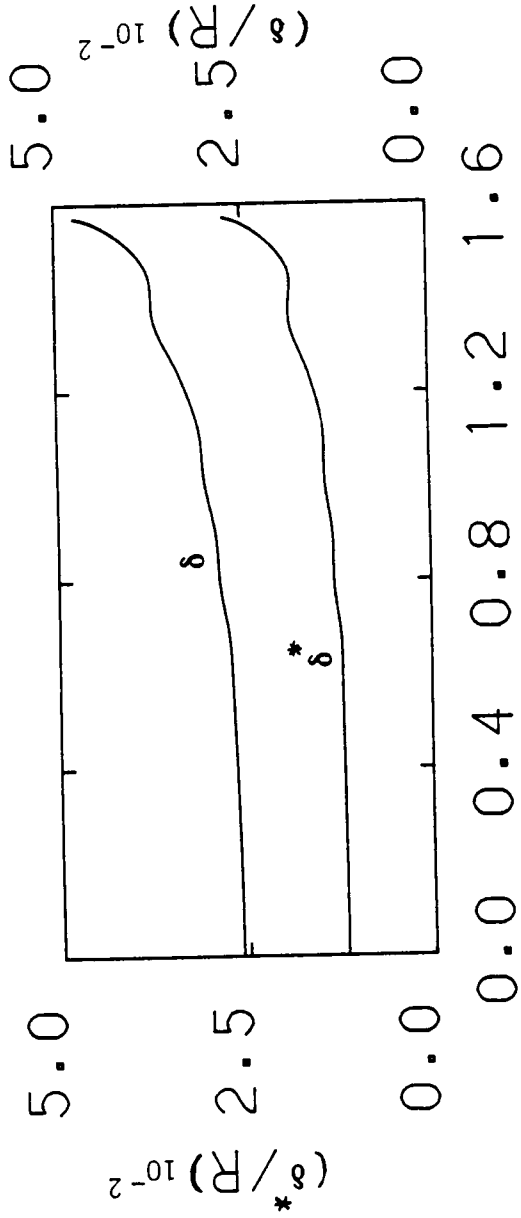


Figure V-4. Displacement and Boundary Layer Thickness of Flow Over Cylinder, Re_o = 2463, Free Stream Velocity = 10 ft/sec.

layer equation was integrated using a variable step size to calculate η_{max} which was then divided into a total of 33 equally spaced points to obtain the boundary layer solution. Velocities in the boundary layer with uniform surface mass transfer were also computed. Figure V-5 and V-6 present nondimensional velocity in the streamwise direction for a number of surface mass transfer rates. These velocity profiles correspond to the location x/R = 1.0 which is approximately 57.3 degrees from the front stagnation point. Wall shear was also calculated for a variety of surface injection velocities and some of the results are presented in Figure V-7. Wall shear decreases in the streamwise direction up to the point of separation, which is a function of surface injection velocity. It was found that separation of the boundary layer occurs much earlier than for the case with no surface injection. In facts as indicated in Figure V-7 even with rather small surface velocity the shear reduction is substantial. Even though the actual location of separation could not be calculated the solution blows up near the separation point), nevertheless curves given in the above figure can be extrapolated to estimate the separation point for the cases shown. Thus boundary layer blow-off is certain for surface velocities considered in both Chapter IV and the experiments performed. To investigate the effect of boundary layer on droplet trajectories, the boundary layer was patched to the potential flow outside the boundary layer and droplet trajectories were calculated by the same procedure discussed in Chapter IV. Less than 2 percent change was realized in

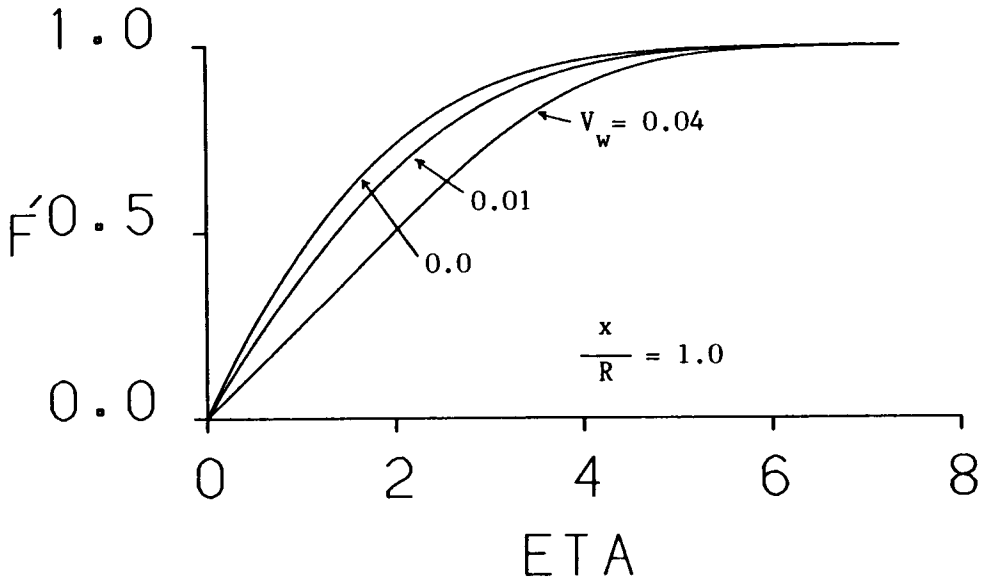


Figure V-5. Effect of Surface Mass Transfer on Boundary Layer Velocity Profile for Flow Over Circular Cylinder, Re = 1000.

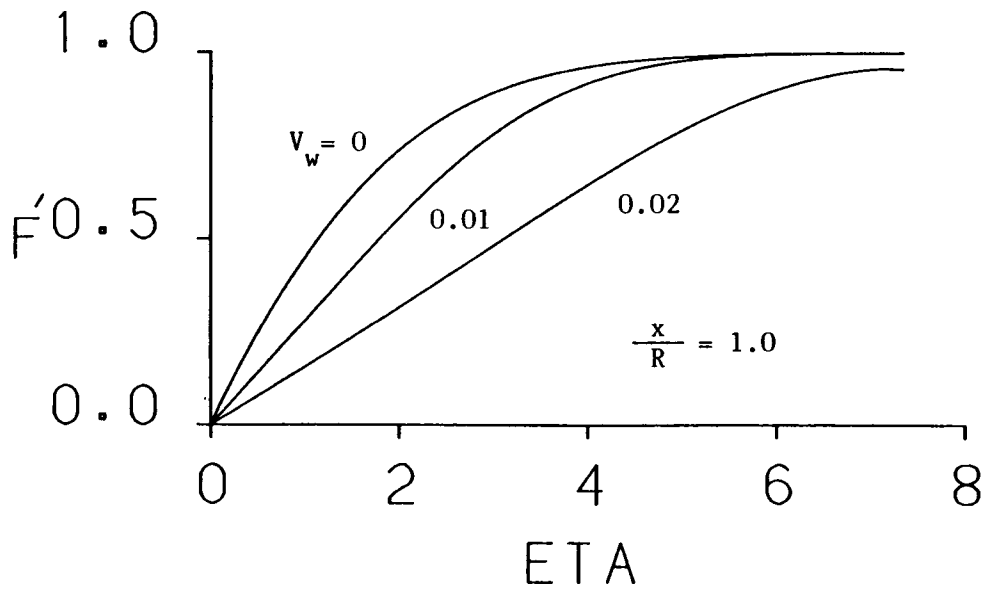


Figure V-6. Effect of Surface Mass Transfer on Boundary Layer Velocity Profile for Flow Over Circular Cylinder, Re = 10,000.

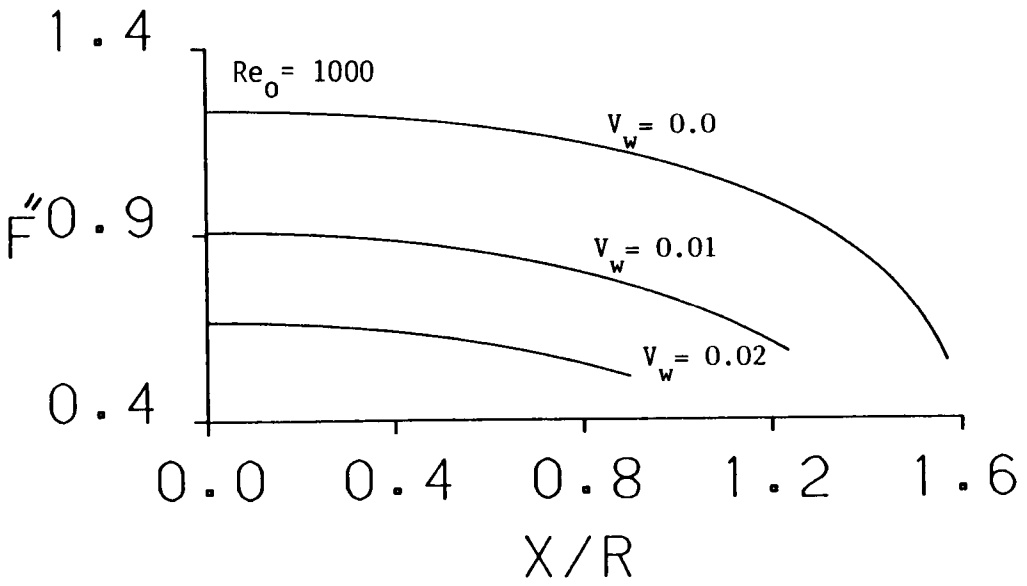


Figure V-7. Effect of Surface Mass Transfer on Wall Shear For Flow Over Circular Cylinder, Boundary Layer Flow.

collection efficiency of the cylinder. This small change was expected since the boundary layer thickness for cases considered was very small as was shown in Figure V-4.

Listings of the computer programs for the 1-equation, 2-equation, and 3-equation models are give in Appendices P, Q, and R respectively. The computer program for calculating the boundary layer and displacement thickness and velocities is given in Appendix S.

CHAPTER VI

MAPPED POTENTIAL FLOW SOLUTION OF FLOW OVER A CIRCULAR CYLINDER WITH SURFACE INJECTION

General

A potential flow solution of flow over a cylinder was obtained numerically by integrating the Laplace equation in terms of stream function. The flow velocities were then calculated from the known values of the stream function at nodal points. The following coordinate systems in connection with the solution of the Laplace equation were examined.

1 – Cartesian coordinates

2 – Polar coordinates

3 – Mapped coordinates

Use of the cartesian coordinate system greatly simplifies application of the boundary conditions far from the cylinder but application of surface boundary conditions and placement of the grid points at the desired locations is difficult. On the other hand the polar coordinate system simplifies handling of the boundary conditions on the cylinder but implementation of the boundary conditions far from the cylinder becomes difficult. However, the mapped coordinate avoids the above problems by mapping the physical plane onto a rectangular cartesian plane where the cylinder is represented by a

straight line. In the mapped plane all the grid lines are equally spaced which makes the finite differencing equations simpler than they otherwise would have been. The Laplace equation with stream function as the dependent variable was then solved in the mapped plane. In the following sections the grid mapping and potential flow solution is briefly discussed (for more information and details, see Appendix I and [50]).

Grid Mapping Procedure

The objective of grid mapping is to produce a body fitted coordinate system. This procedure eliminates the shape of the boundaries as a complicating factor and allows the flow about arbitrary boundaries to be treated essentially in the same manner as that about simple boundaries. A general curvilinear coordinate system having a coordinate line coincident with each boundary of the region of interest was then generated as the solution of two elliptic partial differential equations, one coordinate being specified to be constant on each boundary segment. These partial differential equations are transformed by interchanging the dependent variable (the curvilinear coordinates) and the independent variables (the physical cartesian coordinates) to produce two partial differential equations for the cartesian coordinates as functions of the curvilinear coordinates. The elliptic equations for the curvilinear coordinates are

$$\xi_{xx} + \xi_{yy} = P(\xi,\eta)$$

$$\eta_{xx} + \eta_{yy} = Q(\xi,\eta) \qquad \text{(VI-1)}$$

where P and Q are the control functions used to control the coordinate lines spacing (see Appendix I). The Dirichlet boundary conditions (see Figure VI-1) are

$$\begin{pmatrix} \xi \\ \eta \end{pmatrix} = \begin{pmatrix} \xi_{1\to6}^{(x,y)} \\ \eta_{1\to6} \end{pmatrix}, \ (x,y) \in \Gamma_{1\to6} \qquad \text{(VI-2)}$$

Since it is desired to perform all numerical computations in the uniform rectangular transformed plane, the above equations are transformed ($P(\xi,\eta) = 0$) as

$$\alpha X_{\xi\xi} - 2\beta X_{\xi\eta} + \gamma X_{\eta\eta} = QJ^2 X_{\eta}$$

$$\alpha Y_{\xi\xi} - 2\beta Y_{\xi\eta} + \gamma Y_{\eta\eta} = QJ^2 Y_{\eta} \qquad \text{(VI-3)}$$

where

$$\alpha = X_{\eta}^2 + Y_{\eta}^2$$

$$\beta = X_{\xi} X_{\eta} + Y_{\xi} Y_{\eta}$$

$$\gamma = X_{\xi}^2 + Y_{\xi}^2$$

$$J = X_{\xi} Y_{\eta} - X_{\eta} Y_{\xi} \qquad \text{(VI-4)}$$

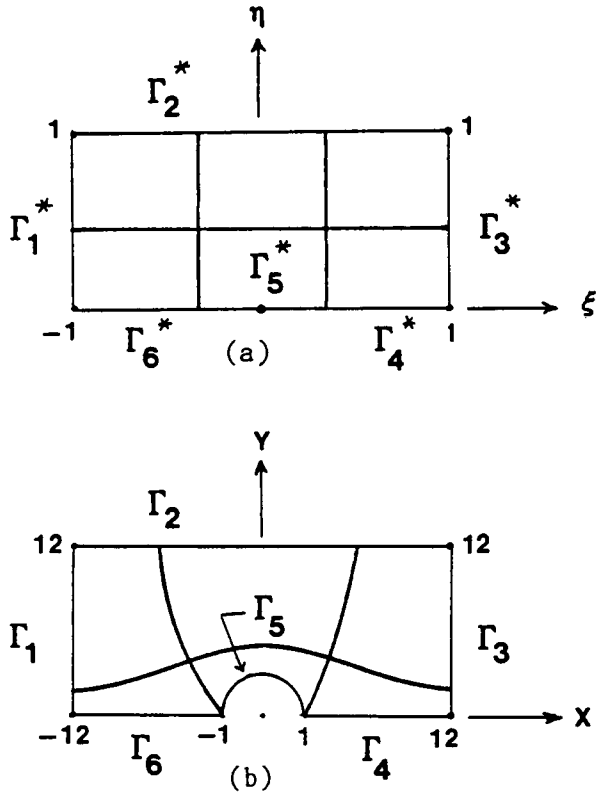


Figure VI-1. Grid Mapping Coordinates,
(a) Transformed plane
(b) Physical plane

with the transformed boundary conditions

$$\begin{pmatrix} x \\ y \end{pmatrix} = \begin{pmatrix} G'_{1\to 6}(\xi, \eta_{1\to 6}) \\ G_{1\to 6}(\xi, \eta_{1\to 6}) \end{pmatrix}, (\xi, \eta_{1\to 6}) \in \Gamma^*_{1\to 6} \qquad \text{(VI-5)}$$

where the "G and G'" functions are simply the desired location from which the grid lines are to be drawn in physical plane. Therefore one can place as many points as desired at the locations where steep gradients in the flow are expected.

Although Equation (VI-3) is considerably more complex than that given by Equation (VI-1), the boundary conditions are specified on straight boundaries and the coordinate spacing in the transformed plane is uniform. A coordinate system was fitted to the cylinder by numerically integrating Equation (VI-3) as follows. First a time derivative term was added to each one of the equations as used by White [51]. The resulting equations were then integrated with time until a steady state solution was reached. This type of integration allows a smooth transition of the initially assumed solution to the final solution of the mapped coordinate.

Solution of the equations was based on the factored implicit finite differencing method by Beam and Warming [52] and is described in Appendix I. Once the solution of the mapped coordinate, i.e. $X(\xi,\eta)$, and $Y(\xi,\eta)$, was obtained then the flow equation was solved in the transformed plane using these data.

For the flow over a circular cylinder with surface mass transfer, the mapped coordinate was obtained by first using the solution of a potential flow over circular cylinder, i.e. stream and potential functions, as the initial guess for the transformation. This initial guess was obtained by using the exact theoretical expressions for the stream and potential functions given (in nondimensional form) by

$$\Psi(x,y) = y\left(1 - \frac{1}{x^2 + y^2}\right)$$

$$\phi(x,y) = x\left(1 + \frac{1}{x^2 + y^2}\right) \qquad \text{(VI-6)}$$

The solution, i.e. x and y at the intersection of the streamlines and potential lines, was obtained by Newton's method. (see Appendix T for listing of computer program) Figure VI-2 presents such a solution. Figure VI-3 presents the coordinate after transformation. It can be seen that the closely spaced grid points on the top boundary produce undesirable effects on the transformed lines. Thus, the top boundary of the initial coordinate was modified as shown in Figure VI-4 and then the transformation was performed. The result of this transformation is shown in Figure VI-5. Focusing our attention on the lines closer to the bottom plane it is desired to have these lines as close to the plane of symmetry as possible. Thus to achieve this, the control terms in the transformation equation had to be activated. Suction was provided at the bottom plane to pull the coordinate lines closer to the plane of symmetry. The final result

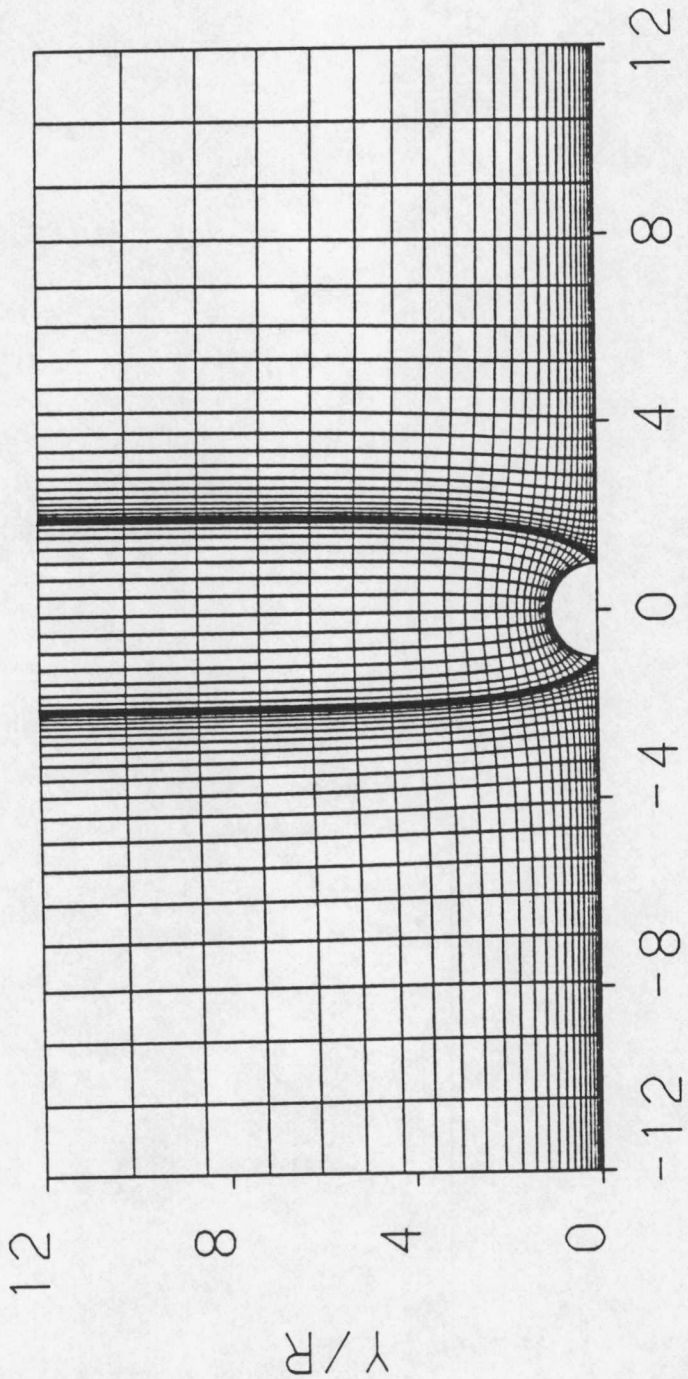


Figure VI-2. Initial Coordinate of Grid Mapping.

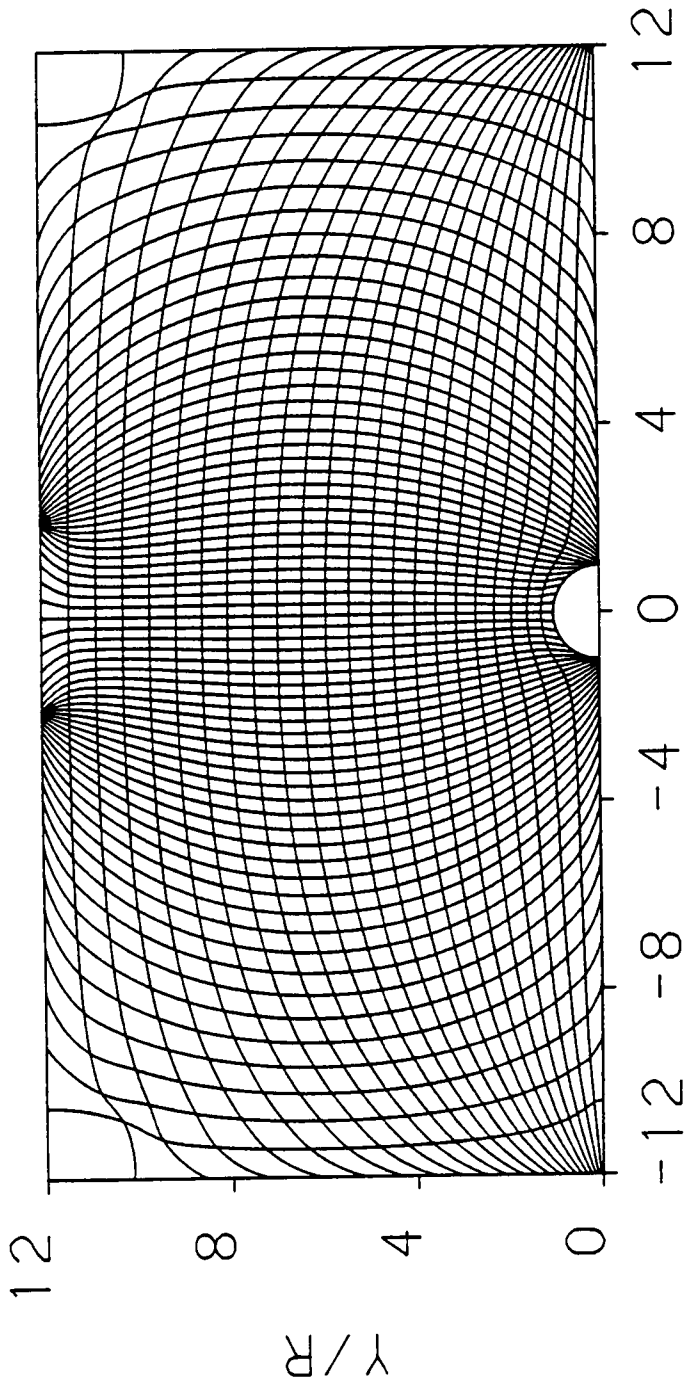


Figure VI-3. Initial Coordinate After Mapping.

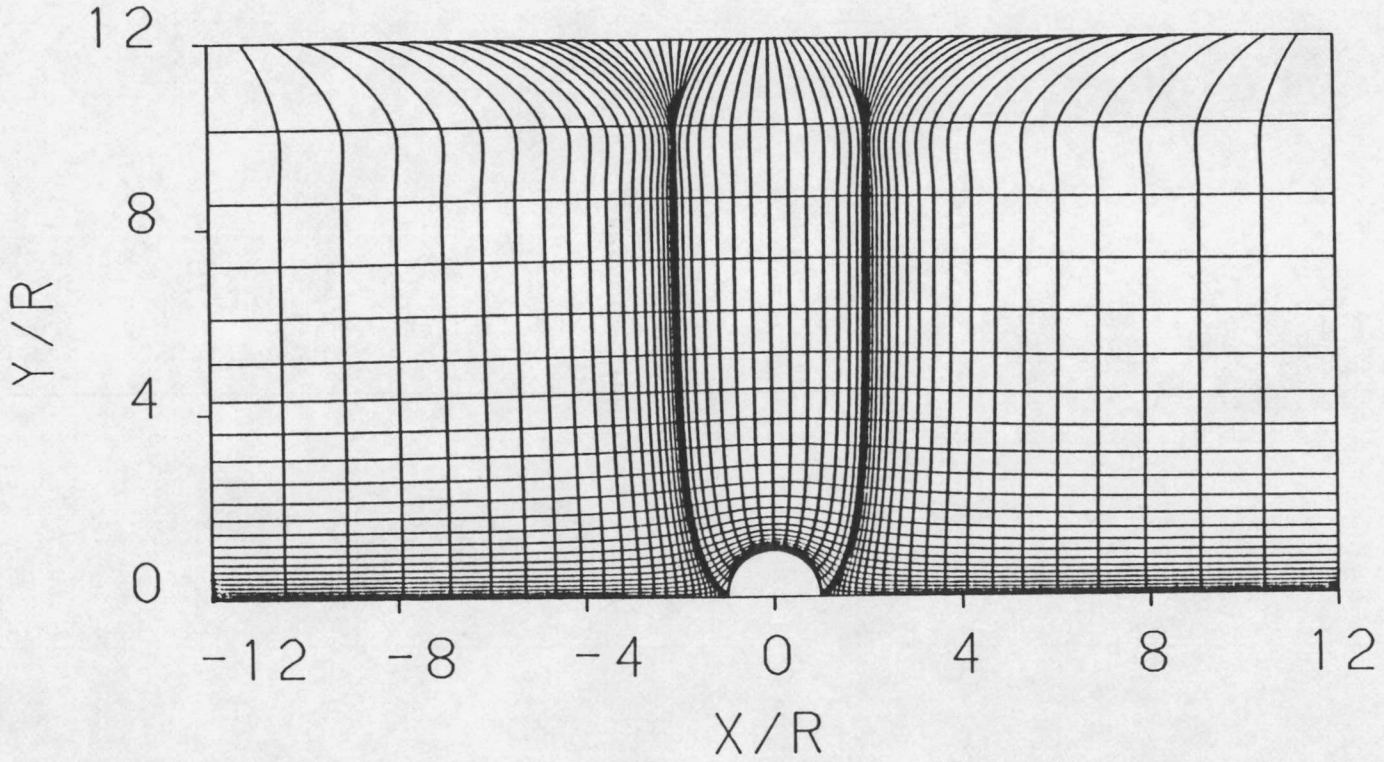


Figure VI-4. Initial Coordinate with Modified Top Boundary.

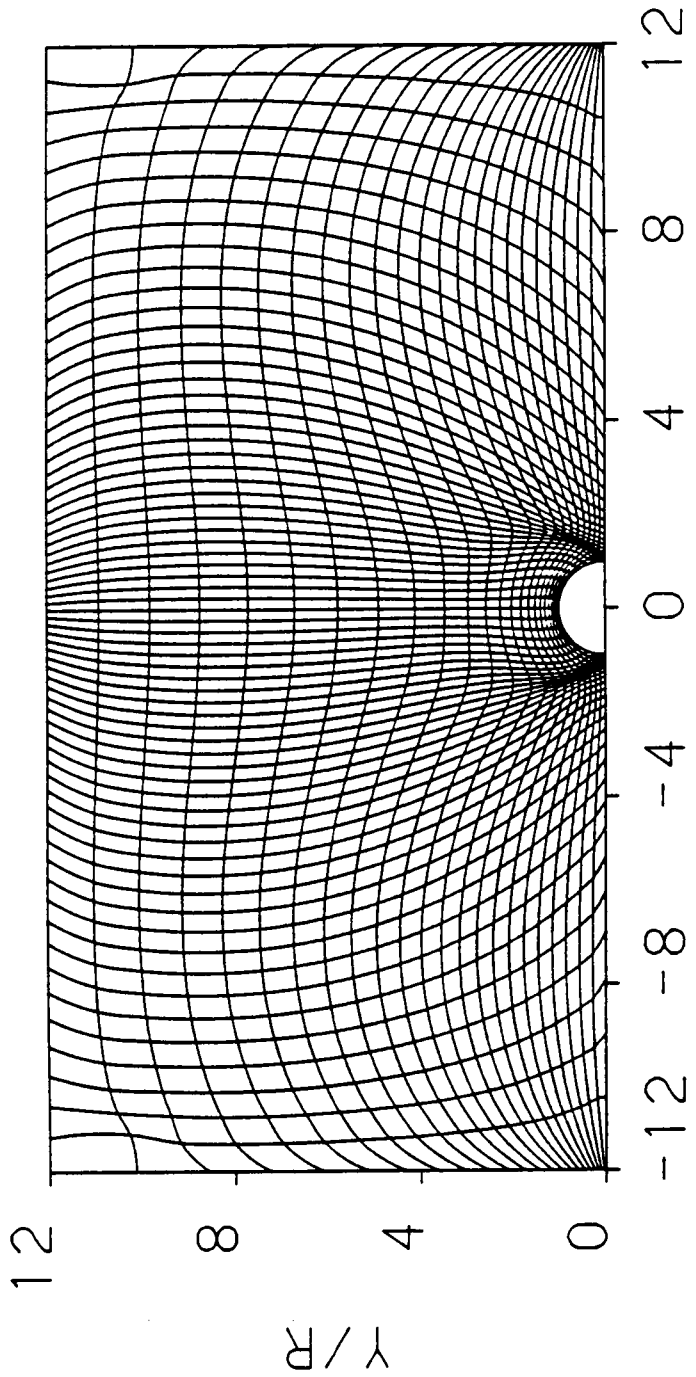


Figure VI-5. Initial Modified Grid After Mapping.

of the transformation is shown in Figure VI-6. This particular coordinate system was used in the computation. A listing of the computer program used for grid mapping is given in Appendix U.

Potential Flow Solution

The stream function for the flow over a cylinder with surface injection was obtained by numerically integrating the following elliptic equation with appropriate boundary conditions. Computations were performed in the mapped plane obtained previously. The transformed stream function equation is (see Appendix J for details)

$$\alpha\Psi_{\xi\xi} - 2\beta\Psi_{\xi\eta} + \gamma\Psi_{\eta\eta} - J^2 Q\,\Psi_{\eta} = 0 \qquad \text{(VI-7)}$$

The boundary conditions are

$$\Psi_{\xi}(\xi = 1, \eta) = 0.0$$

$$\Psi(\xi = -1, \eta) = \eta$$

$$\Psi_{\eta}(\xi, \eta = 1) = 0.0$$

$$\Psi\left(-1 \le \xi < -\frac{1}{12}, \eta = 0\right) = 0$$

$$\Psi\left(-\frac{1}{12} \le \xi \le 1, \eta = 0\right) = -\left(\frac{v_w}{U\infty}\right)\frac{W}{R} \qquad \text{(VI-8)}$$

where W is the width of the injection slot, R is the cylinder radius, and α, β, γ are given in Equation (VI-4).

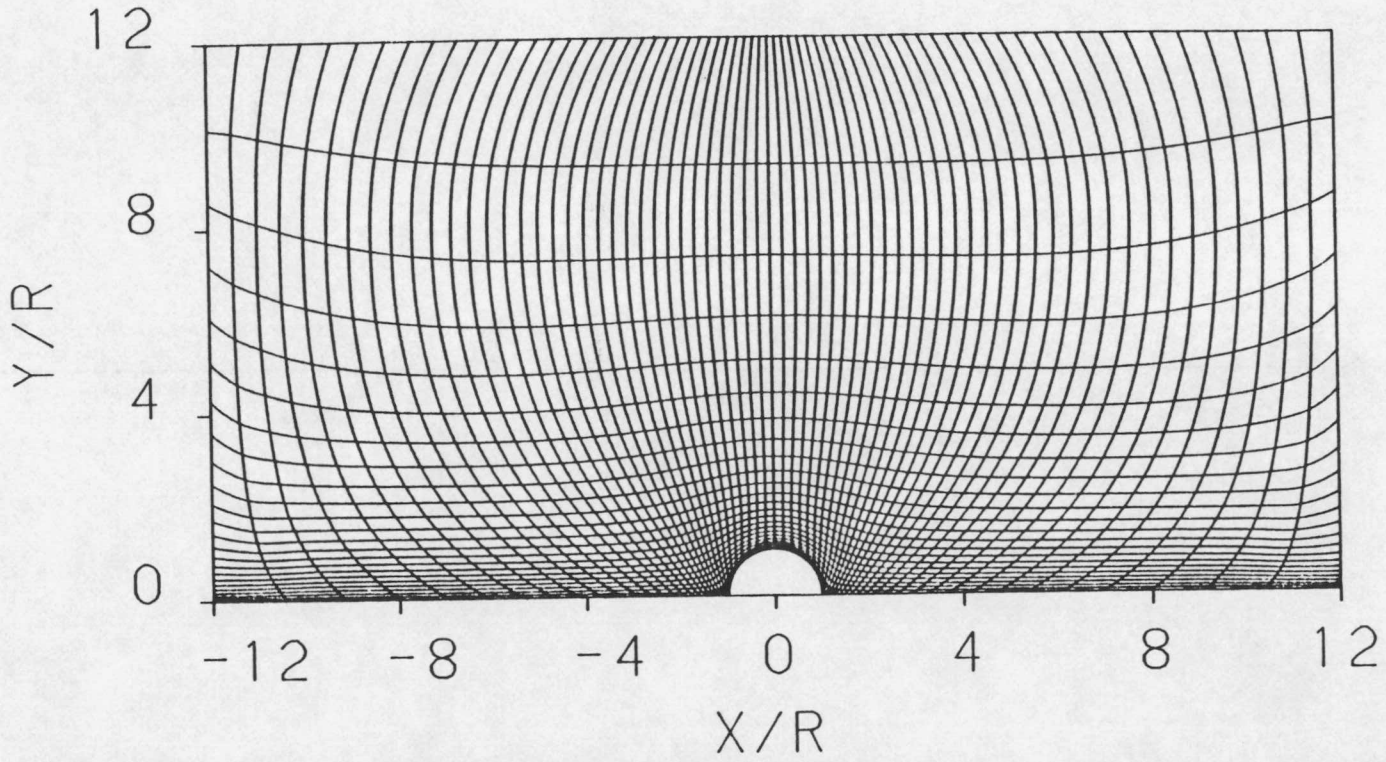


Figure VI-6. Mapped Coordinate of Initial Modified Grid With Suction Applied at the Bottom Plane.

Equations (VI-7,8) were integrated using factored implicit finite differencing described in Appendix J. Appendix V contains a listing of the computer program for calculating stream function in the mapped plane.

Comparison of the numerical results with those obtained from the exact theoretical expression in Chapter IV was done by first calculating the stream functions at the grid points using the exact expression (Equation IV-3). Stream function values calculated from the two methods were found to have a maximum difference of about 15 percent. Slots located at 0 and ±50 degrees from the front stagnation point with slot velocities of up to 17.3 times that of free stream velocity were considered. Location of slots were 0 and ±50 degrees from the front stagnation point. Figure VI-7 presents a sample contour plot of stream lines obtained from the numerical computation. A corresponding contour plot obtained from the method of Chapter IV is shown in Figure VI-8. A contour plot of streamlines for the case of no surface injection is shown in Figure VI-9 for comparison. It should be pointed out that the velocities considered in the numerical computation do not represent the actual flight velocities.

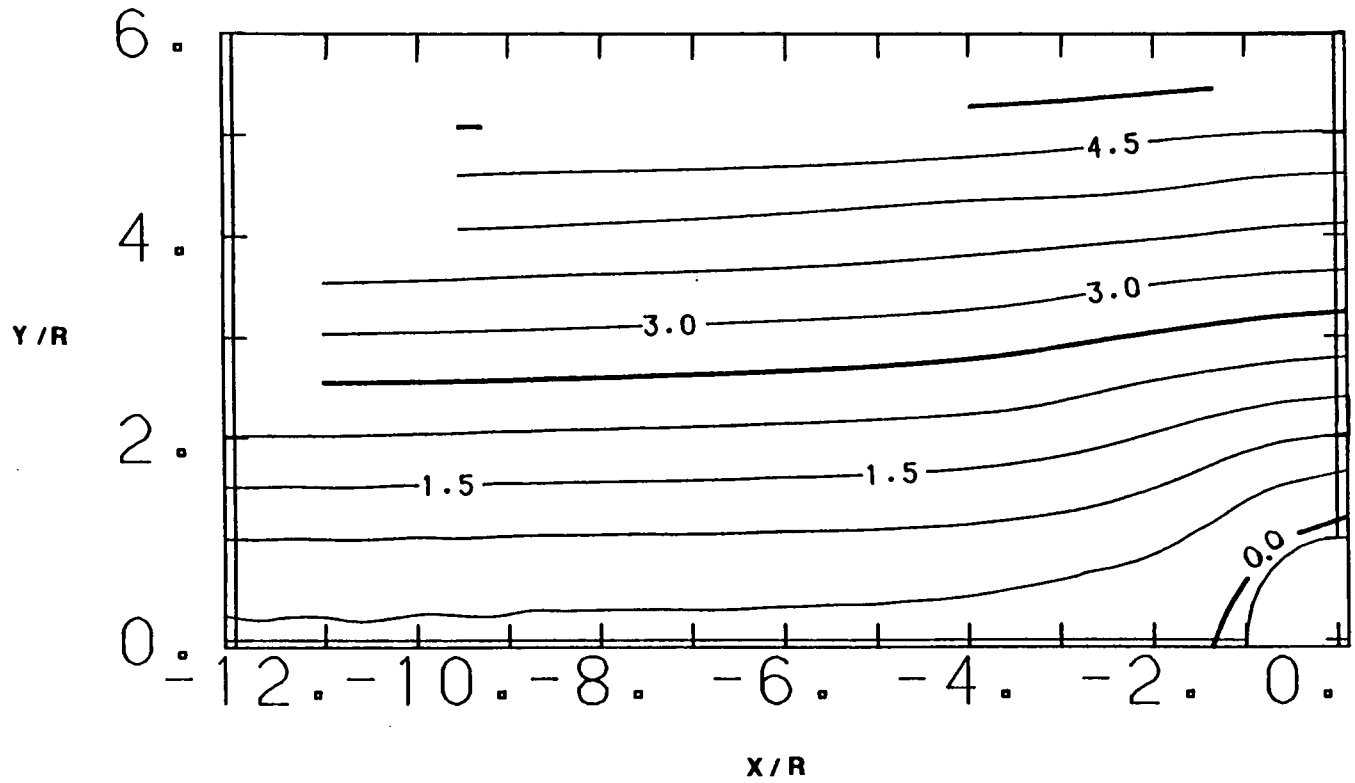


Figure VI-7. Contour Plot of Streamlines Obtained From Mapped Solution With Surface Injection at ±50°, and 0° (Front Stagnation Point), Wall Velocity = 17.3*U_∞.

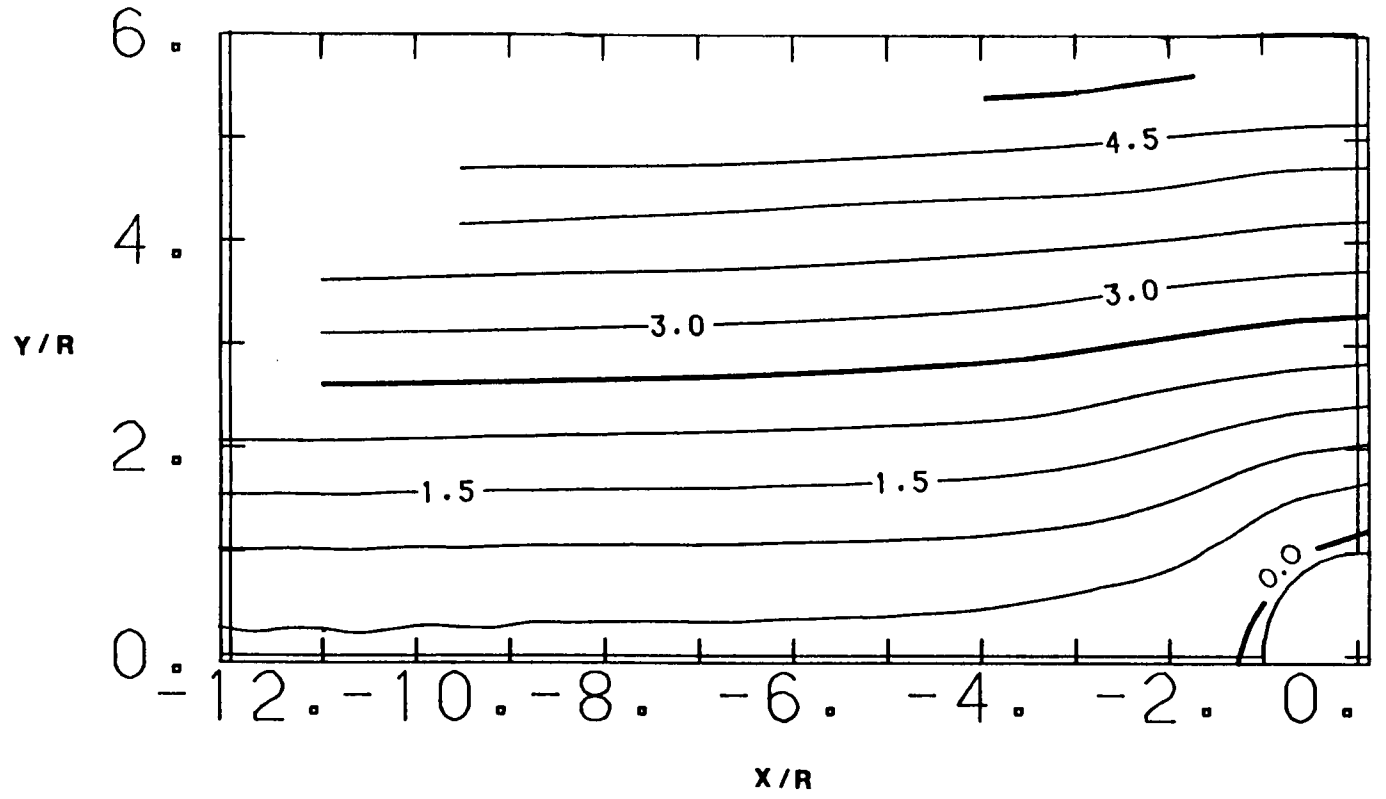


Figure VI-8. Contour Plot of Streamlines Obtained from Theoretical Solution With Surface Injection at ±50° and 0° from Stagnation, Wall Velocity = 17.3*U_∞.

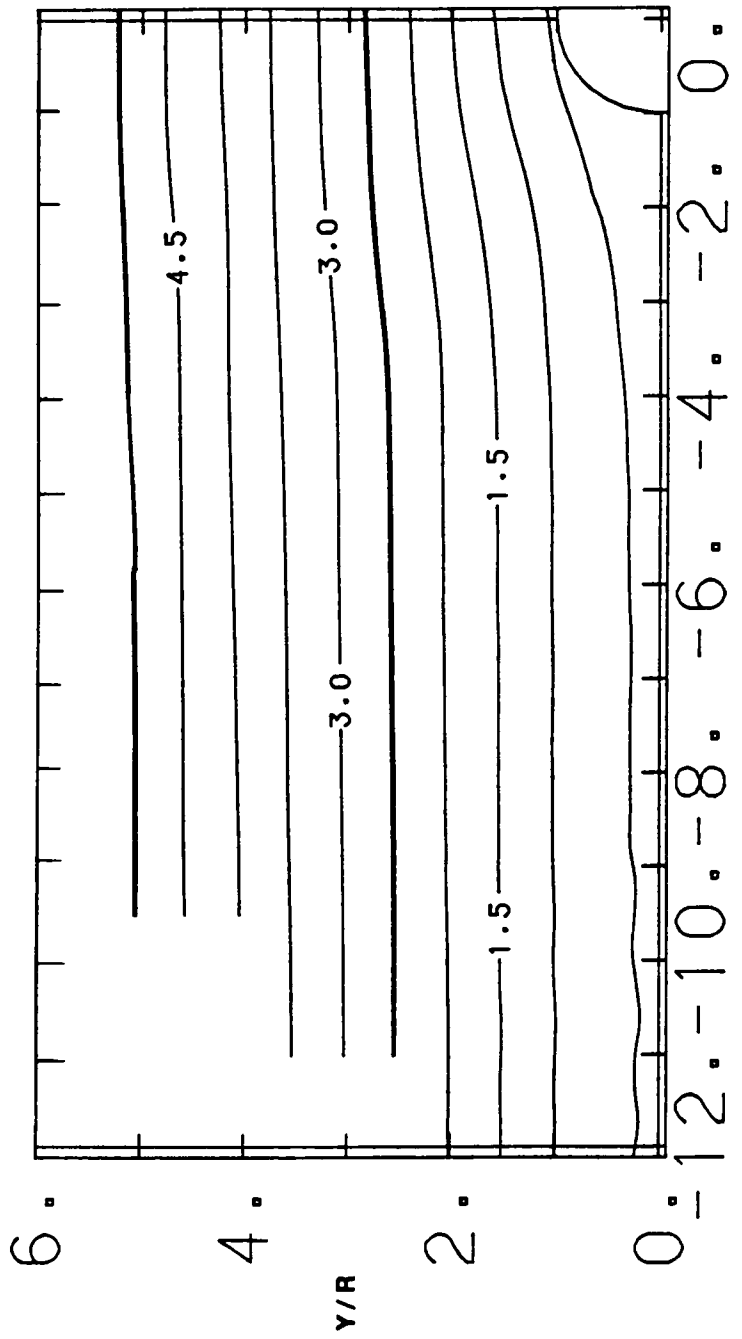


Figure VI-9. Contour Plot of Streamlines Obtained from Theoretical Solution With No Surface Injection.

CHAPTER VII

EXPERIMENTAL INVESTIGATION

General

An experimental study was conducted to complement the analytical study of the anti-icing system. An experimental model, a circular cylinder with three air injection slots at the frontal surface, was tested in the wind tunnel.

Ice is accreted on a surface when supercooled water droplets in the atmosphere strike it. Thus, to simulate the atmospheric icing condition in a wind tunnel, one must be able to cool the air in the tunnel and also produce supercooled water droplets. Closed loop tunnels are best suited for this type of experiments, i.e. two-phase flow problems where the tunnel air condition is to be controlled.

However, due to unavailability of a closed loop two-phase flow tunnel, an open loop single phase tunnel was used in the present study. Since cooling of the air in this tunnel was not possible it was decided to cool the surface of the cylinder by circulating chilled Methanol (-30 °F to -45 °F) through it to freeze the droplets that impinged on the cylinder. Initially air was injected through slots provided on the model in order to reduce ice accretion rate. However, within the first two minutes of testing the moisture in the compressed air condensed and froze due to low surface temperature and slots became clogged with ice. To avoid condensation

of moisture when air (75°F dry bulb temperature) was cooled to −40°F the relative humidity of air should be less than 0.44 percent. An attempt was made to dry the compressed air using a desiccant air dryer. Unfortunately it was found that the use of desiccant was not able to remove enough moisture from the air. Finally, it was decided to substitute nitrogen gas for compressed air. Nitrogen gas provided trouble free operation of the slots. Water droplets were introduced in the tunnel using pneumatic atomizers.

A general description of the wind tunnel, a detailed description of the experimental model, a description of the spray system, and a discussion of experimental procedure is given in the remainder of this chapter.

Wind Tunnel

An open loop wind tunnel with horizontally oriented 13 inch cylindrical test section capable of providing velocities up to 90 MPH in the test section was used as shown photographically in Figure VII-1. A system of flow straighteners consisting of an inlet bell mouth made of styrofoam and 1/4 x 9 inch drinking straws which were stacked inside the tunnel at the inlet, as shown in Figure VII-1, was used to provide a smooth and straight flow at the test section. Pressure drop due to presence of the flow straighteners reduced the maximum attainable velocity in the test section to 45 MPH.

The test section of the tunnel is made of Plexiglass 14 inches in length, 13 inches in diameter, and 1/2 inch in thickness. To provide

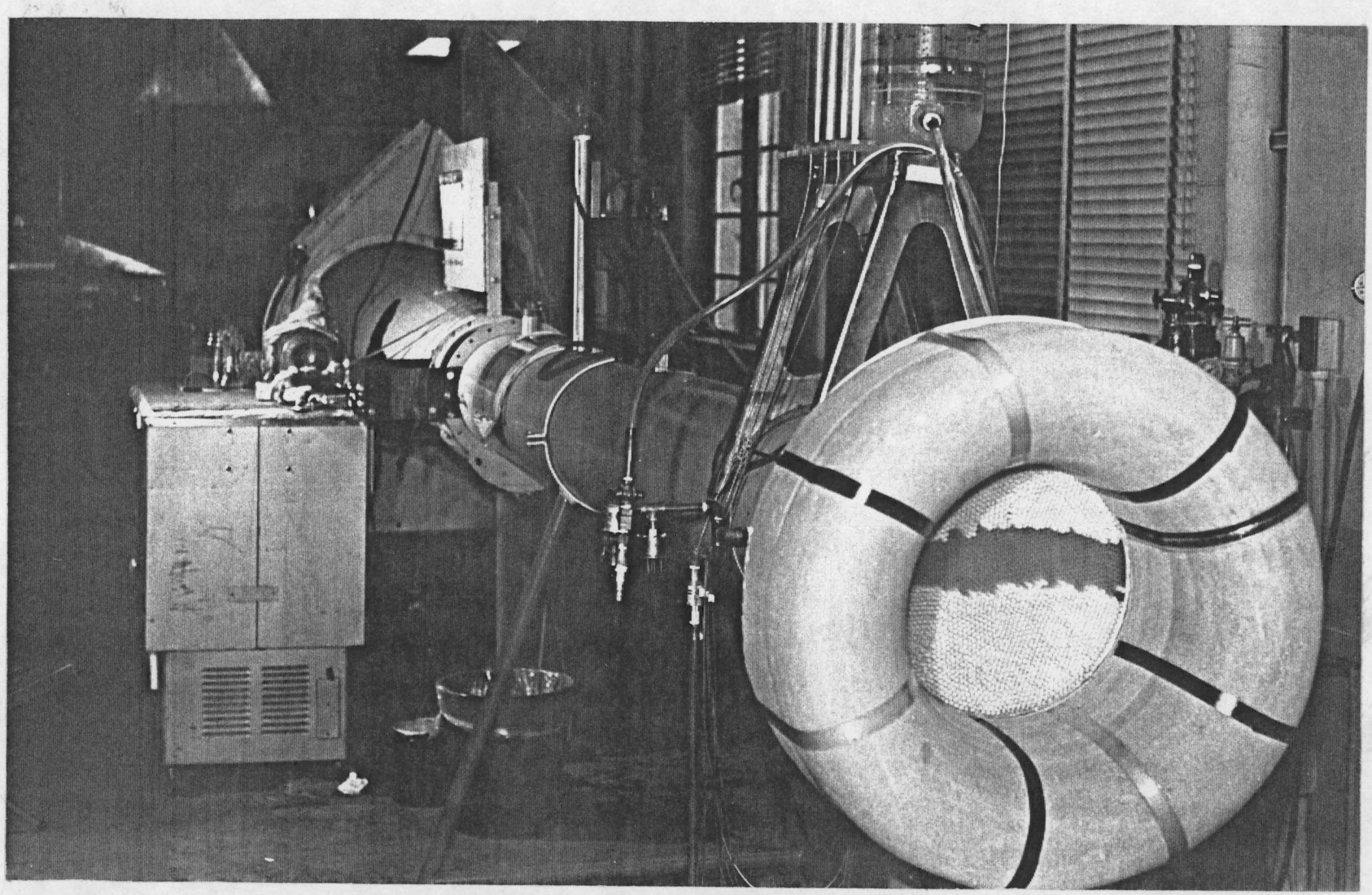


Figure VII-1. Wind Tunnel.

fast and easy access to the model the test section was cut in two halves so that the top half would be removable as shown in Figure VII-2.

Hot wire and hot film sensors were used to obtain velocities in the test section. First, sensors were calibrated using a hot wire/hot film probe calibrator (TSI model 1125) and calibration curves for the sensors were then plotted as shown in Figures K-1 and K-2 in Appendix K. A hot wire/hot film (low air speed/high air speed respectively) sensor was traversed across the test section and the voltage output of the sensor was recorded. An anemometer system, TSI model 1050 shown in Figure VII-3, along with HP computer 9826A and HP data acquisition system were used to measure probe output (in volts). Five hundred voltage samples were taken for each location and average value and standard deviation were then computed. Voltages were related to pressure drops using the calibration data and, in turn, pressure drops were used to calculate velocities. For the four tunnel speeds used in experiments velocity profiles and the corresponding average speeds are shown in Figures K-3, K-4, K-5, and K-6 in Appendix K.

Experimental Model

A model was built to study the feasibility and performance of the proposed anti-icing technique. The model consists of a circular cylinder made of 0.969 inch diameter (1 inch nominal) brass tubing with three air injection slots located at 0, +50, and −50 degrees

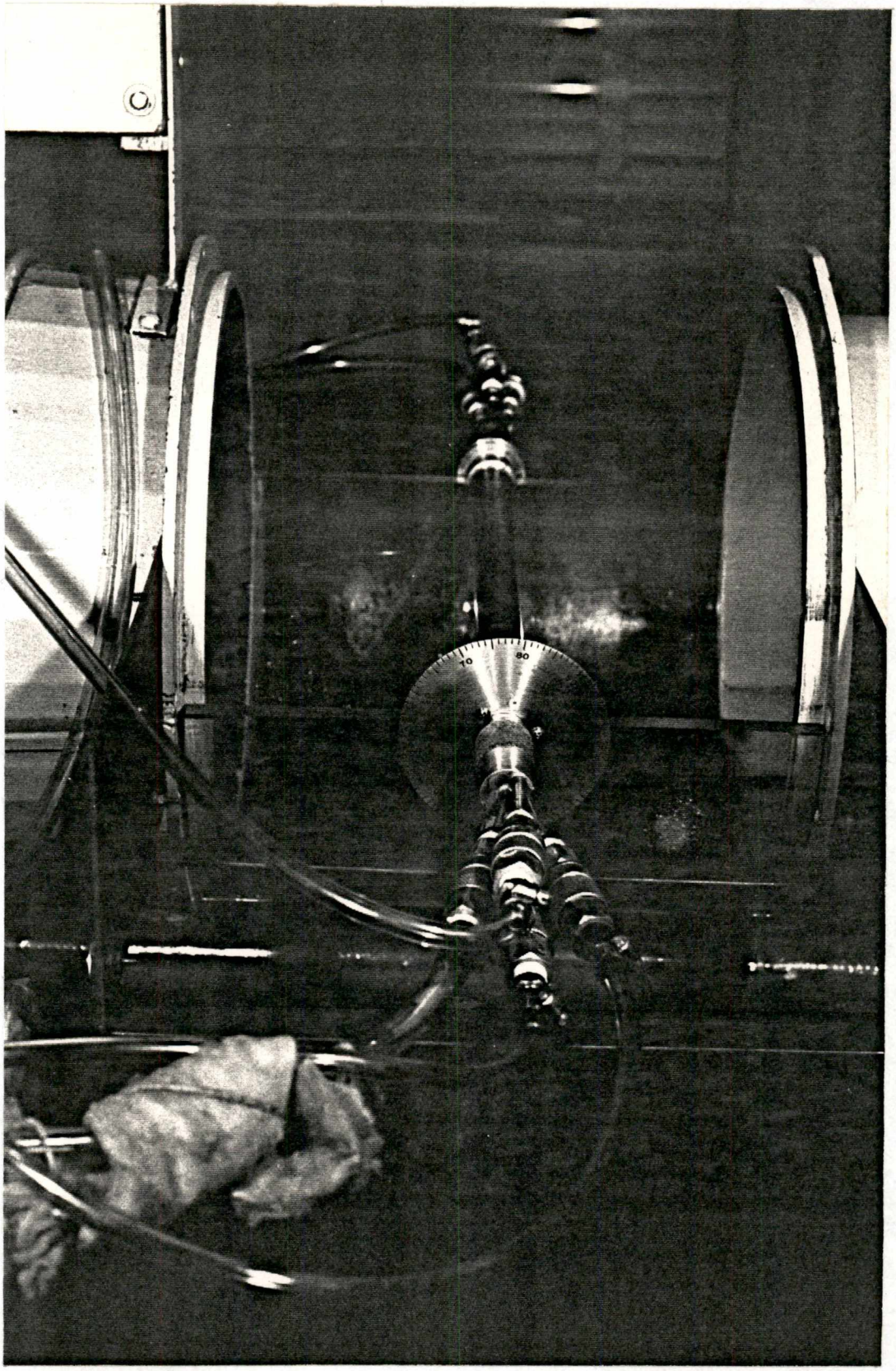


Figure VII-2. Wind Tunnel Test Section And The Model.

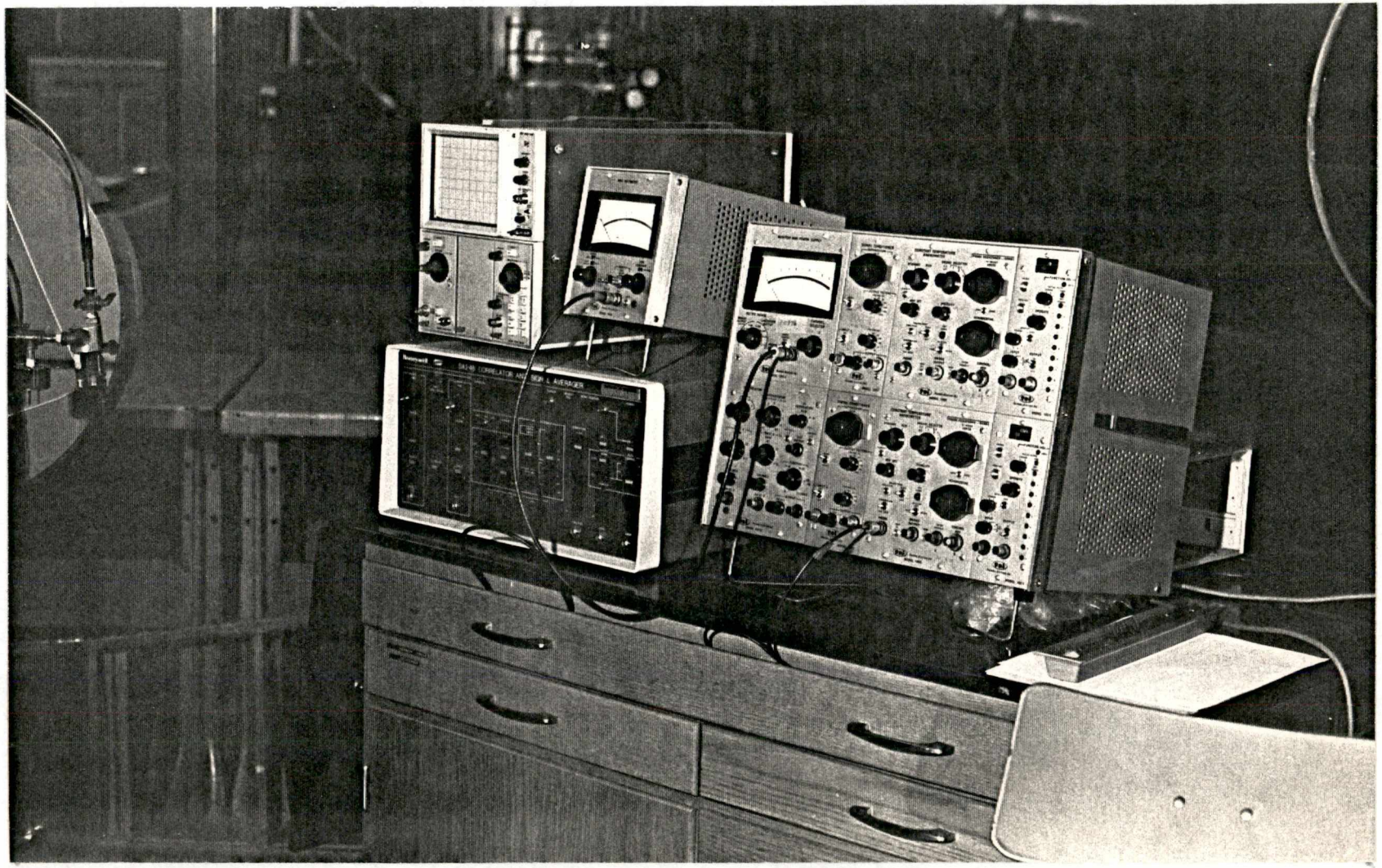


Figure VII-3. Hot Wire/Film Anemometer Used For Velocity Measurement.

where 0 degrees represents the front stagnation point. It should be noted that the angles at which slots are located on either side of the front stagnation point represent the minimum possible angles for the particular arrangement and the size of the cylinder and the nitrogen injection tubes used in constructing the model and that these locations do not represent the optimum location (as discussed in Chapter IV) of the slots operating under the conditions tested. The slots are 4 inches long and 0.014 inch wide and the injected fluid, air or nitrogen, is delivered to each of them through a 0.25 inch copper tube. A photograph of the model is shown in Figure VII-2 and dimensional and descriptive details are given in Figure VII-4, and VII-5 respectively.

Spray System

The atmospheric cloud was simulated by a specially designed pneumatic atomizing system located five feet from the test section in the tunnel. A schematic of the spray system is shown in Figure VII-6. Pneumatic nozzle atomization involves impacting liquid bulk with high velocity gas such as air, thus the mechanism of atomization is one of high velocity gas creating high frictional forces over liquid surfaces causing liquid disintegration into spray droplets. External mixing type pneumatic nozzles shown schematically in Figure VII-7 were used to produce droplets. Another type of pneumatic nozzle, an internal mixing type (spraying system co. model 1/8 JJ-J16) was also tried, but because of its larger size and specially undesirable spray

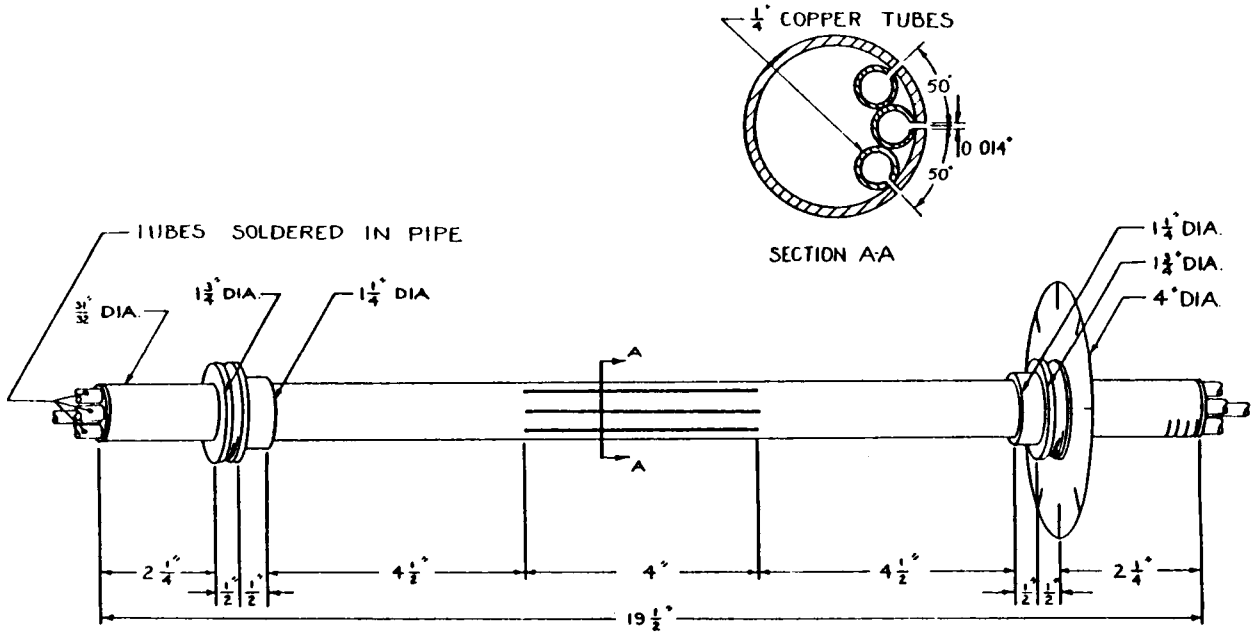


Figure VII-4. Dimensional Details of the Experimental Model.

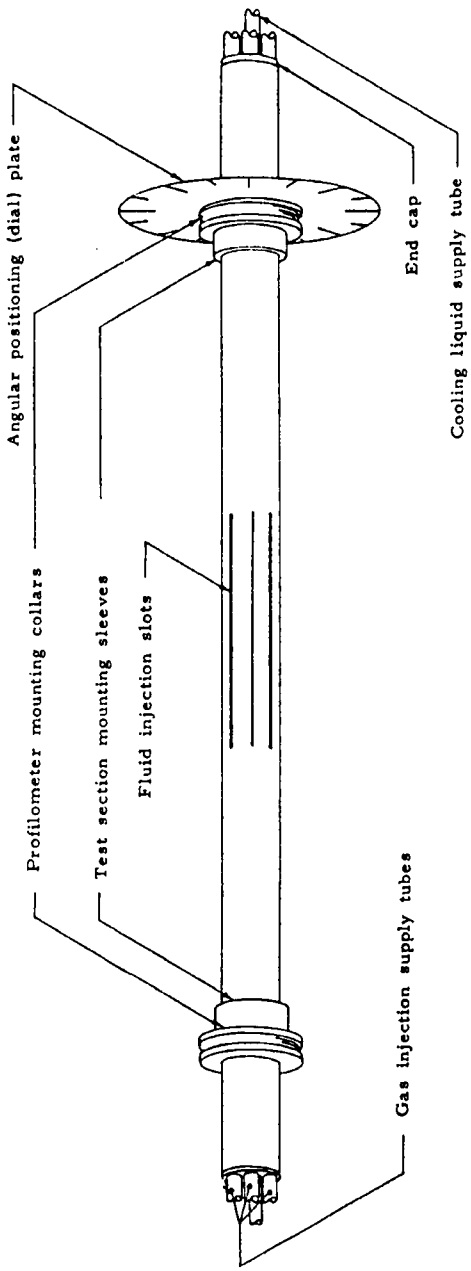


Figure VII-5. Descriptive Details of the Experimental Model.

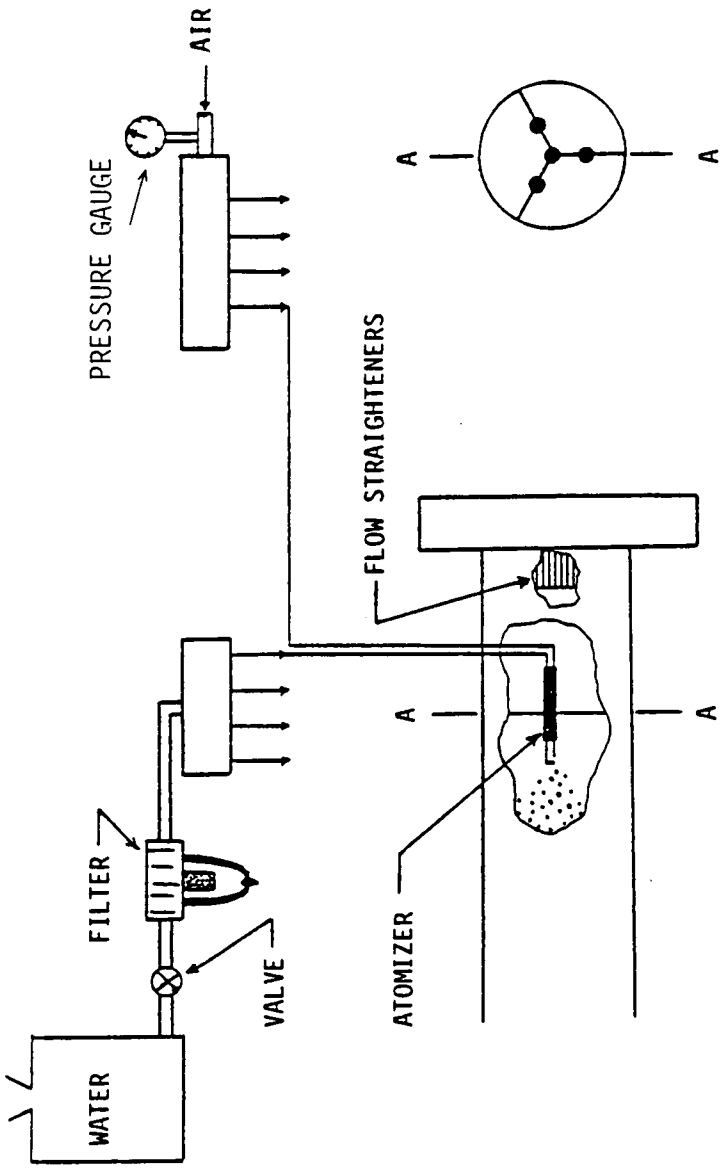


Figure VII-6. Schematics of the Spray System Used In Experiments.

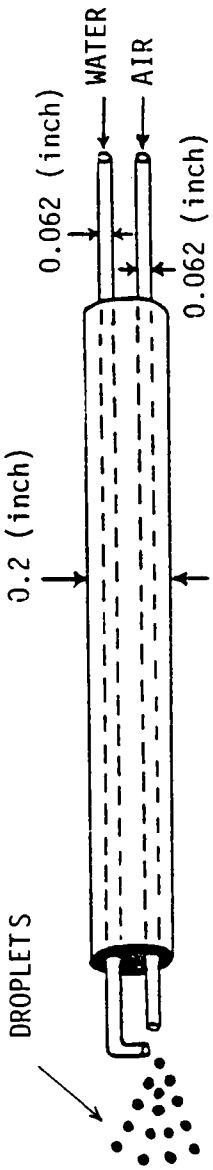


Figure VII-7. Schematic of a Pneumatic Atomizing Nozzle.

pattern (i.e. spray cone angle, nonuniformity of the spray distribution, etc.) it was not used.

Nozzles were calibrated for different water mass flow rates with respect to atomizing air pressure levels and the result is shown in Figure K-7 in Appendix K, the calibration curve gives the total water flow for the whole spray system, i.e. four nozzles. Individual calibration of the nozzles indicated that the water mass flow through nozzles were not the same. Thus in order to have the same water flow through each nozzle, the length of the water supply tube was adjusted. Therefore the water flow through each nozzle is approximately 1/4th of the values indicated in the calibration curve. For atomizing air pressure of 30 psia the water flow rate through each nozzle was 2.803 lbm/hr.

Liquid water content of the tunnel, which is a function of air speed and water mass in the tunnel, was then calculated for the tunnel speeds used in the present experiments. Table K-1 in Appendix K presents such data. An atomizing air pressure of 30 psia was used to produce sprays for all tests.

Droplet Size Distribution

The microscope measuring method was used to determine droplet sizes in the test section. A vaseline coated microscope slide was inserted in the tunnel to capture water droplets from the air. Droplet diameters were then measured under a microscope. The vaseline coating was used to create a non-wetting surface thus

avoiding smearing and flattening of the droplets upon impact. The lifetime of the droplets on the slide was short due to the evaporation which caused measurement difficulties. However, this problem was overcome by using ice water for atomization which produced colder droplets and increased lifetime of the droplets on the slide. Appendix X contains a computer program which was used to process the data obtained from the microscope and generate droplet size distribution for the spray. Table K-2 in Appendix K presents the droplet size distribution and other pertinent data. The percent frequency of occurence of each droplet size in the spray is shown graphically in Figure K-8 in Appendix K. The maximum droplet size measured was 211 microns and the mean droplet size was determined to be 45 microns.

Droplet Velocity in the Test Section

In the theoretical analysis presented in Chapter IV it was assumed that droplets far from the cylinder (10R where R is the cylinder radius which is about 0.5 in.) have the same velocity as the free stream. Since droplets were introduced into the tunnel at a higher velocity than the local air it is necessary to check the validity of this assumption. This is possible by experimentally measuring droplet velocities at the test section. Such measurements have been done by Hodgson [20]. He obtained high speed moving pictures of the flow in the test section from which droplet velocities were calculated. He concluded that droplet velocities were generally the same as that of local tunnel air. Spray droplets

in his experiments were introduced at higher velocities than those in the present experiments. Due to the lack of equipment, droplet velocities in the test section were calculated numerically as follows: A droplet was injected into the free stream at a velocity of $10U_\infty$ where U_∞ is the free stream velocity. The trajectory of the droplet was then obtained by integrating the equations of droplet dynamics (see Chapters III and IV) with respect to time. The new droplet location and corresponding velocities were calculated for every time step of the integration. Droplet velocity was then plotted as a function of distance traveled and presented in Figure VII-8. This figure presents deceleration of a droplet (diameter of 30 microns) injected into the tunnel with an initial velocity equal to 10 times that of the tunnel air. It can be seen that the droplet decelerates quickly and attains the free stream velocity after a distance of 5R. The droplet velocity remains equal to the air velocity along the tunnel until there is a change in the air velocity. The change in the air velocity occurs only at a region very close to the cylinder in the test section. Similarly, a droplet injected into the tunnel at a velocity less than that of the free stream quickly accelerates and attains the free stream velocity. Thus it is reasonable to assume that droplets have essentially no relative velocity away from the cylinder (x = 10R).

Experimental Procedure

To evaluate the effect of the surface injection on the ice accretion rate a series of experiments was performed. A quantitative

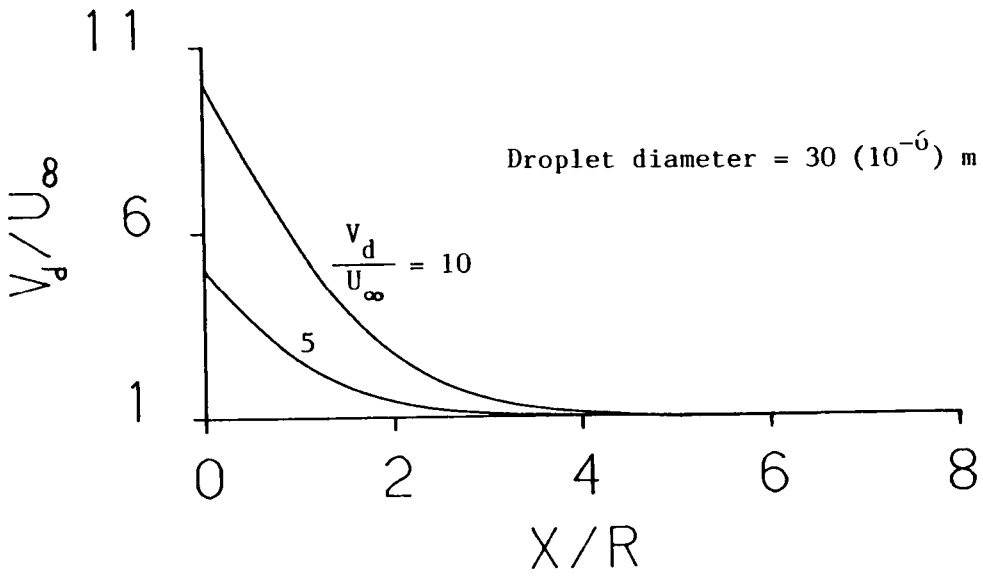


Figure VII-8. Spray Droplet Deceleration Distance.

evaluation of the analytical model and its predictions was performed by measuring the ice weight collected on the model while a qualitative evaluation was performed by comparing the profiles obtained from the ice layer build-ups on the model. The water collected on the model was frozen by cooling the model from the inside using cold Methanol (−45°F). Figure VII-9 presents a schematic of the cooling and the nitrogen supply system used in the experiments. The following procedure was used to carry out the experiments.

The model was first tested with no surface injection and the ice collected on the model was weighed. The total run time for each test was seven minutes (a few tests were performed with longer run times). The ice weights for the speeds of 4.1, 6.3, 13.3, and 39 ft/sec, were obtained. In all the above tests, the water mass injected into the tunnel was kept at a constant value of 7.29 lbm/hr. The results of these tests are presented in Tables VIII-1 and VIII-2, Chapter VIII. The axial ice profiles at the front stagnation point and the angular ice profiles at the center of the model (center of the tunnel) and at the locations 1.25 inches away from the center were obtained using a profilometer. A photograph of the profilometer is shown in Figure VII-10. Appendix L contains the design and the operational details of the profilometer.

The icing of the model with surface injection was next considered. For all tests conducted, the water mass injected into the tunnel was 7.29 lbm/hr. Numerous tests were performed to

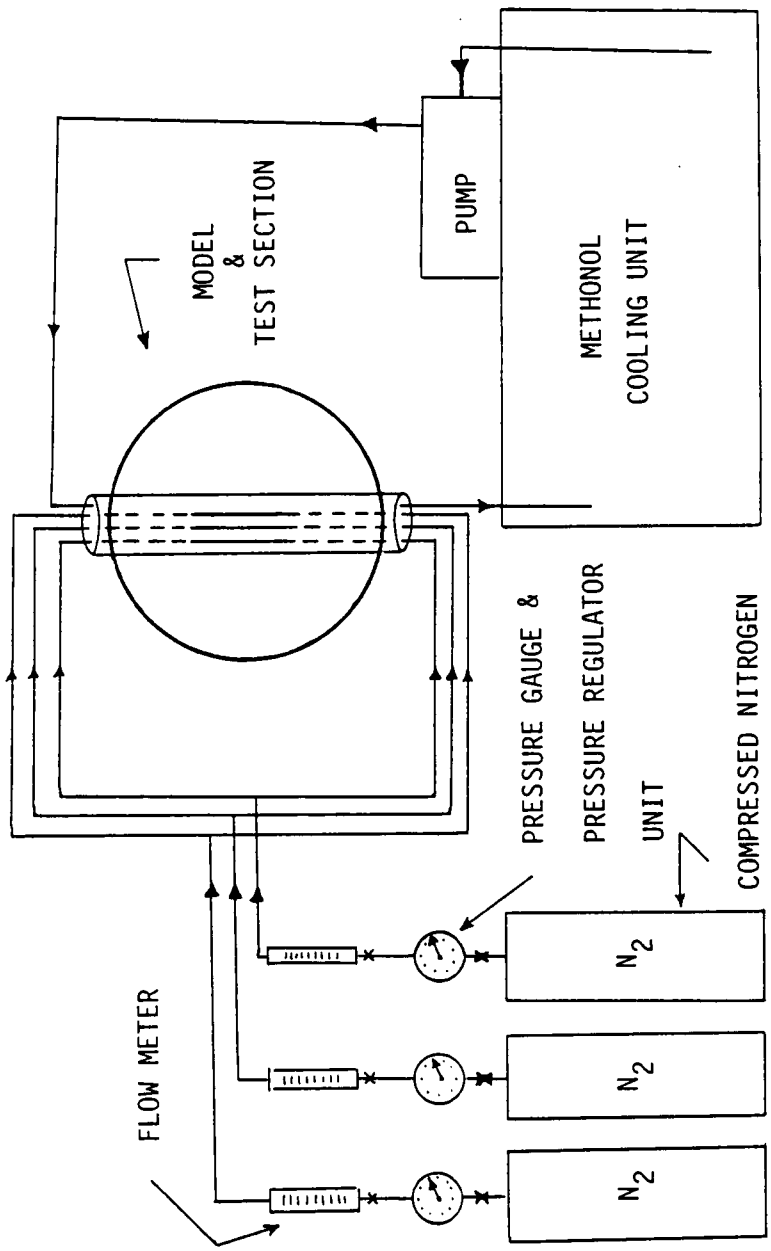


Figure VII-9. Schematic of the Cooling and the Nitrogen Supply System.

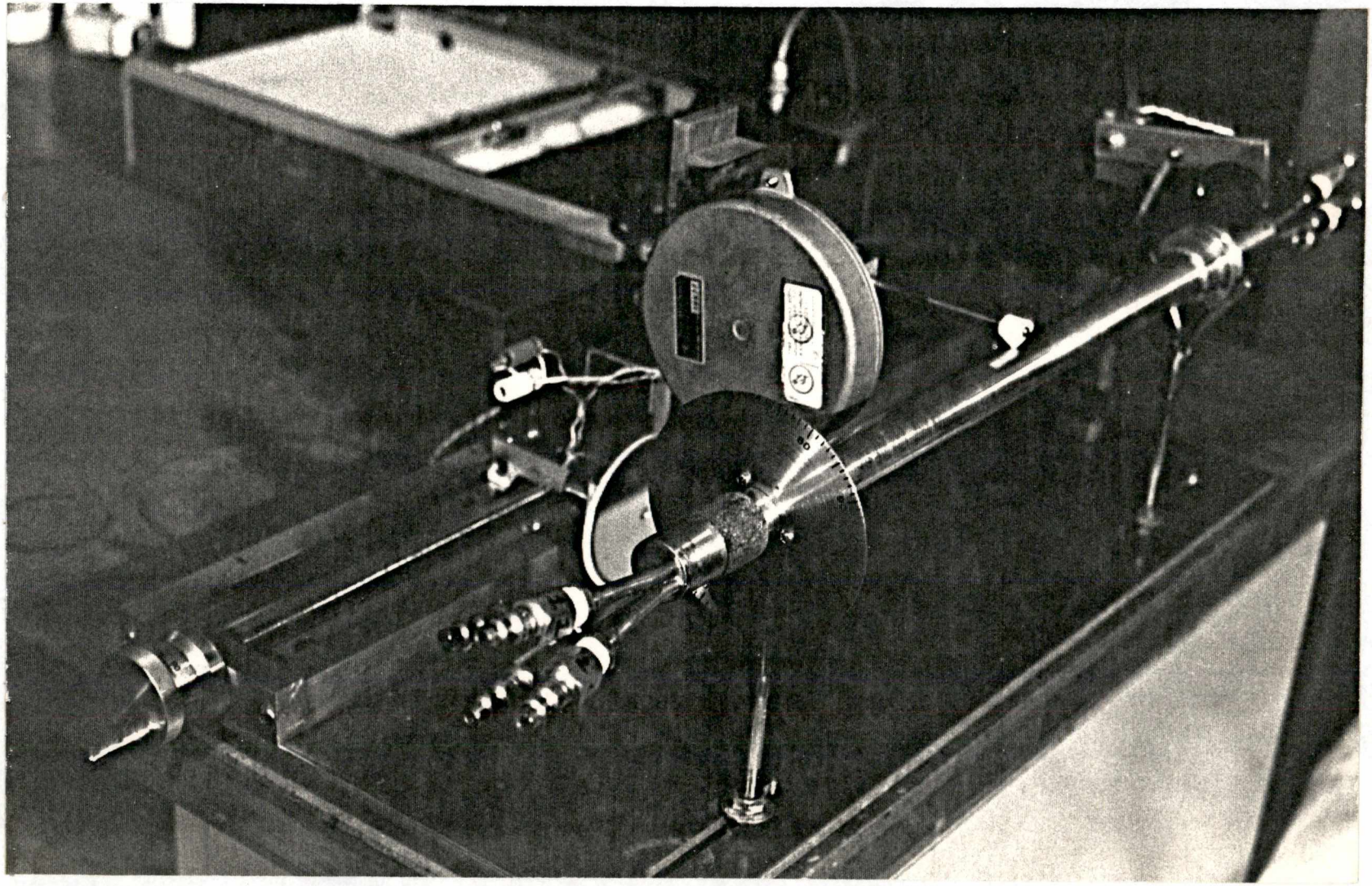


Figure VII-10. Profilometer Used for Ice Profile Measurements, Experimental Model is Also Shown.

investigate the effects of the location of the slots and the number of slots on the model as well as the injection rate through each slot. First the effect of slot flow rate on the reduction of the ice collection was considered using a total of three slots located at 0 and ±50 degrees from the front stagnation point with the flow through each slot set at 25 ft^3/hr. The ice weight collected on the model for seven minutes of exposure at tunnel velocity of 6.3 ft/sec was 13 grams. A test was also run with the flow rate through each slot set at 100 ft^3/hr and all other parameters kept constant; the ice weight for this run was 12.75 grams (these results are shown in Table VIII-1, Chapter VIII). The effect of nonuniform injection, i.e. different flow rate through each slot, was examined by the following three runs (keeping all other parameters constant). For the flow through slots #1 and #3 (+50 and −50 degrees respectively) set at 50 ft^3/hr and through slot #2 (stagnation point) set at 150 ft^3/hr the ice weight collected was 13.8 grams. For the second test the flow rates through slots #1 and #3 were 100 ft^3/hr and through slot #2 was 150 ft^3/hr resulting in an ice weight of 11.25 grams. Finally, for the flow rate of 100 ft^3/hr through slots #1 and #3, and 200 ft^3/hr through slot #2 the ice weight collected was 9.3 grams. Next the effect of the location as well as the number of slots were tested. First, the effect of a single injection slot located at the stagnation point was considered. The slot flow rate was set at 50 ft^3/hr and the resulting ice weight was 11.6 grams. The ice weight was 9.6 grams with the slot flow rate of 200 ft^3/hr. Then tests were conducted with the slot

located at +50 degrees (and at −50 degrees for the purpose of symmetry). The flow rate was set at 50 ft^3/hr and the collected ice weighed at 9.8 grams. Another test was also performed with the flow rate of 100 ft^3/hr which resulted in an ice weight of 8.3 grams. These results are also presented in Table VIII-1. Similar tests were also conducted with the tunnel velocity of 4.1, 13.3, and 39 ft/sec. The results of these tests are shown in Table VIII-2, Chapter VIII.

Measured Ice Profiles

Ice shapes obtained experimentally were different than those found in actual icing situations (see Figure I-1, page 2). Typical ice shapes obtained are shown in Figure VII-11. The effect of slot injection on the ice shapes is also indicated in this figure.

The total run time for each test was chosen to be 7 minutes which was selected primarily for the following reasons. Shorter run times result in lesser ice collection on the model; this is undesirable since weighing of the ice collected on the model was done by a triple beam balance that had an accuracy of about 0.1 grams. On the other hand as ice builds up on the model it insulates the model so that the ice surface temperature increases. Consequently after some time, due to the higher surface temperature, water collected on the model does not freeze and sheds from the surface. This condition is of course undesirable since the results obtained can not be compared to those predicted theoretically which do not include the water shedding.

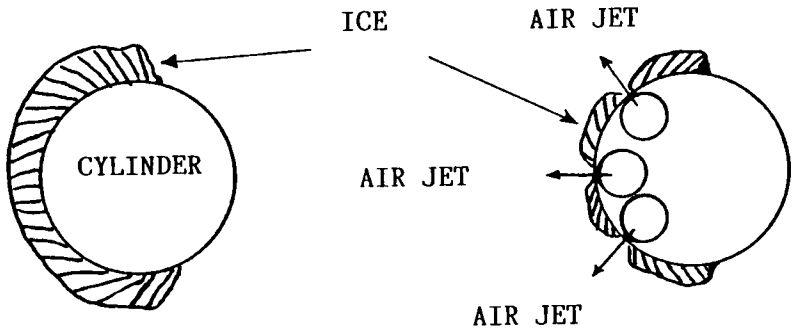


Figure VII-11. Typical Ice Shapes on Cylinder With And Without Surface Injection.

Based on numerous tests it was concluded that 7 minutes of run time provided adequate time for ice collection with no water shedding.

A sample ice profile taken along the front stagnation line with no slot injection is shown in Figure VII-12. The symmetric nature of the test section velocity profile is projected on the ice profile with no injection, i.e. the ice profile is parabolic (rather flat) in shape and symmetric with respect to the center of the model (or tunnel). The ice weight collected (on the 12.5 inch long model) was 7.9 grams which corresponds to the tunnel velocity of 6.3 ft/sec, the flow water content of 0.63×10^{-3} lbm/ft^3, and the average droplet diameter of 45 microns. Profiles indicating the effect of injection at the slots are also shown in this figure, with the reduction in the ice clearly indicated at the location where injection is taking place (noting that the injection slot is only 4 inches long and symmetrically located at the center of the model). Once again symmetry of the flow is shown. Figure VII-13, VII-14, and VII-15 present ice profiles in the angular direction, i.e. around the cylinder, at locations +1.25, 0, −1.25 inches with respect to the center of the model along the cylinder. In these figures the ice profiles for the case of surface injection are compared to those with no injection. The effects of injection are clearly shown by the reduction in the area under each curve. The approximate location of the slot(s) is marked on these curves. The extent of ice reduction can also be observed if one compares these profiles with the axial ice profile shown in Figure VII-12. The angular ice profiles

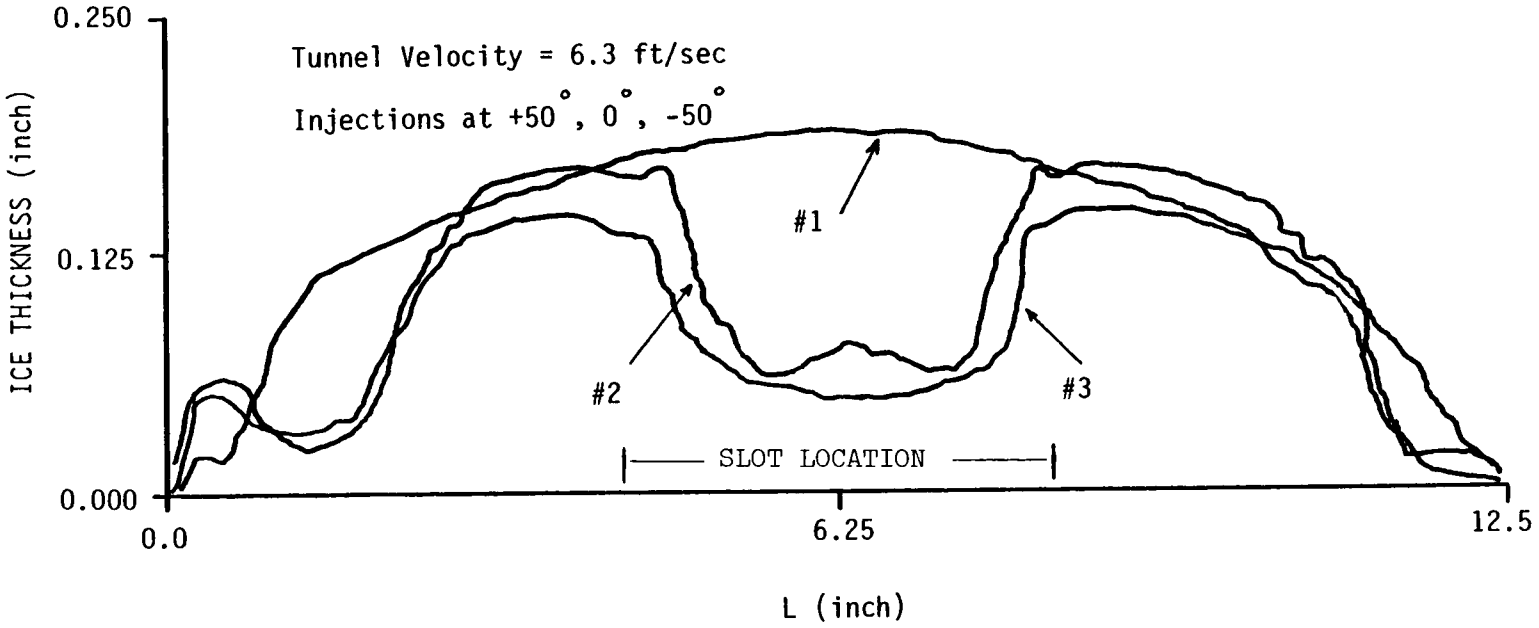


Figure VII-12. Axial Ice Profiles Along the Cylinder at $\theta = +5°$ From the Front Stagnation Point. Injection Rates Are: Curve # 1 = 0, 0, 0; Curve # 2 = 0, 200, 0; Curve # 3 = 100, 200, 100 (ft^3/hr).

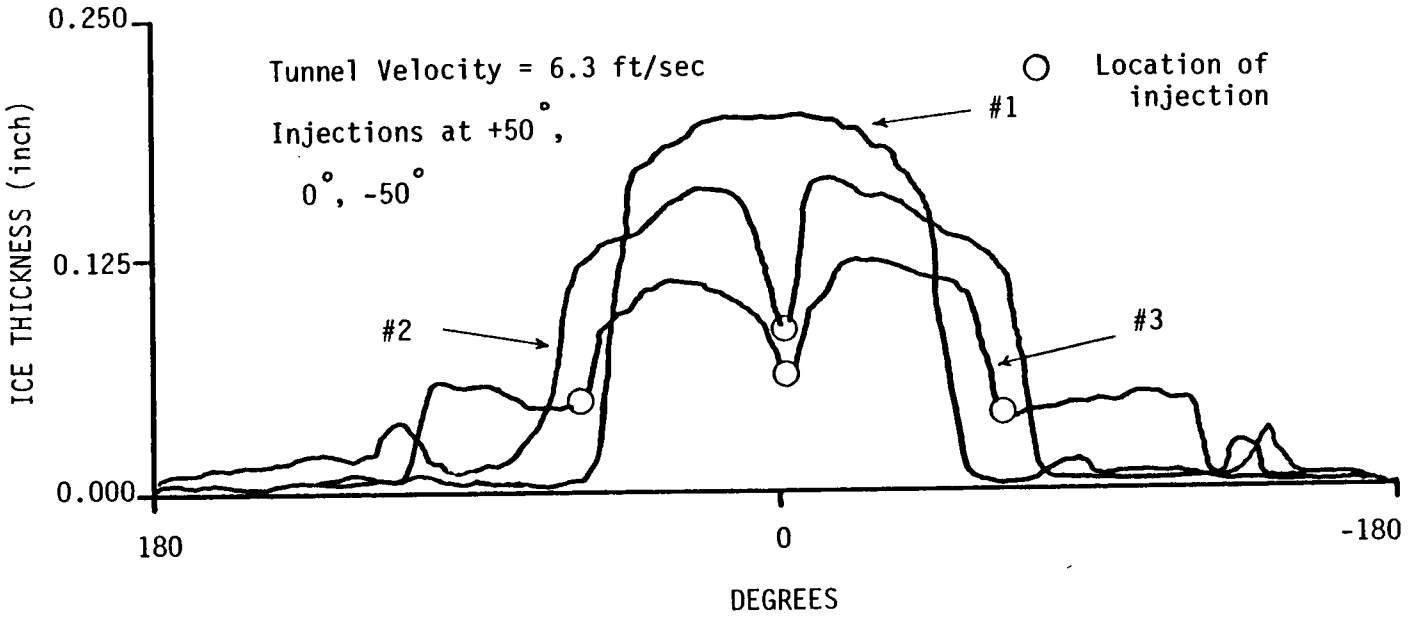


Figure VII-13. Angular Ice Profiles Around the Cylinder at L = 5 inches. The Front Stagnation Point is at $\theta = 0^{\circ}$. Injection Rates Are: Curve # 1 = 0, 0, 0; Curve # 2 = 0, 200, 0; Curve # 3 = 100, 200, 100 (ft^3/hr).

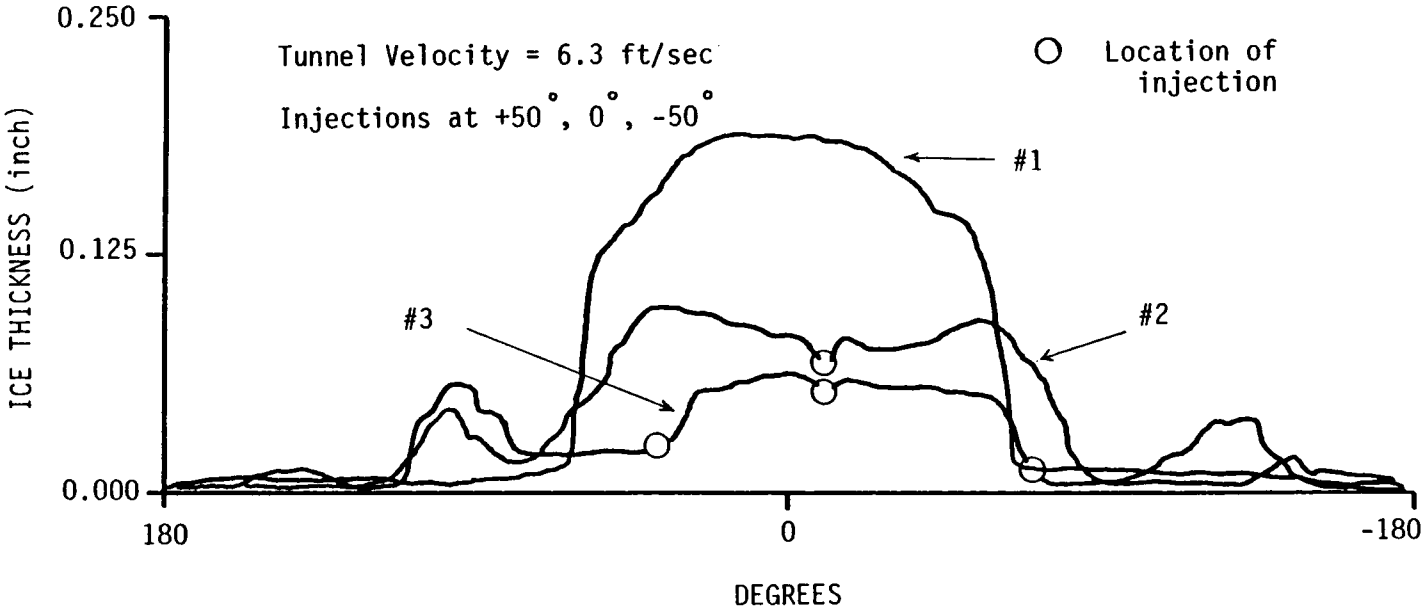


Figure VII-14. Angular Ice Profiles Around the Cylinder at L = 6.25 inches. The Front Stagnation Point is at $\theta = 0°$. Injection Rates Are: Curve # 1 = 0, 0, 0; Curve # 2 = 0, 200, 0; Curve # 3 = 100, 200, 100 (ft^3/hr).

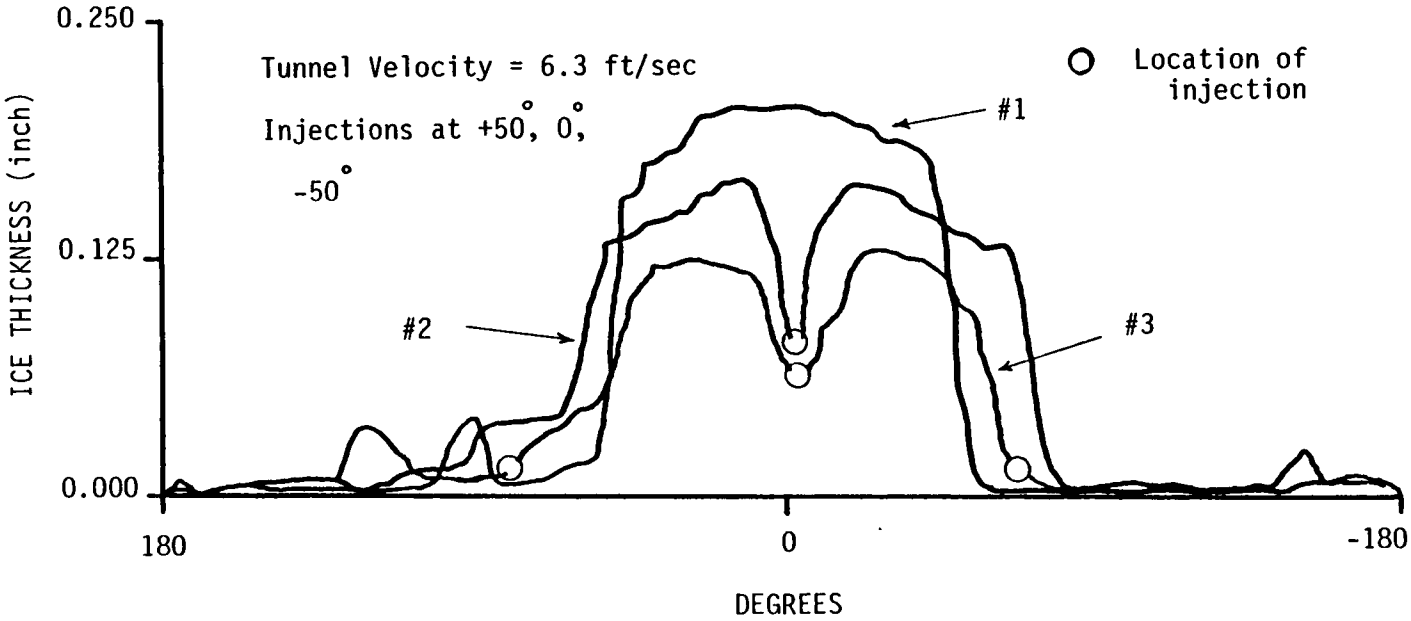


Figure VII-15. Angular Ice Profiles Around the Cylinder at L = 7.5 inches. The Front Stagnation Point is at $\theta = 0^{\circ}$. Injection Rates Are: Curve #1 = 0, 0, 0; Curve #2 = 0, 200, 0; Curve #3 = 100, 200, 100 (ft^3/hr).

indicate that the ice thickness is smaller at the center of the model. This nonuniformity is due to the fact that the jet velocity profile along the slot(s) is not uniform, having instead a parabolic shape. It is expected that a higher jet velocity would result in less ice collection, which is indicated by the ice profile at the center. Figures VII-16 and VII-17 show ice profiles obtained under a higher tunnel velocity, i.e. 13.3 ft/sec. The tunnel liquid water content and the mean droplet diameter were the same as in the previous case. More ice was collected in this case, as was expected, because a higher tunnel speed increases the inertial parameter (or decreases the residence time which is inversely proportional to the inertia parameter) which causes an increase in the collection efficiency (see Figure IV-3, page 28). Equivalently, one might reason that the higher acceleration rate of the flow near the cylinder causes more droplets to deviate from the streamlines and impact on the cylinder. The axial ice profile in this case is more parabolic than that shown previously for the lower tunnel speed. For the uniform droplet distribution it is expected that the ice profiles obtained under different tunnel velocities would be similar. Therefore it can be concluded that a higher air speed tends to keep droplets in the center core of the tunnel and does not permit the droplets to reach the regions close to the wall. Thus droplet mixing does not occur to the same extent as with the lower air speed. Consequently, there are more droplets in the center core of the tunnel. Under this condition, more ice is collected at the center

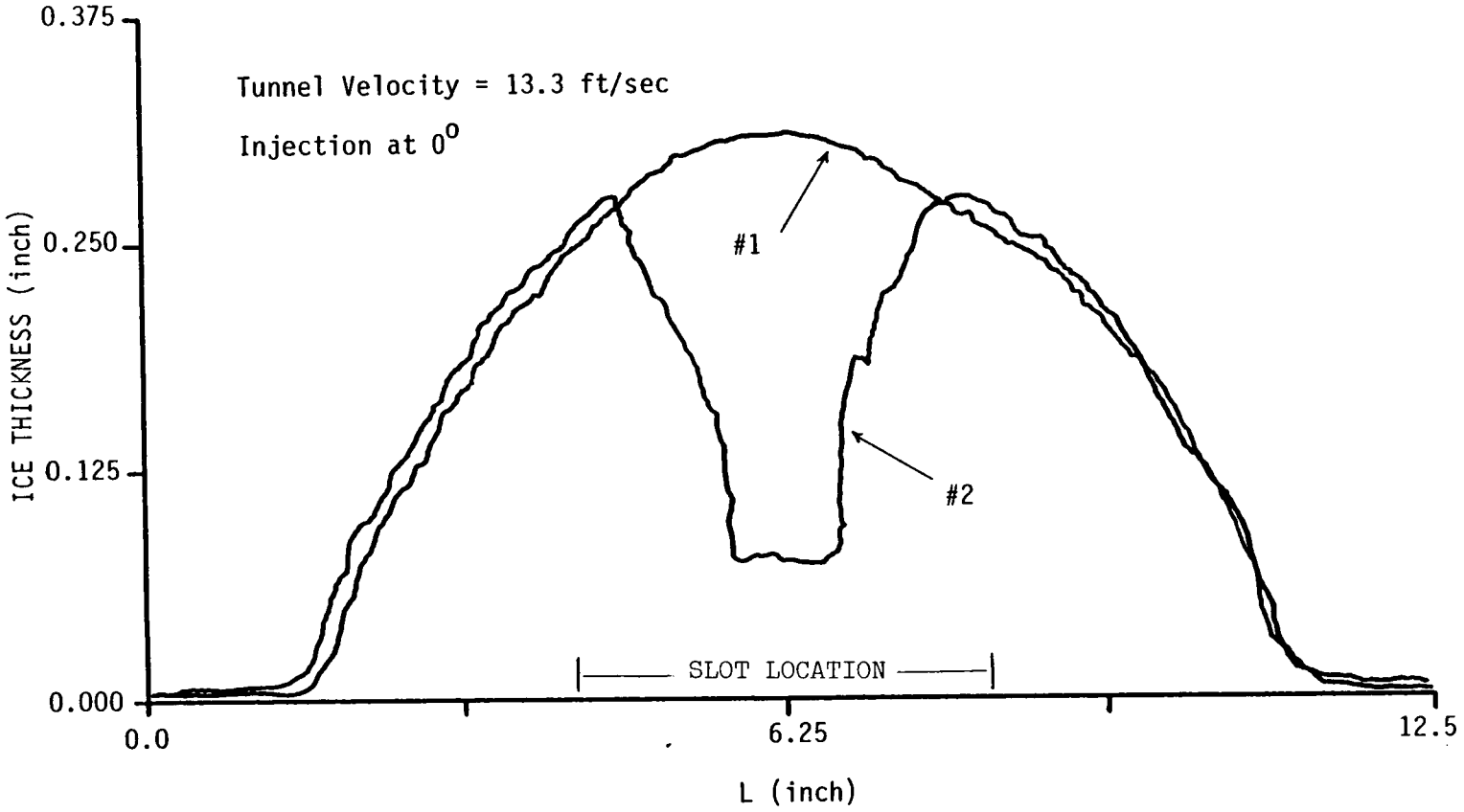


Figure VII-16. Axial Ice Profile Along the Cylinder at $\theta = +5^{\circ}$ From The Front Stagnation Point. Injection Rates Are: Curve #1 = 0; Curve #2 = 200 (ft^3/sec).

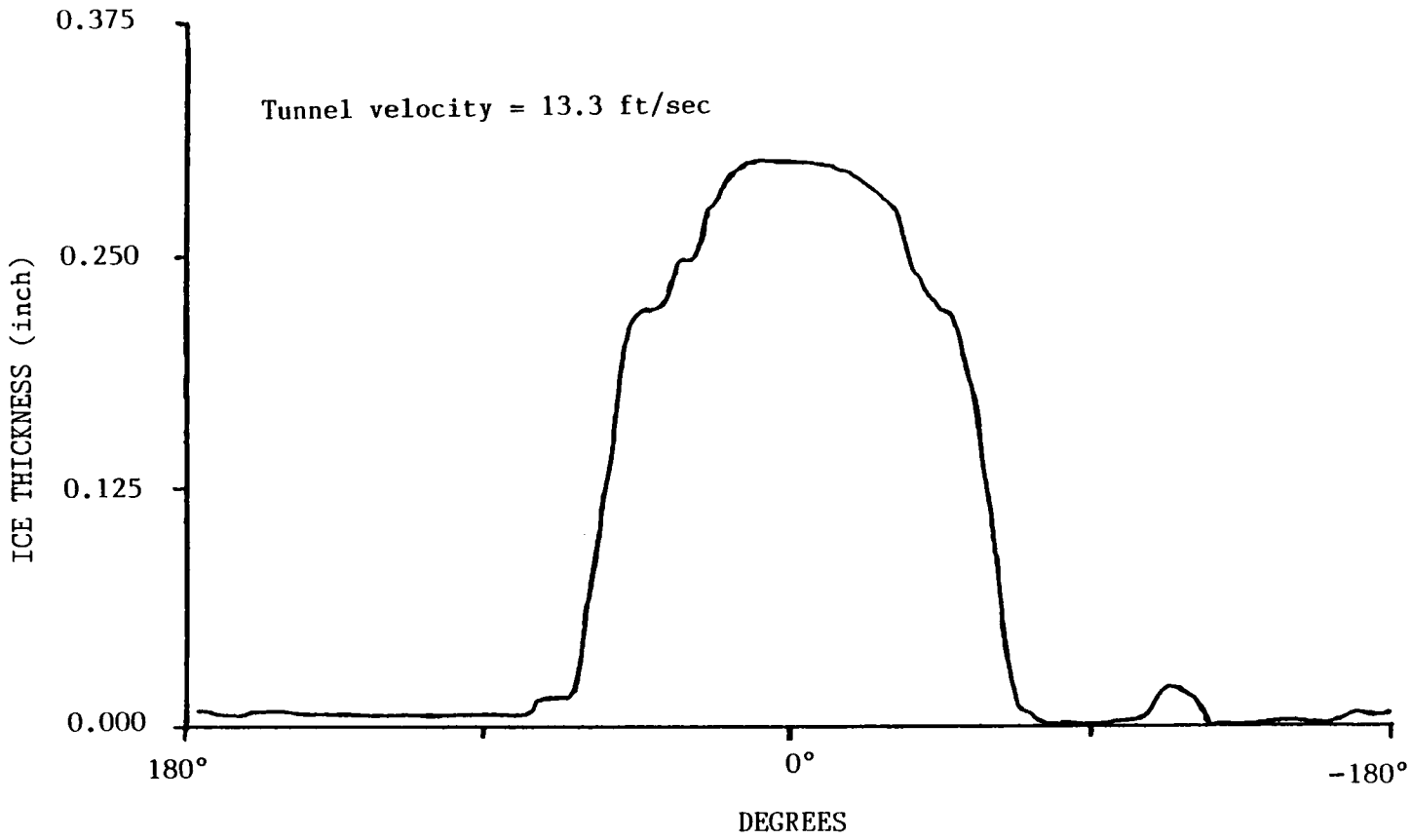


Figure VII-17. Angular Ice Profile Around the Cylinder at L = 6.25 inches.

than any other location on the model resulting in a parabolic shape as shown. The tabulated results of the icing tests are shown in Chapter VIII.

CHAPTER VIII

DISCUSSION OF RESULTS

In the following sections the results of icing tests performed in the tunnel are presented and a comparison is made with the prediction as described in Chapter IV. The effectiveness of the surface injection is discussed and conclusions are drawn.

The tunnel air velocities used in the experiments were 4.1, 6.3, 13.3, and 39 ft/sec. The total water mass injected into the tunnel was 2.025×10^{-3} lbm/sec which was kept constant for all tests. The liquid water content of the airstream for the above tunnel speeds vary from 0.07×10^{-3} to 0.63×10^{-3} lbm/ft^3, with results for all tests shown in Table K-1 in Appendix K. Experimental ice weights for a variety of surface injection rates, with injection slots located at +50, 0 and −50 degrees from the front stagnation line, are shown in Tables VIII-1 and VIII-2. Run times for all experiments was about 7 minutes (see Chapter VII, page 96 for details on the experimental procedure). A triple beam balance was utilized to obtain ice weights collected on the model (no measurable ice sublimation was noticed during weight measurements). Ice profiles were taken by a specially designed profilometer (see Figure VII-10, page 100 and Appendix L for details of the profilometer) and were shown in Figures VII-12 through VII-17, pages 105 through 111.

A reduction in collected ice weights were realized in all tests conducted when injection was used. It is important to keep in mind

Table VIII-1. Experimental Ice Weights Collected on the Model, Set No. 1.

Run[a]	Tunnel[b] Speed	Air injection flow rate[c]			Run[d] Time	Room Air Temp.[e]		Ice[f] weight
		Slot #1[g]	Slot #2	Slot #3		Dry Bulb	Wet Bulb	
1	6.3	0	0	0	7	66	56	14.75
2	6.3	25	25	25	7	70	55	13.00[h]
3	6.3	100	100	100	7	68	57	12.75
4	6.3	100	150	100	7	64	52	11.25
5	6.3	50	150	50	7	70	55	13.80
6	6.3	50	0	50	7	70	55	9.80
7	6.3	100	0	100	7	71	55	8.30
8	6.3	0	200	0	7	71	59	9.60
9	6.3	0	50	0	7	72	59	11.60
10	6.3	100	200	100	7	71	55	9.30

a(Test No.), b(ft/sec), c(ft^3/hr), d(minute), e(°F), f(grams), g(location of slots 1,2,3 are: +50, 0, −50 from the front stagnation point), h(slot clogging experienced)

Table VIII-2. Experimental Ice Weights Collected on the Model, Set No. 2.

Run[a]	Tunnel[b] Speed	Air injection flow rate[c]			Run[d] Time	Room Air Temp.[e]		Ice[f] weight
		Slot #1[g]	Slot #2	Slot #3		Dry Bulb	Wet Bulb	
1	13.3	0	0	0	7	70	53	22.63
2	13.3	100	100	100	7	70	51	19.00
3	13.3	0	200	0	7	70	52	20.80
4	13.3	100	200	100	7	80	65	22.00
5	13.3	100	0	100	7	80	65	21.30
6	13.3	50	150	50	7	80	65	21.60
1	39.0	0	0	0	7	68	53	42.30
2	39.0	100	200	100	7	70	54	40.30[h]
1	4.1	0	0	0	7	70	54	7.90
2	4.1	100	100	100	7	70	54	7.00

a(Test No.), b(ft/sec), c(ft^3/hr), d(minute), e(°F), f(grams), g(location of slots 1,2,3 are: +50, 0, −50 from the front stagnation point), h(water shedding and slot clogging)

that injection at the slots blocks the center core of the test section (jets are opposing the main flow), thereby causing a redistribution of the flow in the remaining region of the test section. Therefore, compared to the case of no injection, higher velocities were realized over the model when injection was taking place. The collection efficiency of the model is higher for a higher air velocity due to the increase in the inertia parameter (K) as was explained previously in Chapter VII and IV. Thus the ice weights obtained are generally higher than those obtained if the test section had been much larger, such that secondary injection effects were negligible. This implies that the flow in the test section is three dimensional.

The effect of room air humidity on the collected ice weight can be seen from the results of runs obtained with a tunnel velocity of 13.3 ft/sec. Run number 4, which corresponds to a higher injection rate than those in run 2 and 3, actually results in more ice collection than those in run 2 and 3. This increase in ice weight is due to the higher humidity of room air. From the dry bulb and wet bulb temperature data listed for each test in Tables VIII-1 and VIII-2 relative humidity for run number 2 and 3 is 20% and that of run number 4 is 45%. Thus ice weights of run 4, 5, and 6 cannot be directly compared with those of run 1, 2, and 3.

Some water shedding and slot clogging occured when a tunnel velocity of 39 ft/sec was used. Higher injection rates (higher than

200 ft^3/hr from the middle slot and $100ft^3/hr$ from the other two) were not possible with the particular set-up used.

Theoretical predictions of ice weights corresponding to the experiments conducted are given in Tables VIII-3 and VIII-4. In these tables two columns are given for the ice weight. The first column gives ice weight per foot of slot (slots were 4 inches long) and the second column gives total ice collected on the model, which includes both that on the section where slots are located and that on the remaining parts of the model. The total effective model length exposed to icing was 12.5 inches.

The overall ice collection reduces as slot flow rate increases as indicated by runs 1 to 3. The ice collection is predicted to be zero (run 5) with slot flow rates of 50, 150, and 50 ft^3/hr (corresponding to slots located at +50, 0, and −50 degrees). The same result is predicted if only the slot along the stagnation line is operating with 200 ft^3/hr flow rate (run 8). Results of other combinations of slot flow rates are also given.

The predicted and experimental ice weights are compared in Table VIII-5. It can be seen that, in general, there are very good agreements between the experimental and the predicted values. The percent difference ranging from 1.9 up to 35.4. Comparing the experimental values for the cases of surface injection with those of no surface injection, the reduction in the ice collection due to the injection appears to follow the pattern predicted by the theoretical analysis presented in Chapter IV, i.e. the effect of slot location as

Table VIII-3. Predicted Ice Weights Collected on the Model For 7 Minutes of Exposure, Set No. 1.

Run[a]	Tunnel[b] Speed	LWC[c] x 10^{+3}	Air flow rate (Q = q/RU)[d]			E[f]	Ice weight[g]	Total weight[h]
			Slot #1[e]	Slot #2	Slot #3			
1	6.3	0.41	0	0	0	0.320	12.712	13.242
2	6.3	0.41	0.0182	0.0182	0.0182	0.314	12.474	13.163
3	6.3	0.41	0.3277	0.3277	0.3277	0.187	7.429	11.481
4	6.3	0.41	0.3277	0.4916	0.3277	0	0	9.005
5	6.3	0.41	0.1639	0.4916	0.1639	0	0	9.005
6	6.3	0.41	0.1639	0	0.1639	0.305	12.116	13.043
7	6.3	0.41	0.3277	0	0.3277	0.290	11.521	12.845
8	6.3	0.41	0	0.6554	0	0	0	9.005
9	6.3	0.41	0	0.1639	0	0.275	10.925	12.646
10	6.3	0.41	0.3277	0.6554	0.3277	0	0	9.005

a(Test No.), b(ft/sec), c(liquid water content, lbm/ft^3), d(R = cylinder radius, and U_∞ is the free stream velocity-ft, ft/sec resp.), e(location: +50°, 0, −50°), f(collection efficiency), g(gm/ft), h(total ice weight on cylinder, gm), cylinder diameter = 31/32 inches, drop diameter = 45 micron.

Table VIII-4. Predicted Ice Weights Collected on the Model For 7 Minutes of Exposure, Set No. 2.

Run[a]	Tunnel[b] Speed	LWC[c] x 10^{+3}	Air flow rate (Q = q/RU)[d]			E[f]	Ice weight[g]	Total weight[h]
			Slot #1[e]	Slot #2	Slot #3			
1	13.3	0.19	0	0	0	0.500	19.433	20.242
2	13.3	0.19	0.155	0.155	0.155	0.433	16.829	19.374
3	13.3	0.19	0	0.310	0	0.441	17.140	19.478
4	13.3	0.19	0.155	0.310	0.155	0.407	15.818	19.037
5	13.3	0.19	0.155	0	0.155	0.460	17.878	19.724
6	13.3	0.19	0.078	0.233	0.078	0.439	17.062	19.452
1	39.0	0.07	0	0	0	0.705	29.601	30.834
2	39.0	0.07	0.053	0.106	0.053	0.683	26.800	29.901
1	4.1	0.63	0	0	0	0.216	8.581	8.939
2	4.1	0.63	0.504	0.504	0.504	0	0	6.078

a(Test No.), b(ft/sec), c(liquid water content, lbm/ft^3), d(R = cylinder radius, and U_∞ is the free stream velocity-ft, ft/sec resp.), e(location: +50°, 0, −50°), f(collection efficiency), g(gm/ft), h(total ice weight on cylinder, gm), cylinder diameter = 31/32 inches, drop diameter = 45 micron.

Table VIII-5. Percent Difference of Predicted and Experimental Ice Weights.

Run	Tunnel Velocity (ft/sec)	% difference
1	6.3	10.22
2	6.3	16.43
3	6.3	9.95
4	6.3	19.96
5	6.3	34.75
6	6.3	24.86
7	6.3	35.38
8	6.3	6.20
9	6.3	8.27
10	6.3	3.17
1	13.3	10.55
2	13.3	1.93
3	13.3	6.36
4	13.3	13.47
5	13.3	7.40
6	13.3	9.94
1	39.0	27.11
2	39.0	25.80
1	4.1	11.61
2	4.1	13.17

well as the slot flow rate. Comparison of the predicted ice weights and those obtained experimentally was rendered difficult for the following reasons. The theoretical model assumes that the flow is two-dimensional, as opposed to the velocity gradient that exists in the test section (along the model). As was mentioned earlier, slot injection increases the three-dimensionality of the flow in the test section. The ice accretion rate was influenced by the change in the room air conditions, i.e. room temperature and humidity, which were different for the tests conducted on different days. The effect of room air conditions as well as the effect of flow turbulence are not incorporated in the theoretical model. The slot flow velocity profile is not perfectly uniform, adding to the three-dimensionality of flow in the test section. Finally, the theoretical model utilizes a single droplet diameter in computation, which is clearly not the case in the spray droplet flow in the tunnel. Slots have different effects on different droplet size, i.e. larger droplets require stronger injection in order to be deflected.

In conclusion, however, it can be stated that experimental results do indicate a general reduction in ice due to slot injection. The performance can be enhanced if a more uniformly distributed droplet flow were produced with uniform droplet size. Also, a larger tunnel test section could reduce the three-dimensional effects. An increase in the number of slots could definitely improve performance. Finally, to eliminate the three-dimensional effects caused by

nonuniform axial velocity at the exit of slots, a porous model surface is favored.

With respect to the boundary layer effects on the collection efficiency the following was concluded. Firstly, in the case of no surface injection it was assumed that the presence of the boundary layer does not have an appreciable effect on the collection efficiency. This was explained by the fact that the displacement thickness (δ^*) was very small, e.g. δ^* is equal to 0.013R to 0.025R for a flow Reynolds number of 2463. The boundary layer thickness for the same cases was in the range of 0.025R to 0.05R. This assumption was substantiated by patching the boundary layer to the potential flow region outside the layer and tracking a droplet from the location $-10R$ away from the cylinder all the way to the point of impact on the cylinder. No appreciable change in the collection efficiency was noticed. It should be pointed out that even though the effect of laminar boundary layer on the collection efficiency is negligible, however, in a turbulent boundary layer flow the effect of boundary layer on the collection rate of droplets on the surface may be noticeable. The velocities in the boundary layer were determined by the method outlined in Chapter V. Secondly, in the case where fluid is blown into the boundary layer with a uniform velocity which is large compared to the velocities in the boundary layer, the skin friction decreases rapidly in the streamwise direction (see Figure V-7, page 65). The angle of separation becomes smaller with an increase in the blowing velocity. As shown in Figure V-7, the

boundary layer separates at about 52 degrees from the front stagnation point for the flow Reynolds number of 1000 when the surface injection velocity is $0.02U_\infty$. The entire boundary layer is detached from the surface and replaced by the injected fluid when the surface injection is larger than $0.5U_\infty$. The experimental investigation indicates that the flow rate through slots operating at a velocity of $0.5U_\infty$ is not sufficient to prevent droplets from impinging on the slot. In fact, at the velocities below approximately $7U_\infty$ slots clog up with ice due to water collection. Thus it can be seen that the boundary layer analysis, in the classical sense, is not applicable to the problem under consideration.

It is concluded that the method of Chapter IV, namely source and sink representation of the flow, is the most effective method for the type of analysis considered in this research. Ice weights predicted by this model for the case of no surface injection closely follow those obtained experimentally as shown in Figure VIII-1. The Attractiveness of this model is due to the following facts. Firstly, the effect of slot injection is best determined by studying a single droplet trajectory. Secondly, integration of the droplet trajectory equation by marching in time requires a knowledge of main stream velocities at the location of the droplet, which is an unknown before integration. Thus this particular model of the flow allows one to derive exact expressions for the velocities as a function of independent parameters. Free stream velocities thus can be

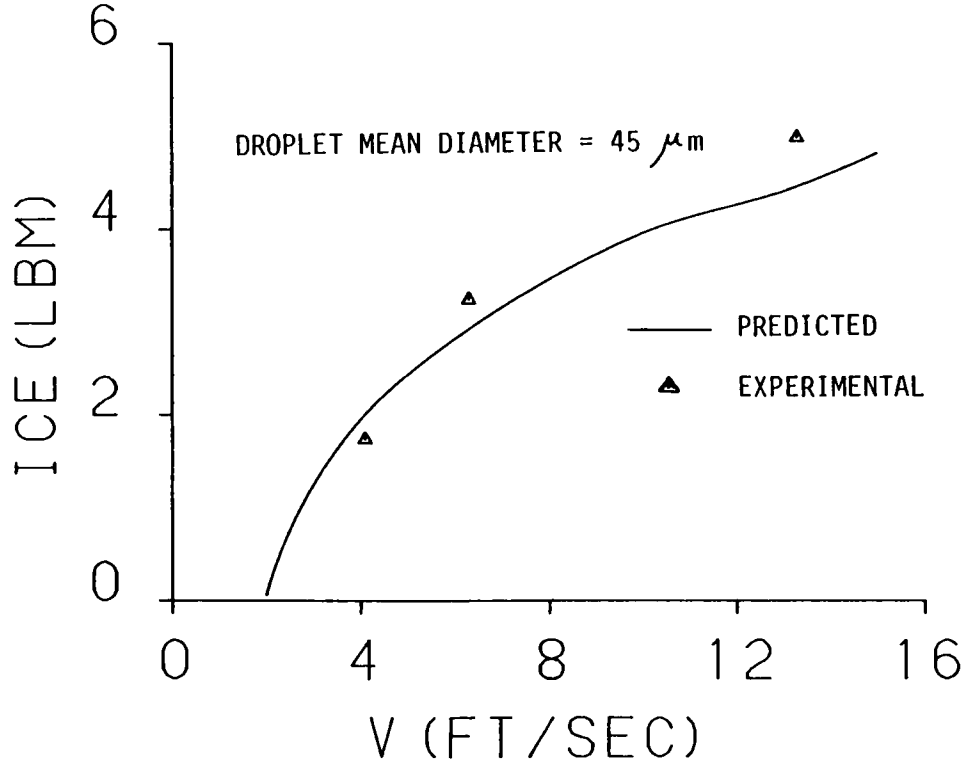


Figure VIII-1. Comparison of Theoretical and Experimental Ice Weights, No Surface Injection.

conveniently calculated wherever they are needed, in contrast to other types of modeling where velocities are calculated beforehand at preselected locations, i.e. grid points. Thus, free stream velocities corresponding to the location of the droplet may now be calculated by interpolating velocities in a particular grid cell, corresponding to the location of the droplet, which obviously is not exact. Additionally, when dealing with a general curvilinear mapped grid system, the droplet dynamics equations will also be transformed. However, to validate the source and sink model in Chapter VI a mapped numerical potential flow solution was obtained. It was shown that the stream function values obtained from the two methods were very close with a maximum difference of 15 percent. This provides confidence in the method of Chapter IV.

A viscous model of flow over a circular cylinder with surface injection was obtained and presented in Appendix M. The flow was considered to be incompressible, laminar, and steady. The momentum equations (Navier-Stokes equations in a polar coordinates) along with an artificial compressibility equation for the pressure were solved. The solution was carried out in a vectorial form using the method of Beam and Warming [52]. Due to the convergence problems at high Reynolds numbers and excessive computer time required for converged solution, only a solution for the Reynolds number of 32 was obtained. The computer CPU for this case was about 7 hours (done on the

DEC-10). Thus the cases for Reynolds numbers of interest (higher than 3000) were not considered. However, some of the results for the case of Re_o = 32 are given in Appendix M.

CHAPTER IX

CONCLUSIONS AND RECOMMENDATIONS

Conclusions

Discussion of the results presented in Chapter VIII leads to the following conclusions:

1 – The ice accretion rate on a surface is best predicted by considering the motion of individual droplets suspended in the flow.

2 – Boundary layer effects can be neglected with no appreciable loss of accuracy, but with substantial saving in the computational cost.

3 – A surface jet represented by a source results in a mathematically simple model for the entire flow, provides an exact expression for the velocity field, lowers the computational cost, and produces reasonably accurate results.

4 – A droplet in an icing environment could accurately be represented by a solid sphere.

5 – The use of a mean droplet size, representing the entire droplet size spectrum in the spray used flow, resulted in a very close prediction of the accreted ice weight.

6 – The reduction in the ice accretion rate on a surface due to slot injection is a function of the injection flow rate, the

location of the slot(s), as well as the number of slots on the surface.

7 – The ice weights predicted by the theoretical model follow the same trend as those experimentally measured.

8 – A qualitative comparison of the ice profiles obtained with and without surface injection supports the theoretical findings.

9 – The ice accretion rate is a function of the room air condition, the relative humidity of the airstream, and the redistribution of the flow in the test section due to the surface injection.

10 – The three dimensionality of the flow in a small test section affects the ice collection rate; the effect is especially pronounced when injection is taking place at the surface of the model.

11 – Finally, it can be claimed that air injection at the icing surface appears to be a quite effective anti-icing technique. However, the effect of injection on the aerodynamic characteristics of the icing surface should be studied if this technique is to be implemented.

Recommendations

The following is a list of the tasks that are suggested in order to further improve the performance of the proposed anti-icing system and provide a more accurate theoretical prediction:

1 – A closed circuit two-phase flow tunnel should be used to produce a saturated air which avoids evaporation of the droplets. Furthermore, tests under a variety of air conditions could also be conducted.

2 – A wind tunnel with a large test section allows the use of more spray nozzles which could produce a nearly uniform droplet distribution in the flow.

3 – Use a cooled air (−10 to −40 F) in the tunnel to simulate the atmospheric icing condition and the ice accretion process in particular. This eliminates the need for cooling the model from the inside in order to freeze the collected droplets.

4 – The injection slot(s) should extend along the entire length of the model to avoid the end effects that would be present if the slot(s) were extended only over a section of the model. This also makes it easier to compare the results of the injecting surface with those of a noninjecting surface.

5 – The effect of surface injection on the ice collection, as well as its effects on the lift and drag on a more realistic model, i.e. an airfoil, should be tested.

6 – Injection through a porous leading edge of an icing surface should be investigated both theoretically and experimentally.

7 – The theoretical model should include the effect of each droplet size present in the flow rather than a mean droplet size.

8 – A numerical model of the flow where the surface shape is changing with time, due to the ice deposition, should be obtained.

9 – The effect of turbulent boundary layer on the collection efficiency of the surface should be investigated.

BIBLIOGRAPHY

BIBLIOGRAPHY

1. Lake, H. B., and Bradley, J., "The Problem of Certifying Helicopters for Flight in Icing Conditions," Aeronautical Journal, Vol. 80, pp. 419-433 (1976).

2. Ashwood, P. F., and Swift, R. D., "Icing Trials on The Front Fuselage and Engine Intakes of Helicopters at Conditions Simulating Forward Flight," AGARD Advisory Report No. 127 (November 1978).

3. Brun, E. A., "Icing Problems and Recommended Solutions," AGARDograph No. 16 (November 1957).

4. Laschka, B., and Jesse, R., "Ice Accretion and Its Effects on Aerodynamics of Unprotected Aircraft Components," AGARD Advisory Report No. 127 (November 1978).

5. Jackson, W. E., "Proceedings of the Aircraft Icing Workshop," Department of the Air Force Document, unpublished (February 13-15, 1979).

6. Armand, C. et al., "Techniques and Facilities Used at the Onera Modane Center for Icing Tests," AGARD Advisory Report No. 127, (November 1978).

7. Messinger, B. L., "Equilibrium Temperature of an Unheated Icing Surface of Air Speed," Journal of Aeronautical Sciences, Vol. 20, pp. 29-42 (January 1953).

8. Keshock, E. G., et al., "Scaling Analysis of the Ice Accretion Process on Aircraft Surfaces," presented at the ASME Winter Annual Meeting, Phoenix, Arizona, Paper No. 82-WA/HT-39 (January 1982).

9. Nichols, C. C., "Ice Protection of Engine Air Inlet for Cruise Missile Applications," ASME paper No. 80-ENAs-2 (1980).

10. Kohlman, D. L., et al., "Icing Tunnel Tests of a Glycol-Exuding Porous Leading Edge Ice Protection System on a General Aviation Airfoil," AIAA paper No. AIAA-81-0405 (1981).

11. Horne, A. T., "Weeping Wings," Pilot, (January, 1984).

12. Hauger, H. H., "Intermittent Heating of Airfoils for Ice Protection, Utilizing Hot Air," ASME Paper No. 53-SA-42 (March 27, 1953).

13. Brun, R. J., et al., "Impingement of Cloud Droplets on a Cylinder and Procedure for Measuring Liquid-Water Content and Droplet Sizes in Supercooled Clouds by Rotating Multicylinder Method," NACA TN No. 1215 (1955).

14. Azzopardi, B. J., "Measurement of Drop Sizes," Int. Journal of Heat Mass Transfer, Vol. 22, pp. 1245-1279 (1979).

15. Kim, K. Y., and Marshall, W. R., "Drop-Size Distributions From Pneumatic Atomizers," AIChE Journal, Vol. 17, No. 3, pp. 575 (May 1971).

16. Schneider, J. M., "The Stability of Electrified Liquid Surfaces," A Ph.D. Dissertation, University of Illinois (1964).

17. Dabora, E. K., "Production of Monodisperse Sprays," The Review of Scientific Instruments, Vol. 38, No. 4 (April 1967).

18. Stallabrass, J. R., et al., "The Icing of an Unheated Non-Rotating Cylinder in Liquid Water Droplet-Ice Crystal Clouds," Report of the National Research Council of Canada (February 1979).

19. Goldstein, M. E., "Boundary Layer Analysis of Two Phase Gas/Liquid Flows Over an Oscillating Flat Plate and Over a Circular Cylinder," A Ph.D. Dissertation, University of Michigan-Ann Arbor (1965).

20. Hodgson, J. W., "Investigation of The Heat Transfer From An Isothermal Cylinder Exposed to Crossflow of a Water-Air Spray," A Ph.D. Dissertation, Georgia Institute of Technology (1967).

21. Spielman, L. A., "Particle Capture From Low-Speed Laminar Flows," Ann. Rev. Fluid Mech., Vol. 9, pp. 297-319 (1977).

22. Peyret, R., and Taylor, T. D., Computational Methods for Fluid Flow, Springer- Verlag, New York (1983).

23. Feiereisen, W., "A Numerical Study of Boundary Layer Injection as a Scale Control Method, " Lawrence Livermore Laboratory Report No. UCID-16909, (September 26, 1975).

24. Menguturk, M. and Sverdrup, E. F., "A Theory For Fine Particle Deposition in Two-Dimensional Boundary Layer Flows and Application to Gas Turbines," Journal of Engineering for Power, Vol. 104 (January, 1982).

25. Lindow, B., and Greber, I., "Similarity Solution For A Laminar, In Compressible Jet Flowing along a Curved Surface," AIAA Journal, Vol. 6, No. 7, (July, 1968).

26. Tennant, J. S., Johnson, W. S., and Keaton, D. D., "On The Calculation of Boundary Layers along Rotating Cylinders," Journal of Hydronautics, Vol. 11, No. 2 (April, 1977).

27. Cole, J. D., and Aroesty, J., "The Blowhard Problem - Inviscid Flows with Surface Injection," Int. Journal of Heat Mass Transfer, Vol. 11, pp. 1167-1183 (June, 1967).

28. Inger, G. R., and Gaitatzes, G. A., "Strong Bowing Into Supersonic Laminar Flows Around Two-Dimensional and Axisymmetric Bodies," AIAA Journal, Vol. 9, No. 3 (June, 1970).

29. Crowe, C. T., "Conservation Equations for Vapor-Droplet Flows Including Boundary-Droplet Effects," Lawrence Livermore Laboratory Report No. UC-66 (1976).

30. Bragg, M. B., et al., "Analytical Approach to Airfoil Icing," Paper 81-0403 presented at the AIAA Aerospace Sciences Meeting, St. Louis, Missouri (January 12-15, 1981).

31. Rubinow, S. I. and Keller, J. B., Journal of Fluid Mech., Vol. 11, pp. 447 (1961).

32. Saffman, P. G., Journal of Fluid Mech., Vol. 22, pp. 385 (1965).

33. Hinze, J. O., Turbulence, McGraw-Hill, New York (1975).

34. Glasser, D., et al., "Aspects of Mixer-Settler Design," Miner. Sci. Eng., Vol. 8, No. 1, pp. 23-45 (1976).

35. Neuringer, J. L., and Rosensweig, R. E., Phys. Fluids, Vol. 7, pp. 1927 (1964).

36. Ailam, G., and Gallily, I, Phys. Fluids Vol. 5, pp. 575 (1962).

37. Masters, K., Spray Drying Handbook, John Wiley Sons, New York (1979).

38. Crowe, C. T., and Sharma, M. P., "Numerical Modeling of Gas Particle Flows," Work shop notes, presented at the ASME Conference, New Orleans (March, 1981).

39. Cliffe, K. A., and Lever, D. A., "The Effect of Evaporation and Temperature-Dependent Fluid Properties on Droplet Drag Coefficients," Paper presented at the 22nd ASME/AIChE National Heat Transfer Conference, Niagra Falls, New York (August, 1984).

40. Lamb, S. H., Hydrodynamics, Dover Publications, New York (1945).

41. Zuber, N., and Ishii, M., "Drag Coefficient and Relative Velocity in Bubbly, Droplet or Particulate Flows," AIChE Journal, Vol. 25, No. 5 (September, 1979).

42. Bergrun, N. R., "A Method for Numerically Calculating the Area and Distribution of Water Impingement on the Leading Edge of an Airfoil in a Cloud," NACA TN No. 1397 (1947).

43. Milne-Thomson, L. M., Theoretical Hydrodynamics, The Macmillan Company, New York, 5th Ed. (1968).

44. Sparrow, E. M., and Yu, H. S., "Local Nonsimilarity Thermal Boundary Layer Solutions," Journal of Heat Transfer, TRANS. ASME, Series C., Vol. 93, pp. 328-334 (1971).

45. Minkowycz, W. J., and Sparrow, E. M., "Local Nonsimilarity Solutions for Natural Convection on a Vertical Cylinder," Journal of Heat Transfer, TRANS. ASME Paper No. 74-HT-Y (Auguts 13, 1973).

46. Nachtsheim, P. R., and Swigert, P., "Satisfaction of Asymptotic Boundary Conditions in Numerical Solution of Systems of Nonlinear Equations of Boundary-Layer Type," NACA TN No. D-3004 (1965).

47. Liu, T. M., and Nachtsheim, P. R., "On Numerical Methods to Impose Asymptotic Boundary Conditions of Boundary-Layer Equations," Computers and Fluids, Vol. 2, pp. 113-116 (1974).

48. Shampine, L. F., and Baca, L. S., "Fixed vs. Variable Order Runge-Kutta," Sandia Report No. 1410-UC-32 (1984).

49. Terrill, R. M., "Laminar Boundary Flow Near Separation With and Without Suction," Philosophical Transactions of the Royal Society of London, Series A, Vol. 253, No. 1022 (September, 1960).

50. Thompson, J. F., Thames, F. C., and Mastin, C. W., "Boundary-Fitted Curvilinear Coordinate Systems for Solution of Partial Differential Equations on Fields Containing Any Number of Arbitrary Two-Dimensional Bodies," NASA CR-2729 (1977).

51. White, J. W., "A General Mapping Procedure for Variable Area Duct Acoustics," AIAA Paper No. 81-0094, presented at AIAA 19th Aerospace Sciences Meeting, St. Louis, Missouri (January 12-15, 1981).

52. Beam, R. M., and Warming, R. F., "An Implicit Factored Scheme for Conservation Laws," SIAM-AMS Proceedings, Vol. 11, pp. 85-129 (1978).

53. Hetsroni, Gad, Handbook of Multiphase Systems, McGraw-Hill, New York (1982).

54. Takami, H., and Keller, H. B., "Steady Two-Dimensional Viscous Flow of an Incompressible Fluid Past a Circular Cylinder," Phys. Fluids, No. 5, Vol. 12 (1969).

APPENDICES

APPENDIX A

TWO-PHASE FLOW EFFECTS

In an air-liquid flow system effect of the liquid droplets on the air phase depends on the droplet loading which is defined by the ratio of the mass of droplets to the mass of air per unit volume. In a dilute flow system where the droplet loading is small (< 0.1), the effect of droplets on the air phase can be neglected [29]. It can also be shown that the ratio of the drag force acting on the air to that acting on the droplets is equal to the droplet loading [19], thus small loadings implies small drag force on the air. Using the following data

Droplet mass flow = 7.29 lbm/hr

Tunnel velocity = 10 ft/sec

Tunnel diameter = 12 inch

Droplet diameter = 45 microns

the droplet loading in the tunnel is equal to

$$Z = 0.003$$

The loading would be even smaller for a higher tunnel velocity. Droplet loading was less than 0.1 in all of the experiments conducted in connection with the icing tests.

The droplet motion is controlled by the air flow rather than droplet-droplet collision if [38]

$$\frac{\text{Aerodynamic Response Time}}{\text{Time Between Collisions}} \simeq Z \frac{Re_{o_d}}{10} << 1.0$$

$$Re_{o_d} = \frac{U_\infty d}{\nu_a} \qquad (A-1)$$

using the above data

$$Re_{o_d} = 8.20$$

then

$$Z \frac{Re_{o_d}}{10} = 0.0025 << 1.0$$

Furthermore the effect of the droplet wakes on each other can be neglected if the spacing between droplets is equal to or greater than 10 times the diameter of the droplet. Assuming that the droplet distribution in the flow field is uniform thus the droplet spacing in the flow can be calculated as follows

Air flow rate (Q) = 7.85 ft^3/sec

Water mass injected (m) = 7.29 lbm/hr

Droplet diameter (d) = 45 microns

Total droplet mass injected per unit time is

$$m_d = \frac{1}{6} \pi d^3 \rho_d N \tag{A-2}$$

where N is the number of droplets. The number of droplets per unit volume is then equal to

$$N_o = N/Q \tag{A-3}$$

For a unit control volume the number of droplets per unit length is

$$N_o^{\frac{1}{3}}$$

Thus the droplet spacing in the unit volume is

$$s/d = 49.2 > 10$$

Therefore, the effect of a droplet wake on the other droplets can be neglected. Based on the above discussion the two-phase flow effects were neglected in the present analysis.

APPENDIX B

EFFECT OF DROPLET EVAPORATION

The evaporation at the droplet surface may effect the dynamics of the droplet. The effect on the droplet dynamics is mainly due to the change in diameter and reduction in the drag force on the droplet.

Mass transfer rates from the droplet in an air under a relative velocity condition can be expressed as [37]

$$\frac{d(d)}{dt} = \frac{2h}{\rho_d h_{fg}} (T_a - T_{wet\ bulb}) \tag{B-1}$$

$$Nu = 2.0 + 0.493\, Re_d^{0.5}\, Pr^{0.33} \tag{B-2}$$

where:

$Nu = h\,d\,/\,k$

Re_d = Reynolds number = $\dfrac{d\left(\left| \bar{U}_a - \bar{U}_d \right| \right)}{\nu}$

Pr = Prandtl number = $\dfrac{\mu_a c_p}{\rho_a}$

$\Delta T = (T_a - T_{wet\ bulb})$

d = Droplet diameter

Equation (B-1) can be integrated in a stepwise manner over a small time interval (Δt) to obtain the change in the droplet diameter. It should be noted that during integration over Δt the droplet diameter is assumed to be constant. The above equation along with the droplet trajectory equation was integrated simultaneously and it was found that for the atmospheric icing condition the evaporation effects, i.e. diameter reduction is negligible due to the magnitude of the ΔT (flow is nearly saturated). The evaporation effects the drag coefficient of the droplet. The drag force on the droplet is reduced by surface injection (evaporation or burning). However, the reduction in drag is appreciable only if the surface injection rate is high. The high surface injection for evaporating droplets corresponds to the case of rapid burning. Thus, if the droplets are evaporating slowly, the reduction in the drag force can be considered to be very small [39]. The reduction in the drag coefficients due to surface injection at a droplet surface is shown in Figure B-1 (taken from reference [39]). It can be seen that the injection effect is substantial for large values of the blowing number, i.e. ratio of the injection velocity to the free stream velocity. In the present study the evaporation effects were considered to be negligible.

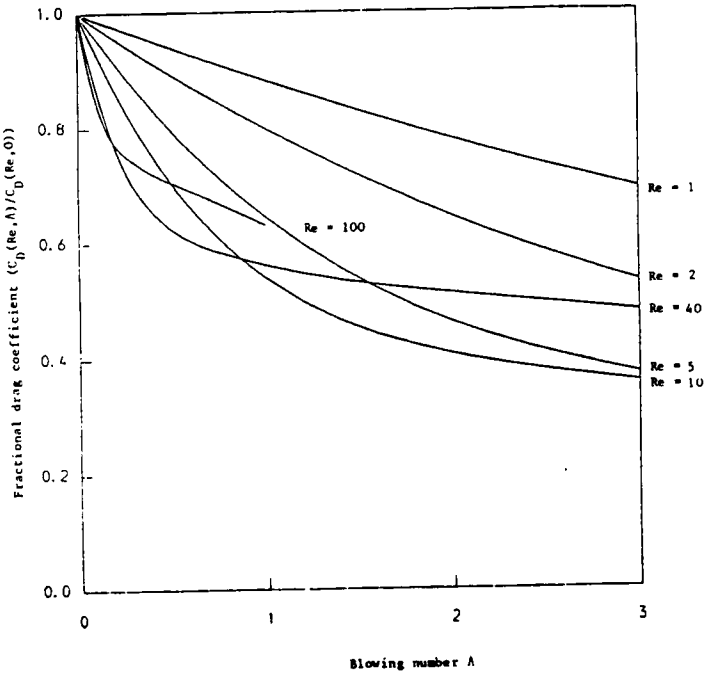


Figure B-1. The Drag Coefficient Divided By That in the Absence of Blowing as a Function of Blowing Number For Various Reynolds Number [39].

APPENDIX C

DROPLET DRAG COEFFICIENT

Circulation inside a droplet delays flow separation which reduces the drag force on the droplet. The drag reduction is due to the smaller vorticity on the surface which is causing the pressure drag and the skin friction to be reduced. Hetsroni [53] reports that for a small internal circulation, drag on a droplet follows closely drag on a solid sphere. He further presents the following limit

$$E\ddot{o} = \frac{g(\rho_d - \rho_a)d^2}{\sigma_d} < 0.4 \qquad (C\text{-}1)$$

$$Re_{o_d} = \frac{U_\infty d}{\nu} < 300 \qquad (C\text{-}2)$$

where $E\ddot{o}$ is the Eötvos number, d, and σ_d are the droplet diameter and the interfacial surface tension respectively. For a 100 micron water droplet, $E\ddot{o}$ is equal to 0.0014 which is well below the limit given above. Thus use of the drag coefficient of a solid sphere in the place of that of a droplet is justified. All the calculations in the present study were done based on the experimental drag coefficient of a solid sphere. These coefficients are presented in Table C-1.

Table C-1. Experimental Drag Coefficient of Solid Sphere [42].

R	$\frac{C_D R}{24}$	R	$\frac{C_D R}{24}$
0.00	1.00	200	6.52
.05	1.009	250	7.38
.1	1.013	300	8.26
.2	1.037	350	9.00
.4	1.073	400	9.82
.6	1.103	500	11.46
.8	1.142	600	12.97
1.0	1.176	800	15.81
1.2	1.201	1000	18.62
1.4	1.225	1200	21.3
1.6	1.246	1400	24.0
1.8	1.267	1600	26.9
2.0	1.285	1800	29.8
2.5	1.332	2000	32.7
3.0	1.374	2500	40.4
3.5	1.412	3000	47.8
4.	1.447	3500	55.6
5.	1.513	4000	63.7
6.	1.572	5000	80.0
8.	1.678	6000	96.8
10.	1.782	8000	130.6
12.	1.901	10000	166.3
14.	2.009	12000	204.
16.	2.109	14000	243.
18.	2.198	16000	285.
20.	2.291	18000	325.
25.	2.489	20000	365.
30.	2.673	25000	470.
35.	2.851	30000	574.
40.	3.013	35000	674.
50.	3.327	40000	778.
60.	3.60	50000	980.
80.	4.11	60000	1175.
100.	4.59	80000	1552.
120.	5.01	10^5	1905.
140.	5.40	1.2×10^5	2234.
160.	5.76	1.4×10^5	2549.
180.	6.16	1.6×10^5	2851.

APPENDIX D

DERIVATION OF THE TRAJECTORY EQUATION

The droplet dynamics equation is obtained by the application of Newton's second law. For a droplet suspended in the air with a relative velocity the trajectory equation has the form of

$$m_d(\bar{S})_{tt} = \bar{F}_g + \bar{F}_a + \bar{F}_d \tag{D-1}$$

where $\bar{F}_g$, $\bar{F}_a$, and $\bar{F}_d$ are the gravity, apparent mass, and the drag force respectively. $\bar{S}$ is the coordinate vector defined in Figure III-1, page 19. Substituting the corresponding expressions

$$m_d(\bar{U}_d)_t = \frac{4}{3}\pi\frac{d^3}{8}(\rho_d - \rho_a)\bar{g} + \frac{1}{2}\frac{\pi}{6}d^3\rho_a\left[(\bar{U}_a)_t - (\bar{U}_d)_t\right]$$

$$+ \frac{1}{8}\pi d^2\rho_a C_D \left|\bar{U}_a - \bar{U}_d\right|(\bar{U}_a - \bar{U}_d) \tag{D-2}$$

assuming $(U_a)_t = 0$, and rearranging

$$(\bar{U}_d)_t = \frac{2(\rho_d - \rho_a)}{(2\rho_d + \rho_a)}\bar{g} + \frac{3}{2}\frac{1}{d}\frac{\rho_a C_D}{(2\rho_d + \rho_a)}\left|\bar{U}_a - \bar{U}_d\right|(\bar{U}_a - \bar{U}_d) \tag{D-3}$$

for $\rho_d >> \rho_a$ then Equation (D-3) after nondimesionalizing becomes

$$\ddot{\bar{S}}^* = \frac{1}{Fr^2}\frac{\bar{g}}{g} + \frac{C_D Re_d}{24K}(\bar{U}_a^* - \dot{\bar{S}}^*) \qquad (D\text{-}4)$$

where:

$$Re_d = \frac{\rho_a d}{\mu_a}\left|\bar{U}_a - \bar{U}_d\right|$$

where:

$$\bar{S}^* = \bar{S}/R$$

$$t^* = tU_\infty/R$$

$$\bar{U}_a^* = \bar{U}_a/U_\infty$$

$$\dot{\bar{S}}^* = \bar{U}_d^* = d\bar{S}^*/dt^*$$

$$\ddot{\bar{S}}^* = (\dot{\bar{S}}^*)_{t^*}$$

Fr = Froude number $= U_\infty/(Rg)^{\frac{1}{2}}$

K = Inertia parameter $= \rho_d d^2 U_\infty/9D\mu_a$

R = Cylinder radius $(D/2)$ (D-5)

The aerodynamic response time and the residence time of a droplet is expressed as

$$\tau_A = \rho_d d^2/18 \qquad \text{(aerodynamic response time)} \qquad (D\text{-}6)$$

$$\tau_R = R/U_\infty \qquad \text{(residence time)} \qquad \text{(D-7)}$$

Thus the inertia parameter can be expressed as

$$K = \tau_A/\tau_R \qquad \text{(D-8)}$$

Equation (D-4) was used to obtain the droplet trajectories by integrating it in both the x and y directions. The modified Euler integration scheme was utilized for the integration procedure.

APPENDIX E

SOURCE AND SINK MODEL OF A FLOW OVER A CIRCULAR CYLINDER WITH SURFACE INJECTION

Uniform flow over a circular cylinder with surface mass transfer was modeled theoretically using the potential flow approximation. The entire flow was represented by a series of sources and sinks. To model the effects of slots on the flow it is helpful to first consider the potential flow model of a source outside a cylinder. The model consists of a source located outside the cylinder, an image source located inside the cylinder at the inverse point, a sink at the center of the cylinder and a doublet representing the cylinder as shown in Figure E-1. It can be seen that as the outside source approaches the cylinder the image source moves away from the center and finally both the source and its image come together at the cylinder surface. Thus a slot on a cylinder can be modeled by a source at the same location and a sink with half the strength of the source located at the center of the cylinder. Therefore the potential flow model of a uniform flow past a circular cylinder with surface injection consists of the following:

1 - A uniform flow

2 - Source(s) on the cylinder

3 - Sink(s) with half the strength of sources at the center of the cylinder

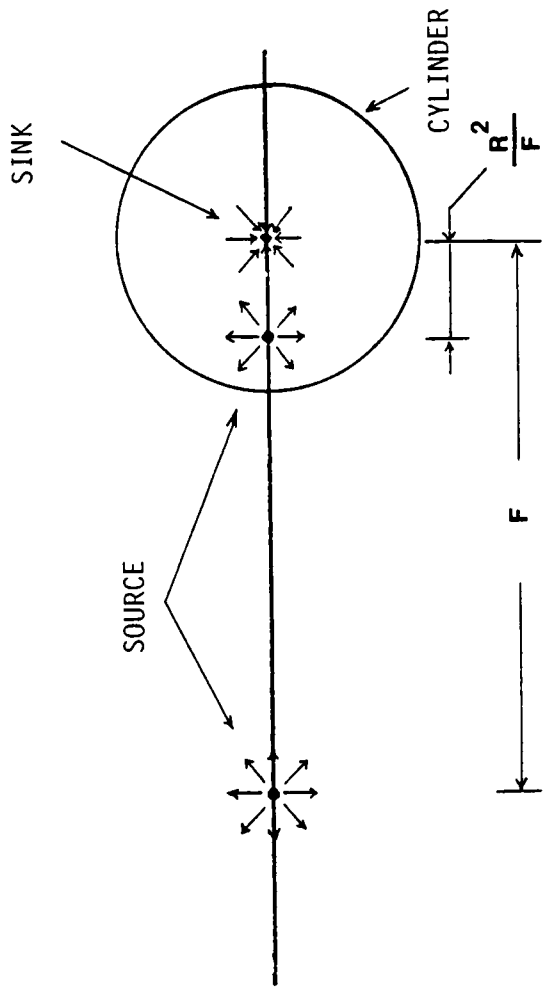


Figure E-1. Potential Flow Model of a Source Near a Cylinder.

4 - A doublet

The potential and stream function for the flow can now be obtained by adding the potential and stream functions of the items 1 through 4 listed above.

APPENDIX F

1-EQUATION MODEL OF LOCAL NONSIMILARITY AND SOLUTION PROCEDURE

The transformed boundary layer equation in ξ, η coordinate is

$$(f''' + ff'') + \beta(1 - f'^2) + \gamma f'' = 2\xi(f'_\xi f' - f_\xi f'') \tag{F-1}$$

where:

$$\beta = \frac{2\cos(x/R)}{1 + \cos(x/R)}$$

$$\gamma = \frac{-Re_o^{\frac{1}{2}}\left[1 - \cos(x/R)\right]^{\frac{1}{2}}}{\sin(x/R)}\left(\frac{V_w}{U_\infty}\right)$$

$$\xi = 2\left[1 - \cos(x/R)\right]$$

$$Re_o = \frac{RU_\infty}{\nu}$$

$V_w < 0$ Suction

$V_w > 0$ Injection (F-2)

Local similarity solution or 1-equation local similarity solution of Equation (F-1) could be obtained if one assumes that

$$\xi\frac{\partial}{\partial\xi}[\quad] \sim 0 \tag{F-3}$$

The above assumption is justified if ξ or $\partial/\partial\xi$ is small. Using Equation (F-3), boundary conditions for Equation (F-1) become:

$$\begin{aligned} \eta = 0 \qquad & f'(\xi,0) = 0 \\ \eta = 0 \qquad & f(\xi,0) = 0 \\ \eta = \infty \qquad & f'(\xi,\infty) = 1.0 \end{aligned} \tag{F-4}$$

Solution Procedure

The method of Nachtsheim and Swigert [46] is used in conjunction with the 4th order Runge-Kutta integration scheme with variable step size. Equation (F-1) (with right hand side deleted) was integrated along with the boundary conditions given in Equations (F-4) and

$$f''(\xi,0) = x \tag{F-5}$$

$$f''(\xi,\eta_{max}) = 0.0 \tag{F-6}$$

where x is the initial guess for the wall shear and Equation (F-6) is the asymptotic condition at η_{max}, η_{max} is an assumed value of the boundary layer thickness. Then, integrating the above along η from $\eta = 0$ to $\eta = \eta_{max}$ the $f'(\xi,\eta_{max})$ and $f''(\xi,\eta_{max})$ were calculated. With these values the correction to the initial guess (x) was made as follows.

$$1 = f'(\xi,\eta_{max}) + \Delta x\, f'_x(\xi,\eta_{max})$$

$$0 = f''(\xi,\eta_{max}) + \Delta x\, f''_x(\xi,\eta_{max}) \qquad \text{(F-7)}$$

The correction for x, i.e. Δx, was calculated from Equation (F-7). However, since there are two equations and only one unknown thus a least square solution is required. The least square solution was obtained as

$$r_1 = f'(\xi,\eta_{max}) - 1.0 + \Delta x\, f'_x(\xi,\eta_{max})$$

$$r_2 = f''(\xi,\eta_{max}) + \Delta x\, f''_x(\xi,\eta_{max})$$

$$\sum_i (r_i)^2 = \text{minimum}$$

$$\sum_{i=1}^{n} r_i \frac{\partial r_i}{\partial c_k} = 0, \quad k = 1, m \qquad \text{(F-8)}$$

where m is the number of unknowns, n is the number of equations, and c_k is the unknowns, i.e. $c_1 = \Delta x$. In this problem since there is only one unknown (Δx) then

$$\Delta x = \frac{-f'_x(f' - 1) - f'' f''_x}{f'^2_x + f''^2_x} \qquad \text{(F-9)}$$

If the value of Δx is greater than a small value, i.e. $\Delta x > \varepsilon(10^{-4})$, then the integation should be repeated from $\eta = 0$ to η_{max} until $\Delta x \leq \varepsilon$. Finally, the following condition was imposed on the solution at $\eta = \eta_{max}$

$$E = (f' - 1)^2 + (f'')^2 \qquad \text{(F-10)}$$

If $E > \varepsilon$ then the assumed value for the η_{max} was adjusted as $\eta_{max} = \eta_{max} + \Delta\eta$ and once again the integration was repeated until both E and Δx were less than $\varepsilon(10^{-4})$. This completes the boundary layer solution at a particular ξ or x. The integration was actually performed on a set of first order ordinary differential equations which were obtained from the boundary layer equation, i.e. Equation (F-1) with the right hand side set equal to zero. These first order ODE's are listed in the following Table F-1 along with the initial values and derivatives which are required by the integration scheme.

Table F-1. First Order Equations For 1-Equation Model

1st Order ODE	Initial Values at $\eta = 0$	1st Derivative
$S(1) = f$	0	$S'(1) = S(2)$
$S(2) = f'$	0	$S'(2) = S(3)$
$S(3) = f''$	x	$S'(3)$ = from equation (F-1)
$S(4) = f_x$	0	$S'(4) = S(5)$
$S(5) = f'_x$	0	$S'(5) = S(6)$
$S(6) = f''_x$	1.0	$S'(6)$ = from $\partial/\partial x$ (F-1)

APPENDIX G

2-EQUATION MODEL OF LOCAL NONSIMILARITY AND SOLUTION PROCEDURE

Recall the boundary layer equation from Appendix F Equation (F-1)

$$(f''' + ff'') + \beta(1 - f'^2) + \gamma f'' = 2\xi(f'_\xi f' - f_\xi f'') \tag{G-1}$$

with boundary conditions

$$\begin{aligned} &\eta = 0 \qquad f'(\xi,0) = 0 \\ &\eta = 0 \qquad f(\xi,0) + 2\xi f_\xi(\xi,0) = 0 \\ &\eta = \infty \qquad f'(\xi,\infty) = 1.0 \end{aligned} \tag{G-2}$$

The two equation model was obtained by differentiating Equation (G-1) and its boundary conditions with respect to ξ and defining the following

$$\begin{aligned} &g = f_\xi \qquad g' = f'_\xi \\ &g'' = f''_\xi \qquad g''' = f'''_\xi \end{aligned} \tag{G-3}$$

then the resulting equation is

$$g''' + fg'' + f''g - 2\beta f'g' + \gamma g'' + (1 - f'^2)\beta_\xi + \gamma_\xi f'' - 2(g'f' - gf'') =$$

$$+2\xi(g'^2 + f'g_\xi' - g_\xi f'' - gg'') \tag{G-4}$$

The boundary conditions are

$$\begin{aligned}
&\eta = 0 \qquad f'(\xi,0) = 0 \\
&\eta = 0 \qquad 3g(\xi,0) + 2\xi(f_\xi)_\xi = 0 \\
&\eta = 0 \qquad g'(\xi,0) = 0 \\
&\eta = 0 \qquad f(\xi,0) + 2\xi f_\xi(\xi,0) = 0 \\
&\eta = \infty \qquad f'(\xi,\infty) = 1.0 \\
&\eta = \infty \qquad g'(\xi,\infty) = 0
\end{aligned} \tag{G-5}$$

Once again assuming that g_ξ and g'_ξ are small then they can be neglected. These terms were also deleted from the boundary conditions, Equations (G-5). The resulting equations are the 2-equation model of the local nonsimilarity.

Solution Procedure

The procedure presented in Appendix F was used to solve the 2-equation model except that now an initial guess for the function (g") should also be provided. In addition, the asymptotic condition for the $g''(\xi,\eta_{max})$ is also required. Then

$$\eta = 0 \qquad f''(\xi,0) = x$$

$$\eta = 0 \qquad g''(\xi,0) = y \tag{G-6}$$

$$\eta = \eta_{max} \qquad f''(\xi,\eta_{max}) = 0.0$$

$$\eta = \eta_{max} \qquad g''(\xi,\eta_{max}) = 0.0 \tag{G-7}$$

The corrections for x and y were calculated from the following

$$1 = f'(\xi,\eta_{max}) + \Delta x\, f'_x(\xi,\eta_{max}) + \Delta y\, f'_y(\xi,\eta_{max})$$

$$0 = f''(\xi,\eta_{max}) + \Delta x\, f''_x(\xi,\eta_{max}) + \Delta y\, f''_y(\xi,\eta_{max})$$

$$0 = g'(\xi,\eta_{max}) + \Delta x\, g'_x(\xi,\eta_{max}) + \Delta y\, g'_y(\xi,\eta_{max})$$

$$0 = g''(\xi,\eta_{max}) + \Delta x\, g''_x(\xi,\eta_{max}) + \Delta y\, f''_y(\xi,\eta_{max}) \tag{G-8}$$

Once again since there are 4 equations but only two unknowns, a least square solution is needed to obtain Δx and Δy. Table G-1 presents the listing of the first order ODE's which were used in the integration. These equations were obtained from Equations (G-1) and (G-4).

Table G-1. First Order Equations For 2-Equation Model

1st Order ODE	Initial Values at $\eta = 0$	1st Derivative
$S(1) = f$	0	$S'(1) = S(2)$
$S(2) = f'$	0	$S'(2) = S(3)$
$S(3) = f''$	x	$S'(3)$ = from equation (G-1)
$S(4) = f_x$	0	$S'(4) = S(5)$
$S(5) = f'_x$	0	$S'(5) = S(6)$
$S(6) = f''_x$	1.0	$S'(6)$ = from $\partial/\partial x$ (G-1)
$S(7) = f_y$	0	$S'(7) = S(8)$
$S(8) = f'_y$	0	$S'(8) = S(9)$
$S(9) = f''_y$	0	$S'(9)$ = from $\partial/\partial y$ (G-1)
$S(10) = g$	0	$S'(10) = S(11)$
$S(11) = g'$	0	$S'(11) = S(12)$
$S(12) = g''$	y	$S'(12)$ = from equation (G-4)
$S(13) = g_x$	0	$S'(13) = S(14)$
$S(14) = g'_x$	0	$S'(14) = S(15)$
$S(15) = g''_x$	0	$S'(15)$ = from $\partial/\partial x$ (G-4)
$S(16) = g_y$	0	$S'(16) = S(17)$
$S(17) = g'_y$	0	$S'(17) = S(18)$
$S(18) = g''_y$	1.0	$S'(18)$ = from $\partial/\partial y$ (G-4)

APPENDIX H

3-EQUATION MODEL OF LOCAL NONSIMILARITY AND SOLUTION PROCEDURE

The 3-equation model was obtained by differentiating Equation (G-4) in Appendix G with respect to ξ. Then by defining the following

$$h = g_\xi \qquad h' = g'_\xi$$

$$h'' = g''_\xi \qquad h''' = g'''_\xi \tag{H-1}$$

and deleting terms h_ξ, h'_ξ, and h''_ξ the 3-equation model of local nonsimilarity takes the form of

$$h''' + (6g + 2\gamma_\xi)g'' + (-2\beta g' - 4g' - 4\beta_\xi f')g'$$

$$+ (f + \gamma)h'' + 5f''h - (4 + 2\beta)f'h'$$

$$+ (1 - f'^2)\beta_{\xi\xi} + \gamma_{\xi\xi} f'' = 0 \tag{H-2}$$

and the corresponding boundary conditions are

$$\eta = 0 \qquad f'(\xi,0) = 0$$

$$\eta = 0 \qquad g'(\xi,0) = 0$$

$$\eta = 0 \qquad h'(\xi,0) = 0$$

$$\eta = 0 \qquad f(\xi,0) + 2\xi g(\xi,0) = 0$$

$$\eta = 0 \qquad 3g(\xi,0) + 2\xi h(\xi,0) = 0$$

$$\eta = 0 \qquad 5h(\xi,0) = 0$$

$$\eta = \infty \qquad f'(\xi,\infty) = 1.0$$

$$\eta = \infty \qquad g'(\xi,\infty) = 0.0$$

$$\eta = \infty \qquad h'(\xi,\infty) = 0.0 \qquad \text{(H-3)}$$

Solution Procedure

The procedure presented in Appendix F and G was used to solve the 3-equation model. However, in this case there are three unknown functions, i.e. f, g, and h, that were needed to be evaluated. The initial guesses at η = 0 and the asymptotic conditions for this case are

$$\eta = 0 \qquad f''(\xi,0) = x$$

$$\eta = 0 \qquad g''(\xi,0) = y$$

$$\eta = 0 \qquad h''(\xi,0) = z \qquad \text{(H-4)}$$

$$\eta = \eta_{max} \qquad f''(\xi,\eta_{max}) = 0$$

$$\eta = \eta_{max} \qquad g''(\xi,\eta_{max}) = 0$$

$$\eta = \eta_{max} \qquad h''(\xi,\eta_{max}) = 0 \tag{H-5}$$

The corrections to the x, y, and z were calculated from the least square solution of the following

$$1 = f' + \Delta x\, f'_x + \Delta y\, f'_y + \Delta z\, f'_z$$

$$0 = f'' + \Delta x\, f''_x + \Delta y\, f''_y + \Delta z\, f''_z$$

$$0 = g' + \Delta x\, g'_x + \Delta y\, g'_y + \Delta z\, g'_z$$

$$0 = g'' + \Delta x\, g''_x + \Delta y\, g''_y + \Delta z\, g''_z$$

$$0 = h' + \Delta x\, h'_x + \Delta y\, h'_y + \Delta z\, h'_z$$

$$0 = h'' + \Delta x\, h''_x + \Delta y\, h''_y + \Delta z\, h''_z \tag{H-6}$$

Once again Equations (G-1) and (G-4) (see Appendix G) and Equation (H-2) were written in terms of first order ODEs and integrated as discussed in Appendix G. Table H-1 presents the ODEs used in the integration.

Table H-1. First Order Equations For 3-Equation Model

1st Order ODE	Initial Values at $\eta = 0$	1st Derivative
$S(1) = f$	0	$S'(1) = S(2)$
$S(2) = f'$	0	$S'(2) = S(3)$
$S(3) = f''$	x	$S'(3)$ = from equation (G-1)
$S(4) = f_x$	0	$S'(4) = S(5)$
$S(5) = f'_x$	0	$S'(5) = S(6)$
$S(6) = f''_x$	1.0	$S'(6)$ = from $\partial/\partial x$ (G-1)
$S(7) = f_y$	0	$S'(7) = S(8)$
$S(8) = f'_y$	0	$S'(8) = S(9)$
$S(9) = f''_y$	0	$S'(9)$ = from $\partial/\partial y$ (G-1)
$S(10) = f_z$	0	$S'(10) = S(11)$
$S(11) = f'_z$	0	$S'(11) = S(12)$
$S(12) = f''_z$	0	$S'(12)$ = from $\partial/\partial z$ (G-1)
$S(13) = g$	0	$S'(13) = S(14)$
$S(14) = g'$	0	$S'(14) = S(15)$
$S(15) = g''$	y	$S'(15)$ = from equation (G-4)
$S(16) = g_x$	0	$S'(16) = S(17)$
$S(17) = g'_x$	0	$S'(17) = S(18)$
$S(18) = g''_x$	0	$S'(18)$ = from $\partial/\partial x$ (G-4)

Table H-1 (cont.)

1st Order ODE	Initial Values at $\eta = 0$	1st Derivative
$S(19) = g_y$	0	$S'(19) = S(20)$
$S(20) = g'_y$	0	$S'(20) = S(21)$
$S(21) = g''_y$	1.0	$S'(21) =$ from $\partial/\partial y$ (G-4)
$S(22) = g_z$	0	$S'(22) = S(23)$
$S(23) = g'_z$	0	$S'(23) = S(24)$
$S(24) = g''_z$	0	$S'(24) =$ from $\partial/\partial z$ (G-4)
$S(25) = h$	0	$S'(25) = S(26)$
$S(26) = h'$	0	$S'(26) = S(27)$
$S(27) = h''$	z	$S'(27) =$ from equation (H-2)
$S(28) = h_x$	0	$S'(28) = S(29)$
$S(29) = h'_x$	0	$S'(29) = S(30)$
$S(30) = h''_x$	0	$S'(30) =$ from $\partial/\partial x$ (H-2)
$S(31) = h_y$	0	$S'(31) = S(32)$
$S(32) = h'_y$	0	$S'(32) = S(33)$
$S(33) = h''_y$	0	$S'(33) =$ from $\partial/\partial y$ (H-2)
$S(34) = h_z$	0	$S'(34) = S(35)$
$S(35) = h'_z$	0	$S'(35) = S(36)$
$S(36) = h''_z$	1.0	$S'(36) =$ from $\partial/\partial z$ (H-2)

APPENDIX I

GRID MAPPING EQUATIONS AND PROCEDURE

General grid transformation technique presented in this appendix is based on the procedure developed by Thompson [50]. Before describing the mapping technique it is worth while to explain some of the reasons for mapping a coordinate system. Most often in numerical computations it is desired to concentrate a greater number of grid points in the region of steep gradients, e.g. in a boundary layer etc., this of course, gives rise to a nonuniform grid system for which the discritized equations become rather complex. In addition, some times due to the irregular geometries involved in a given problem satisfying the necessary boundary conditions is very difficult if not impossible. Thus it is desirable to find an alternate coordinate system and perform all the computation in that plane instead of the physical plane. Such an alternate coordinate system is, ideally, a cartesian coordinate system where grid lines are equally spaced. The question that now remains is how one can identify the particular cartesian coordinate system that corresponds to the actual physical plane. For very simple geometries, however, one can derive the exact relationship for the transformations based on the conformal mapping technique. However, even though transformation from a physical plane onto a cartesian coordiante is possible with these analytical expression, in general, equal grid spacing is not guaranteed. Thus a general grid mapping technique is

desired to satisfy all of the above concerns. The method outlined below is based on a procedure which numerically generates mapped grid coordinates. While the boundary grid points may be placed arbitrary in the physical plane, the mapping locates them equally spaced on the corresponding segments in the transformed plane. This important feature of the mapping technique can allow a greater number of points around the regions of interest in the physical plane and lesser number of points in the regions where changes in dependent parameters are small or gradual. The computation can now be performed over the uniformally spaced grid in the transformed plane where the finite differencing approximations can be used with high degree of accuracy. Each point on the rectangular plane corresponds to a point on the physical plane which is not known beforehand except the boundary points. The locations of the interior points in the physical plane are obtained by solving the mapping equations presented below. The system of elliptic partial differential equations defining the mapping is the following

$$\nabla^2 \xi = P(\xi,\eta)$$

$$\nabla^2 \eta = Q(\xi,\eta) \qquad \text{(I-1)}$$

where ξ, and η are the coordinate system in the transformed plane corresponding to the x, and y in the physical plane. Parameters $P(\xi,\eta)$, and $Q(\xi,\eta)$ are the grid control terms which are used to control interior grid spacing and shapes. The variables in Equation (I-1) can be interchanged using

$$f_\xi = f_x X_\xi + f_y Y_\xi$$

$$f_\eta = f_x X_\eta + f_y Y_\eta \qquad \text{(I-2)}$$

Equations (I-2) are then solved for f_x and f_y to give

$$f_x = (f_\xi Y_\eta - f_\eta Y_\xi)/J$$

$$f_y = (f_\eta X_\xi - f_\xi X_\eta)/J \qquad \text{(I-3)}$$

where

$$J = X_\xi Y_\eta - X_\eta Y_\xi \qquad \text{(I-4)}$$

Then the coordinates of the transformed plane can be differentiated using (I-3) to give

$$\xi_x = Y_\eta/J \qquad \xi_y = -X_\eta/J$$

$$\eta_x = -Y_\xi/J \qquad \eta_y = X_\xi/J \qquad \text{(I-5)}$$

The Laplacian operators would then appear as

$$J^3\nabla^2\xi = X_\eta[\alpha Y_{\xi\xi} - 2\beta Y_{\xi\eta} + \gamma Y_{\eta\eta}] - Y_\eta[\alpha X_{\xi\xi} - 2\beta X_{\xi\eta} + \gamma X_{\eta\eta}]$$

$$J^3\nabla^2\eta = X_\xi[\alpha Y_{\xi\xi} - 2\beta Y_{\xi\eta} + \gamma Y_{\eta\eta}] - Y_\xi[\alpha X_{\xi\xi} - 2\beta X_{\xi\eta} + \gamma X_{\eta\eta}] \qquad \text{(I-6)}$$

where

$$\alpha = X_\eta^2 + Y_\eta^2$$

$$\beta = X_\xi X_\eta + Y_\xi Y_\eta$$

$$\gamma = X_\xi^2 + Y_\xi^2 \qquad \text{(I-7)}$$

Combining Equations (I-6) and (I-1) produces a system of coupled quasi-linear elliptic equations which is given by

$$\alpha X_{\xi\xi} - 2\beta X_{\xi\eta} + \gamma X_{\eta\eta} = J^2 Q X_\eta - J^2 P X_\xi$$

$$\alpha Y_{\xi\xi} - 2\beta Y_{\xi\eta} + \gamma Y_{\eta\eta} = J^2 Q Y_\eta - J^2 P Y_\xi \qquad \text{(I-8)}$$

A damping time derivative is then added to Equations (I-8) resulting in

$$\alpha X_{\xi\xi} - 2\beta X_{\xi\eta} + \gamma X_{\eta\eta} - J^2 Q X_\eta + J^2 P X_\xi = X_t$$

$$\alpha Y_{\xi\xi} - 2\beta Y_{\xi\eta} + \gamma Y_{\eta\eta} - J^2 Q Y_\eta + J^2 P Y_\xi = Y_t \qquad \text{(I-9)}$$

The coupled system above is then solved in the transformed plane for the physical coordinates, x and y, using a factored implicit finite difference scheme. An outline of the numerical solution of Equations (I-9) will now be presented.

Each one of the Equations (I-9) was split into two parts by spatial factoring, i.e. equations were factored out in the η and ξ direction. The two parts were then solved by alternating direction.

The solution of each step requires a tridiagonal matrix inversion which is the result of the central differencing of the above equations. Using the Crank-Nicholson averaging, the finite difference form of Equations (I-9) becomes

$$X^{k+1} - X^k = \left(\frac{\Delta t}{2}\right)\left[(\alpha X_{\xi\xi} - 2\beta X_{\xi\eta} + \gamma X_{\eta\eta} - QX_\eta + PX_\xi)^{k+1}\right.$$

$$\left. + (\alpha X_{\xi\xi} - 2\beta X_{\xi\eta} + \gamma X_{\eta\eta} - QX_\eta + PX_\xi)^k\right] / J^2$$

$$Y^{k+1} - Y^k = \left(\frac{\Delta t}{2}\right)\left[(\alpha Y_{\xi\xi} - 2\beta Y_{\xi\eta} + \gamma Y_{\eta\eta} - QY_\eta + PY_\xi)^{k+1}\right.$$

$$\left. + (\alpha Y_{\xi\xi} - 2\beta Y_{\xi\eta} + \gamma Y_{\eta\eta} - QY_\eta + PY_\xi)^k\right] / J^2 \qquad \text{(I-10)}$$

After rearranging Equations (I-10) and neglecting fourth order derivatives, Equations (I-10) become

$$\left(1 - \alpha\left(\frac{\Delta t}{2J^2}\right)\delta_{\xi\xi}\right)\left(1 - \gamma\left(\frac{\Delta t}{2J^2}\right)\delta_{\eta\eta}\right)(X^{k+1} - X^k) =$$

$$\left[\alpha X^k_{\xi\xi} - 2\beta X^k_{\xi\eta} + \gamma X^k_{\eta\eta}\right]\frac{\Delta t}{J^2} - \beta\left[X^k_{\xi\eta} - X^{k-1}_{\xi\eta}\right]\frac{\Delta t}{J^2}$$

$$+ \Delta t\left[QX^k_\eta - PX^k_\xi\right] \qquad \text{(I-11)}$$

$$\left(1 - \alpha\left(\frac{\Delta t}{2J^2}\right)\delta_{\xi\xi}\right)\left(1 - \gamma\left(\frac{\Delta t}{2J^2}\right)\delta_{\eta\eta}\right)(Y^{k+1} - Y^k) =$$

$$\left[\alpha Y^k_{\xi\xi} - 2\beta Y^k_{\xi\eta} + \gamma Y^k_{\eta\eta}\right]\frac{\Delta t}{J^2} - \beta\left[Y^k_{\xi\eta} - Y^{k-1}_{\xi\eta}\right]\frac{\Delta t}{J^2}$$

$$+ \Delta t\left[QY^k_\eta - PY^k_\xi\right] \qquad \text{(I-11)}$$

The coefficients (α,β,γ) in Equations (I-11) are nonlinear in nature and are treated explicitly in time. Similarly, parameters $P(\xi,\eta)$ and $Q(\xi,\eta)$ were treated explicitly. Thus the right hand side of Equation (I-11) is made up of known quantities denoted by ϕ_1 and ϕ_2. Equations (I-11) then appear as

$$(1 - L_\xi)(1 - L_\eta)\Delta X^k = \phi_1$$

$$(1 - L_\xi)(1 - L_\eta)\Delta Y^k = \phi_2 \qquad \text{(I-12)}$$

where L_ξ and L_ξ are linear difference operators in the ξ and η directions, respectively, and

$$\Delta X^k = X^{k+1} - X^k$$

$$\Delta Y^k = Y^{k+1} - Y^k \qquad \text{(I-13)}$$

Equations (I-12) are split as

$$(1 - L_\xi)\Delta X^* = \phi_1$$

$$(1 - L_\eta)\Delta X^k = \Delta X^*$$

$$(1 - L_\xi)\Delta Y^* = \phi_2$$

$$(1 - L_\eta)\Delta Y^k = \Delta Y^* \qquad \text{(I-14)}$$

where the (*) denotes an intermediate time level between (k) and (k+1). After obtaining the solution for Δx and Δy then the x and y values were updated using Equations (I-13).

The mapping was controlled in the η direction by the parameter $Q(\xi,\eta)$ which had the following form

$$Q(\eta) = \pm A(\eta) e^{-D(\eta)\eta_0}$$

$$\eta_0 = (J - 1)\Delta\eta \qquad \text{(I-15)}$$

In the above expression, Q is a function of η only which means that the coordinates were controlled only in η direction. Other choice of expressions could also be used if an extensive control of grid lines is required. The coefficient $A(\eta)$ is the amplitude of control and $D(\eta)$ is the decay factor. Large values of $D(\eta)$ localizes the effect of control while small values spreads out the effect over the range indicated by η_0, i.e. number lines to be affected. The grid control can be achieved either by suction ($Q<0$) at a boundary or by blowing ($Q>0$). The values of $A(\eta)$ and $D(\eta)$ used in the present transformation were 1.0 and 3.0 respectively.

The procedure was repeated until the sum of all the changes in x or y over the entire field is less than a small value (ε) at that point a steady state solution is said to have reached. The x and y values now represent the grid locations in the physical plane.

APPENDIX J

MAPPED POTENTIAL FLOW EQUATIONS

The mapped potential flow solution of flow over a circular cylinder was obtained by a factored implicit finite differencing. The elliptic Laplace equation for stream function was mapped from the physical plane onto a cartesian uniformally spaced grid coordinates using coordinate mapping results obtained from Appendix I. The stream function equation in the physical plane is

$$\Psi_{xx} + \Psi_{yy} = 0 \tag{J-1}$$

Boundary conditions are:

$$\Psi(x = -12, y) = y$$

$$\Psi_y(x, y = 12) = 0$$

$$\Psi_x(x = +12, y) = 0$$

$$\Psi(-1 < x < 12,\ \sqrt{x^2 + y^2} = 1\ \&\ y = 0) = -\int_0^{\frac{w}{R}} \left(\frac{v_w}{U_\infty}\right) ds$$

$$\Psi(x = -12, y = 0) = 0 \tag{J-2}$$

Transformed equations using relationships given in Appendix I become

$$\alpha\Psi_{\xi\xi} - 2\beta\Psi_{\xi\eta} + \gamma\Psi_{\eta\eta} = J^2 Q \Psi_\eta - J^2 P \Psi_\xi \tag{J-3}$$

Boundary conditions become:

$$\Psi(\xi = -1, \eta) = \eta$$

$$\Psi_{\eta}(\xi, \eta = 1) = 0$$

$$\Psi_{\xi}(\xi = +1, \eta) = 0$$

$$\Psi\left(-\frac{1}{12} < \xi < +1, \eta = 0\right) = -\int_0^{\frac{w}{R}} \left(\frac{v_w}{U_\infty}\right) ds$$

$$\Psi\left(\xi < -\frac{1}{12}, \eta = 0\right) = 0 \qquad \text{(J-4)}$$

w = slot width

where α, β, and γ are given in Equations (I-7) and J is given in Equation (I-4), Appendix I.

The solution of Equation (J-3) with the boundary conditions, Equations (J-4), was obtained by adding a time derivative term to Equation (J-3) then integrating by spatial factoring as discussed in Appendix I. The final factored equations take the form of

$$\left(1 - \alpha \frac{\Delta t}{2J^2} \delta_{\xi\xi}\right)\left(1 - \gamma \frac{\Delta t}{2J^2} \delta_{\eta\eta}\right)(\Psi^{k+1} - \Psi^k) =$$

$$\left[\alpha \Psi^k - 2\beta \Psi^k_{\xi\eta} + \gamma \Psi^k_{\eta\eta}\right] \frac{\Delta t}{J^2}$$

$$- \beta\left[\Psi^k_{\xi\eta} - \Psi^{k-1}_{\xi\eta}\right] \frac{\Delta t}{J^2} + \Delta t \left[Q \Psi^k_{\eta} - P \Psi^k_{\xi}\right] \qquad \text{(J-5)}$$

subject to the boundary conditions given in Equations (J-4).

All the coordinate information were obtained from the analysis presented in Appendix I. Appendices V and W contain programs for calculating the mapped potential flow solution and velocities respectively.

APPENDIX K

THE TUNNEL FLOW AND SPRAY CHARACTERISTICS

Velocity Profiles

The tunnel velocities at the test section were measured using a hot wire and a hot film anemometer. The calibration curves for the probes are shown in Figures K-1 and K-2. The velocity profiles at the test section were calculated using the calibration data and the equations provided in these figures. The velocity profiles at the test section are shown in Figures K-3, K-4, K-5, and K-6.

Spray System

The spray system used to produce droplets consisted of the following components (see Figure VII-6, page 92)

1. A water supply tank
2. A water filter
3. A reservoir which distributes water to the atomizing nozzles
4. A compressed air supply source
5. A reservoir which distributes compressed air to the atomizing nozzles
6. Four external mixing type pneumatic nozzles

The spray nozzles were calibrated for the water flow rate with respect to the atomizing air pressure and the results are shown in Figure K-7. Water was supplied to the nozzles by gravity feed. The

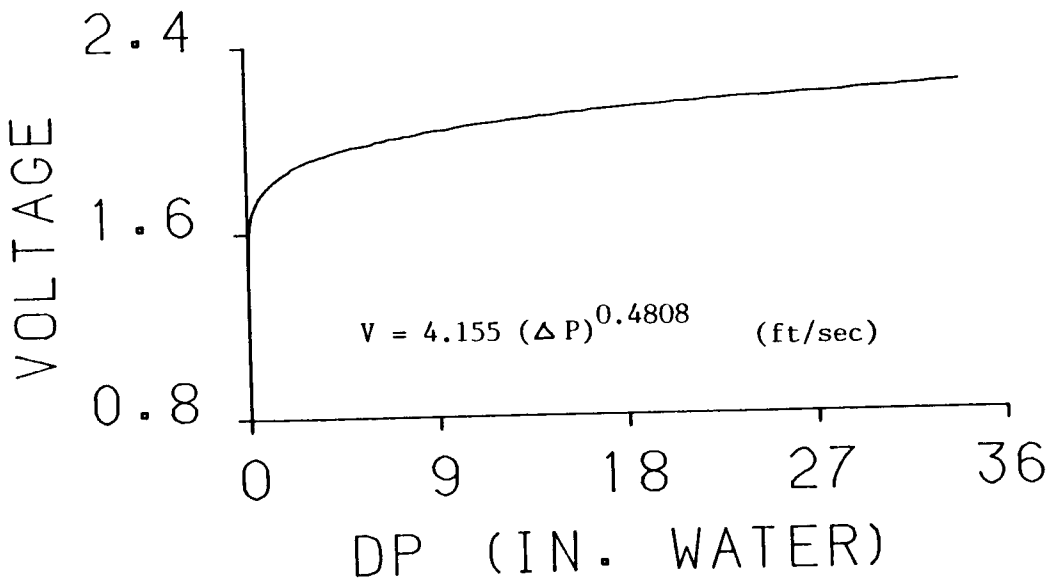


Figure K-1. Hot Wire Probe Calibration Curve and Velocity Equation.

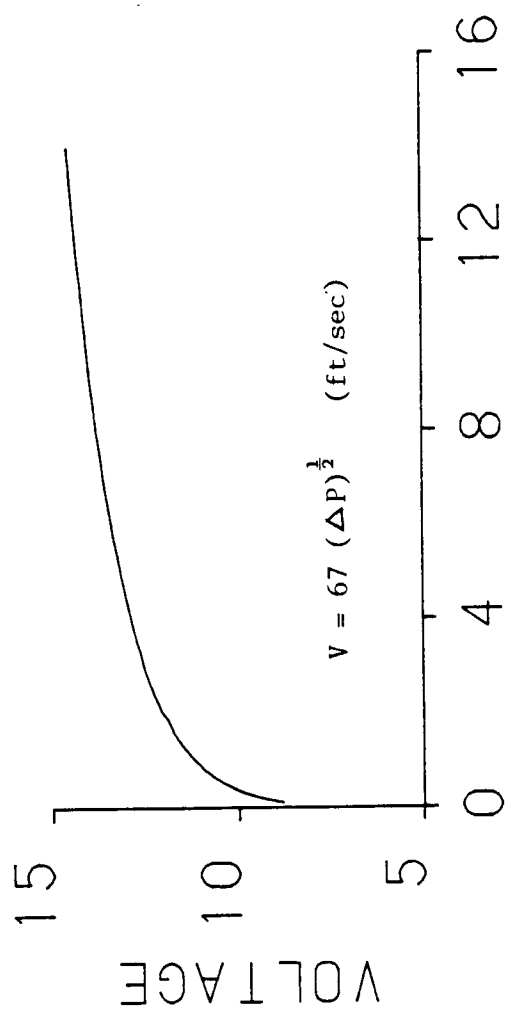


Figure K-2. Hot Film Probe Calibration Curve and Velocity Equation.

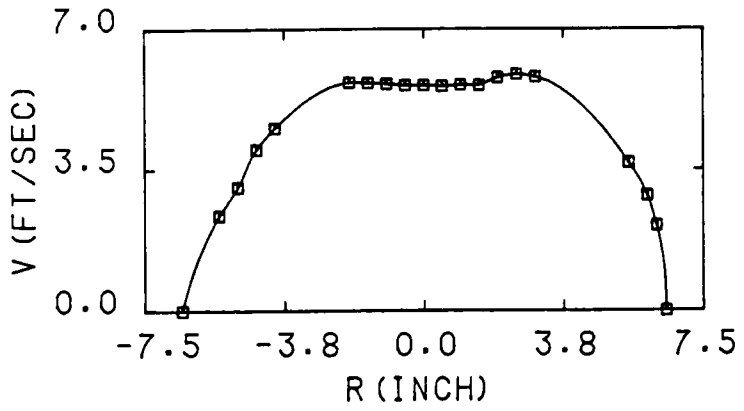


Figure K-3. Test Section Velocity Profile, Average Velocity = 4.1 ft/sec.

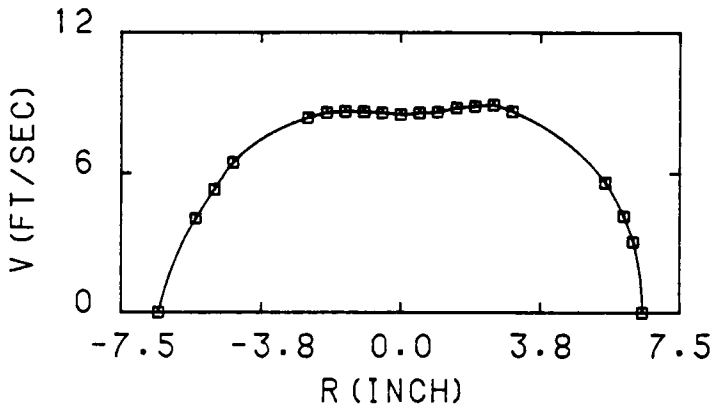


Figure K-4. Test Section Velocity Profile, Average Velocity = 6.3 ft/sec.

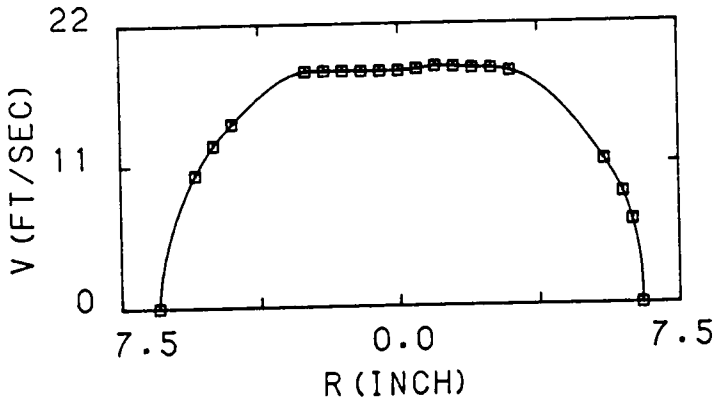


Figure K-5. Test Section Velocity Profile, Average Velocity 13.3 ft/sec.

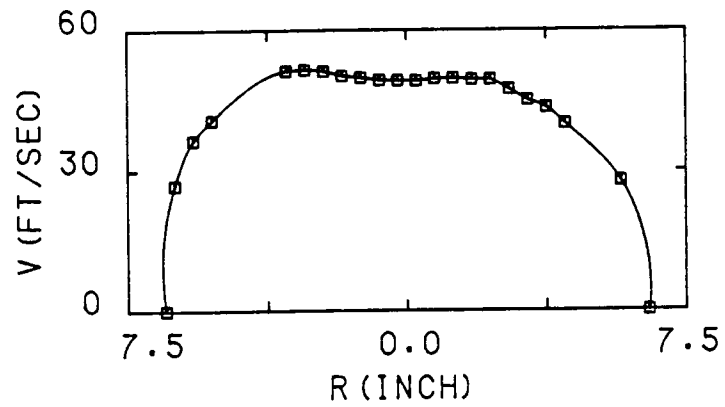


Figure K-6. Test Section Velocity Profile, Average Velocity 39 ft/sec.

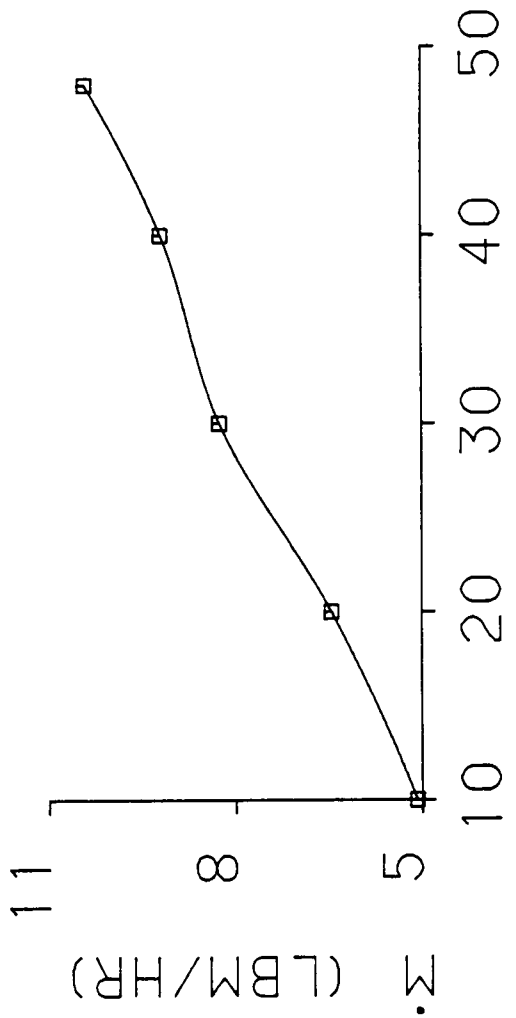


Figure K-7. Pneumatic Nozzle Water Mass Flow Calibration Curve.

water head was kept constant at about 1.5-1.8 feet. The water mass flow given in the calibration curve is the total water flow through the spray nozzles (four nozzles). For example, for air pressure of 30 psig the water flow rate through each nozzle is 7.29 lbm/hr. The liquid water content of the tunnel was calculated based on the tunnel and spray system operating conditions and are shown in Table K-1.

The spray droplet distribution data were obtained using a microscope. A sample distribution data is shown in Table K-2 and Figure K-8. These data correspond to the atomizing air pressure of 30 psig. The mean droplet size in the spray was determined to be 45 microns.

Table K-1. Nozzle Water Flow Rate Calibration Data and Tunnel LWC.

P[a]	m[b] x 10^3	Tunnel Liquid Water Content[c] x 10^3			
		V[d] = 4.1	6.3	13.3	39
48	2.893	0.9	0.58	0.28	0.09
40	2.554	0.79	0.52	0.24	0.08
30	2.025	0.63	0.41	0.19	0.07
20	1.792	0.56	0.36	0.17	0.06
10	1.410	0.44	0.28	0.13	0.05

a(nozzle air pressure, psig), b(nozzle water mass flow rate, lbm/sec), c(LWC, lbm/ft^3 of air), d(tunnel air velocity, ft/sec)

Table K-2. Spray Droplet Characterization

Compressed Air Pressure	(psig)	= 30.0
Spray Water Temperature	(°F)	= 32.0
Room Air Pressure	(In. Hg)	= 29.6
Room Air Dry Bulb Temp.	(°F)	= 70.0
Room Air Wet Bulb Temp.	(°F)	= 56.0
Wind Tunnel Velocity	(Ft/sec)	= 6.30
Sampling Location, Distance From Nozzle	(Ft)	= 5.0

Number of Samples Taken	:	169
Number of Drop Sizes Present	:	24
Mean Drop Diameter (Micron)	:	44.9
Standard Deviation	:	40.40

Drop Dia. (Micron)	Frequency	(%)
5	30	11.15
11	36	13.38
16	31	11.52
21	18	6.69
26	19	7.06
32	16	5.95
37	13	4.83
42	7	2.60
47	4	1.49
53	11	4.09
58	5	1.86
63	6	2.23
68	9	3.35
74	8	2.97
79	2	0.74
84	5	1.86
89	1	0.37
95	14	5.20
105	16	5.95
116	5	1.86
126	3	1.12
137	1	0.37
158	8	2.97
211	1	0.37

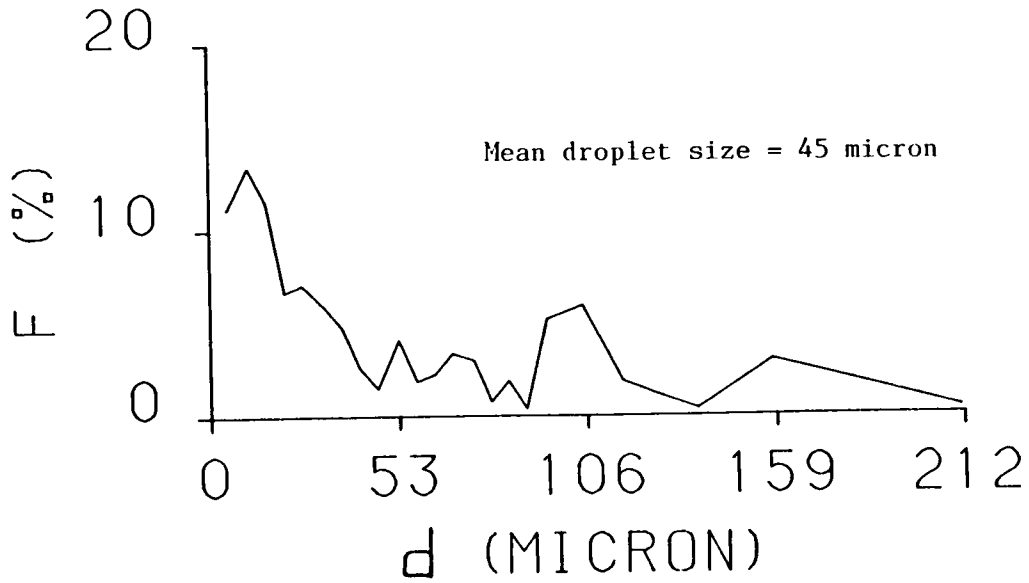


Figure K-8. Frequency of Occurence of a Droplet Size in the Spray.

APPENDIX L

MISCELLANEOUS INSTRUMENTS AND EQUIPMENT

Adjustable flow meters (Dwyer RM 0-100, 0-200 ft/hr) were used to control the nitrogen volume flow rate supplied to each slot on the model.

A freezer with a capacity of 25 gallons was used to store and cool Methanol used to cool the model. The minimum attainable temperature in the freezer was $-45°F$. During a typical run of 7 minutes, methanol temperature increased about $4°F$.

A profilometer was built to obtain the ice profiles on the cylinder. A photograph of the profilometer is shown in Figure VII-10, page 100. This photograph also shows the experimental model in the cradles with the profiling arm placed on it. A X-Y plotter (model HP 7035 A), connected to the profilometer, produced graphs of the ice profiles in the axial and the angular direction. The profilometer system consisted of the following components:

1 – Three precision potentiometers (a single turn straight wire, a single turn wire wound, and a 10 turn wire wound)

2 – A 25 volts power supply

3 – Two Potentiometer mounting wheels

4 – A travers

5 – A profilling arm with a pointer

6 – Two potentiometer mounting brackets

7 – A base plate

8 – Test model mounting cradles

9 – X-Y graph recorder

Due to the high sensitivity requirement, a single turn straight wire potentiometer was used to measure the ice thickness on the cylinder. The axial ice profiles were obtained by traversing the profilling arm along the cylinder at the angular position of interest. The angular ice profiles were obtained by manually rotating the cylinder while holding the profiller at the desired location along the cylinder. The ice profiles were plotted on a X-Y recorder with the X axis representing the location along the cylinder (for the axial profiles) or around the cylinder (for the angular profiles) and the Y axis representing the ice thickness. A 10 turn wire wound potentiometer was used to generate the X axis of the plots. This potentiometer was attached to the bracket on the traverse and the wheel connected to it rolled on the base plate along the cylinder (see Figure VII-10). The X-axis for the angular profile was generated by a single turn wire wound potentiometer which was placed on the cylinder and the wheel connected to it turned as the cylinder was rotated (see Figure VII-10). The X-axis on the angular profiles represented the circumference of the cylinder.

The profilometer calibrations are:

X-axis 1-inch = 1.7857 inch actual (axial profiles)

X-axis 1-inch = 0.4682 inch actual (angular profiles)

Y-axis 1-inch = 0.1000 inch actual (ice thickness)

A triple beam balance was used to weigh the ice accreted on the cylinder.

Smoke was used to visualize the flow field around and about the cylinder with surface mass transfer. To produce a large quantity of dense smoke, a smoke generator was built. As shown in Figure L-1, sawdust or tobacco in the cylindrical chamber was lit by an electrically heated filament (fixed permanently in the chamber). Air was then allowed to enter the chamber and carry smoke out into the tunnel. Wire mesh screens were used to keep the sawdust from blowing out of the chamber.

A neon laser light was used to visualize the droplet flow field approaching the cylinder with surface mass transfer, however, the result was not satisfactory. A strobelight was also tried with unsatisfactory results.

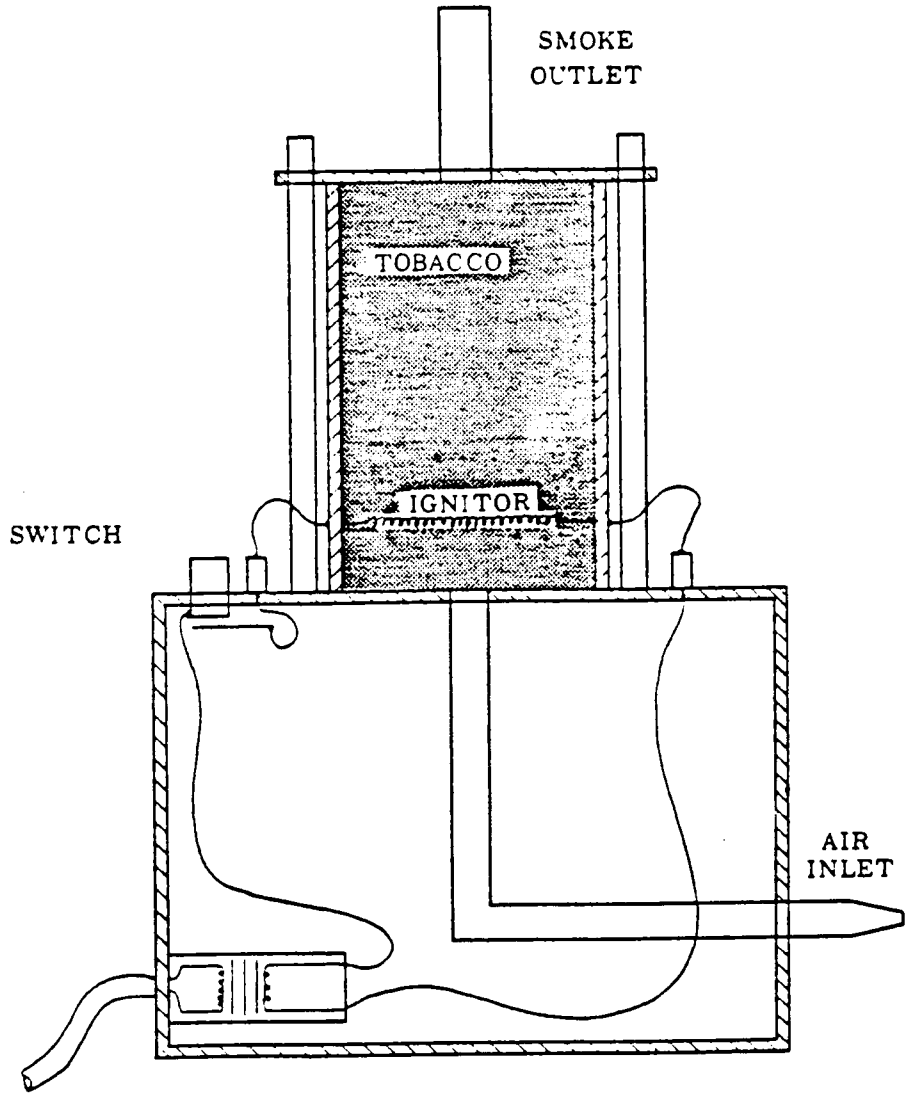


Figure L-1. Schematic of Smoke Generator.

APPENDIX M

INCOMPRESSIBLE VISCOUS FLOW OVER A CIRCULAR CYLINDER WITH SURFACE INJECTION

Viscous laminar incompressible flow over a circular cylinder with surface injection was modeled numerically using a factored implicit finite differencing. The unsteady momentum (Navier-Stokes) equations were solved, in polar coordinates, for u (θ direction velocity) and v (r direction velocity). The pressure values were obtained from an artificial compressibliity equation. The nondimensional form of the equations (in conservative form) are

θ-momentum

$$\frac{\partial u}{\partial t} + \frac{\partial u^2}{\partial r} + \frac{\partial uv}{r\partial\theta} + \frac{2vu}{r} = -\frac{\partial P}{r\partial\theta}$$

$$+ \frac{1}{Re_o}\left(\frac{\partial^2 u}{\partial r^2} + \frac{1}{r}\frac{\partial u}{\partial r} - \frac{u}{r^2} + \frac{\partial^2 u}{r^2\partial\theta^2} + \frac{2}{r}\frac{\partial r}{r\partial\theta}\right) \qquad \text{(M-1)}$$

r-momentum

$$\frac{\partial v}{\partial t} + \frac{\partial vu}{\partial r} + \frac{\partial v^2}{r\partial\theta} + \frac{(v^2 - u^2)}{r} = -\frac{\partial P}{\partial r}$$

$$+ \frac{1}{Re_o}\left(\frac{\partial^2 v}{\partial r^2} + \frac{1}{r}\frac{\partial v}{\partial r} - \frac{v}{r^2} + \frac{\partial^2 v}{r^2\partial\theta^2} - \frac{2}{r}\frac{\partial u}{r\partial\theta}\right) \qquad \text{(M-2)}$$

pressure equation

$$\frac{\partial P}{\partial t} + \omega\left(\frac{\partial v}{\partial r} + \frac{\partial u}{r\partial\theta} + \frac{v}{r}\right) = 0 \qquad \text{(M-3)}$$

where ω is a constant in Equation (M-3). Boundary conditions are:

Cylinder surface:

$$u(\theta, r=0) = 0 \quad , \quad v(\theta, r=0) = v_w$$

$$\frac{\partial P}{\partial r} = \text{From r-momentum, Equation (M-2)}$$

Far field ($r \to \infty$):

$$\text{For } 0 \le \theta \le 90 \ , \ r \to \infty$$

$$u = -\sin(\pi - \theta)$$

$$v = +\cos(\pi - \theta)$$

$$p = P_\infty$$

For $90 \leq \theta \leq 180$, $r \rightarrow \infty$

$$\frac{\partial u}{\partial r} = 0$$

$$\frac{\partial v}{\partial r} = 0$$

$$\frac{\partial P}{\partial r} = 0$$

Plane of symmetry:

$\theta = 0°$ and $180°$, $r = 1$ to ∞

$$u = 0$$

$$\frac{\partial v}{\partial \theta} = 0$$

$$\frac{\partial P}{\partial \theta} = 0$$

Equation (M-1, 2, 3) can be written in the form of

$$\frac{\partial f}{\partial t} + \frac{\partial F}{r d\theta} + \frac{\partial G}{\partial r} + \frac{H}{r} = 0 \qquad \text{(M-4)}$$

where

$$f = \begin{vmatrix} u \\ v \\ P \end{vmatrix}$$

$$F = \begin{vmatrix} (u^2 + P) - \frac{1}{Re_o}\left(\frac{\partial u}{r d\theta} + \frac{2v}{r}\right) \\ uv - \frac{1}{Re_o}\left(\frac{\partial v}{r d\theta} - \frac{2u}{r}\right) \\ \omega u \end{vmatrix}$$

$$G = \begin{vmatrix} uv - \frac{1}{Re_o}\left(\frac{\partial u}{\partial r} + \frac{u}{r}\right) \\ (v^2 + P) - \frac{1}{Re_o}\left(\frac{\partial v}{\partial r} + \frac{v}{r}\right) \\ \omega v \end{vmatrix}$$

$$H = \begin{vmatrix} 2uv \\ v^2 - u^2 \\ \omega v \end{vmatrix}$$

Dividing F, G, and H into two components, i.e. viscous and inviscid,

$$F = F_I - \frac{1}{Re_o} F_v$$

$$G = G_I - \frac{1}{Re_o} G_v$$

$$H = H_I - \frac{1}{Re_o} H_v \qquad \text{(M-5)}$$

where

$$F_I = \begin{vmatrix} u^2 + P \\ uv \\ \omega u \end{vmatrix} \quad , \quad G_I = \begin{vmatrix} uv \\ v^2 + P \\ \omega v \end{vmatrix} \quad , \quad H_I = \begin{vmatrix} 2\,uv \\ v^2 - u^2 \\ \omega v \end{vmatrix}$$

$$F_v = \begin{vmatrix} \dfrac{\partial u}{r\,d\theta} + \dfrac{2v}{r} \\ \dfrac{\partial v}{r\,\partial\theta} - \dfrac{2u}{r} \\ 0 \end{vmatrix} \quad , \quad G_v = \begin{vmatrix} \dfrac{\partial u}{\partial r} + \dfrac{u}{r} \\ \dfrac{\partial v}{\partial r} + \dfrac{v}{r} \\ 0 \end{vmatrix}$$

$$H_v = \begin{vmatrix} 0 \\ 0 \\ 0 \end{vmatrix}$$

Expressing $\partial f/\partial t$ in three level time differencing, Equation (M-4) becomes

$$\frac{1}{2\Delta t}(3f^{n+1} - 4f^n + f^{n-1}) + \left(\frac{\partial F}{r\,d\theta}\right)^{n+1} + \left(\frac{\partial G}{\partial r}\right)^{n+1} + \left(\frac{H}{r}\right)^{n+1} = 0 \qquad \text{(M-6)}$$

The second term of Equation (M-6) can be written as

$$\left(\frac{\partial F}{r\,d\theta}\right)^{n+1} = \left(\frac{\partial F_I}{r\,\partial\theta}\right)^{n+1} - \frac{1}{Re_o}\left(\frac{\partial F_I}{r\,\partial\theta}\right)^{n+1} \qquad \text{(M-7)}$$

and F_I^{n+1} can be linearized as

$$F_I^{n+1} \simeq F_I^n + A^n(f^{n+1} - f^n) \qquad \text{(M-8)}$$

where

$$A = \frac{\partial F_I}{\partial f} = \begin{vmatrix} 2u & 0 & 1 \\ v & u & 0 \\ \omega & 0 & 0 \end{vmatrix}$$

and

$$\left(\frac{\partial F_I}{r\partial\theta}\right)^{n+1} = \left(\frac{\partial F_I}{r\partial\theta}\right)^{n} + \frac{\partial}{r\partial\theta}\left([A]^n \Delta f\right) \qquad \text{(M-9)}$$

where

$$\Delta f = f^{n+1} - f^n$$

the viscous part of F can be separated as

$$F_V = F_{V1}\left(f, \frac{\partial f}{r\partial\theta}\right) + F_{V2}\left(f, \frac{\partial f}{\partial r}\right) \qquad \text{(M-10)}$$

Thus

$$F_{V1} = \begin{vmatrix} \frac{\partial u}{r\partial\theta} + \frac{2V}{r} \\ \frac{\partial v}{r\partial\theta} - \frac{2u}{r} \\ 0 \end{vmatrix}, \quad F_{V2} = \begin{vmatrix} 0 \\ 0 \\ 0 \end{vmatrix}$$

Linearizing F_{V1} as

$$F_{V1}^{n+1} = F_{V1}^{n} + M^n (f^{n+1} - f^n) + P^n\left(\frac{\partial f^{n+1}}{r\partial\theta} - \frac{\partial f^n}{r\partial\theta}\right) \qquad \text{(M-11)}$$

where

$$M = \frac{\partial F_{V1}}{\partial f} = \begin{vmatrix} 0 & 2r^{-1} & 0 \\ -2r^{-1} & 0 & 0 \\ 0 & 0 & 0 \end{vmatrix}$$

$$P = \frac{\partial F_{V1}}{\partial\left(\frac{\partial f}{r\partial\theta}\right)} = \begin{vmatrix} 1 & 0 & 0 \\ 0 & 1 & 0 \\ 0 & 0 & 0 \end{vmatrix}$$

Equation (M-11) can be expressed as

$$F_{V1}^{n+1} \simeq F_{V1}^{n} + \left(M - \frac{\partial P}{r\partial\theta}\right)^{n} \Delta f + \frac{\partial}{r\partial\theta}[P]^{n} \Delta f \qquad \text{(M-12)}$$

Thus

$$\left(\frac{\partial F_{v}}{r\partial\theta}\right)^{n+1} \simeq \left(\frac{\partial F_{v}}{r\partial\theta}\right)^{n} + \frac{\partial}{r\partial\theta}\left[\left(M - \frac{\partial P}{r\partial\theta}\right) + \frac{\partial}{r\partial\theta} P\right]^{n} \Delta f \qquad \text{(M-13)}$$

Equation (M-7) in linear form becomes

$$\left(\frac{\partial F}{r\partial\theta}\right)^{n+1} \simeq \left(\frac{\partial F}{r\partial\theta}\right)^{n} + \frac{\partial}{r\partial\theta}\left\{\left[A - \frac{1}{Re_{o}}\left(\left(M - \frac{\partial P}{r\partial\theta}\right) + \frac{\partial P}{r\partial\theta}\right)\right]^{n} \Delta f\right\} \qquad \text{(M-14)}$$

Similarly:

$$G_{I}^{n+1} \simeq G_{I}^{n} + B^{n}(f^{n+1} - f^{n}) \qquad \text{(M-15)}$$

where

$$B = \frac{\partial G_I}{\partial f} = \begin{vmatrix} v & u & 0 \\ 0 & 2v & 1 \\ 0 & \omega & 0 \end{vmatrix}$$

$$G_V = G_{V1}\left(f, \frac{\partial f}{r\partial\theta}\right) + G_{V2}\left(f, \frac{\partial f}{\partial r}\right) \qquad \text{(M-16)}$$

where

$$G_{V1} = \begin{vmatrix} 0 \\ 0 \\ 0 \end{vmatrix} \quad , \quad G_{V2} = \begin{vmatrix} \frac{\partial u}{\partial r} + \frac{u}{r} \\ \frac{\partial v}{\partial r} + \frac{v}{r} \\ 0 \end{vmatrix}$$

$$G_{V2}^{n+1} \simeq G_{V2}^{n} + N(f^{n+1} - f^{n}) + Q\left(\frac{\partial f^{n+1}}{\partial r} - \frac{\partial f^{n}}{\partial r}\right) \qquad \text{(M-17)}$$

where

$$N = \frac{\partial G_{V2}}{\partial f} = \begin{vmatrix} r^{-1} & 0 & 0 \\ 0 & r^{-1} & 0 \\ 0 & 0 & 0 \end{vmatrix}$$

$$Q = \frac{\partial G_{V2}}{\partial\left(\frac{\partial f}{\partial r}\right)} = \begin{vmatrix} 1 & 0 & 0 \\ 0 & 1 & 0 \\ 0 & 0 & 0 \end{vmatrix}$$

Thus

$$\left(\frac{\partial G}{\partial r}\right)^{n+1} \simeq \left(\frac{\partial G}{\partial r}\right)^{n} + \frac{\partial}{\partial r}\left\{\left[B - \frac{1}{Re_o}\left(\left(N - \frac{\partial Q}{\partial r}\right) + \frac{\partial Q}{\partial r}\right)\right|^{n} \Delta f\right\} \qquad \text{(M-18)}$$

Finally, H^{n+1} is expressed as

$$H^{n+1} = H_I^{n+1} - \frac{1}{Re_o} H_V^{n+1} \tag{M-19}$$

$$H_I^{n+1} \simeq H_I^n + C^n (f^{n+1} - f^n) \tag{M-20}$$

where

$$C = \frac{\partial H_I}{\partial f} = \begin{vmatrix} 2v & 2u & 0 \\ -2u & 2v & 0 \\ 0 & \omega & 0 \end{vmatrix}$$

Rearranging Equation (M-6)

$$\Delta f = -\frac{2\Delta t}{3}\left(\frac{\partial F}{r\partial\theta} + \frac{\partial G}{\partial r} + \frac{H}{r}\right)^{n+1} + \frac{1}{3}(f^n - f^{n-1}) \tag{M-21}$$

Equation (M-21) can be expressed as

$$\left[(I + C) + \frac{\partial \Lambda}{r\partial\theta} + \frac{\partial \Gamma}{\partial r}\right] \Delta f = R \tag{M-22}$$

where I is the identity matrix. Equation (M-22) can be rewritten as

$$\left(I + g\frac{\partial \Lambda}{r\partial\theta} + g\frac{\partial \Gamma}{\partial r}\right) = gR \tag{M-23}$$

where

$$g = [I + C]^{-1}$$

$$\frac{\partial \Lambda}{r\partial\theta} = \frac{2\Delta t}{3}\left\{\frac{\partial}{r\partial\theta}\left(\left[A^n - \frac{1}{Re_0}\left(M^n - \frac{\partial P^n}{r\partial\theta}\right)\right]\Delta f\right) - \frac{1}{Re_0}\frac{\partial^2}{r^2\partial\theta^2}[P^n \Delta f]\right\}$$

$$\frac{\partial \Gamma}{\partial r} = \frac{2\Delta t}{3}\left\{\frac{\partial}{\partial r}\left(\left[B^n - \frac{1}{Re_0}\left(N^n - \frac{\partial Q^n}{\partial r}\right)\right]\Delta f\right) - \frac{1}{Re_0}\frac{\partial^2}{\partial r^2}[Q^n \Delta f]\right\}$$

$$R = -\frac{2\Delta t}{3}\left(\frac{\partial F}{r\partial\theta} + \frac{\partial G}{\partial r} + \frac{H}{r}\right)^n + \frac{1}{3}(f^n - f^{n-1})$$

Equation (M-23) can be split as

$$\left(I + g\frac{\partial \Lambda}{r\partial\theta}\right)\Delta f^* = g\,R \qquad \text{(M-24)}$$

$$\left(I + g\frac{\partial \Gamma}{\partial r}\right)\Delta f = \Delta f^* \qquad \text{(M-25)}$$

Equation (M-24) was first solved for the intermediate values of Δf^*, then Equation (M-25) was integrated to obtain the values of Δf at a particular time level. The procedure was repeated until a steady state solution is reached.

The finite difference expressions used for the derivatives for nonuniform grid spacing are

$$\left.\frac{\partial f}{\partial r}\right|_j = \frac{f_{j+1} + (S^2 - 1)f_j - S^2 f_{j-1}}{(1+S)\Delta r_j} \qquad \text{(M-26)}$$

$$\left.\frac{\partial^2 f}{\partial r^2}\right|_j = \frac{f_{j+1} - (S+1) f_j + S f_{j-1}}{\left(\frac{S+1}{2S}\right) \Delta r_j^2} \qquad \text{(M-27)}$$

where

$$S = \frac{\Delta r_j}{\Delta r_{j-1}}$$

Similar expressions were used in the θ direction. The difference form of Equation (M-24) becomes

$$a\,\Delta f^*_{i+1,j} + b\,\Delta f^*_{i,j} + c\,\Delta f^*_{i-1,j} = g\,R \qquad \text{(M-28)}$$

where a, b, and c are the constant coefficients.
Equation (M-28) leads to the solution of a block tridiagonal matrix system. The solution was carried out using a factorization technique. Similarly, Equation (M-25) was expressed as

$$a\,\Delta f_{i,j+1} + b\,\Delta f_{i,j} + c\,\Delta f_{i,j-1} = \Delta f^*_{i,j} \qquad \text{(M-29)}$$

and a similar procedure was used to solve for Δf. Appendices Y and Z contain the computer programs used for calculating the velocities and stream function values respectively.

Solution of the above equations was carried out using a non-uniform grid system in a polar coordinate with a total of 1575 (35x45) grid points. The far field, r = ∞, was approximated by

r = 13R, and the horizontal flow over the cylinder was assumed to be symmetric with respect to the horizontal plane. The program execution time (CPU on the DEC System 10) for a converged solution at the Reynolds number of 32 (based on the cylinder radius) was about 7 hours. The convergence rate was slower for higher Reynolds numbers. Due to the larger CPU time requirement and the cost, it was decided not to obtain the solutions for higher Reynolds numbers which were desired. The results of computations for the case of Re_0 = 32 with no surface injection indicate that the flow separation is taking place at about 56 degrees from the rear stagnation point. The length of standing vortices behind the cylinder is about 7.9R. These results are in excellent agreement with the experimental and numerical results given by Takami, et al [54].

APPENDIX N

COMPUTER PROGRAM FOR DROPLET TRAJECTORY

CALCULATION

```
CC C C C
```

```
      COMMON /TYPE/FLTY,FLINJ
      DATA NYI,NCASE,DC/100,1,0.0807292/
      DATA RHOA,RHOD,VISCA,XI/0.0747,62.4,1.224E-05,-10.0/
      DATA DELT,DTPR,EPSI,TMAX,PI/0.0010,.10,.00001,15.0,3.141529654/
      OPEN(1,FILE='CDRE.DAT')
      READ(1,*,END=1)(REYNOL(I),CDRE(I),I=1,200)
1     NPTS=I-1
      CLOSE(1,FILE='CDRE.DAT')
5     WRITE(5,7)
7     FORMAT(1X,'POTENTIAL FLOW ONLY? (Y/N)   ',$)
      READ(5,*,ERR=5)FLTY
      IF(FLTY.EQ.'N') THEN
10    WRITE(5,12)
12    FORMAT(1X,' ENTER BOUNDARY LAYER DATA FILE NAME    ',$)
      READ(5,*,ERR=10)BLFILE
      OPEN(UNIT=1,FILE=BLFILE)
      READ(1,* )NPX,NPY,RERC,VJET,U0,RC
13    FORMAT(2(2X,I10),4(2X,D15.8))
      DO 14 I=1,NPX
14    READ(1,* )IX1,XX1,XX1,XX1,XX1
15    FORMAT(2X,I2,4(2X,D15.8))
      DO 16 I=1,NPX
      DO 16 J=1,NPY
      READ(1,* )I1,J1,XC(I),ETA,YBL(I,J),UBL(I,J),VBL(I,J)
      YBL(I,J)=YBL(I,J)/RC
      UBL(I,J)=UBL(I,J)/U0
      VBL(I,J)=VBL(I,J)/U0
16    CONTINUE
17    FORMAT(2(2X,I2),5(2X,D15.8))
      REDC=RERC*2.0
      DC=RC*2.0
      WRITE(5,18)
18    FORMAT(2X,'ENTER DROP DIA (METERS)    ',$)
      READ(5,*)DD1
      DD=DD1*3.28
      ELSE
      WRITE(5,19)
19    FORMAT(2X,'IS THERE ANY SURFACE INJECTION (Y/N) ?    ',$)
      READ(5,*)FLINJ
      IF(FLINJ.EQ.'Y')THEN
      WRITE(5,20)
20    FORMAT(2X,'ENTER # OF SOURCES ON THE SURFACE    ',$)
      READ(5,*)NS
      WRITE(5,21)
21    FORMAT(2X,'ENTER SOURCE ANGLES(90-->270 DEG.)   ',$)
      READ(5,*)(ANGLE(I),I=1,NS)
      WRITE(5,22)
22    FORMAT(2X,'ENETR SOURCE STRENGTH     ',$)
      READ(5,*)(Q(I),I=1,NS)
      DO 23 I=1,NS
```

```
      ALFA=ANGLE(I)*PI/180.0
      XS(I)=COS(ALFA)
      YS(I)=SIN(ALFA)
23    CONTINUE
      END IF
      WRITE(5,24)
24    FORMAT(2X,'ENTER U0(FT/S),DD(MICRON)      ',$)
      READ(5,*)U0,DD1
      DD=DD1*3.28*1E-06
      END IF
      DO 150 KCASE=1,NCASE
      TYPE *,'  ENTER INITIAL Y AND DELTAY'
      READ(5,*)Y0(KCASE),DELTAY
      YI=Y0(KCASE)
      Y=YI
      K=RHOD*U0*DD*DD/(9.0*DC*VISCA)
      PHI=9.0*DC*U0*RHOA*RHOA/(VISCA*RHOD)
      TYPE *,K,PHI
      REDD=RHOA*U0*DD/VISCA
      REDC=RHOA*U0*DC/VISCA
25    DO 130 JJ=1,NYI
      T=0.0
      TPR=DELT
      X=XI
      Y=YI
      CALL VEL(X,Y,U,V)
      XD=U
      YD=V
      RED=REDD*SQRT((ABS(U-XD))**2+(ABS(V-YD))**2)
      CALL DRAG(RED,STOKE)
C
      XDD=STOKE*(U-XD)/K
      YDD=STOKE*(V-YD)/K
C
27    XD1=XD+XDD*DELT
      YD1=YD+YDD*DELT
C
C     CALCULATE NEW VALUES OF X,Y WITH THE P(XD,YD)
C
      X1=X+(XD+XD1)/2.*DELT
      Y1=Y+(YD+YD1)/2.*DELT
C
30    CALL VEL(X1,Y1,U,V)
      RED=REDD*SQRT((ABS(U-XD))**2+(ABS(V-YD))**2)
      CALL DRAG(RED,STOKE)
C
      XDD1=STOKE*(U-XD1)/K
      YDD1=STOKE*(V-YD1)/K
C
      XD1C=XD+(XDD+XDD1)/2.*DELT
```

```
      YD1C=YD+(YDD+YDD1)/2.*DELT
C
      DIFXD=XD1C-XD1
      DIFYD=YD1C-YD1
C
      IF(ABS(DIFXD)-EPSI) 40,60,60
40    IF(ABS(DIFYD)-EPSI) 70,60,60
C
60    XD1=XD1C
      YD1=YD1C
      X1=X+(XD+XD1C)/2.*DELT
      Y1=Y+(YD+YD1C)/2.*DELT
C
      GO TO 30
C
C     PROCEED TO THE NEXT TIME STEP
C
70    X1=X+(XD+XD1C)/2.*DELT
      Y1=Y+(YD+YD1C)/2.*DELT
      CALL VEL(X1,Y1,U,V)
      RED=REDD*SQRT((ABS(U-XD))**2+(ABS(V-YD))**2)
      CALL DRAG(RED,STOKE)
C
      XDD1=STOKE*(U-XD1C)/K
      YDD1=STOKE*(V-YD1C)/K
C
      T=T+DELT
      RAD=SQRT((ABS(X1))**2+(ABS(Y1))**2)
      DRAD=DD/2.
      RDIFF=0.5*DC*(RAD-1.0)
      IF(RDIFF.LE.DRAD) GO TO 92
      TPR=TPR+DTPR
90    FORMAT(1X,F7.3,4F13.4)
      IF(X1-0.0) 110,120,120
92    TYPE 95,X1,Y1,YI,K
95    FORMAT('   TOUCH DOWN'/
      17X,'X1= ',F15.8,5X,'Y1= ',F15.8,5X,'YI= ',F15.8/
      27X,' K= ',F15.8)
      GO TO 140
110   IF(ABS(X1).LE.1.0) DELT=0.010
      X=X1
      Y=Y1
      IF(FLTY.EQ.'N')THEN
      ANGP=ATAN(Y/ABS(X))
      RP=SQRT(X*X+Y*Y)
      IF(RP.LE.1.11) DELT=0.005
      END IF
      XD=XD1C
      YD=YD1C
      XDD=XDD1
```

```
      YDD=YDD1
C
      GO TO 27
120   YI=YI-DELTAY
      Y=YI
      IF(Y.LE.0.0) GO TO 140
130   CONTINUE
140   TYPE *,' WOULD YOU LIKE TO CHANGE DELTAY '
      READ(5,*)YINCR
      IF(YINCR.EQ.'N') GO TO 145
      YI=YI+DELTAY
      TYPE *,' ENTER DELTAY'
      READ(5,*)DELTAY
      YI=YI-DELTAY
      GO TO 25
145   TYPE 96,REDD,REDC,PHI,U0,DD,DD1,DC
96    FORMAT(' '  REDD= ',F12.3/
     1       '     REDC= ',F12.3/
     2       '      PHI= ',F12.3/
     3       '       U0= ',F12.3,'  FT/SEC'/
     4       '       DD= ',F12.9,'  FT',5X,F12.9,'  METERS'/
     5       '       DC= ',F12.3,'  FT')
150   CONTINUE
      STOP
      END
      SUBROUTINE VEL(X,Y,U,V)
      CHARACTER*6 FLTY,FLINJ
      COMMON /BOUND/YBL(50,50),XC(30),VBL(50,50),UBL(50,50)
      COMMON /INJECT/Q(100),XS(100),YS(100),NS
      COMMON /PRAM/NPX,NPY,PI
      COMMON /TYPE/FLTY,FLINJ
      IF(FLTY.EQ.'N')THEN
      ANGP=ATAN(Y/ABS(X))
      RP=SQRT(X*X+Y*Y)
      IF(RP.GE.1.11) GO TO 50
      DANG=0.5*PI/(NPX-1)
      AIANGP=ANGP*(NPX-1)/(PI*0.5)
      IANGP=AIANGP
      REMAIN=AIANGP-IANGP
      IPD=IANGP
      IPU=IANGP+1
C     TYPE *,'ANGP,RP,DANG,IANGP,REMAIN,IPD,IPU,X,Y'
C     TYPE *,ANGP,RP,DANG,IANGP,REMAIN,IPD,IPU,X,Y
      IF(REMAIN.EQ.0.0) THEN
C     PARTICLE IS ON THE LINE
      IP=IPD
      IF(RP.GE.YBL(IP,NPY)+1.0) GO TO 50
      DO 10 JBL=NPY-1,1,-1
      IF(RP.GE.YBL(IP,JBL)+1.0) GO TO 15
10    CONTINUE
```

```
      TYPE *,' TOUCH DOWN 2'
15    U=UBL(IP,JBL)+(UBL(IP,JBL+1)-UBL(IP,JBL))*(RP-YBL(IP,JBL)-1.0)
      1 /(YBL(IP,JBL+1)-YBL(IP,JBL))
      V=VBL(IP,JBL)+(VBL(IP,JBL+1)-VBL(IP,JBL))*(RP-YBL(IP,JBL)-1.0)
      1 /(YBL(IP,JBL+1)-YBL(IP,JBL))
      TYPE 16,U,V
16    FORMAT(2X,'U,V ON THE LINE   ',2F15.5)
      ELSE
      FACT=(ANGP-DANG*IANGP)/DANG
      RMIDBL=YBL(IPD,NPY)+(YBL(IPU,NPY)-YBL(IPD,NPY))*FACT
      IF(RP.GE.RMIDBL+1.0) GO TO 50
      RMIDUP=RMIDBL
      DO 20 JBL=NPY-1,1,-1
      RMIDLO=YBL(IPD,JBL)+(YBL(IPU,JBL)-YBL(IPD,JBL))*FACT
      IF(RP.GE.RMIDLO+1.0) GO TO 25
      RMIDUP=RMIDLO
20    CONTINUE
25    ULO=UBL(IPD,JBL)+(UBL(IPU,JBL)-UBL(IPD,JBL))*FACT
      UUP=UBL(IPD,JBL+1)+(UBL(IPU,JBL+1)-UBL(IPD,JBL+1))*FACT
      VLO=VBL(IPD,JBL)+(VBL(IPU,JBL)-VBL(IPD,JBL))*FACT
      VUP=VBL(IPD,JBL+1)+(VBL(IPU,JBL+1)-VBL(IPD,JBL+1))*FACT
      U=ULO+(UUP-ULO)*(RP-RMIDLO-1.0)/(RMIDUP-RMIDLO)
      V=VLO+(VUP-VLO)*(RP-RMIDLO-1.0)/(RMIDUP-RMIDLO)
      TYPE 49,U,V
49    FORMAT(2X,'U,V   ',2F15.5)
      END IF
      ELSE
      IF(FLINJ.EQ.'Y')THEN
      USO=0.0
      USI=0.0
      VSO=0.0
      VSI=0.0
      UUD=1.0-(X*X-Y*Y)/((X*X+Y*Y)**2)
      DO 55 I=1,NS
      USO=USO+Q(I)*(X-XS(I))/(2*PI*((X-XS(I))*(X-XS(I))+
      1   (Y-YS(I))*(Y-YS(I))))
      USI=USI-Q(I)*X/(4*PI*(X*X+Y*Y))
      VSO=VSO+Q(I)*(Y-YS(I))/(2*PI*((X-XS(I))*(X-XS(I))+
      1   (Y-YS(I))*(Y-YS(I))))
      VSI=VSI-Q(I)*Y/(4*PI*(X*X+Y*Y))
55    CONTINUE
      VUD=-2*X*Y/((X*X+Y*Y)**2)
      U=UUD+USO+USI
      V=VUD+VSO+VSI
      ELSE
50    U=1.0-(X*X-Y*Y)/((X*X+Y*Y)**2)
      V=-2.*X*Y/((X*X+Y*Y)**2)
      END IF
      END IF
      RETURN
```

```
      END
      SUBROUTINE DRAG(RED,STOKE)
      COMMON REYNOL(200),CDRE(200),NPTS
      DO 10 I=1,NPTS
      IF(REYNOL(I).LE.RED) GO TO 10
      STOKE=CDRE(I-1)+(RED-REYNOL(I-1))*(CDRE(I)-CDRE(I-1))/
     1     (REYNOL(I)-REYNOL(I-1))
      GO TO 20
10    CONTINUE
30    TYPE *,'NO MATCH IN THE CDRE TABLE'
      STOP
20    RETURN
      END
```

APPENDIX O

COMPUTER PROGRAM FOR STREAMLINES CALCULATION

```
C C C
```

```
      DO 20 I=1,NS
      ALFA=ANGLE(I)*PI/180.0
      XS(I)=COS(ALFA)
      YS(I)=SIN(ALFA)
20    CONTINUE
      DO 200 NL=1,NLINES
      IF(NAM1.EQ.'Y'.OR.NAM1.EQ.'YES') THEN
      X=XI
      Y=PSI(NL)
      ELSE
      Y=PSI(NL)
      X=XI
C     NOTE THAT XI=XDROP(1,NL)
      PSIUD=Y*(1.0-1.0/(X*X+Y*Y))
      PSISO=0.0
      PSISI=0.0
      DO 30 I=1,NS
      PSISO=PSISO+Q(I)*(ATAN((Y-YS(I))/(X-XS(I))))/(2.*PI)
      PSISI=PSISI-Q(I)*(ATAN(Y/X))/(4.*PI)
30    CONTINUE
      PSI(NL)=PSIUD+PSISO+PSISI
      WRITE(5,35)PSI(NL)
35    FORMAT(2X,'STREAM LINES    ',F10.3)
      END IF
      I=1
40    CALL NEWTON(F,FDERV,Y,1.E-4,1.E-4,150,IFLAG)
      IF(IFLAG.GT.1) STOP
      FY=F(Y)
      IF(ABS(X).GT.4.0) GO TO 50
      XPSI(I,NL)=X
      YPSI(I,NL)=Y
      I=I+1
50    IF(ABS(X).GT.1.0) X=X+0.1
      IF(ABS(X).LE.1.0) X=X+0.01
      IF(X     .LT.XEND) GO TO 40
      WRITE(1,*)I-1
      WRITE(1,*)(XPSI(K,NL),K=1,I-1)
      WRITE(1,*)(YPSI(K,NL),K=1,I-1)
      TYPE *,I-1
200   CONTINUE
      CLOSE(UNIT=1,FILE=NAM2)
999   FORMAT(2X,'ENTER OUTPUT DATA FILE NAME   ',$)
1000  FORMAT(2X,'GENERATING STREAM LINES PLOT ONLY? (Y/N)   ',$)
1100  FORMAT(2X,'ENTER XI,XEND,NS(90-->270),NLINES    ',$)
1200  FORMAT(2X,'ENTER SOURCE ANGLES(90-->270)    ',$)
1300  FORMAT(2X,'ENTER SOURCE STRENGTH(90-->270)    ',$)
1400  FORMAT(2X,'ENTER STREAM LINES OR INITIAL DROP YS   ',$)
1500  FORMAT(2X,'ENTER THE INPUT DATA FILE NAME    ',$)
      END
      SUBROUTINE NEWTON(F,FDERV,Y,YTOL,FTOL,NTOL,IFLAG)
```

```
      COMMON PSI(10),XS(100),YS(100),ANGLE(100),Q(100),X,NS,NL,PI
      IFLAG=0.0
      DO 10 N=1,NTOL
      FY=F(Y)
      IF(ABS(FY).LT.FTOL) RETURN
      DERIV=FDERV(Y)
      IF(DERIV.EQ.0.0) GO TO 30
      DELTAY=FY/DERIV
      Y=Y-DELTAY
10    IF(ABS(DELTAY).LT.YTOL) RETURN
      WRITE(5,20)
20    FORMAT(2X,'NO CONVERGENCE')
      IFLAG=2
      RETURN
30    WRITE(5,40)
40    FORMAT(2X,'DIVISION BY ZERO')
      IFLAG=2
      RETURN
      END
      FUNCTION F(Y)
      COMMON PSI(10),XS(100),YS(100),ANGLE(100),Q(100),X,NS,NL,PI
      PSIUD=Y*(1.0-1.0/(X*X+Y*Y))
C     CALCULATE TOTAL SOURCE STREAM FUNCTION
      PSISO=0.0
      DO 40 I=1,NS
      DELY=Y-YS(I)
      DELX=X-XS(I)
      IF(DELX.NE.0.0) GO TO 10
      ARCTAN=0.0
      IF(DELY.GT.0.0) ARCTAN=-PI/2.0
      IF(DELY.LT.0.0) ARCTAN=+PI/2.0
      IF(ARCTAN.NE.0.0) GO TO 30
      WRITE(5,5)I
5     FORMAT(2X,'STREAM LINE IS PASSING THROUGH SOURCE NO.  ',I2)
      STOP
10    IF(DELY.NE.0.0) GO TO 20
      IF(DELX.LT.0.0) ARCTAN=0.0
      IF(DELX.GT.0.0) ARCTAN=-PI
      GO TO 30
20    IF(DELX.GT.0.0.AND.DELY.GT.0.0) ARCTAN=-PI+ATAN(DELY/DELX)
      IF(DELX.LT.0.0.AND.DELY.GT.0.0) ARCTAN=+ATAN(DELY/DELX)
      IF(DELX.LT.0.0.AND.DELY.LT.0.0) ARCTAN=ATAN(DELY/DELX)
      IF(DELX.GT.0.0.AND.DELY.LT.0.0) ARCTAN=+PI+ATAN(DELY/DELX)
30    PSISO=PSISO+Q(I)*ARCTAN/(2.*PI)
40    CONTINUE
C     CALCULATE SINK STREAM FUNCTION
      PSISI=0.0
      DO 80 I=1,NS
      IF(X.NE.0.0) GO TO 50
      ARCTAN=0.0
```

```
      IF(Y.GT.0.0) ARCTAN=-PI/2.0
      IF(Y.LT.0.0) ARCTAN=+PI/2.0
      IF(ARCTAN.NE.0.0) GO TO 70
      WRITE(5,45)I
45    FORMAT(2X,'STREAM LINE IS PASSING THROUGH SINK NO.  ',I2)
      STOP
50    IF(Y.NE.0.0) GO TO 60
      IF(X.LT.0.0) ARCTAN=0.0
      IF(X.GT.0.0) ARCTAN=-PI
      GO TO 70
60    IF(X.GT.0.0.AND.Y.GT.0.0) ARCTAN=-PI+ATAN(Y/X)
      IF(X.LT.0.0.AND.Y.GT.0.0) ARCTAN=+ATAN(Y/X)
      IF(X.LT.0.0.AND.Y.LT.0.0) ARCTAN=+ATAN(Y/X)
      IF(X.GT.0.0.AND.Y.LT.0.0) ARCTAN=+PI+ATAN(Y/X)
70    PSISI=PSISI-Q(I)*ARCTAN/(4.*PI)
80    CONTINUE
CC    TYPE *,PSISO,PSISI,PSIUD,PSI(NL),F
      F=-PSI(NL)+PSIUD+PSISO+PSISI
      RETURN
      END
      FUNCTION FDERV(Y)
      COMMON PSI(10),XS(100),YS(100),ANGLE(100),Q(100),X,NS,NL,PI
      FDERUD=(1.0-(X*X-Y*Y)/((X*X+Y*Y)**2.0))
      FDERSO=0.0
      FDERSI=0.0
      DO 10 I=1,NS
      FDERSO=FDERSO+Q(I)*(X-XS(I))/(((X-XS(I))**2+(Y-YS(I))**2)*2*PI)
      FDERSI=FDERSI-Q(I)*X/((X*X+Y*Y)*4.*PI)
10    CONTINUE
      FDERV=FDERUD+FDERSO+FDERSI
      RETURN
      END
```

APPENDIX P

COMPUTER PROGRAM FOR 1-EQUATION MODEL

```
C C C
```

```
          TYPE 1020,IT,ETAEND,X
10        ETA=0.
          DO 15 I=1,NEQ
15        S(I)=0D0
          S(1)=0.0
          S(3)=X
          S(6)=1D0
          IF(NETA.EQ.NETAF.AND.IT.EQ.1)THEN
          ETA=0D0
          WRITE(1,1016)IXI,IT-1,XC(IXI),ETA,S(1),S(2),S(3),S(4)
          END IF
          IFLAG=1
         CALL RKF45(DERIV,NEQ,S,ETA,ETAEND,RELERR,ABSERR,IFLAG,WORK,
          1          IWORK)
          IF(IFLAG.NE.2)THEN
          WRITE(5,1040)IFLAG
          WRITE(1,1040)IFLAG
          GO TO 800
          END IF
          IF(NETA.EQ.NETAF)GO TO 75
C
C*******LEAST SQUARE SOLUTION
C
          CORR=(-S(5)*(S(2)-1)-S(3)*S(6))/(S(5)*S(5)+S(6)*S(6))
C
C********CORRECTIONS TO THE INITIAL GUESS I.E. X
C
          X=X+CORR
          E=ABS(1-S(2))**2+S(3)**2
          C1=CORR/X
          IF(DABS(C1).GT.ABSERR)GO TO 10
          ERR=0.1*ABSERR
          IF(E.LT.ERR)GO TO 105
75        IF(NETA.EQ.NETAF)THEN
          WRITE(1,1016)IXI,IT,XC(IXI),ETAEND,S(1),S(2),S(3),S(4)
          END IF
100       CONTINUE
105       IF(NETA.EQ.NETAF) GO TO 110
          NETA=NETAF
          ETAINF(IXI)=ETAEND
          ETAEND=0.0
          GO TO 5
110       CONTINUE
800       CLOSE(1)
          WRITE(1,*)(ETAINF(K),K=1,NPX)
          STOP
1010      FORMAT(2X,'ENTER NPX,NPY,RE,VWALL,FILE NAME      ',$)
1015      FORMAT(2(2X,I10),2(2X,D15.8))
1016      FORMAT(2(2X,I2),5(2X,D15.8))
1017      FORMAT(43X,3(2X,D15.8))
1020      FORMAT(2X,'ETA ITERATION = ',I2,2X,'ETA END = ',F10.5,2X,F10.5)
1040      FORMAT('  IWORK ',I2)
```

```
END
SUBROUTINE DERIV(ETA,S,SP)
IMPLICITREAL*8(A-H,O-Z)
DIMENSION S(6),SP(6)
COMMON XI,BETA,GAMA
SP(1)=S(2)
SP(2)=S(3)
SP(3)=-GAMA*S(3)-BETA*
1     (1D0-S(2)*S(2))-S(1)*S(3)
SP(4)=S(5)
SP(5)=S(6)
SP(6)=
1     -S(4)*S(3)-S(1)*S(6)+2D0*BETA*S(2)*S(5)-GAMA*S(6)
RETURN
END
```

APPENDIX Q

COMPUTER PROGRAM FOR 2-EQUATION MODEL

```
C C C
```

```
          S(1)=0D0
          S(3)=X
          S(6)=1D0
          S(12)=Y
          S(18)=1D0
          IFLAG=1
         CALL RKF45(DERIV,NEQ,S,ETA,ETAEND,RELERR,ABSERR,IFLAG,WORK,
          1          IWORK)
          IF(IFLAG.NE.2)WRITE(5,10110)IFLAG
10110     FORMAT('  IWORK ',I2)
          WRITE(5,10050)ETA,(S(I),I=2,3),(S(I),I=11,12)
10050     FORMAT(2X,'ETA=',F10.2,2X,' FP=',F12.8,2X,' FPP=',F12.8/
          1      18X,'GP=',F12.8,2X,'GPP=',F12.8)
C
C*******LEAST SQUARE SOLUTION
C
          F(1,1)=S(5);F(1,2)=S(8)
          F(2,1)=S(6);F(2,2)=S(9)
          F(3,1)=S(14);F(3,2)=S(17)
          F(4,1)=S(15);F(4,2)=S(18)
          DO 80 I=1,4
          DO 80 J=1,2
80        FT(J,I)=F(I,J)
          DO 85 I=1,2
          DO 85 J=1,2
          FM(I,J)=0D0
          DO 85 K=1,4
85        FM(I,J)=FM(I,J)+FT(I,K)*F(K,J)
          YI(1)=1D0-S(2);YI(2)=-S(3);YI(3)=-S(11);YI(4)=-S(12)
          DO 90 I=1,2
          B(I)=0D0
          DO 90 K=1,4
90        B(I)=B(I)+FT(I,K)*YI(K)
          DO 106 K=1,2
          AIN=1./FM(K,K)
          DO 101 J=1,2
          IF(J.NE.K)THEN
          FM(K,J)=FM(K,J)*AIN
          END IF
101       CONTINUE
          FM(K,K)=AIN
          DO 103 I=1,2
          IF(I.NE.K)THEN
          DO 102 J=1,2
          IF(J.NE.K)THEN
          FM(I,J)=FM(I,J)-FM(K,J)*FM(I,K)
          END IF
102       CONTINUE
          END IF
103       CONTINUE
```

```
      DO 106 I=1,2
      IF(I.NE.K)THEN
      FM(I,K)=-FM(I,K)*FM(K,K)
      END IF
106   CONTINUE
      DO 107 I=1,2
      C(I)=0.0
      DO 107 K=1,2
107   C(I)=C(I)+FM(I,K)*B(K)
C
C********CORRECTIONS TO THE INITIAL GUESSES I.E. X AND Y
C
      X=X+C(1)
      Y=Y+C(2)
      E=ABS(1D0-S(2))**2+S(3)**2+S(11)**2+S(12)**2
      WRITE(5,10115)E,C(1),C(2)
10115 FORMAT(' E,DX,DY ',3(1PD12.4))
      WRITE(5,10059)C(1)/X,C(2)/Y,X
10059 FORMAT(2X,'DX/X=',E15.8,3X,'DY/Y=',E15.8/
     1      3X,'X = ',F15.8,3X,'Y = ',F15.8)
      IF((DABS(C(1)/X).OR.DABS(C(2)/Y)).GT.ABSERR)GO TO 10
      ERR=0.1*ABSERR
      IF(E.LT.ERR)GO TO 111
100   CONTINUE
111   WRITE(5,10060)XI,E,C(1),C(2),X,Y
10060 FORMAT(2X,'XI=',F20.5,2X,'E=',F20.5,2X,'C1=',F20.5/
     1      'C2=',F20.5,'X=',F20.5,'Y=',F20.5)
110   CONTINUE
      STOP
      END
      SUBROUTINE DERIV(ETA,S,SP)
      IMPLICITREAL*8(A-H,O-Z)
      DIMENSION S(18),SP(18)
      COMMON XI,BETA,GAMA,BETX,BETXX,GAMX,GAMXX
      SP(1)=S(2)
      SP(2)=S(3)
      SP(3)=2D0*XI*(S(2)*S(11)-S(3)*S(10))-GAMA*S(3)-BETA*
     1     (1D0-S(2)*S(2))-S(1)*S(3)
      SP(4)=S(5)
      SP(5)=S(6)
      SP(6)=2D0*XI*(S(2)*S(14)+S(5)*S(11)-S(3)*S(13)-S(6)*S(10))
     1     -S(4)*S(3)-S(1)*S(6)+2D0*BETA*S(2)*S(5)-GAMA*S(6)
      SP(7)=S(8)
      SP(8)=S(9)
      SP(9)=2D0*XI*(S(2)*S(17)+S(8)*S(11)-S(3)*S(16)-S(9)*S(10))
     1     -S(7)*S(3)-S(1)*S(9)+2D0*BETA*S(2)*S(8)-GAMA*S(9)
      SP(10)=S(11)
      SP(11)=S(12)
      SP(12)=2D0*(S(2)*S(11)-S(3)*S(10))-GAMA*S(12)+2D0*BETA*S(2)
     1     *S(11)-BETX*(1D0-S(2)*S(2))-GAMX*S(3)-S(10)*S(3)
```

```
1     -S(1)*S(12)
SP(13)=S(14)
SP(14)=S(15)
SP(15)=2D0*(S(2)*S(14)+S(5)*S(11)-S(3)*S(13)-S(6)*S(10))
1     -S(4)*S(12)-S(1)*S(15)-S(13)*S(3)-S(10)*S(6)+2D0*BETA
1     *S(2)*S(14)+2D0*BETA*S(5)*S(11)-GAMA*S(15)+2D0*BETX
1     *S(2)*S(5)-GAMX*S(6)
SP(16)=S(17)
SP(17)=S(18)
SP(18)=2D0*(S(2)*S(17)+S(8)*S(11)-S(3)*S(16)-S(9)*S(10))
1     -S(7)*S(12)-S(1)*S(18)-S(16)*S(3)-S(10)*S(9)+2D0*BETA
1      *S(2)*S(17)+2D0*BETA*S(8)*S(11)-GAMA*S(18)+2D0*BETX
1     *S(2)*S(8)-GAMX*S(9)
RETURN
END
```

APPENDIX R

COMPUTER PROGRAM FOR 3-EQUATION MODEL

```
C C C
```

```
      X=1.
      Y=0.1
      Z=0.1
      ETAEND=4.80
      DO 750 IXI=1,NPX
      XC=XC1(IXI)
      XI=2D0*(1D0-COS(XC))
      BETA=1D0-XI/(4D0-XI)
      BETX=-4D0/((4D0-XI)*(4D0-XI))
      BETXX=-8D0/((4D0-XI)**3D0)
      GAMA=-4D0*SQRT(RE)*VJET/(SQRT(4D0-XI))
      GAMX=-2D0*SQRT(RE)*VJET/((4D0-XI)**15D-01)
      GAMXX=-3D0*SQRT(RE)*VJET/((4D0-XI)**25D-01)
      NETA=NETAI
      DETA=DETAI
      IF(XC.GT.1.4585673)ETAEND=1.5
C     ETAEND=ETAEND-2.*DETA
      ETAEND=ETAEND-1.45
50    DO 650 IT=1,NETA
      ITX=0
      IF(NETA.NE.NETAI)THEN
      IF(IT.EQ.1)THEN
      IF(YSPACE.EQ.'Y') THEN
      DETAF=ETAINF(IXI)/FLOAT(NETAF)
      DO 10 J=1,NPY-1
10    DEF(J)=DETAF
      ELSE
      WRITE(5,1013)
      READ(5,*)(DEF(J),J=1,NPY-1)
      END IF
      END IF
      ETAEND=ETAEND+DEF(IT)
      ELSE
      ETAEND=ETAEND+DETA
      END IF
      TYPE 1020,IT,ETAEND,X
100   ETA=0.
      ITX=ITX+1
C     WRITE(5,1030)ITX
      DO 150 I=1,NEQ
150   S(I)=0D0
      S(3)=X
      S(6)=1D0
      S(15)=Y
      S(21)=1D0
      S(27)=Z
      S(36)=1D0
      IF(NETA.EQ.NETAF.AND.IT.EQ.1)THEN
      ETA=0D0
      WRITE(1,1016)IXI,IT-1,XC,ETA,S(1),S(2),S(3),S(4)
```

```
          WRITE(1,1017)S(13),S(14),S(15),S(16)
          WRITE(1,1017)S(25),S(26),S(27),S(28)
          END IF
          IFLAG=1
         CALL RKF45(DERIV,NEQ,S,ETA,ETAEND,RELERR,ABSERR,IFLAG,WORK,
          1          IWORK)
          IF(IFLAG.NE.2)THEN
          WRITE(5,1040)IFLAG
          WRITE(1,1040)IFLAG
          GO TO 800
          END IF
C         WRITE(5,1050)S(2),S(14),S(26),S(3),S(15),S(27)
          IF(NETA.EQ.NETAF)GO TO 600
C
C*******LEAST SQUARE SOLUTION
C
          F(1,1)=S(5);F(1,2)=S(8);F(1,3)=S(11)
          F(2,1)=S(6);F(2,2)=S(9);F(2,3)=S(12)
          F(3,1)=S(17);F(3,2)=S(20);F(3,3)=S(23)
          F(4,1)=S(18);F(4,2)=S(21);F(4,3)=S(24)
          F(5,1)=S(29);F(5,2)=S(32);F(5,3)=S(35)
          F(6,1)=S(30);F(6,2)=S(33);F(6,3)=S(36)
          DO 200 I=1,6
          DO 200 J=1,3
200       FT(J,I)=F(I,J)
          DO 250 I=1,3
          DO 250 J=1,3
          FM(I,J)=0D0
          DO 250 K=1,6
250       FM(I,J)=FM(I,J)+FT(I,K)*F(K,J)
          YI(1)=1.0-S(2);YI(2)=-S(3);YI(3)=-S(14);YI(4)=-S(15)
          YI(5)=-S(26);YI(6)=-S(27)
          DO 300 I=1,3
          B(I)=0D0
          DO 300 K=1,6
300       B(I)=B(I)+FT(I,K)*YI(K)
          DO 500 K=1,3
          AIN=1./FM(K,K)
          DO 350 J=1,3
          IF(J.NE.K)THEN
          FM(K,J)=FM(K,J)*AIN
          END IF
350       CONTINUE
          FM(K,K)=1.*AIN
          DO 450 I=1,3
          IF(I.NE.K)THEN
          DO 400 J=1,3
          IF(J.NE.K)THEN
          FM(I,J)=FM(I,J)-FM(K,J)*FM(I,K)
          END IF
400       CONTINUE
```

```
          END IF
450       CONTINUE
          DO 500 I=1,3
          IF(I.NE.K)THEN
          FM(I,K)=-FM(I,K)*FM(K,K)
          END IF
500       CONTINUE
          DO 550 I=1,3
          C(I)=0.0
          DO 550 K=1,3
550       C(I)=C(I)+FM(I,K)*B(K)
C
C********CORRECTIONS TO THE INITIAL GUESSES I.E. X,Y AND Z
C
          X=X+C(1)
          Y=Y+C(2)
          Z=Z+C(3)
          E=ABS(1D0-S(2))**2+S(3)**2
C         WRITE(5,1060)E,X,Y,Z
          C1=C(1)/X
          C2=C(2)/Y
          C3=C(3)/Z
C         WRITE(5,1070)C1,C2,C3
          IF(ABS(C1).GT.ABSERR) GO TO 100
          IF(ABS(C2).GT.ABSERR) GO TO 100
          IF(ABS(C3).GT.ABSERR) GO TO 100
          ERR=0.1*ABSERR
          IF(E.LT.ERR)GO TO 700
600       IF(NETA.EQ.NETAF)THEN
C          WRITE(5,1080)S(1),S(2),ETAEND,XC
          WRITE(1,1016)IXI,IT,XC,ETAEND,S(1),S(2),S(3),S(4)
          WRITE(1,1017)S(13),S(14),S(15),S(16)
          WRITE(1,1017)S(25),S(26),S(27),S(28)
          END IF
650       CONTINUE
700       IF(NETA.EQ.NETAF) GO TO 750
C         WRITE(5,1090)XC,E,ETAEND,X,Y,Z
          NETA=NETAF
C         DETA=ETAEND/NETAF
          ETAINF(IXI)=ETAEND
          ETAEND=0.0
          GO TO 50
750       CONTINUE
          WRITE(1,*)(ETAINF(K),K=1,NPX)
800       CLOSE(UNIT=1,FILE=NAM1)
          STOP
1010      FORMAT(2X,'ENTER NPX,NPY,UINF(FT/S),VJET,FILE NAME  ',$)
1011      FORMAT(2X,'EQUAL SPACING IN X & Y (Y/N)?    ',$)
1012      FORMAT(2X,'ENTER X LOCATIONS ON THE CYLINDER    ',$)
1013      FORMAT(2X,'ENTER DELA ETA IN THE B.L.    ',$)
1015      FORMAT(2(2X,I10),4(2X,D15.8))
```

```
1016     FORMAT(2(2X,I2),6(2X,D15.8))
1017     FORMAT(42X,4(2X,D15.8))
1020     FORMAT(2X,'ETA ITERATION = ',I2,2X,'ETA END = ',F10.5,2X,F10.5)
1030    FORMAT(2X,'X,Y, AND Z ITERATION = ',I2)
1040     FORMAT('  IWORK ',I2)
1050     FORMAT(2X,' FP = ',F10.5,2X,' GP = ',F10.5,2X,' HP = ',F10.5/
         1      2X,'FPP = ',F10.5,2X,'GPP = ',F10.5,2X,'HPP = ',F10.5)
1060     FORMAT(' E,X,Y,Z = ',E10.3,3(2X,F10.5))
1070     FORMAT(2X,'C1/X = ',D10.3,2X,'C2/Y = ',D10.3,2X,'C3/Z= ',D10.3)
1080     FORMAT(2X,'F,FP,ETAEND,XC      ',4(2X,F10.5))
1090     FORMAT(2X,'X/R = ',F6.2,2X,'ERROR = ',D10.3,2X,'ETAEND = '
         1      ,F10.5/
         1      2X,' X = ',F10.5,2X,' Y = ',F10.5,2X,' Z = ',F10.5)
         END
         SUBROUTINE DERIV(ETA,S,SP)
         IMPLICITREAL*8(A-H,O-Z)
         DIMENSION S(36),SP(36)
         COMMON XI,BETA,GAMA,BETX,BETXX,GAMX,GAMXX
         SP(1)=S(2)
         SP(2)=S(3)
         SP(3)=2D0*XI*(S(2)*S(14)-S(3)*S(13))-GAMA*S(3)-BETA*
         1     (1D0-S(2)*S(2))-S(1)*S(3)
         SP(4)=S(5)
         SP(5)=S(6)
         SP(6)=2D0*XI*(S(2)*S(17)+S(5)*S(14)-S(3)*S(16)-S(6)*S(13))
         1     -S(4)*S(3)-S(1)*S(6)+2D0*BETA*S(2)*S(5)-GAMA*S(6)
         SP(7)=S(8)
         SP(8)=S(9)
         SP(9)=2D0*XI*(S(2)*S(20)+S(8)*S(14)-S(3)*S(19)-S(9)*S(13))
         1     -S(7)*S(3)-S(1)*S(9)+2D0*BETA*S(2)*S(8)-GAMA*S(9)
         SP(10)=S(11)
         SP(11)=S(12)
         SP(12)=2D0*XI*(S(2)*S(23)+S(11)*S(14)-S(3)*S(22)-S(12)*S(13))
         1     -S(10)*S(3)-S(1)*S(12)+2D0*BETA*S(2)*S(11)-GAMA*S(12)
         SP(13)=S(14)
         SP(14)=S(15)
         SP(15)=2D0*(S(2)*S(14)-S(3)*S(13))-GAMA*S(15)+2D0*BETA*S(2)
         1     *S(14)-BETX*(1D0-S(2)*S(2))-GAMX*S(3)-S(13)*S(3)
         1     -S(1)*S(15)+2D0*XI*(S(14)*S(14)+S(2)*S(26)
         1     -S(25)*S(3)-S(13)*S(15))
         SP(16)=S(17)
         SP(17)=S(18)
         SP(18)=2D0*(S(2)*S(17)+S(5)*S(14)-S(3)*S(16)-S(6)*S(13))
         1     -S(4)*S(15)-S(1)*S(18)-S(16)*S(3)-S(13)*S(6)+2D0*BETA
         1     *S(2)*S(17)+2D0*BETA*S(5)*S(14)-GAMA*S(18)+2D0*BETX
         1     *S(2)*S(5)-GAMX*S(6)+2D0*XI*(2D0*S(14)*S(17)+S(2)*S(29)
         1     +S(5)*S(26)-S(25)*S(6)-S(28)*S(3)-S(13)*S(18)
         1     -S(16)*S(15))
         SP(19)=S(20)
         SP(20)=S(21)
```

```
SP(21)=2D0*(S(2)*S(20)+S(8)*S(14)-S(3)*S(19)-S(9)*S(13))
1      -S(7)*S(15)-S(1)*S(21)-S(19)*S(3)-S(13)*S(9)+2D0*BETA
1       *S(2)*S(20)+2D0*BETA*S(8)*S(14)-GAMA*S(21)+2D0*BETX
1      *S(2)*S(8)-GAMX*S(9)+2D0*XI*(2D0*S(14)*S(20)+S(2)*S(32)
1      +S(8)*S(26)-S(25)*S(9)-S(31)*S(3)-S(13)*S(21)
1      -S(19)*S(15))
SP(22)=S(23)
SP(23)=S(24)
SP(24)=2D0*(S(2)*S(23)+S(11)*S(14)-S(3)*S(22)-S(12)*S(13))
1      -S(10)*S(15)-S(1)*S(24)-S(22)*S(3)-S(13)*S(12)+2D0*BETA
1      *S(2)*S(23)+2D0*BETA*S(11)*S(14)-GAMA*S(24)+2D0*BETX
1      *S(2)*S(11)-GAMX*S(12)+2D0*XI*(2D0*S(14)*S(23)
1      +S(2)*S(35)+S(11)*S(26)-S(25)*S(12)-S(34)*S(3)
1      -S(13)*S(24)-S(22)*S(15))
SP(25)=S(26)
SP(26)=S(27)
SP(27)=-(S(1)+GAMA)*S(27)-2D0*(3D0*S(13)+GAMX)*S(15)+(4D0+
1      2D0*BETA)*S(2)*S(26)-5D0*S(25)*S(3)+(2D0*BETA+4D0)*
1      S(14)*S(14)+4D0*BETX*S(2)*S(14)-GAMXX*S(3)-(1D0-S(2)*S(2)
1      )*BETXX
SP(28)=S(29)
SP(29)=S(30)
SP(30)=-S(4)*S(27)-S(1)*S(30)-GAMA*S(30)-6D0*S(16)*S(15)
1      -6D0*S(13)*S(18)-2D0*GAMX*S(18)+(4D0+2D0*BETA)*S(2)*
1      S(29)+(4D0+2D0*BETA)*S(5)*S(26)-5D0*S(25)*S(6)-5D0*
1      S(28)*S(3)+4D0*(2D0+BETA)*S(14)*S(17)+4D0*BETX*S(2)*
1      S(17)+4D0*BETX*S(5)*S(14)-GAMXX*S(6)+2D0*BETXX*S(2)*S(5)
SP(31)=S(32)
SP(32)=S(33)
SP(33)=-S(7)*S(27)-S(1)*S(33)-GAMA*S(33)-6D0*S(19)*S(15)
1      -6D0*S(13)*S(21)-2D0*GAMX*S(21)+(4D0+2D0*BETA)*S(2)*
1      S(32)+(4D0+2D0*BETA)*S(8)*S(26)-5D0*S(25)*S(9)-5D0*
1      S(31)*S(3)+4D0*(2D0+BETA)*S(14)*S(20)+4D0*BETX*S(2)*
1      S(20)+4D0*BETX*S(8)*S(14)-GAMXX*S(9)+2D0*BETXX*S(2)*S(8)
SP(34)=S(35)
SP(35)=S(36)
SP(36)=-S(10)*S(27)-S(1)*S(36)-GAMA*S(36)-6D0*S(22)*S(15)
1      -6D0*S(13)*S(24)-2D0*GAMX*S(24)+(4D0+2D0*BETA)*S(2)*
1      S(35)+(4D0+2D0*BETA)*S(11)*S(26)-5D0*S(25)*S(12)-5D0*
1      S(34)*S(3)+4D0*(2D0+BETA)*S(14)*S(23)+4D0*BETX*S(2)*
1    S(23)+4D0*BETX*S(11)*S(14)-GAMXX*S(12)+2D0*BETXX*S(2)*S(11)
RETURN
END
```

APPENDIX S

COMPUTER PROGRAM FOR BOUNDARY LAYER AND DISPLACEMENT

THICKNESS AND VELOCITY CALCULATION

```
C C C
```

```
      XIX=2D0*SIN(XC(I))/R
      UEX=2D0*U0*COS(XC(I))/R
      TYPE *,I,UE(I),XI
      DO 100 J=1,NPY
      U(I,J)=UE(I)*FP(I,J)
      ETX=ETA(I,J)*(XI*UEX-0.5*UE(I))/(UE(I)*XI)
      V(I,J)=-SQRT(2.*NU*NU*RE)*0.5*XIX*F(I,J)/SQRT(XI)
     1       -SQRT(2.*NU*NU*RE*XI)*(FP(I,J)*ETX+G(I,J)*XIX)
     1       +VJET*U0
100   CONTINUE
      CLOSE(1)
      DO 115 J=1,NPY
      IF(F(1,J).LE.0.995) GO TO 115
      ETINF=ETA(1,J)+(ETA(1,J+1)-ETA(1,J))*(F(1,J+1)-0.995)/
     1     (F(1,J+1)-F(1,J))
      GO TO 117
115   CONTINUE
117   A=R/(SQRT(2*RE))
      DELSTA(1)=A*(ETINF-0.995)
      DEL(1)=A*ETINF
      DO 150 I=2,NPX
      DO 120 J=1,NPY
      IF(F(I,J).LE.0.995) GO TO 120
      ETINF=ETA(I,J)+(ETA(I,J+1)-ETA(I,J))*(F(I,J+1)-0.995)/
     1     (F(I,J+1)-F(I,J))
      GO TO 130
120   CONTINUE
130   A=R*SQRT(1.-COS(XC(I)))/(SQRT(RE)*SIN(XC(I)))
      DELSTA(I)=A*(ETINF-0.995)
      DEL(I)=A*ETINF
      DO 150 J=1,NPY
      Y(I,J)=A*ETA(I,J)
150   CONTINUE
      WRITE(5,1050)
      READ(5,*)NAM2
      OPEN(1,FILE=NAM2)
      WRITE(1,*    )NPX,NPY,RE,VJET,U0,R
      DO 175 I=1,NPX
175   WRITE(1,*    )I,ETA(I,NPY),Y(I,NPY),DELSTA(I)/R,DEL(I)/R,UE(I)
      DO 200 I=1,NPX
      DO 200 J=1,NPY
      WRITE(1,*    )I,J,XC(I),ETA(I,J),Y(I,J),U(I,J),V(I,J)
200   CONTINUE
      CLOSE(1)
C
1010  FORMAT(2X,'ENTER INPUT FILE NAME     ',$)
1020  FORMAT(2(2X,I10),4(2X,D15.8))
1030  FORMAT(2(2X,I2),6(2X,D15.8))
1040  FORMAT(42X,4(2X,D15.8))
1050  FORMAT(2X,'ENTER OUTPUT FILE NAME     ',$)
1055  FORMAT(2(2X,I10),4(2X,D15.8))
```

```
1060      FORMAT(2(2X,I2),5(2X,D15.8))
1070      FORMAT(2X,I2,4(2X,D15.8))
C
          END
```

APPENDIX T

COMPUTER PROGRAM FOR INITIAL GRID GENERATION

```
C C C
```

```
      WRITE(5,72)NJ,Y(1,NJ),RY,DY1
72    FORMAT(2X,'NJ = 'I4,' YMAX = ',F6.1,' RATIO = ',F9.6,
     1       '  FIRST Y = ',F8.5/)
      END IF
      IF(ANS.NE.'Y')THEN
      TYPE *,'ENTER NJ,YMAX'
      READ(5,*)NJ,YMAX
      DY=YMAX/(NJ-1)
      DO 90 J=1,NJ
90    Y(1,J)=DY*(J-1)
      DY1=DY
      RY=1.0
      END IF
C------THERE IS A SYMMETRY AT X=0.0. THUS ONLY FIRST QUADRANT OF
C------THE DOMIAN IS DISCRETIZED  AND MIRROR IMAGE IS USED FOR THE
C------BACK SIDE.   THIS REGION IS DIVIDED INTO TWO SECTION:
C----------1) 1/4   OF THE CYLINDER SURRFACE
C----------2) AHEAD OF THE CYLINDER ALONG X AND Y=0.0
C------THE CHOICE OF GEOMETRIC PROGRESSION IS GIVEN FOR TWO SECTION
C
      WRITE(5,92)
92    FORMAT(2X,'# PTS AHEAD OF CYL' /
     1       2X,'# PTS ON CYL (ODD NUMBER)'/
     1       2X,'# PTS BEHIND CYL     ',$)
      READ(5,*)NIA,NC,NIB
      NCH=(NC-1)/2
      DANG=(3.141592654-0.3)/(NC-1-4)
      X(NIA+1,1)=-1D0
      X(NIA+2,1)=-COS(0.05)
      X(NIA+3,1)=-COS(0.1)
      Y(NIA+1,1)=0D0
      Y(NIA+2,1)=SIN(0.05)
      Y(NIA+3,1)=SIN(0.1)
      X(NIA+NC,1)=+1D0
      X(NIA+NC-1,1)=+COS(0.05)
      X(NIA+NC-2,1)=+COS(0.1)
      Y(NIA+NC,1)=0D0
      Y(NIA+NC-1,1)=+SIN(0.05)
      Y(NIA+NC-2,1)=+SIN(0.1)
      ANGLE=0.15+DANG
      DO 105 I=4,NC-3
      X(NIA+I,1)=-COS(DANG*(I-4)+ANGLE)
      Y(NIA+I,1)=+SIN(DANG*(I-4)+ANGLE)
105   CONTINUE
      TYPE *,'GEOMETRIC PROGRESSION IN X (1 TO XMAX) (Y/N)?'
      READ(5,25)ANS
      IF(ANS.EQ.'Y')THEN
115   WRITE(5,120)
120   FORMAT(2X,'XMAX,AND FIRST DX BEHIND CYL= ',$)
      READ(5,*)XMAX,DX1
```

```
      XMAX=XMAX-1.0
      R=1.5
      DO 125 I=1,500
      ROLD=R
      FX=R-1.-DX1*(R**NIB-1.)/XMAX
      FXP=1.-DX1*NIB*R**(NIB-1)/XMAX
      R=R-FX/FXP
      IF(ABS(R-ROLD).LE.0.0000001)GO TO 130
125   CONTINUE
      TYPE *,'THE +X DIR GEOMETRIC PROGRESSION DID NOT CONVERGE'
      WRITE(5,127)R,ABS(R-ROLD)
127   FORMAT(2X,' GEO. RATIO = ',F8.5,'  RESIDUAL = ',F8.7)
      GO TO 1000
130   RXB=R
      RXA=RXB
      DX=DX1
      X(NIA+NC+1,1)=1.0+DX1
      X(NIA,1)=-1.0-DX1
      DO 150 I=2,NIB
      DX=DX*RXB
      X(NIA+NC+I,1)=X(NIA+NC+I-1,1)+DX
150   X(NIA-I+1,1)=+X(NIA-I+2,1)-DX
      XMAX=X(NI,1)
      XMIN=X(1,1)
      WRITE(5,155)NIB,NIA,RXB,RXA,X(NIB+NIA+NC,1),X(1,1),DX1
155   FORMAT(2X,'# PTS BEHIND CYL = ',I4/
     1      2X,'# PTS AHEAD OF CYL = 'I4/
     1      2X,'PROGRESSION RATIO BEHIND & AHEAD OF CYL  =',2F10.5/
     1      2X,'XMAX & XMIN  = ',2F15.5/
     1      2X,'FIRST DX     =',F10.5/)
      END IF
      IF(ANS.NE.'Y')THEN
      TYPE *,'ENTER XMAX'
      READ(5,*)XMAX
      DX=(XMAX-1.0)/NIB
      DO 160 I=1,NIB
      Y(NIB+NC+I,1)=0.0
      Y(NIA-I+1,1)=0.0
      X(NIB+NC+I,1)=DX*I+1.0
160   X(NIA-I+1,1)=-DX*I  -1.0
      DX1=DX
      RXB=1.0
      RXA=1.0
      XMIN=-XMAX
      END IF
      NI=NIB+NIA+NC
      WRITE(5,*)(X(I,1),I=1,NIB+NIA+NC)
      WRITE(5,*)(Y(I,1),I=1,NIB+NIA+NC)
      WRITE(5,*)(Y(1,J),J=1,NJ)
      DO 180 J=1,NJ
```

```
        X(NI,J)=X(NI,1)
180     Y(NI,J)=Y(1,J)
C------PSI=Y(1-1/R**2),  PHI=X(1+1/R**2)
        DO 200 J=1,NJ
        X(1,J)=+X(1,1)
        AAA=ABS(X(1,J))
200     PSI(J)=Y(1,J)*(1.-1./(AAA**2.+Y(1,J)**2.))
        DO 300 I=1,NI
        AAA=ABS(X(I,1))
300     PHI(I)=X(I,1)*(1.+1./(AAA**2.+Y(I,1)**2.))
C
C-----FIND THE COORDINATES OF THE INTERSECTION OF PSI & PHI
C
        DO 600 I=NI-1,2,-1
        DO 600 J=2,NJ
        X(I,J)=X(I,J-1)
        Y(I,J)=Y(I+1,J)
        AA=X(I,J)*X(I,J)+Y(I,J)*Y(I,J)
        F=-PSI(J)+Y(I,J)*(1.0-1.0/AA)
        G=-PHI(I)+X(I,J)*(1.0+1.0/AA)
        DO 400 ITER=1,NGITER
        F=-PSI(J)+Y(I,J)*(1.0-1.0/AA)
        G=-PHI(I)+X(I,J)*(1.0+1.0/AA)
        FX=+2.*X(I,J)*Y(I,J)/(AA*AA)
        FY=1.0-1./AA+2*Y(I,J)*Y(I,J)/(AA*AA)
        GX=1.0+1.0/AA-2*X(I,J)*X(I,J)/(AA*AA)
        GY=-2.*X(I,J)*Y(I,J)/(AA*AA)
        DELTAX=(-F*GY+G*FY)/(FX*GY-FY*GX)
        DELTAY=(-G*FX+F*GX)/(FX*GY-FY*GX)
        X(I,J)=X(I,J)+DELTAX
        Y(I,J)=Y(I,J)+DELTAY
        AA=X(I,J)*X(I,J)+Y(I,J)*Y(I,J)
        F=-PSI(J)+Y(I,J)*(1.0-1.0/AA)
        G=-PHI(I)+X(I,J)*(1.0+1.0/AA)
        IF(AMAX1(ABS(DELTAX),ABS(DELTAY),ABS(F),ABS(G)).LT.1.E-6)
        1GO TO 600
400     CONTINUE
        WRITE(5,450)ITER,I,J
450     FORMAT(2X,'NO CONVERGENCE AFTER  ',I4,'  ITERATIONS'/
        1      2X,' I  = ',I3,'  J  =  ',I3)
        GO TO 1000
600     CONTINUE
       WRITE(5,601)
601    FORMAT(2X,'ENTER INITIAL DATA FILE NAME IN QOUTS   ',$)
       READ(5,*)NAMI
        OPEN(UNIT=1,FILE=NAMI)
        WRITE(1,*)NI,NJ
        DO 700 J=NJ,1,-1
        WRITE(1,800)(I,J,X(I,J),I=1,NI)
700     WRITE(1,800)(I,J,Y(I,J),I=1,NI)
800    FORMAT(5(1X,I4,I4,D16.8))
```

```
      WRITE(1,850)NI,NJ,RY,RXB,RXA,DY1,DX1,XMAX,XMIN,YMAX
850   FORMAT(2X,'NI & NJ = ',2I6/
     1       2X,'RY,RXB,RXA = ',3F15.5/
     1       2X,'DY1 & DX1 = ',2F15.5/
     1       2X,'XMAX,XMIN,YMAX =',3(2X,F8.2))
      CLOSE(UNIT=1,FILE=NAMI)
1000  STOP
      END
```

APPENDIX U

COMPUTER PROGRAM FOR GRID MAPPING

```
C C C
```

```
 23     FORMAT(2X,'ENTER GRID FILE NAME IN QOUTS  ',$)
        READ(5,*,ERR= 22)NAM2
        DETA=1./(NJ-1)
        DXI=2./(NI-1)
        DDE1=DT*0.25*(NJ-1)
        DZZ1=(NI-1)*(NI-1)*0.25
        DEE1=(NJ-1)*(NJ-1)
        DDZ=DT*0.5*DZZ1
        DDE=DT*0.5*DEE1
        DE2=0.5*(NJ-1.)
        DZ2=0.25*(NI-1.)
        DEZ=0.125*(NI-1.)*(NJ-1.)
        WRITE(5,40)
40      FORMAT(2X,'ENTER AMP. & DECAY FACTOR     ',$)
        READ(5,*)AMP,DEC
        IF(AMP.EQ.0.0.AND.DEC.EQ.0.0)THEN
        DO 25 J=1,NJ
25      Q(J)=0
        ELSE
        WRITE(5,30)
30      FORMAT(2X,'ENTER # OF LINES FROM Y=0.0 TO BE CONTROLLED   ',$)
        READ(5,*)NLFB
C       WRITE(5,35)
C35     FORMAT(2X,'ENTER RANGE IN THE X DIR TO BE CONTROLLED   ',$)
C       READ(5,*)NRANX1,NRANX2
C       DO 50 I=1,(NI-1)/2+1
        I=2
        NRANX1=1
        NRANX2=NI
        DO 50 J=2,NJ
C       IF(I.LT.NRANX1.OR.I.GT.NRANX2)THEN
C       Q(J)=0.0
C       ELSE
        IF(J.GT.NLFB+1)THEN
        Q(J)=0.0
        ELSE
        NJINF=NLFB+2
        AQ=AMP*(J-NJINF)/NLFB
        Q(J)=+AQ*EXP(-DEC*DETA*(J-1))
        END IF
C       END IF
50      CONTINUE
        GO TO 70
        NN1=NI-NRANX2+1
        NN2=NI-NRANX1+1
        DO 60 I=(NI-1)/2+1,NI
        DO 60 J=1,NJ
        IF(I.LT.NN1.AND.I.GT.NN2)THEN
        Q(J)=0.0
        ELSE
```

```
      IF(J.GT.NLFB+1)THEN
      Q(J)=0.0
      ELSE
      NJINF=NLFB+2
      AQ=AMP*(J-NJINF)/NLFB
      Q(J)=AQ*EXP(-DEC*DETA*(J-1))
      END IF
      END IF
60    CONTINUE
      END IF
70    CONTINUE
      DO 500 ITIME=1,900
      DO 200 J=2,NJ-1
      ALFY(1)=0.
      ALFX(1)=0.
      BETY(1)=0.
      BETX(1)=0.
      DO 100 I=2,NI-1
      A1=(X(I,J+1)-X(I,J-1))*DE2
      A2=(Y(I,J+1)-Y(I,J-1))*DE2
      B1=(X(I+1,J)-X(I-1,J))*DZ2
      B2=(Y(I+1,J)-Y(I-1,J))*DZ2
      AJJ=B1*A2-A1*B2
      AJJ2=AJJ*AJJ
      BETA=B1*A1+B2*A2
      GAMA=B1*B1+B2*B2
      ALFA=A1*A1+A2*A2
      DYDZZ=(Y(I+1,J)-2*Y(I,J)+Y(I-1,J))*DZZ1
      DYDEE=(Y(I,J+1)-2*Y(I,J)+Y(I,J-1))*DEE1
      DXDZZ=(X(I+1,J)-2*X(I,J)+X(I-1,J))*DZZ1
      DXDEE=(X(I,J+1)-2*X(I,J)+X(I,J-1))*DEE1
      DYDZE=(Y(I+1,J+1)-Y(I-1,J+1)-Y(I+1,J-1)+Y(I-1,J-1))*DEZ
      DYDZE1=(Y1(I+1,J+1)-Y1(I-1,J+1)-Y1(I+1,J-1)+Y1(I-1,J-1))*DEZ
      DXDZE=(X(I+1,J+1)-X(I-1,J+1)-X(I+1,J-1)+X(I-1,J-1))*DEZ
      DXDZE1=(X1(I+1,J+1)-X1(I-1,J+1)-X1(I+1,J-1)+X1(I-1,J-1))*DEZ
      A=-ALFA*DDZ
      B=1.+2.*ALFA*DDZ
      C=A
      DY=DT*(ALFA*DYDZZ+GAMA*DYDEE-2.*BETA*DYDZE-BETA*(DYDZE-DYDZE1))
     1  +DT*Q(J)*A2*AJJ2
      DX=DT*(ALFA*DXDZZ+GAMA*DXDEE-2.*BETA*DXDZE-BETA*(DXDZE-DXDZE1))
     1  +DT*Q(J)*A1*AJJ2
      DENY=B+C*BETY(I-1)
      DENX=B+C*BETX(I-1)
      ALFY(I)=(DY-C*ALFY(I-1))/DENY
      BETY(I)=-A/DENY
      ALFX(I)=(DX-C*ALFX(I-1))/DENX
      BETX(I)=-A/DENX
100   CONTINUE
      DO 150 II=2,NI-1
```

```
      I=NI-II+1
      DYY(I,J)=ALFY(I)+BETY(I)*DYY(I+1,J)
      DXX(I,J)=ALFX(I)+BETX(I)*DXX(I+1,J)
150   CONTINUE
200   CONTINUE
      DO 400 I=2,NI-1
      ALFY(1)=0.
      ALFX(1)=00.
      BETY(1)=0.0
      BETX(1)=0.
      DO 300 J=2,NJ-1
      A1=(X(I,J+1)-X(I,J-1))*DE2
      A2=(Y(I,J+1)-Y(I,J-1))*DE2
      B1=(X(I+1,J)-X(I-1,J))*DZ2
      B2=(Y(I+1,J)-Y(I-1,J))*DZ2
      AJJ=B1*A2-A1*B2
      AJJ2=AJJ*AJJ
      GAMA=B1*B1+B2*B2
      A=-GAMA*DDE -Q(J)*DDE1*AJJ2
      B=1.+2.*GAMA*DDE
      C=-GAMA*DDE +Q(J)*DDE1*AJJ2
      DY=DYY(I,J)
      DX=DXX(I,J)
      DENY=B+C*BETY(J-1)
      ALFY(J)=(DY-C*ALFY(J-1))/DENY
      DENX=B+C*BETX(J-1)
      ALFX(J)=(DX-C*ALFX(J-1))/DENX
      BETY(J)=-A/DENY
      BETX(J)=-A/DENX
300   CONTINUE
      DYY(I,NJ)=0.0
      DXX(I,NJ)=0.0
      RESX=0.0
      RESY=0.0
      DO 350 JJ=2,NJ-1
      J=NJ-JJ+1
      Y1(I,J)=Y(I,J)
      X1(I,J)=X(I,J)
      DYY(I,J)=ALFY(J)+BETY(J)*DYY(I,J+1)
      Y(I,J)=Y(I,J)+DYY(I,J)
      DXX(I,J)=ALFX(J)+BETX(J)*DXX(I,J+1)
      X(I,J)=X(I,J)+DXX(I,J)
      RESY=RESY+ABS(DYY(I,J))
      RESX=RESX+ABS(DXX(I,J))
350   CONTINUE
400   CONTINUE
      IF(MOD(ITIME,20).EQ.0)THEN
      WRITE(5,*)ITIME,RESX,RESY
      OPEN(UNIT=1,FILE=NAM2)
      WRITE(1,*)NI,NJ
```

```
      DO 610 J=NJ,1,-1
      WRITE(1,615)(I,J,X(I,J),I=1,NI)
610   WRITE(1,615)(I,J,Y(I,J),I=1,NI)
      I=2
      WRITE(1,615)(I,J,Q(J),J=1,NJ)
615   FORMAT(5(1X,I4,I4,D16.8))
      WRITE(1,650)ITIME,RESX,RESY,NI,NJ,DT,DEC,AMP,NLFB,NRANX1,NRAN
      CLOSE(1,FILE=NAM2)
      END IF
      IF(RESX.LE.EPSI.AND.RESY.LE.EPSI)GO TO 580
500   CONTINUE
580   OPEN(UNIT=1,FILE=NAM2)
      WRITE(1,*)NI,NJ
      DO 611 J=NJ.1,-1
      WRITE(1,615)(I,J,X(I,J),I=1,NI)
611   WRITE(1,615)(I,J,Y(I,J),I=1,NI)
      I=2
      WRITE(1,615)(I,J,Q(J),J=1,NJ)
      WRITE(1,650)ITIME,RESX,RESY,NI,NJ,DT,DEC,AMP,NLFB,NRANX1,NRAN
650   FORMAT(1X,'# OF TIME ITER.= ',I4/
     1       1X,'RESX= ',D15.8,'   RESY= ',D15.8/
     1       1X,'# OF X POINTS = ',I4,'  # OF Y POINTS = ',I4/
     1       1X,'TIME STEP = ',D15.8/
     1       1X,'CONTROL TERMS ARE :'/
     1    1X,'DECAY FACTOR = ',F10.5,'  CONTROL AMPLITUDE = ',F10.5
     1      /1X,'# OF LINES FROM BOTTOM TO BE EFFECTED  = ',I2/
     1       1X,'X DIR RANGE OF CONTROL  =',I2,',',I2)
      CLOSE(UNIT=1,FILE=NAM2)
      J=2
      WRITE(5,*)ITIME-1,RESX,RESY
     STOP
      END
```

APPENDIX V

COMPUTER PROGRAM FOR MAPPED POTENTIAL FLOW

```
C C C
```

```
      READ(1,*)NI,NJ
      DZ=FLOAT(NI-1)/2.0
      DE=FLOAT(NJ-1)/1.0
      DZZ=DZ*DZ
      DEE=DE*DE
      DO 10 J=NJ,1,-1
      READ(1,118)(K,K,X(I,J),I=1,NI)
10    READ(1,118)(K,K,Y(I,J),I=1,NI)
      READ(1,118)(K,K,Q(J),J=1,NJ)
      CLOSE(UNIT=1,FILE=NAMD)
      DO 20 I=2,NI-1
      DO 20 J=2,NJ-1
      DXDE=(X(I,J+1)-X(I,J-1))*0.5*DE
      DXDE2=DXDE*DXDE
      DXDZ=(X(I+1,J)-X(I-1,J))*0.5*DZ
      DXDZ2=DXDZ*DXDZ
      DYDE=(Y(I,J+1)-Y(I,J-1))*0.5*DE
      DYDE2=DYDE*DYDE
      DYDZ=(Y(I+1,J)-Y(I-1,J))*0.5*DZ
      DYDZ2=DYDZ*DYDZ
      DXDZZ=(X(I+1,J)-2.*X(I,J)+X(I-1,J))*DZZ
      DXDEE=(X(I,J+1)-2.*X(I,J)+X(I,J-1))*DEE
      DYDZZ=(Y(I+1,J)-2.*Y(I,J)+Y(I-1,J))*DZZ
      DYDEE=(Y(I,J+1)-2.*Y(I,J)+Y(I,J-1))*DEE
      DXDZE=(X(I+1,J+1)-X(I-1,J+1)-X(I+1,J-1)+X(I-1,J-1))*0.25*DE*DZ
      DYDZE=(Y(I+1,J+1)-Y(I-1,J+1)-Y(I+1,J-1)+Y(I-1,J-1))*0.25*DE*DZ
      AJJ=DXDZ*DYDE-DXDE*DYDZ
      AJJ2=AJJ*AJJ
      AL(I,J)=(DXDE2+DYDE2)/AJJ2
      GA(I,J)=(DXDZ2+DYDZ2)/AJJ2
      BE(I,J)=2.0*(DXDZ*DXDE+DYDZ*DYDE)/AJJ2
      QTJ(I,J)=+DT*Q(J)
20    CONTINUE
      IF(ICOND) CALL INICON
      IF(IREAD) CALL READ1
      IF(VJET.GT.0.)THEN
      DO 25 I=25,30
C25   PSI(I,1)=-0.01445*VJET
25    PSI(I,1)=-VJET/4
      DO 27 I=31,NI
C27   PSI(I,1)=-0.04335*VJET
27    PSI(I,1)=-0.75*VJET
      END IF
      IF(IPRT1) CALL PRINT1
      IF(IPRT2) CALL PRINT2
      IF(IPRT4) CALL PRINT4
      IF(.NOT.IPRT4)IPRT4=.TRUE.
      IF(NTITER.EQ.0) GO TO 55
      DT2=DT*0.5
      WRITE(5,35)
35    FORMAT(2X,'ENTER DATA FILE NAME FOR PSI     ',$)
```

```
          READ(5,*)NAMP
40        IF(MOD(NITER,40).EQ.0)THEN
          OPEN(UNIT=1,FILE=NAMP)
          WRITE(1,*)NI,NJ
          DO 41 J=NJ,1,-1
41        WRITE(1,118)(I,J,PSI(I,J),I=1,NI)
          WRITE(1,120)NITER,DT,RESP,VJET
          CLOSE(UNIT=1,FILE=NAMP)
          END IF
          TYPE *,NITER,RESP
          NITER=NITER+1
          IF(IPSI) CALL CALPSI
          IF(MOD(NITER,INTVLP).NE.0) GO TO 45
          WRITE(5,107)
          IERR=3
42        READ(5,*,ERR=115)NPRT
          WRITE(5,104)NITER,RESP
          IF(IPRT3) CALL PRINT3
          WRITE(5,106)
          IERR=4
43        READ(5,*,ERR=115)CHINTP
          IF(CHINTP.NE.0.0) INTVLP=CHINTP
45       CONTINUE
C
C------CONVERGENCE TEST
C
          IF(NITER.GE.NTITER) GO TO 50
C         IF(RESP.GT.PSIEPS) GO TO 50
          GO TO 40
50        WRITE(5,108)
          IERR=5
52        READ(5,*,ERR=115)NNIT,DDT
          IF(NNIT.EQ.0)THEN
          TYPE *,'NO. OF VARIABLES FOR FINAL PRINT ?'
          IERR=6
53        READ(5,*,ERR=115)NPRT
          IF(NPRT.NE.0)CALL PRINT4
          END IF
          IF(NNIT.EQ.0) GO TO 55
          IF(DDT.NE.0.)DT=DDT
          NTITER=NNIT
          GO TO 40
55       CONTINUE
          WRITE(5,102)
          IERR=7
57        READ(5,103,ERR=115)SAVE
          IF(SAVE.EQ.'Y') CALL STORE
          GO TO 60
115       WRITE(5,116)
          GO TO(3,5,42,43,52),IERR
60        STOP
```

```
101     FORMAT(10F12.7)
102     FORMAT(5X,'IF YOU LIKE TO SAVE TYPE Y OR N    ',$)
103     FORMAT(A4)
104     FORMAT(2X,'NO. OF TIME ITERATIONS= ',I5/
     1         2X,'RESIDUE PSI= ',D15.5)
105     FORMAT(2X,'ENTER DT,NTITER,INTVLP,VJET         ',$)
106     FORMAT(2X,'ENTER NEW PRINT INTERVAL OR 0    ',$)
107     FORMAT(2X,'ENTER NO. VARIABLES FOR INT. PRINT     ',$)
108     FORMAT(2X,'ENTER NO. OF TIME ITER AND DT TO CONTINUE    ',$)
109     FORMAT(2X,'ENTER IREAD,IGRID,IPRT1,IPRT2,IPRT3,IPRT4     ',$)
111     FORMAT(6(L1))
112     FORMAT(6(L1))
116      FORMAT(2X,'RE-ENTER THE VALUE =  ',$)
118      FORMAT(5(1X,I4,I4,D16.8))
120      FORMAT(2X,'# ITER = ',I4,'   DT =  ',F10.5,/
         1      2X,'RESIDUAL PSI = ',D15.8,'   VJET = ',F10.2)
         END
         SUBROUTINE INICON
C
         IMPLICITREAL*8(A-H,O-Z)
                    COMMON
     1 /FVAR/PSI(100,50),DPSI(100,50),PSI1(100,50)
     1 /COORD/X(100,50),Y(100,50),Q(50)
     1 /INTEG/NI,NJ,NTITER
     1 /PROP/DT,VJET
C
C------CALCULATE THE FLOW REYNOLD NUMBER BASED ON THE REF. VALUES.
C
         DO 10 I=1,NI
         DO 10 J=1,NJ
         DPSI(I,J)=0.0
         PSI(I,J)=Y(I,J)*(1.-1./(X(I,J)*X(I,J)+Y(I,J)*Y(I,J)))
10       PSI1(I,J)=PSI(I,J)
         DO 20 I=2,NI-1
         DO 20 J=2,NJ-1
         PSI1(I,J)=PSI1(I,J)*0.0
20       PSI(I,J)=PSI(I,J)*0.0
30       CONTINUE
C
C-----INITIALIZE ALL THE NONDIMENSIONAL FIELD VARIABLES
C
         RETURN
         END
         SUBROUTINE CALPSI
         IMPLICITREAL*8(A-H,O-Z)
                    COMMON
     1 /FVAR/PSI(100,50),DPSI(100,50),PSI1(100,50)
     1 /COORD/X(100,50),Y(100,50),Q(50)
     1 /PROP/DT,VJET
     1 /EPSI/PSIEPS
```

```
     1 /RES/RESP,DT2,DZ,DZZ,DE,DEE
     1 /INTEG/NI,NJ,NTITER
     1 /COEF/QTJ(100,50),AL(100,50),GA(100,50),BE(100,50)
       DIMENSION ALFA(100),BETA(100)
C
C------GENERATE THE TDM COEFFICIENTS IN THE XI  DIRECTION
C
       DTZ=DT2*DZ/2.0
       DTZZ=DT2*DZZ
       DTE=DT2*DE/2.0
       DTEE=DT2*DEE
       DO 40 J=2,NJ-1
       ALFA(1)=0.0
       BETA(1)=0.0
       DO 30 I=2,NI-1
       COF1=AL(I,J)*DTZZ
C--------C=C(I-1,J),B=B(I,J),AND A=A(I+1,J)
C
       C=-COF1
       B=1.0+COF1*2.0
       A=-COF1
       DPDZZ=(PSI(I+1,J)-2.*PSI(I,J)+PSI(I-1,J))*DZZ
       DPDEE=(PSI(I,J+1)-2.*PSI(I,J)+PSI(I,J-1))*DEE
       DPDZ=(PSI(I+1,J)-PSI(I-1,J))*DZ*0.5
       DPDE=(PSI(I,J+1)-PSI(I,J-1))*DE*0.5
       DPDZE=(PSI(I+1,J+1)-PSI(I-1,J+1)-PSI(I+1,J-1)+PSI(I-1,J-1))
       1     *0.25*DE*DZ
       DPDZE1=(PSI1(I+1,J+1)-PSI1(I-1,J+1)-PSI1(I+1,J-1)+
       1     PSI1(I-1,J-1))*0.25*DE*DZ
       D=+DT*(AL(I,J)*DPDZZ+GA(I,J)*DPDEE-BE(I,J)*DPDZE)
       1  -DT2*(DPDZE-DPDZE1)*BE(I,J)+QTJ(I,J)*DPDE
       DEN=B+C*BETA(I-1)
       ALFA(I)=(D-C*ALFA(I-1))/DEN
       BETA(I)=-A/DEN
30     CONTINUE
       IF(VJET.GT.0.0)THEN
       DPSI(NI,J)=ALFA(NI-1)/(1.-BETA(NI-1))
       END IF
       DO 35 I=NI-1,2,-1
       DPSI(I,J)=ALFA(I)+BETA(I)*DPSI(I+1,J)
35     CONTINUE
40     CONTINUE
C
C-------ETA DIR INTEGRATION
C
       RESP=0.0
       DO 80 I=2,NI-1
       ALFA(1)=0.0
       BETA(1)=0.0
       DO 60 J=2,NJ-1
```

```
          COF3=GA(I,J)*DTEE
          COF4=QTJ(I,J)*0.25*DE
          C=-COF3+COF4
          B=1.0+COF3*2.0
          A=-COF3-COF4
          D=DPSI(I,J)
          DEN=B+C*BETA(J-1)
          ALFA(J)=(D-C*ALFA(J-1))/DEN
          BETA(J)=-A/DEN
60        CONTINUE
          DO 65 J=NJ-1,2,-1
          PSI1(I,J)=PSI(I,J)
          DPSI(I,J)=ALFA(J)+BETA(J)*DPSI(I,J+1)
          PSI(I,J)=PSI(I,J)+DPSI(I,J)
          RESP=RESP+ABS(DPSI(I,J))
65        CONTINUE
80        CONTINUE
          IF(VJET.GT.0.0)THEN
          DO 90 J=2,NJ-1
          DPSI(NI,J)=DPSI(NI-1,J)
          PSI1(NI,J)=PSI(NI,J)
          PSI(NI,J)=PSI(NI,J)+DPSI(NI,J)
90        CONTINUE
          END IF
          RETURN
          END
C           ***************************************************************
                          SUBROUTINE PRINT
C           ***************************************************************
C
          IMPLICITREAL*8(A-H,O-Z)
          CHARACTER*6 NAMP
          COMMON
     1 /LOGIC/IPSI,IPRT1,IPRT2,
     2        IPRRT3,IPRT4,IREAD,ISTORE,IGRID
     1 /FVAR/PSI(100,50),DPSI(100,50),PSI1(100,50)
     1 /COORD/X(100,50),Y(100,50),Q(50)
     1 /INTEG/NI,NJ,NTITER
     1 /PROP/DT,VJET
     1 /EPSI/PSIEPS
     1 /RES/RESP,DT2,DZ,DZZ,DE,DEE
     1 /PRTVAR/NPRT,INTVLP,NITER
        LOGICAL IPSI,IPRT1,IPRT2,
     1          IPRT3,IPRT4,IREAD,ISTORE,IGRID
C
C
C                       ++++++++++++
                         ENTRY PRINT1
C                       ++++++++++++
C
```

```
      WRITE(5,107)
      WRITE(5,130)NI,NJ,NTITER,DT
      WRITE(5,150)PSIEPS
C
107   FORMAT(2X,' LIST OF THE INPUT DATA'/,
     1       2X,'**************************'///)
130   FORMAT(2X,'NUMBER OF NODES IN THE X DIR. = ',I5/
      1     ,2X,'NUMBER OF NODES IN THE Y DIR. = ',I5/
      1     ,2X,'NUMBER OF ITERATIONS FOR TIME       = ',I5/
      1     ,2X,'TIME INCREMENTS (NONDIM.)= ',F7.4//)
150   FORMAT(2X,'CONVERGENCE CRITERION FOR PSI-VEL = ',F8.6)
      RETURN
C
C               ++++++++++++
                ENTRY PRINT2
C               ++++++++++++
C
      WRITE(5,201)NI,NJ
      WRITE(5,210)
      WRITE(5,211)((X(I,J),I=1,NI),J=1,NJ)
      WRITE(5,212)
      WRITE(5,213)((Y(I,J),I=1,NI),J=1,NJ)
C
201   FORMAT(2X,' NUMBER OF GRID NODES IN THE X DIR.= ',I5/
     1       2X,' NUMBER OF GRID NODES IN THE Y DIR= ',I5/)
210   FORMAT(2X,' DX(I) VALUES :')
211   FORMAT(2X,40D15.8//)
212   FORMAT(2X,' DY(J) VALUES :')
213   FORMAT(2X,40D15.8//)
C
      RETURN
C
C                ++++++++++++
                 ENTRY PRINT3
C                ++++++++++++
C
300   CONTINUE
      I=MOD(NPRT,10)
      NPRT=(NPRT-I)/10
      IF(I.EQ.0) GO TO 365
      GO TO (310),I
310   WRITE(5,380)
      DO 320 JJ=1,NJ,NJ/4
      J=NJ-JJ+1
320   WRITE(5,370)(PSI(I,J),I=2,NI,NI/11)
370   FORMAT(2X,20(3X,D15.8))
380   FORMAT(2X,' STREAM FUNCTION')
365   RETURN
C
C                 ++++++++++++
```

```
                    ENTRY PRINT4
C                   ++++++++++++
C
        I=MOD(NPRT,10)
        NPRT=(NPRT-I)/10
        IF(I.EQ.0) GO TO 570
        GO TO (510),I
510     WRITE(5,575)
        DO 515 JJ=1,NJ
        J=NJ-JJ+1
515     WRITE(5,605)(PSI(I,J),I=1,NI)
575      FORMAT(2X,'STREAM FUNCTION    =    ')
570     CONTINUE
C
605     FORMAT(1X,20(3X,D15.8))
C
        RETURN
C
C
C                   ++++++++++++
                    ENTRY READ1
C                   ++++++++++++
C
        TYPE 781
        READ(5,*)NAMP
       OPEN(UNIT=1,FILE=NAMP)
        READ(1,*)NI,NJ
        DO 710 J=NJ,1,-1
710     READ(1,711)(K,K,PSI(I,J),I=1,NI)
711      FORMAT(5(1X,I4,I4,D16.8))
        CLOSE(UNIT=1,FILE=NAMP)
781     FORMAT(2X,'ENTER THE INITIAL PSI DATA FILE NAME ')
        RETURN
C
C                   ++++++++++++
                    ENTRY STORE
C                   ++++++++++++
C
        TYPE 1000
        READ(5,*)NAMP
       OPEN(UNIT=1,FILE=NAMP)
        WRITE(1,*)NI,NJ
        DO 820 J=NJ,1,-1
820     WRITE(1,825)(I,J,PSI(I,J),I=1,NI)
825      FORMAT(5(1X,I4,I4,D16.8))
        WRITE(1,1020)NITER,DT
        WRITE(1,1030)RESP,VJET
        CLOSE(UNIT=1,FILE=NAMP)
        RETURN
1000    FORMAT(2X,'ENTER PSI DATA FILE NAME TO STORE')
1002    FORMAT(A4)
1020    FORMAT(2X,'THESE VALUES ARE AT ITERATION ',I4/
```

```
     1      2X,'WITH THE TIME INC. OF ',D9.2/)
1030 FORMAT(2X,'RESP = ',D12.5,3X,' JET VELOCITY = ',D12.5)
     END
```

APPENDIX W

COMPUTER PROGRAM FOR VELOCITY CALCULATION FROM STREAM FUNCTION DATA IN MAPPED PLANE

```
C C C
```

```
      DXDE=0.0
      DYDZ=(4.*Y(2,J)-Y(3,J)-3.*Y(1,J))*DZ*0.5
      DYDE=(Y(1,J+1)-Y(1,J-1))*DE*0.5
      DPDE=(PSI(1,J+1)-PSI(1,J-1))*DE*0.5
      DPDZ=(4.*PSI(2,J)-PSI(3,J)-3.*PSI(1,J))*DZ*0.5
      AJJ=DXDZ*DYDE
      U(1,J)=+DPDE*DXDZ/AJJ
      V(1,J)=-DPDZ*DYDE/AJJ+DPDE*DYDZ/AJJ
      DXDZ=(X(NI-2,J)-4.*X(NI-1,J)+3.*X(NI,J))*DZ*0.5
      DYDZ=(Y(NI-2,J)-4.*Y(NI-1,J)+3.*Y(NI,J))*DZ*0.5
      DYDE=(Y(NI,J+1)-Y(NI,J-1))*DE*0.5
      DPDE=(PSI(NI,J+1)-PSI(NI,J-1))*DE*0.5
      DPDZ=(PSI(NI-2,J)-4.*PSI(NI-1,J)+3.*PSI(NI,J))*DZ*0.5
      AJJ=DXDZ*DYDE
      U(NI,J)=DPDE*DXDZ/AJJ
      V(NI,J)=-DPDZ*DYDE/AJJ+DPDE*DYDZ/AJJ
50    CONTINUE
      DO 55 I=2,NI-1
      DXDE=(4.*X(I,2)-X(I,3)-3.*X(I,1))*DE*0.5
      DXDZ=(X(I+1,1)-X(I-1,1))*DZ*0.5
      DYDE=(4.*Y(I,2)-Y(I,3)-3.*Y(I,1))*DE*0.5
      DYDZ=0.0
      DPDZ=(PSI(I+1,1)-PSI(I-1,1))*DZ*0.5
      DPDE=(4.*PSI(I,2)-PSI(I,3)-3.*PSI(I,1))*DE*0.5
      AJJ=DXDZ*DYDE
      U(I,1)=+DPDE*DXDZ/AJJ -DPDZ*DXDE/AJJ
      V(I,1)=-DPDZ*DYDE/AJJ
      DXDE=(X(I,NJ-2)-4.*X(I,NJ-1)+3.*X(I,NJ))*DE*0.5
      DXDZ=(X(I+1,NJ)-X(I-1,NJ))*DZ*0.5
      DYDE=(Y(I,NJ-2)-4.*Y(I,NJ-1)+3.*Y(I,NJ))*DE*0.5
      DYDZ=(Y(I+1,NJ)-Y(I-1,NJ))*DZ*0.5
      DPDZ=(PSI(I+1,NJ)-PSI(I-1,NJ))*DZ*0.5
      DPDE=(PSI(I,NJ-2)-4.*PSI(I,NJ-1)+3.*PSI(I,NJ))*DE*0.5
      AJJ=DXDZ*DYDE-DXDE*DYDZ
      U(I,NJ)=DPDE*DXDZ/AJJ-DPDZ*DXDE/AJJ
      V(I,NJ)=-DPDZ*DYDE/AJJ+DPDE*DYDZ/AJJ
55    CONTINUE
      TYPE *,'ENTER VELOCITY DATA FILE NAME'
      READ(5,*)NAMV
      OPEN(UNIT=1,FILE=NAMV)
      WRITE(1,*)NI,NJ
      DO 60 J=NJ,1,-1
60    WRITE(1,20)(I,J,U(I,J),I=1,NI)
      DO 70 J=NJ,1,-1
70    WRITE(1,20)(I,J,V(I,J),I=1,NI)
      CLOSE(UNIT=1,FILE=NAMV)
      END
```

APPENDIX X

COMPUTER PROGRAM FOR GENERATING SPRAY

DROPLET DISTRIBUTION DATA

```
C C C
```

```
      TYPE *,'ENTER THE MICROSCOPE READINGS (NO. OF DIVISIONS)'
      I=1
10    WRITE(5,20)I
20    FORMAT(2X,'NO. ',I3,'  ',$)
      READ(5,*,ERR=40)D(I)
      IF(D(I).EQ.999)GO TO 60
      I=I+1
      GO TO 10
40    TYPE *,'RE-ENTER THE DIAMETER'
      GO TO 10
60    NP=I-1
      END IF
      DO 70 I=1,NP
      P(I)=D(I)
      TEMP=D(I)*100./MAG
      D(I)=D(I)*100./MAG
      IF(TEMP-D(I).GE.0.5)D(I)=D(I)+1
70    CONTINUE
      DO 90 J=1,NP-1
      M=J
      MA=J+1
      DO 80 I=MA,NP
      IF(D(I).LT.D(M))M=I
80    CONTINUE
      TEMP=D(J)
      D(J)=D(M)
      D(M)=TEMP
90    CONTINUE
      NF=1
      N=1
      DO 110 I=1,NP-1
      IF(D(I+1).EQ.D(I))THEN
      NF=NF+1
      IF(I.EQ.NP-1)THEN
      T(N,1)=D(I)
      T(N,2)=NF
      END IF
      END IF
      IF(D(I+1).GT.D(I))THEN
      T(N,1)=D(I)
      T(N,2)=NF
      N=N+1
      NF=1
      IF(I.EQ.NP-1)THEN
      T(N,1)=D(I+1)
      T(N,2)=1
      END IF
      END IF
110   CONTINUE
      SUM=0.0
```

```
      DO 155 I=1,NP
155   SUM=SUM+D(I)
      DBAR=SUM/NP
      SUM=0.0
      DO 160 I=1,NP
160   SUM=SUM+(ABS(D(I)-DBAR))**2
      SD=SQRT(SUM/NP)
      TYPE *,'ENTER DATA FILE NAME IN QUOTES'
      READ(5,*)NAME
      OPEN(UNIT=1,FILE=NAME)
      WRITE(1,*)NP
      WRITE(1,*)(P(I),I=1,NP)
      WRITE(1,*)(D(I),I=1,NP)
      WRITE(1,*)N
      WRITE(1,*)(T(I,1),I=1,N)
      WRITE(1,*)(T(I,2),I=1,N)
      CLOSE(UNIT=1,FILE=NAME)
      TYPE *,'ENTER OUTPUT FILE NAME IN QUOTES'
      READ(5,*)NAME
      OPEN(UNIT=1,FILE=NAME)
      WRITE(1,130)AIRP,WTEMP,RAIRP,RADRY,RAWET,VEL,DIS,NP,N,DBAR,SD
130   FORMAT(2X,'SPRAY SYSTEM CHARACTERIZATION '/
     1      2X,'************************************ '//
     1      2X,'TEST CONDITIONS'/
     1      2X,'==============='//
     1      2X,'.....................................'/
     1      2X,'COMPRESSED AIR PRESSURE ( PSIG ) = ',F5.1/
     1      2X,'SPRAY WATER TEMPERATURE (DEG. F) = ',F5.1/
     1      2X,'ROOM AIR PRESSURE       (IN. HG) = ',F5.1/
     1      2X,'ROOM AIR DRY BULB TEMP. (DEG. F) = ',F5.1/
     1      2X,'ROOM AIR WET BULB TEMP. (DEG. F) = ',F5.1/
     1      2X,'WIND TUNNEL VELOCITY    (FT/SEC) = ',F5.2/
     1      2X,'SAMPLING LOCATION ,'/
     1      2X,'DISTANCE FROM NOZZEL    (  FT  ) = ',F5.1/
     1      2X,'.....................................'///
     1      2X,'       NUMBER OF SAMPLES TAKEN     : ',I3/
     1      2X,'       NUMBER OF DROP SIZES PRESENT: ',I3/
     1      2X,'       MEAN DROP DIAMETER (MICRON) : ',F4.1/
     1      2X,'       STANDARD DEVIATION          : ',F5.2//
     1      2X,'  DROP DIA.(MICRON)      FREQUENCY    (%)'/
     1      2X,'  ********************    **********   *****'/)
      DO 140 I=1,N
      PERC=100.*(FLOAT(T(I,2))/FLOAT(NP))
140   WRITE(1,150)T(I,1),T(I,2),PERC
150   FORMAT(10X,I3,19X,I2,6X,F5.2)
      CLOSE(UNIT=1,FILE=NAME)
      END
```

APPENDIX Y

COMPUTER PROGRAM FOR VISCOUS FLOW SOLUTION

```
C C C
```

```
      DC=DC*0.3048
      TYPE *,'ENTER U VEL FILE'
      ACCEPT 1,NAM1
1     FORMAT(A4)
      TYPE *,'ENTER V VEL FILE'
      ACCEPT 1,NAM2
      TYPE *,'ENTER P FILE'
      ACCEPT 1,NAM3
      UINF=2.*RE*AIRVIS/(AIRDEN*DC)
      REINV=1./RE
      TYPE 2,RE,REINV,UINF
2     FORMAT(2X,'RE # = ',F10.1,4X,'1/RE = ',E10.3,
     1       'UINF = ',E10.3/)
      ICOND=.TRUE.
      IDRIV=.TRUE.
      ISVUP=.TRUE.
      WRITE(5,109)
      IERR=1
3     READ(5,111,ERR=115)IREAD,IPRT1,IPRT2,IPRT3,IPRT4
      IF(IREAD)ICOND=.FALSE.
      NITER=0
      WRITE(5,5)
5     FORMAT(1X,'ENTER NI    ',$)
      READ(5,*)NI
      PI=3.141592654
      DX(1)=PI/180.
      DX(2)=2.5*DX(1)
      DX(NI-1)=DX(1)
      DX(NI-2)=DX(2)
      SI(2)=DX(2)/DX(1)
      SI(NI-1)=DX(NI-1)/DX(NI-2)
      DDX=173./(NI-5)
      DO 7 I=3,NI-3
      DX(I)=DDX*3.141592654/180.0
7     SI(I)=DX(I)/DX(I-1)
      SI(NI-2)=DX(NI-2)/DX(NI-3)
8     WRITE(5,9)
9     FORMAT(1X,'ENTER NJ,STEP SIZE,FIRST DY    ',$)
      READ(5,*)NJ,RY,DY1
      Y2=DY1*(RY**(NJ-1) -1)/(RY-1)
      WRITE(5,10)Y2
10    FORMAT(1X,'THE YMAX IS = ',F6.2)
      TYPE *,' IS YMAX OK (Y/N) ?'
      READ(5,11)ANS
11    FORMAT(A4)
      IF(ANS.NE.'Y')GO TO 8
      Y2=Y2+1.0
      Y1=1.0
      YMIN=DC/2.0
      YMAX=Y2*YMIN
```

```
      REFL=YMIN
      XMAX=180.
      XMIN=0.0
      DY(1)=DY1
      DO 12 J=2,NJ-1
      SJ(J)=RY
12    DY(J)=RY*DY(J-1)
      WRITE(5,105)
      IERR=2
35    READ(5,*,ERR=115)DT,NTITER,INTVLP,OMEGA,ZETAX,ZETAY
      ZETAX=ZETAX/8.0
      ZETAY=ZETAY/8.0
      NPRT=123
     IF(ICOND) CALL INICON
      IF(IREAD) CALL READ1
      IF(IDRIV) CALL DRIV
      IF(IPRT1) CALL PRINT1
      IF(IPRT2) CALL PRINT2
      IF(IPRT4) CALL PRINT4
      IPRT4=.TRUE.
40    IF(MOD(NITER,10).EQ.0.AND.NITER.GT.0)THEN
      WRITE(30,39)NITER,RESU,RESV,RESP
39    FORMAT(1X,' # OF ITERATION = ',I4,' RESU = ',D15.5,' RESV = ',
     1      D15.5,' RESP = ',D15.5)
      TYPE 39,NITER,RESU,RESV,RESP
      END IF
      IF(MOD(NITER,10).EQ.0.AND.NITER.GT.0)THEN
      OPEN(UNIT=1,FILE=NAM1)
      DO 200 J=NJ,1,-1
200   WRITE(1,37)(I,J,U(I,J),I=1,NI)
      WRITE(1,38)NITER,DT,OMEGA,ZETAX,ZETAY,RESU,RESV,RESP
38    FORMAT(1X,'# OF ITERATION = ',I4,'  TIME STEP = ',F8.5/
     1      1X,'OMEGA = ',F5.1,'  ZETAX,ZETAY = ',2(2X,F5.3)/
     1      1X,'RESU = ',D15.5,'  RESV = ',D15.5,'  RESP = ',D15.5)
      CLOSE(UNIT=1,FILE=NAM1)
      OPEN(UNIT=1,FILE=NAM2)
      DO 201 J=NJ,1,-1
201   WRITE(1,37)(I,J,V(I,J),I=1,NI)
      CLOSE(UNIT=1,FILE=NAM2)
      OPEN(UNIT=1,FILE=NAM3)
      DO 202 J=NJ,1,-1
202   WRITE(1,37)(I,J,P(I,J),I=1,NI)
      CLOSE(UNIT=1,FILE=NAM3)
37    FORMAT(50(I3,I3,2X,D15.8))
      END IF
      NITER=NITER+1
      IF(NTITER.EQ.0) GO TO 55
      IF(ISVUP) CALL CALVUP
      IF(IDRIV) CALL DRIV
      IF(MOD(NITER,INTVLP).NE.0) GO TO 45
```

```
          WRITE(5,107)
          IERR=3
42        READ(5,*,ERR=115)NPRT
          WRITE(5,104)NITER,RESU,RESV,RESP
          IF(IPRT3) CALL PRINT3
          WRITE(5,106)
          IERR=4
43        READ(5,*,ERR=115)CHINTP
          IF(CHINTP.NE.0.0) INTVLP=CHINTP
45       CONTINUE
C
C------CONVERGENCE TEST
C
          IF(NITER.GE.NTITER) GO TO 50
          IF(RESU.GT.UEPSI.OR.RESV.GT.VEPSI) GO TO 50
          GO TO 40
50        WRITE(5,108)
          IERR=5
52        READ(5,*,ERR=115)NNIT,DDT
          IF(NNIT.EQ.0)THEN
          TYPE *,'NO. OF VARIABLES FOR FINAL PRINT ?'
          IERR=6
53        READ(5,*,ERR=115)NPRT
          IF(NPRT.NE.0)CALL PRINT4
          END IF
          IF(NNIT.EQ.0) GO TO 55
          IF(DDT.NE.0.)DT=DDT
          NTITER=NNIT
          GO TO 40
55       CONTINUE
          WRITE(5,102)
          IEER=7
57        READ(5,103,ERR=115)SAVE
          IF(SAVE.EQ.'Y') CALL STORE
          GO TO 60
115       WRITE(5,116)
          GO TO (3,35,42,43,52),IERR
60        STOP
101      FORMAT(10F12.7)
102      FORMAT(5X,'IF YOU LIKE TO SAVE TYPE Y OR N    ',$)
103      FORMAT(A4)
104      FORMAT(2X,'NO. OF TIME ITERATIONS= ',I5/
     1         2X,'RESIDUE U= ',D15.5/
     2         2X,'RESIDUE V= ',D15.5/
     3         2X,'RESIDUE P= ',D15.5)
105      FORMAT(2X,'ENTER DT,NTITER,INTVLP,OMEGA ,ZETAX,ZETAY    ',$)
106      FORMAT(2X,'ENTER NEW PRINT INTERVAL OR 0    ',$)
107      FORMAT(2X,'ENTER NO. VARIABLES FOR INT. PRINT    ',$)
108      FORMAT(2X,'ENTER NO. OF TIME ITER AND DT TO CONTINUE     ',$)
109      FORMAT(2X,'ENTER IREAD,IPRT1,IPRT2,IPRT3,IPRT4     ',$)
111      FORMAT(5(L1))
116       FORMAT(2X,'RE-ENTER THE VALUE =    ',$)
```

```
      END
      SUBROUTINE INICON
C
      IMPLICITREAL*8(A-H,O-Z)
                COMMON
     1 /FVAR/U(40,50),V(40,50),P(40,50),
     3       DUDX(40,50),DUDY(40,50),
     4       DVDX(40,50),DVDY(40,50),
     6       DUDXX(40,50),DUDYY(40,50),DPDY(40,50),
     7       DVDXX(40,50),DVDYY(40,50),DPDX(40,50)
     1 /DELF/DF(40,50,3)
     1 /COORD/DX(50),DY(50),SI(50),SJ(50)
     1 /INTEG/NI,NJ,NTITER
     1 /PROP/UINF,PINF,AIRVIS,AIRDEN,DT,RE,REINV
     1 /GEOM/REFL,XMAX,YMAX,YMIN,RY,Y1,Y2
C
C-----INITIALIZE ALL THE NONDIMENSIONAL FIELD VARIABLES
C
      PI=3.141592654
      NIM1=NI-1
      NJM1=NJ-1
      DYS1=Y2
      DYS=DYS1*DYS1
      DO 120 J=NJ,1,-1
      ANGLE=0.0
      DO 110 I=1,NI
      IF(J.LE.10)THEN
      U(I,J)=(J-1)*U(I,J+1)/10.
      END IF
      IF(J.GT.10)THEN
      U(I,J)=-(1.+1./DYS)*SIN(PI+ANGLE)
      END IF
      ANGLE=ANGLE+DX(I)
110   CONTINUE
      IF(J.EQ.1)GO TO 120
      DYS1=DYS1-DY(J-1)
      DYS=DYS1*DYS1
120   CONTINUE
      DYS1=1.0
      DYS=DYS1*DYS1
      DO 125 J=1,NJ
      ANGLE=0.0
      DO 127 I=1,NI
      V(I,J)=(1-1./DYS)*COS(PI+ANGLE)
      ANGLE=ANGLE+DX(I)
127   CONTINUE
      IF(J.EQ.NJ)GO TO 125
      DYS1=DYS1+DY(J)
      DYS=DYS1*DYS1
125   CONTINUE
```

```
          V(1,1)=0.0
          DO 130 I=1,NI
          DO 130 J=1,NJ
          P(I,J)=0.5*(1-(U(I,J)**2.+V(I,J)**2.))
130       CONTINUE
          RETURN
          END
          SUBROUTINE CALVUP
          IMPLICITREAL*8(A-H,O-Z)
                    COMMON
     1 /FVAR/U(40,50),V(40,50),P(40,50),
     3       DUDX(40,50),DUDY(40,50),
     4       DVDX(40,50),DVDY(40,50),
     6       DUDXX(40,50),DUDYY(40,50),DPDY(40,50),
     7       DVDXX(40,50),DVDYY(40,50),DPDX(40,50)
     1 /DELF/DF(40,50,3)
     1 /COORD/DX(50),DY(50),SI(50),SJ(50)
     1 /PROP/UINF,PINF,AIRVIS,AIRDEN,DT,RE,REINV
     1 /EPSI/PEPSI,UEPSI,VEPSI,OMEGA,ZETAX,ZETAY
     1 /RES/RESU,RESV,RESP
     1 /INTEG/NI,NJ,NTITER
     1 /GEOM/REFL,XMAX,YMAX,YMIN,RY,Y1,Y2
          COMMON WORK(3,3)
          DIMENSION DUMMY1(3,3),DUMMY2(3,3)
          DIMENSION AW1(3,1),PQ(3,3),IDEN(3,3)
          DIMENSION A(3,3),B(3,3),C(3,3),D(3,1),G(3,3),Z(3,3)
          DIMENSION ALFA(3,3),W(3,1,50),GAMA(3,3,50)
          NSE=3
          DO 100 IC=1,NSE
100       IDEN(IC,IC)=1.0
          PQ(1,1)=1.0
          PQ(1,2)=0.0
          PQ(1,3)=0.0
          PQ(2,1)=0.0
          PQ(2,2)=1.0
          PQ(2,3)=0.0
          PQ(3,1)=0.0
          PQ(3,2)=0.0
          PQ(3,3)=0.0
          DT2=0.5*DT
          NIM1=NI-1
          NJM1=NJ-1
C
C------GENERATE THE TDM COEFFICIENTS IN THE X DIRECTION
C
          R=1.0
          DO 140 J=2,NJM1
          RD1=1./R
          R=R+DY(J-1)
          RU1=1./(R+DY(J))
```

```
          R1=1.0/R
          R2=R1*R1
          RDT=R1*DT2
          DO 130 I=2,NIM1
          T1=+1.0/((SI(I)+1)*DX(I))
          T2=T1/DX(I)
          T3=SI(I)*SI(I)
          T4=(SI(I)-1)/DX(I)
          T5=2*SI(I)/(DX(I)*DX(I))
          WORK(1,1)=1.+2*V(I,J)*RDT
          WORK(1,2)=2*U(I,J)*RDT
          WORK(1,3)=0.0
          WORK(2,1)=-2*U(I,J)*RDT
          WORK(2,2)=1.0+2*V(I,J)*RDT
          WORK(2,3)=0.0
          WORK(3,1)=0.0
          WORK(3,2)=OMEGA*RDT
          WORK(3,3)=1.0
          CALL INV
          Z(1,1)=2*U(I,J)
          Z(1,2)=-2*REINV*R1
          Z(1,3)=1.0
          Z(2,1)=V(I,J)+2*REINV*R1
          Z(2,2)=U(I,J)
          Z(2,3)=0.0
          Z(3,1)=OMEGA
          Z(3,2)=0.0
          Z(3,3)=0.0
          DO 102 IC=1,NSE
          DO 102 JC=1,NSE
          DUMMY1(IC,JC)=0.0
          DUMMY2(IC,JC)=0.0
          DO 102 KC=1,NSE
          DUMMY1(IC,JC)=DUMMY1(IC,JC)+WORK(IC,KC)*Z(KC,JC)
102       DUMMY2(IC,JC)=DUMMY2(IC,JC)+WORK(IC,KC)*PQ(KC,JC)
          DO 103 IC=1,NSE
          DO 103 JC=1,NSE
103       B(IC,JC)=IDEN(IC,JC)+DT2*(T4*R1*DUMMY1(IC,JC)+
          1         REINV*R2*T5*DUMMY2(IC,JC))
          Z(1,1)=2*U(I-1,J)
          Z(2,1)=V(I-1,J)+2*REINV*R1
          Z(2,2)=U(I-1,J)
C------THE [ P ] IS THE SAME AT ANY I.
          DO 104 IC=1,NSE
          DO 104 JC=1,NSE
          DUMMY1(IC,JC)=0.0
          DO 104 KC=1,NSE
104       DUMMY1(IC,JC)=DUMMY1(IC,JC)+WORK(IC,KC)*Z(KC,JC)
          DO 105 IC=1,NSE
          DO 105 JC=1,NSE
105       C(IC,JC)=DT2*(-T1*T3*R1*DUMMY1(IC,JC)-2*T2*T3*R2*REINV
```

```
     1        *DUMMY2(IC,JC))
      Z(1,1)=2*U(I+1,J)
      Z(2,1)=V(I+1,J)+2*REINV*R1
      Z(2,2)=U(I+1,J)
C--------THE [ P ] IS THE SAME AT ANY I
      DO 106 IC=1,NSE
      DO 106 JC=1,NSE
      DUMMY1(IC,JC)=0.0
      DO 106 KC=1,NSE
106   DUMMY1(IC,JC)=DUMMY1(IC,JC)+WORK(IC,KC)*Z(KC,JC)
      DO 107 IC=1,NSE
      DO 107 JC=1,NSE
107   A(IC,JC)=DT2*(T1*R1*DUMMY1(IC,JC)-2*SI(I)*T2*R2*REINV
     1        *DUMMY2(IC,JC))
      IF(I.GT.2.AND.I.LT.NIM1)THEN
      CORRU=-(U(I+2,J)-4.*U(I+1,J)+6.*U(I,J)-4.*U(I-1,J)+U(I-2,J))
      CORRV=-(V(I+2,J)-4.*V(I+1,J)+6.*V(I,J)-4.*V(I-1,J)+V(I-2,J))
      CORRP=-(P(I+2,J)-4.*P(I+1,J)+6.*P(I,J)-4.*P(I-1,J)+P(I-2,J))
      ELSE
      CORRU=0.0
      CORRV=0.0
      CORRP=0.0
      END IF
      SJ2=SJ(J)*SJ(J)
      DENY=1./((SJ(J)+1)*DY(J))
      US1=U(I-1,J)*U(I-1,J)
      US2=U(I,J)*U(I,J)
      US3=U(I+1,J)*U(I+1,J)
      VS1=V(I,J-1)*V(I,J-1)
      VS2=V(I,J)*V(I,J)
      VS3=V(I,J+1)*V(I,J+1)
      UVI1=U(I-1,J)*V(I-1,J)
      UVI2=U(I,J)*V(I,J)
      UVI3=U(I+1,J)*V(I+1,J)
      UVJ1=U(I,J-1)*V(I,J-1)
      UVJ2=UVI2
      UVJ3=U(I,J+1)*V(I,J+1)
      DUSDX=R1*T1*(US3+(T3-1)*US2-T3*US1)
      DUVDY=(UVJ3+(SJ2-1)*UVJ2-SJ2*UVJ1)*DENY
      DUVDX=(UVI3+(T3-1)*UVI2-T3*UVI1)*R1*T1
      DVSDY=(VS3+(SJ2-1)*VS2-SJ2*VS1)*DENY
      DURDY=(U(I,J+1)*RU1+(SJ2-1)*U(I,J)*R1-SJ2*
     1     U(I,J-1)*RD1)*DENY
      DVRDY=(V(I,J+1)*RU1+(SJ2-1)*V(I,J)*R1-SJ2*
     1     V(I,J-1)*RD1)*DENY
      D(1,1)=DT*(-DUSDX-DUVDY-2*U(I,J)*V(I,J)*R1-R1*DPDX(I,J)
     1      +REINV*(DUDYY(I,J)+DURDY
     2       +R2*DUDXX(I,J)+2*R2*DVDX(I,J)))
      D(2,1)=DT*(-DUVDX-DVSDY-(V(I,J)*V(I,J)-U(I,J)*U(I,J))*R1
     1      -DPDY(I,J)+REINV*(DVDYY(I,J)+DVRDY
```

```
          2      +R2*DVDXX(I,J)-2*R2*DUDX(I,J)))
          D(3,1)=DT*OMEGA*(-R1*DUDX(I,J)-DVDY(I,J)-V(I,J)*R1)
          DO 108 IC=1,NSE
          AW1(IC,1)=0.0
          DO 108 KC=1,NSE
108       AW1(IC,1)=AW1(IC,1)+WORK(IC,KC)*D(KC,1)
          D(1,1)=AW1(1,1)+CORRU*ZETAX
          D(2,1)=AW1(2,1)+CORRV*ZETAX
          D(3,1)=AW1(3,1)+CORRP*ZETAX
          IF(I.EQ.NIM1)THEN
          DO 109 IJ=1,3
          DO 109 JI=2,3
109       B(IJ,JI)=B(IJ,JI)+A(IJ,JI)
          END IF
          IF(I.EQ.2)THEN
C------I=2 AND J
          DO 110 IJ=1,3
          DO 110 JI=2,3
          B(IJ,JI)=B(IJ,JI)+C(IJ,JI)
110       WORK(IJ,JI)=B(IJ,JI)
          END IF
          IF(I.EQ.2) THEN
C------B=ALFA=WORK
          CALL INV
          DO 113 IC=1,NSE
          W(IC,1,I)=0.0
          DO 113 KC=1,NSE
113      W(IC,1,I)=W(IC,1,I)+WORK(IC,KC)*D(KC,1)
          DO 114 IC=1,NSE
          DO 114 JC=1,NSE
          GAMA(IC,JC,I)=0.0
          DO 114 KC=1,NSE
114      GAMA(IC,JC,I)=GAMA(IC,JC,I)+WORK(IC,KC)*A(KC,JC)
          END IF
          IF(I.NE.2)THEN
         DO 116 IC=1,NSE
          DO 116 JC=1,NSE
          WORK(IC,JC)=0.0
          DO 116 KC=1,NSE
116      WORK(IC,JC)=WORK(IC,JC)+C(IC,KC)*GAMA(KC,JC,I-1)
          DO 117 JC=1,NSE
          DO 117 IC=1,NSE
          ALFA(IC,JC)=B(IC,JC)-WORK(IC,JC)
          WORK(IC,JC)=ALFA(IC,JC)
117      CONTINUE
          CALL INV
          DO 118 IC=1,NSE
          DO 118 JC=1,1
          AW1(IC,JC)=0.0
          DO 118 KC=1,NSE
118      AW1(IC,JC)=AW1(IC,JC)+C(IC,KC)*W(KC,JC,I-1)
```

```
          DO 119 IC=1,NSE
          W(IC,1,I)=0.0
          DO 119 KC=1,NSE
119       W(IC,1,I)=W(IC,1,I)+WORK(IC,KC)*(D(KC,1)-AW1(KC,1))
          DO 120 IC=1,NSE
          DO 120 JC=1,NSE
          GAMA(IC,JC,I)=0.0
          DO 120 KC=1,NSE
120       GAMA(IC,JC,I)=GAMA(IC,JC,I)+WORK(IC,KC)*A(KC,JC)
          END IF
130       CONTINUE
          DO 132 IC=1,NSE
          DF(NIM1,J,IC)=W(IC,1,NIM1)
132       CONTINUE
          DO 135 II=4,NI
          I=NI-II+2
          DO 133 IC=1,NSE
          AW1(IC,1)=0.0
          DO 133 KC=1,NSE
133       AW1(IC,1)=AW1(IC,1)+GAMA(IC,KC,I)*DF(I+1,J,KC)
          DO 134 IC=1,NSE
          DF(I,J,IC)=W(IC,1,I)-AW1(IC,1)
134       CONTINUE
135       CONTINUE
140       CONTINUE
          DO 142 J=1,NJ
          DO 142 K=2,3
          DF(1,J,K)=DF(2,J,K)
142       DF(NI,J,K)=DF(NI-1,J,K)
C------START THE Y DIRECTION SWEEP
          ANGLE=0.0
          DO 240 I=2,NIM1
          ANGLE=ANGLE+DX(I-1)
          R=1.0
          DO 210 J=2,NJM1
          RD1=1./R
          R=R+DY(J-1)
          RU1=1./(R+DY(J))
          R1=1.0/R
          RDT=R1*DT2
          R2=R1*R1
          T1=1.0/((SJ(J)+1.)*DY(J))
          T2=T1/DY(J)
          T3=SJ(J)*SJ(J)
          T4=(SJ(J)-1)/DY(J)
          T5=2*SJ(J)/(DY(J)*DY(J))
          WORK(1,1)=1.+2*V(I,J)*RDT
          WORK(1,2)=2*U(I,J)*RDT
          WORK(1,3)=0.0
          WORK(2,1)=-2*U(I,J)*RDT
```

```
          WORK(2,2)=1.0+2*V(I,J)*RDT
          WORK(2,3)=0.0
          WORK(3,1)=0.0
          WORK(3,2)=OMEGA*RDT
           WORK(3,3)=1.0
          CALL INV
          Z(1,1)=V(I,J)-REINV*R1
          Z(1,2)=U(I,J)
          Z(1,3)=0.0
          Z(2,1)=0.0
          Z(2,2)=2*V(I,J)-REINV*R1
          Z(2,3)=1.0
          Z(3,1)=0.0
          Z(3,2)=OMEGA
          Z(3,3)=0.0
C-------[ Q ] 'S ARE THE SAME AS [ P ] 'S GIVEN IN X-DIR. (DESG. [PQ])
          DO 158 IC=1,NSE
          DO 158 JC=1,NSE
          DUMMY1(IC,JC)=0.0
          DUMMY2(IC,JC)=0.0
          DO 158 KC=1,NSE
          DUMMY1(IC,JC)=DUMMY1(IC,JC)+WORK(IC,KC)*Z(KC,JC)
158       DUMMY2(IC,JC)=DUMMY2(IC,JC)+WORK(IC,KC)*PQ(KC,JC)
          DO 159 IC=1,NSE
          DO 159 JC=1,NSE
159       B(IC,JC)=IDEN(IC,JC)+DT2*(T4*DUMMY1(IC,JC)+T5*REINV*
          1         DUMMY2(IC,JC))
          Z(1,1)=V(I,J-1)-REINV*RD1
          Z(1,2)=U(I,J-1)
          Z(2,2)=2*V(I,J-1)-REINV*RD1
C------SAME [ PQ ] 'S APPLY AT J-1
          DO 160 IC=1,NSE
          DO 160 JC=1,NSE
          DUMMY1(IC,JC)=0.0
          DO 160 KC=1,NSE
160       DUMMY1(IC,JC)=DUMMY1(IC,JC)+WORK(IC,KC)*Z(KC,JC)
          DO 162 IC=1,NSE
          DO 162 JC=1,NSE
162       C(IC,JC)=DT2*(-T3*T1*DUMMY1(IC,JC)-2*T2*T3*REINV*
          1         DUMMY2(IC,JC))
          Z(1,1)=V(I,J+1)-REINV*RU1
          Z(1,2)=U(I,J+1)
          Z(2,2)=2*V(I,J+1)-REINV*RU1
C------SAME [ PQ ] 'S APPLY
          DO 163 IC=1,NSE
          DO 163 JC=1,NSE
          DUMMY1(IC,JC)=0.0
          DO 163 KC=1,NSE
163       DUMMY1(IC,JC)=DUMMY1(IC,JC)+WORK(IC,KC)*Z(KC,JC)
          DO 165 IC=1,NSE
```

```
      DO 165 JC=1,NSE
165   A(IC,JC)=DT2*(T1*DUMMY1(IC,JC)-2*SJ(J)*T2*REINV*DUMMY2(IC,JC))
      IF(J.GT.2.AND.J.LT.NJM1)THEN
      CORRU=U(I,J+2)-4.*U(I,J+1)+6.*U(I,J)-4.*U(I,J-1)+U(I,J-2)+DF(I,
      1J+2,1)-4.*DF(I,J+1,1)+6.*DF(I,J,1)-4.*DF(I,J-1,1)+DF(I,J-2,1)
      CORRV=V(I,J+2)-4.*V(I,J+1)+6.*V(I,J)-4.*V(I,J-1)+V(I,J-2)+DF(I,
      1J+2,2)-4.*DF(I,J+1,2)+6.*DF(I,J,2)-4.*DF(I,J-1,2)+DF(I,J-2,2)
      CORRP=P(I,J+2)-4.*P(I,J+1)+6.*P(I,J)-4.*P(I,J-1)+P(I,J-2)+DF(I,
      1J+2,3)-4.*DF(I,J+1,3)+6.*DF(I,J,3)-4.*DF(I,J-1,3)+DF(I,J-2,3)
      ELSE
      IF(J.EQ.2)THEN
      CORRU=U(I,J+2)-4.*U(I,J+1)+6.*U(I,J)-4.*U(I,J-1)-U(I,J+2)+DF(I,
      1J+2,1)-4.*DF(I,J+1,1)+6.*DF(I,J,1)-4.*DF(I,J-1,1)-DF(I,J+2,1)
      CORRV=V(I,J+2)-4.*V(I,J+1)+6.*V(I,J)-4.*V(I,J-1)-V(I,J+2)+DF(I,
      1J+2,2)-4.*DF(I,J+1,2)+6.*DF(I,J,2)-4.*DF(I,J-1,2)-DF(I,J+2,2)
      CORRP=P(I,J+2)-4.*P(I,J+1)+6.*P(I,J)-4.*P(I,J-1)-P(I,J+2)+DF(I,
      1J+2,3)-4.*DF(I,J+1,3)+6.*DF(I,J,3)-4.*DF(I,J-1,3)-DF(I,J+2,3)
      ELSE
      CORRU=0.0
      CORRV=0.0
      CORRP=0.0
      END IF
      END IF
      D(1,1)=DF(I,J,1) -CORRU*ZETAY
      D(2,1)=DF(I,J,2) -CORRV*ZETAY
      D(3,1)=DF(I,J,3) -CORRP*ZETAY
      GO TO 169
      IF(J.EQ.NJM1)THEN
C-----J=NJM1 AND I
      PI2=3.141592/2.0
      IF(ANGLE.GT.PI2)THEN
      DO 167 JI=1,3
      DO 167 IJ=1,3
167   B(IJ,JI)=B(IJ,JI)+A(IJ,JI)
      END IF
      END IF
169   CONTINUE
      IF(J.EQ.2)THEN
C-----J=2AND I
C-----RCYL=YMIN/REFL =1.0
      TER1=(1 -2./(DY(1)*SJ(2)))*REINV-2.*V(I,1)
      TER2=(2./(DY(1)*SJ(2)*(SJ(2)+1.)))*REINV
      B(1,2)=B(1,2)+TER1*C(1,3)
      B(1,3)=B(1,3)+C(1,3)
      B(2,2)=B(2,2)+TER1*C(2,3)
      B(2,3)=B(2,3)+C(2,3)
      B(3,2)=B(3,2)+TER1*C(3,3)
      B(3,3)=B(3,3)+C(3,3)
      A(1,2)=A(1,2)+TER2*C(1,3)
      A(2,2)=A(2,2)+TER2*C(2,3)
```

```
          A(3,2)=A(3,2)+TER2*C(3,3)
          END IF
          IF(J.EQ.2)THEN
          DO 171 IC=1,3
          DO 171 JC=1,3
171       WORK(IC,JC)=B(IC,JC)
C------B=ALFA=WORK
          CALL INV
          DO 175 IC=1,NSE
          W(IC,1,J)=0.0
          DO 175 KC=1,NSE
175      W(IC,1,J)=W(IC,1,J)+WORK(IC,KC)*D(KC,1)
          DO 180 IC=1,NSE
          DO 180 JC=1,NSE
          GAMA(IC,JC,J)=0.0
          DO 180 KC=1,NSE
180      GAMA(IC,JC,J)=GAMA(IC,JC,J)+WORK(IC,KC)*A(KC,JC)
          END IF
          IF(J.NE.2) THEN
          DO 186 IC=1,NSE
          DO 186 JC=1,NSE
          WORK(IC,JC)=0.0
          DO 186 KC=1,NSE
186      WORK(IC,JC)=WORK(IC,JC)+C(IC,KC)*GAMA(KC,JC,J-1)
          DO 190 JC=1,NSE
         DO 190 IC=1,NSE
          ALFA(IC,JC)=B(IC,JC)-WORK(IC,JC)
          WORK(IC,JC)=ALFA(IC,JC)
190      CONTINUE
          CALL INV
          DO 195 IC=1,NSE
          AW1(IC,1)=0.0
          DO 195 KC=1,NSE
195      AW1(IC,1)=AW1(IC,1)+C(IC,KC)*W(KC,1,J-1)
          DO 200 IC=1,NSE
          W(IC,1,J)=0.0
          DO 200 KC=1,NSE
200       W(IC,1,J)=W(IC,1,J)+WORK(IC,KC)*(D(KC,1)-AW1(KC,1))
          DO 205 IC=1,NSE
          DO 205 JC=1,NSE
          GAMA(IC,JC,J)=0.0
          DO 205 KC=1,NSE
205      GAMA(IC,JC,J)=GAMA(IC,JC,J)+WORK(IC,KC)*A(KC,JC)
          END IF
210       CONTINUE
          DO 215 IC=1,NSE
          DF(I,NJM1,IC)=W(IC,1,NJM1)
215      CONTINUE
          DO 230 JJ=4,NJ
          J=NJ-JJ+2
```

```
          DO 220 IC=1,NSE
          AW1(IC,1)=0.0
          DO 220 KC=1,NSE
220       AW1(IC,1)=AW1(IC,1)+GAMA(IC,KC,J)*DF(I,J+1,KC)
          DO 225 IC=1,NSE
          DF(I,J,IC)=W(IC,1,J)-AW1(IC,1)
225       CONTINUE
230       CONTINUE
240       CONTINUE
          RESU=0.0
          RESV=0.0
          RESP=0.0
          DO 245 J=2,NJM1
          DO 245 I=2,NIM1
          V(I,J)=V(I,J)+DF(I,J,2)
          U(I,J)=U(I,J)+DF(I,J,1)
          P(I,J)=P(I,J)+DF(I,J,3)
          RESU=RESU+ABS(DF(I,J,1))
          RESV=RESV+ABS(DF(I,J,2))
          RESP=RESP+ABS(DF(I,J,3))
245       CONTINUE
C------CALCULATE THE V,U,P AT THE BOUNDARY
C------CALCULATE P ON THE SURFACE ,J=1,FROM Y MOMENTUM EQ.
          ANGLE=0.
          SJP1=1+SJ(2)
          SJ2=SJP1*SJP1
          DENY=1./(SJ(2)*SJP1*DY(1)*DY(1))
          DO 250 I=1,NI
          POLD=P(I,1)
          ANGLE=ANGLE+DX(I)
          DVDY(I,1)=(V(I,2)*SJ2-V(I,3)-V(I,1)*(SJ2-1.))*DENY*DY(1)
          DVDYY(I,1)=(V(I,3)-V(I,2)*SJP1+SJ(2)*V(I,1))*2.*DENY
          IF(I.EQ.1)DVDXX(1,1)=(V(3,1)-V(2,1)*(1+SI(2))+SI(2)*V(1,1))*2.
          1/(SI(2)*(1.+SI(2))*DX(1)*DX(1))
          IF(I.EQ.NI)DVDXX(NI,1)=(-V(NI-1,1)*(SI(NI-1)+1.)+V(NI-2,1)*SI(
          1NI-1)+V(NI,1))*2./(SI(NI-1)*(1.+SI(NI-1))*DX(NI-1)**2.)
          IF(I.GT.1.AND.I.LT.NI)DVDXX(I,1)=2.*SI(I)*(V(I+1,1)-V(I,1)*
          1(1.+SI(I))+V(I-1,1))/((1.+SI(I))*DX(I)*DX(I))
          P(I,1)=P(I,2)-DY(1)*(-2.*V(I,1)*DVDY(I,1)-V(I,1)*V(I,1)
          1+REINV*(DVDYY(I,1)+DVDY(I,1)-V(I,1)+DVDXX(I,1)))
          DF(I,1,3)=P(I,1)-POLD
          GO TO 250
          IF(ANGLE.GT.PI2)THEN
          P(I,NJ)=P(I,NJ-1)
          U(I,NJ)=U(I,NJ-1)
          V(I,NJ)=V(I,NJ-1)
          DF(I,NJ,1)=DF(I,NJ-1,1)
          DF(I,NJ,2)=DF(I,NJ-1,2)
          DF(I,NJ,3)=DF(I,NJ-1,3)
          END IF
250       CONTINUE
```

```
      DO 260 J=2,NJ-1
      U(1,J)=0.0
      U(NI,J)=0.0
      V(1,J)=V(2,J)
      V(NI,J)=V(NI-1,J)
      P(1,J)=P(2,J)
      P(NI,J)=P(NI-1,J)
      DF(1,J,1)=0.0
      DF(1,J,2)=DF(2,J,2)
      DF(1,J,3)=DF(2,J,3)
      DF(NI,J,1)=0.0
      DF(NI,J,2)=DF(NI-1,J,2)
      DF(NI,J,3)=DF(NI-1,J,3)
260   CONTINUE
C
      RETURN
      END
      SUBROUTINE INV
      IMPLICITREAL*8(A-H,O-Z)
      COMMON WORK(3,3)
      DO 6 K=1,3
      AIN=1./WORK(K,K)
      DO 4 J=1,3
      IF(J.NE.K)THEN
      WORK(K,J)=WORK(K,J)*AIN
      END IF
4     CONTINUE
      WORK(K,K)=AIN
      DO 5 I=1,3
      IF(I.NE.K)THEN
      DO 10 J=1,3
      IF(J.NE.K)THEN
      WORK(I,J)=WORK(I,J)-WORK(K,J)*WORK(I,K)
      END IF
10    CONTINUE
      END IF
5     CONTINUE
      DO 6 I=1,3
      IF(I.NE.K)THEN
      WORK(I,K)=-WORK(I,K)*WORK(K,K)
      END IF
6     CONTINUE
      RETURN
      END
      SUBROUTINE DRIV
      IMPLICITREAL*8(A-H,O-Z)
            COMMON
     1 /FVAR/U(40,50),V(40,50),P(40,50),
     3       DUDX(40,50),DUDY(40,50),
     4       DVDX(40,50),DVDY(40,50),
```

```
     6       DUDXX(40,50),DUDYY(40,50),DPDY(40,50),
     7       DVDXX(40,50),DVDYY(40,50),DPDX(40,50)
     1 /INTEG/NI,NJ,NTITER
     1 /COORD/DX(50),DY(50),SI(50),SJ(50)
         NIM1=NI-1
         NJM1=NJ-1
         DO 120 J=2,NJM1
         DO 120 I=2,NIM1
C
         F1=SI(I)*SI(I)
         F2=SJ(J)*SJ(J)
         F3=1./((SI(I)+1.)*DX(I))
         F4=1./((SJ(J)+1.)*DY(J))
         F5=1./((SI(I)+1.)*DX(I)*DX(I)/(2.*SI(I)))
         F6=1./((SJ(J)+1.)*DY(J)*DY(J)/(2.*SJ(J)))
         DUDY(I,J)=(U(I,J+1)+(F2-1.)*U(I,J)-U(I,J-1)*F2)*F4
         DUDX(I,J)=(U(I+1,J)+(F1-1.)*U(I,J)-U(I-1,J)*F1)*F3
         DUDYY(I,J)=(U(I,J+1)-(SJ(J)+1.)*U(I,J)+U(I,J-1)*SJ(J))*F6
         DUDXX(I,J)=(U(I+1,J)-(SI(I)+1.)*U(I,J)+U(I-1,J)*SI(I))*F5
C        DUDYX(I,J)=F3*(F4*(U(I+1,J+1)+(F2-1.)*U(I+1,J)-F2*U(I+1,J-1))
C        1   +       (F1-1.)*F4*(U(I,J+1)+(F2-1.)*U(I,J)-F2*U(I,J-1))
C        1   -       F1*F4*(U(I-1,J+1)+(F2-1.)*U(I-1,J)-F2*U(I-1,J-1)))
         DVDY(I,J)=(V(I,J+1)+(F2-1.)*V(I,J)-V(I,J-1)*F2)*F4
         DVDX(I,J)=(V(I+1,J)+(F1-1.)*V(I,J)-V(I-1,J)*F1)*F3
         DVDYY(I,J)=(V(I,J+1)-(SJ(J)+1.)*V(I,J)+V(I,J-1)*SJ(J))*F6
         DVDXX(I,J)=(V(I+1,J)-(SI(I)+1.)*V(I,J)+V(I-1,J)*SI(I))*F5
C        DVDYX(I,J)=F3*(F4*(V(I+1,J+1)+(F2-1.)*V(I+1,J)-F2*V(I+1,J-1))
C        1   +       (F1-1.)*F4*(V(I,J+1)+(F2-1.)*V(I,J)-F2*V(I,J-1))
C        1   -       F1*F4*(V(I-1,J+1)+(F2-1.)*V(I-1,J)-F2*V(I-1,J-1)))
         DPDY(I,J)=(P(I,J+1)+(F2-1.)*P(I,J)-P(I,J-1)*F2)*F4
         DPDX(I,J)=(P(I+1,J)+(F1-1.)*P(I,J)-P(I-1,J)*F1)*F3
C        DPDYY(I,J)=(P(I,J+1)-(SJ(J)+1.)*P(I,J)+P(I,J-1)*SJ(J))*F6
C        DPDXX(I,J)=(P(I+1,J)-(SI(I)+1.)*P(I,J)+P(I-1,J)*SI(I))*F5
120     CONTINUE
         RETURN
         END
C          ************************************************************
                        SUBROUTINE PRINT
C          ************************************************************
C
         IMPLICITREAL*8(A-H,O-Z)
         COMMON
     1 /LOGIC/ISVUP,IPRT1,IPRT2,
     2        IPRRT3,IPRT4,IREAD,ISTORE,IDRIV
     1 /FVAR/U(40,50),V(40,50),P(40,50),
     3       DUDX(40,50),DUDY(40,50),
     4       DVDX(40,50),DVDY(40,50),
     6       DUDXX(40,50),DUDYY(40,50),DPDY(40,50),
     7       DVDXX(40,50),DVDYY(40,50),DPDX(40,50)
     1 /COORD/DX(50),DY(50),SI(50),SJ(50)
```

```
      1 /GEOM/REFL,XMAX,YMAX,YMIN,RY,Y1,Y2
      1 /INTEG/NI,NJ,NTITER
      1 /PROP/UINF,PINF,AIRVIS,AIRDEN,DT,RE,REINV
      1 /EPSI/PEPSI,UEPSI,VEPSI,OMEGA,ZETAX,ZETAY
      1 /RES/RESU,RESV,RESP
      1 /PRTVAR/NPRT,INTVLP,NITER
          LOGICAL ISVUP,IPRT1,IPRT2,
     1           IPRT3,IPRT4,IREAD,ISTORE,IDRIV
C
C
C                       ++++++++++++
                         ENTRY PRINT1
C                       ++++++++++++
C
          OPEN(UNIT=1,FILE='PRINT1.DAT')
          WRITE(1,107)
          WRITE(1,110)Y2,Y1
          WRITE(1,120)XMAX,XMIN,YMAX,YMIN,RY
          WRITE(1,130)NI,NJ,NTITER,DT
          WRITE(1,140)UINF,PINF,AIRVIS,AIRDEN,RE
          WRITE(1,150)UEPSI,PEPSI,VEPSI,OMEGA,ZETAX,ZETAY
          WRITE(1,160)NVIPRT,NVFPRT,INTVLP
          CLOSE(UNIT=1,FILE='PRINT1.DAT')
C
107       FORMAT(2X,' LIST OF THE INPUT DATA'/,
     1           2X,'*****************************'///)
110        FORMAT(2X,'THE NONDIM. YMAX  =',F10.3/
           1     ,2X,'THE NONDIM. YMIN  =',F10.3/)
120       FORMAT(2X,'THE MAXIMUM X     = ',F10.3,2X,'(DEGREE)'/
           1     ,2X,'THE MINIMUM X     = ',F10.3,2X,'(DEGREE)'/
           1     ,2X,'THE MAXIMUM Y     = ',F10.3,2X,'(METERS)'/
           1     ,2X,'THE MINIMUM Y     = ',F10.3,2X,'(METERS)'/
           1     ,2X,'THE RATE OF CHANGE OF DY IS=',(F8.6,3X)//)
130       FORMAT(2X,'NUMBER OF NODES IN THE X DIR. = ',I5/
           1     ,2X,'NUMBER OF NODES IN THE Y DIR. = ',I5/
           1     ,2X,'NUMBER OF ITERATIONS FOR TIME       = ',I5/
           1     ,2X,'TIME INCREMENTS (NONDIM.)= ',F7.4//)
140       FORMAT(2X,'FAR FIELD AIR VELOCITY = ',E9.2,2X,'(M/SEC)'
           1    ,/2X,'FAR FIELD AIR PRESSURE = ',E9.2,2X,'(N/M**2)'
           1    ,/2X,'FAR FIELD AIR VISCOSITY= ',E9.2,2X,'(KG/MS)'
           1    ,/2X,'FAR FIELD AIR DENSITY  = ',E9.2,2X,'(KG/M**3)'
           1    ,/2X,'AIR REYNOLD NUMBER BASED'
           1    ,/2X,'ON THE CYL. DIA.  = ',E11.3//)
150       FORMAT(2X,'CONVERGENCE CRITERION FOR U-VEL = ',F8.6/
           1      2X,'//     ///    ////    /// PRESSURE = ',F8.6/
           1      2X,'//     ///    ////    /// V-VEL    = ',F8.6/
           1      2X,'SCALE FACTOR FOR PRESSURE= ',F8.2/
           1      2X,'DAMPING FACTOR FOR X = ',F8.3/
           1      2X,'DAMPING FACTOR FOR Y = ',F8.3//)
160       FORMAT(2X,'NUMBER OF VARIABLES FOR WHICH INTERMEDIATE'/
```

```
     1      2X,'RESULTS TO BE PRINTED, NOTE: U=1,V=2,P=3',I7//
     1      2X,'NUMBER OF VARIABLES FOR WHICH FINAL RESULTS'/
     1      2X,'TO BE PRINTED          = ',I7//
     1      2X,'TIME INTERVAL FOR PRINT = ',I5//)
      RETURN
C
C              ++++++++++++
               ENTRY PRINT2
C              ++++++++++++
C
      OPEN(UNIT=1,FILE='PRINT2.DAT')
      WRITE(1,201)NI,NJ
      WRITE(1,210)
      WRITE(1,211)(DX(I),I=1,NI)
      WRITE(1,212)
      WRITE(1,213)(DY(J),J=1,NJ)
      WRITE(1,214)
      WRITE(1,216)(SI(I),I=1,NI)
      WRITE(1,215)
      WRITE(1,216)(SJ(J),J=1,NJ)
      CLOSE(UNIT=1,FILE='PRINT2.DAT')
C
201   FORMAT(2X,' NUMBER OF GRID NODES IN THE X DIR.= ',I5/
     1       2X,' NUMBER OF GRID NODES IN THE Y DIR= ',I5/)
210   FORMAT(2X,' DX(I) VALUES :')
211   FORMAT(2X,40D15.8//)
212   FORMAT(2X,' DY(J) VALUES :')
213   FORMAT(2X,40D15.8//)
214   FORMAT(2X,'RATIO OF DX(I)/DX(I-1):')
215   FORMAT(2X,'RATIO OF DY(J)/DY(J-1):')
216   FORMAT(2X,50D15.8//)
C
      RETURN
C
C              ++++++++++++
               ENTRY PRINT3
C              ++++++++++++
C
300   CONTINUE
      I=MOD(NPRT,10)
      NPRT=(NPRT-I)/10
      IF(I.EQ.0) GO TO 365
      GO TO (310,330,350),I
310   WRITE(5,380)
      DO 320 JJ=1,NJ,NJ/4
      J=NJ-JJ+1
320   WRITE(5,370)(U(I,J),I=1,NI,NI/4)
330   WRITE(5,385)
      DO 340 JJ=1,NJ,NJ/4
      J=NJ-JJ+1
340   WRITE(5,370)(V(I,J),I=1,NI,NI/4)
350   WRITE(5,390)
```

```
      DO 360 JJ=1,NJ,NJ/4
      J=NJ-JJ+1
360   WRITE(5,370)(P(I,J),I=1,NI,NI/4)
      GO TO 300
365   CONTINUE
370   FORMAT(2X,20(3X,D15.8))
380   FORMAT(2X,' U-VELOCITY')
385   FORMAT(2X,' V-VELOCITY')
390   FORMAT(2X,' PRESSURE')
      RETURN
C
C                  ++++++++++++
                   ENTRY PRINT4
C                  ++++++++++++
C
500   CONTINUE
      I=MOD(NPRT,10)
      NPRT=(NPRT-I)/10
      IF(I.EQ.0) GO TO 570
      GO TO (510,520,530),I
510   WRITE(5,575)
      DO 515 JJ=1,NJ
      J=NJ-JJ+1
515   WRITE(5,605)(U(I,J),I=1,NI)
      GO TO 500
520   WRITE(5,580)
      DO 525 JJ=1,NJ
      J=NJ-JJ+1
525   WRITE(5,605)(V(I,J),I=1,NI)
      GO TO 500
530   WRITE(5,585)
      DO 535 JJ=1,NJ
      J=NJ-JJ+1
535   WRITE(5,605)(P(I,J),I=1,NI)
      GO TO 500
570   CONTINUE
C
575   FORMAT(2X,'U-VELOCITY'/2X,'************'//)
580   FORMAT(2X,'V-VELOCITY'/2X,'************'//)
585   FORMAT(2X,'PRESSURE  '/2X,'************'//)
605   FORMAT(1X,20(3X,D15.8))
C
      RETURN
C
C
C                  ++++++++++++
                   ENTRY READ1
C                  ++++++++++++
C
      TYPE 781
```

```
        ACCEPT 780,UVEL
       OPEN(UNIT=1,FILE=UVEL)
        DO 710 J=NJ,1,-1
710    READ(1,999)(I,K,U(I,J),I=1,NI)
        CLOSE(UNIT=1,FILE=UVEL)
        TYPE 782
        ACCEPT 780,VVEL
       OPEN(UNIT=1,FILE=VVEL)
        DO 725 J=NJ,1,-1
725    READ(1,999)(I,K,V(I,J),I=1,NI)
        CLOSE(UNIT=1,FILE=VVEL)
        TYPE 783
        ACCEPT 780,PRESS
       OPEN(UNIT=1,FILE=PRESS)
         DO 740 J=NJ,1,-1
740    READ(1,999)(I,K,P(I,J),I=1,NI)

        CLOSE(UNIT=1,FILE=PRESS)
999     FORMAT(50(I3,I3,2X,D15.8))
780    FORMAT(A4)
781    FORMAT(2X,'ENTER THE U-VEL DATA FILE SPECS.')
782    FORMAT(2X,'ENTER THE V-VEL DATA FILE SPECS.')
783    FORMAT(2X,'ENTER THE PRESS DATA FILE SPECS.')
        RETURN
C
C                  ++++++++++++
                   ENTRY STORE
C                  ++++++++++++
C
        TYPE 1000
        ACCEPT 1002,UVEL
       OPEN(UNIT=1,FILE=UVEL)
        DO 820 J=NJ,1,-1
820    WRITE(1,995)(I,J,U(I,J),I=1,NI)
        WRITE(1,1020)NITER,DT,OMEGA,ZETAX,ZETAY,RE,REINV,UINF
        WRITE(1,1030)DY(1),DY(NJ-1),RY
        WRITE(1,1040)DX(1),DX(NI-1)
        CLOSE(UNIT=1,FILE=UVEL)
        TYPE 1004
        ACCEPT 1002,VVEL
       OPEN(UNIT=1,FILE=VVEL)
        DO 850 J=NJ,1,-1
850    WRITE(1,995)(I,J,V(I,J),I=1,NI)
        WRITE(1,1020)NITER,DT,OMEGA,RE,REINV,UINF
        CLOSE(UNIT=1,FILE=VVEL)
        TYPE 1006
        ACCEPT 1002,PRESS
       OPEN(UNIT=1,FILE=PRESS)
        DO 880 J=NJ,1,-1
880    WRITE(1,995)(I,J,P(I,J),I=1,NI)
```

```
      WRITE(1,*)NITER,DT,OMEGA,RE,REINV,UINF
      CLOSE(UNIT=1,FILE=PRESS)
      RETURN
995   FORMAT(50(I3,I3,2X,D15.8))
1000  FORMAT(2X,'ENTER U-VEL DATA FILE SPECS. TO STORE')
1002  FORMAT(A4)
1004  FORMAT(2X,'ENTER V-VEL DATA FILE SPECS. TO STORE')
1006  FORMAT(2X,'ENTER PRESS DATA FILE SPECS. TO STORE')
1020  FORMAT(2X,'THESE VALUES ARE AT ITERATION ',I3/
     1      2X,'WITH THE TIME INC. OF ',D9.2/
     1      2X,'WITH OMEGA OF ',D11.4/
     1      2X,'WITH DAMPING FACTOR FOR X ',D11.4/
     1      2X,'WITH DAMPING FACTOR FOR Y ',D11.4/
     1      2X,'WITH   RE OF ',D11.4/
     1      2X,'WITH REINV OF ',D11.4/
     1      2X,'WITH UINF OF ',D11.4)
1030  FORMAT(2X,'FIRST DY = ',D12.5,3X,'LAST DY = ',D12.5/
     1      2X,'INITIAL DY(J)/DY(J-1) = ',D12.7/)
1040  FORMAT(2X,'FIRST DX = ',D12.5,3X,'LAST DX = ',D12.5/)
      END
```

APPENDIX Z

COMPUTER PROGRAM FOR STREAM FUNCTION CALCULATION

FROM VELOCITY DATA OF VISCOUS FLOW SOLUTION

```
C C C
```

```
      IT=IT+1
      DO 300 I=2,NI-1
      R=1.0
      DR=DY1
      DO 200 J=2,NJ
      R=R+DR
      DR=DR*S
      T1=2*S/(DR*DR)
      T2=T1/(S+1)
      T3=1./R
      A=AA*T3/R
      B=-2*A
      C=A
      POLD=PSI(I,J)
      IF(J.EQ.NJ) GO TO 150
      PSI(I,J)=PSI(I,J)-1.4*((DUDR(I,J)-DVDX(I,J)-A*PSI(I+1,J)
     1        -C*PSI(I-1,J)-T2*PSI(I,J+1)-S*T2*PSI(I,J-1))/(B-T1)
     1        +PSI(I,J))
      GO TO 170
150   PSI(I,J)=PSI(I,J)-1.4*((-DVDX(I,J)-A*PSI(I+1,J)-C*PSI(I-1,J)
     1        )/B+PSI(I,J))
170   RES=RES+ABS(PSI(I,J)-POLD)
200   CONTINUE
300   CONTINUE
      WRITE(5,400)IT,RES
      IF(RES.GT.0.00001)GO TO 100
      WRITE(5,400)IT,RES
400   FORMAT(2X,'# OF ITERATION = ',I4,'  RESIDUAL = ',F10.5)
      OPEN(UNIT=1,FILE='PSI.DAT')
      DO 500 J=NJ,1,-1
500   WRITE(1,20)(I,J,PSI(I,J),I=1,NI)
      CLOSE(UNIT=1,FILE='PSI.DAT')
      END
```

VITA

Abdollah Haddad Tabrizi was born in Tabriz, Iran on December 1, 1954. He graduated from Ferdousi high school in Tabriz, Iran in June, 1973.

He entered the University of Tulsa in June, 1974 and graduated in August, 1977, receiving a B.S. degree in Mechanical Engineering. He then continued his education at Oklahoma State University receiving a M.S. degree in Mechanical Engineering in May, 1979. He then entered the University of Tennessee. For a year and a half he conducted research with the aid of a grant from NASA. Since then he has been involved in studying and teaching at the Mechanical Engineering department at the University of Tennessee.

The author is a member of Sigma Xi, Tau Beta Pi, Pi Tau Sigma, and Phi Eta Sigma. He is the representative of the Mechanical Engineering Department in the Graduate Student Council at the University of Tennessee.